MITIGATING WIND-INDUCED FATIGUE IN STEEL TRAFFIC SIGNAL SUPPORT STRUCTURES

A Dissertation

by

KYLE THOMAS WIEGHAUS

Submitted to the Office of Graduate and Professional Studies of
Texas A&M University
in partial fulfillment of the requirements for the degree of

DOCTOR OF PHILOSOPHY

Chair of Committee,	Stefan Hurlebaus
Co-Chair of Committee,	John B. Mander
Committee Members,	W. Lynn Beason
	Ibrahim Karaman
Head of Department,	Robin Autenrieth

August 2015

Major Subject: Civil Engineering

ABSTRACT

Traffic signal structures undergo wind-induced vibrations that result in fatigue damage accumulation and reduced service life. Mast arms have failed and required removal while in service. A dual experimental and analytical modeling approach is taken to mitigate fatigue and fracture in steel traffic supporting structures.

A full-scale prototype structure is instrumented to study natural wind response. Excitation mechanisms are identified, and response is characterized statistically by a lognormal distribution. Helical strakes are found to reduce the vortex-induced vibration of cantilevered traffic signal structures, however are not a panacea for fatigue mitigation as marginal service life gains occur in severe wind environments.

A probabilistic framework is extended to assess the risk of wind-induced fatigue and estimate service life while considering uncertainties in fatigue demand and capacity. The framework is successfully demonstrated against compiled inspection records. Locations with higher prevailing winds are susceptible to wind-induced fatigue, but the prevalence of low-speed vortex-induced response is primarily responsible for the early fatigue failures in more mild environments.

A low-cost damage avoidance system is proposed to mitigate fatigue and fracture in steel traffic supporting structures. Applied prestress introduces a fail-safe, supplementary load path to balance dead load moment, eradicating the detrimental tensile mean stress found in traffic signal structure connections. Field observations are made without and with the proposed system installed. The benefit of applied prestress is

quantified by determining service life without and with the system based on changes in response and fatigue resistance using: (i) a code-based technique; and (ii) the proposed probabilistic framework. Fatigue performance is modeled as mean stress-dependent by modifying nominal stress-life relationships. Service life is shown to increase by an order of magnitude, regardless of wind environment. The concept shows potential to reduce the detrimental effects of non-redundancy for a variety of similar, fatigue-critical infrastructure components.

The validity of simplified mean stress-dependent connection modeling is explored. A fracture mechanics-based, total life (initiation-propagation) model is used to demonstrate the detrimental effect mean stress has on tube-to-transverse base plate fatigue resistance. Using fatigue strength curves derived from total life analyses, probabilistic analyses are repeated to justify the use of simplified models.

DEDICATION

To my family.

ACKNOWLEDGEMENTS

I would like to thank my committee chair Dr. Stefan Hurlebaus, and co-chair Dr. John Mander, for their constant support and guidance throughout my study. This work would not have been possible without their vision, thoughts, and advice. I am deeply grateful to Dr. Hurlebaus, Dr. Mander, Texas A&M Transportation Institute, and the Zachry Department of Civil Engineering for the financial support that I received at various times during my stay at Texas A&M University.

I would also like to thank Dr. W. Lynn Beason and Dr. Ibrahim Karaman for serving on my committee. Thank you also to Dr. Gary Fry for assisting with field instrumentation; to Dr. Keating and the High-Bay laboratory technicians for allowing me to borrow tools; and to the department's faculty and staff for making my time at Texas A&M University a fond experience. I also want to acknowledge and thank my dear colleagues Mr. Madhu Karthik, Dr. Jaeyong Baik, Dr. Stacey Tucker, Mr. Joshua White, and numerous other friends at Texas A&M University for their constant support and friendship.

Last, but never least, I would like to thank my family (Tom, Sheryl, and Emily Wieghaus) for their constant support, encouragement, love, and prayers, and especially to my wife, Marianne Wieghaus, for her patience and faith in me.

TABLE OF CONTENTS

LIST OF FIGURES

LIST OF TABLES

1 INTRODUCTION

1.1 Background and Motivation

Under excitation from wind, traffic signal supporting structures often exhibit large amplitude vibrations that can result in reduced service life of fatigue-critical details in these structures. With an estimated 3 million intersections in the United States, over 300,000 are signalized, many using cantilevered structures. The results of a recent multi-state survey show that over 10 percent cantilevered traffic signal structures are classified as cracked when inspected (Price et al. 2008). This number has been observed to vary from 3 percent in Connecticut (Christenson and Hoque 2011) to 33 percent in Wyoming (Hamilton et al. 2000). As depicted in Figure 1-1, there have been several known instances where the mast-to-arm connection has completely failed or nearly failed and required removal while in service.

In response to sequential cantilevered traffic signal collapses in Michigan, which resulted in property damage, injuries and a fatality, AASHTO identified the need for new specifications in the early 1990's (Culp 1990). The specification would include designing for vibration and fatigue. Much research was done concerning fatigue loading types, identifying fatigue prone details, and the development of a simplified design methodology. Although the current AASHTO specifications (AASHTO 2013) now reflect consideration of most of these issues, Price et al. (2008) shows the average structure in inspection records predates the 2001 AASHTO specifications (2001), where fatigue provisions were first

introduced. As a result, the majority of steel traffic support structures were designed not properly taking fatigue into consideration.

As a result, there is great need for a fatigue and fracture mitigation measure for implementation not only on both existing and new traffic support structures, but other fatigue susceptible steel traffic support structures. Because other proposed vibration mitigation devices have been shown to have limited effectiveness due to the varying nature of traffic support structure configurations and the lack of a complete understanding of governing excitation mechanisms, mitigation measures must be viable for the vast majority of not only cantilevered traffic signal structures, but many other steel traffic support structures.

The proposed research takes note that fatigue failures only occur if a connection experiences tensile cyclic loads. The removal of tensile bending stresses in traffic signal connections would eliminate the susceptibility of fatigue failures. The underlying approach is to use post-tensioned (PT) prestress concepts. This concept is not new; engineers have been doing exactly using this for decades by applying prestress to concrete bridge girders, building frames and floors, etc. Although concrete is a material strong in compression and weak in tension (strength), engineers tend to overlook that steel, particularly at its connections, is weak in tension also. This is not a strength weakness; rather a fatigue weakness. Fatigue is a phenomenon that primarily occurs if partial or full tensile stress or strain cycles exist. Therefore, by simply post-tensioning a mast arm with an appropriate degree of prestress, preferably with some load-balancing attributes, there is the potential to remove tensile bending stresses. The proposed work will focus primarily

on steel traffic signal structures, and will determine the statistical risk of fatigue and explore several options to mitigate fatigue in the arm-pole and pole-foundation connections.

1.2 Research Hypothesis and Questions

It can be seen that much research has been performed to study the fatigue life of traffic signal structures, from finding a better understanding of the excitation mechanisms that result in vibrations to the development of methods to enhance the fatigue performance of these structures. Enhancing the fatigue performance has been approached by attempting to reduce fatigue demand on or by increasing connection fatigue capacity by detail modification or weld treatment.

It has been demonstrated that even with large research projects and wind tunnel testing, previous research has been unable entirely address the issues related to wind-induced vibrations of traffic signal structures. Each traffic signal supporting structure is different in location, equipment (signal, sign camera, etc.), wind speed, wind direction, size, etc. It would be impractical to look at the wind-induced demands and the resulting mechanisms of every possible traffic signal type and location. Moreover, wind tunnel testing in the past has been performed on reduced scale models. Scaling a structural problem and using similitude relations introduces uncertainties which are critical for excitation sensitive parameters, such as size, wind speed, etc. These uncertainties have led to vague results and not surprisingly previous research has not reached a consensus.

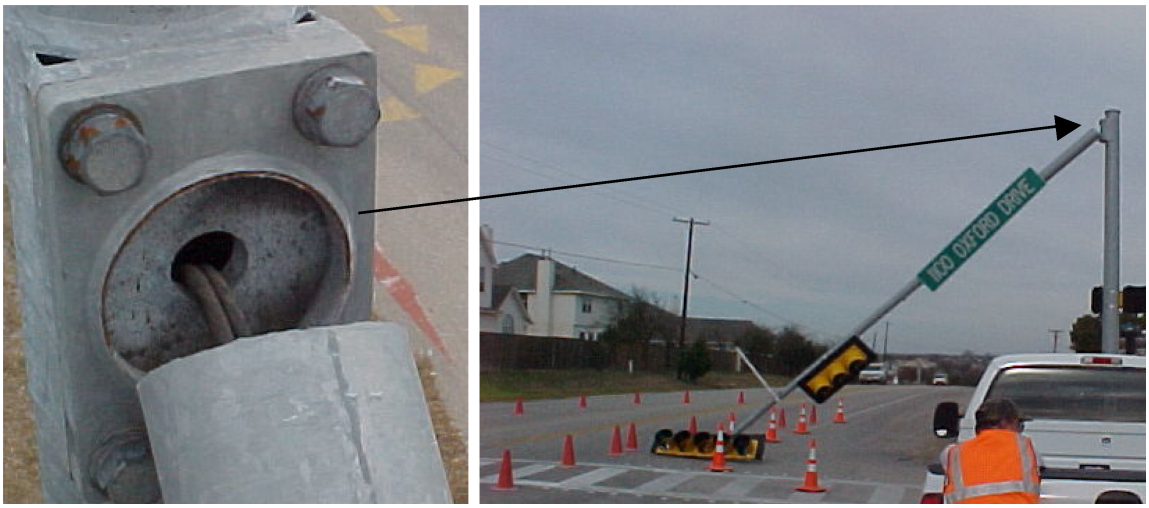

Figure 1-1. Failure of traffic signal supporting structure (Frank, 2005).

What is the primary excitation mechanism responsible for traffic signal structure vibrations and reduced fatigue/dependable service life? Have mitigation strategies aimed at excitation reduction taken this into consideration?

Previous research has not been able to entirely address the issues related to wind-induced vibrations of traffic signal structures. The mechanism behind observed large amplitude vibrations had been attributed to wind-induced galloping of the signal clusters (McDonald et al. 1995). Later, this was reaffirmed by showing that vortex shedding was not an excitation mechanism (Kaczinski et al. 1998); as a result, fatigue design loads were specified to account for natural wind gust, truck-induced gusts, and galloping in the specifications (AASHTO 2001).

Various types of mitigation devices and measures, such as damper plates were developed based on this understanding. However, the effectiveness of these mitigation devices has varied, indicating a potential inadequacy in the current understanding of the problem. In support of this notion, following studies have found that the structural vibrations with signals attached closely resembled vibrations due to vortex shedding (Letchford et al. 2008; Cruzado et al. 2013), and related the vibrations to the height of the attached signal clusters. As a result of identifying vortex shedding as an excitation mechanism, both galloping and vortex shedding were both directly accounted for in the fatigue provisions of the 2009 Standard Specifications (AASHTO 2009). More recent works have attributed them to the aerodynamic instability of the cantilever tapered cylinders (Zou and Letchford 2010), disregarding any explanation on the dependence of

signal cluster dimension. Current specifications (AASHTO 2013) no longer directly account for vortex-induced vibrations for fatigue design.

With uncertainty regarding vortex shedding as an excitation mechanism for cantilevered traffic signal structures, no vibration mitigation measures have considered it as a primary source of fatigue damage accumulation. Although there have been mitigation measures developed as excitation independent, all have had limited success, since each traffic signal supporting structure is different in location, equipment (signal, sign camera, etc.), wind speed, wind direction, size, etc. Verifying vortex shedding as an excitation mechanism will not only justify its place in new design specifications, but it will also provide reason to consider classical measures to reduce vortex shedding as a method of vibration suppression/mitigation. Vibration suppression will lead to decreased fatigue demand on cantilevered traffic signal structures, elongating their dependable service life.

Is there a probabilistic methodology available for the rapid assessment of the statistical risk of fatigue cracking in traffic signal structure connections?

Service life estimation strategies for traffic support structures presented in past works must be improved upon. The presented models have not come to a consensus on the vibrations critical to fatigue damage. The model proposed by South (1994) took only damage accumulated by out-of-plane (along-wind) vibrations into account. Later, a very similar method proposed by Chen et al. (2001) was recommended, but again only estimated the number of out-of-plane vibration cycles occurring after gusts. The proposed model in Letchford et al. (2008) has similarities to the procedures proposed by South (1994) and Chen et al. (2001), except it considers the effect of wind direction and estimates

damage based on in-plane (across-wind) vibrations, the location identified as fatigue prone in the Chen et al. (2002) study. None of the above risk assessment methodologies take into account uncertainties present in estimation.

A probabilistic risk assessment model should be developed as the recommended fatigue service life estimation strategies in past do not conform to concepts seen in reliability theory and new design. The uncertainty in fatigue life estimation needs to be taken into account. A probabilistic methodology is necessary to conduct a genuine risk assessment on populations of installed cantilevered traffic signal structures. Assigning service life estimates to a prescribed non-exceedance probability is possible using available wind data, field measured strain data, and fatigue test results. A model can be developed to incorporate the quantification of uncertainties, yet be assessable for rapid implementation. Such a model can offer an improved method for the evaluation of fatigue mitigation procedures.

Is there an alternative fatigue mitigation strategy that would improve the fatigue capacity of traffic signal structure connections?

More effective mitigation strategies, with a wider range of applicability, to decrease failures of mast-to-arm connections have the potential for development. There has been no research toward solutions that have the potential to eliminate the possibility of fatigue from the connection entirely, while conforming to the same standards to which the traditional connections adhere. They must resist the specified loads and signify a beneficial change not only in fatigue performance, but also response amplitude.

Concepts principle to the damage avoidance design (DAD) methodology should be considered for a solution; unlike those proposed by other researchers, an effective mitigation strategy should aim to remove damage accumulation at fatigue prone connections and provide energy dissipation. With that, traditional PT concepts hold the key to the development of a low-cost, highly-effective fatigue retrofit for cantilevered steel traffic signal and similar structure connections. As utilized in DAD designs, PT has the ability to lessen or eliminate the tensile mean stresses present in steel traffic support structure connections and reduce the load demands transmitted through the welded component. The reduction (or elimination) of tensile mean stresses will significantly reduce fatigue damage accumulation; high-cycle fatigue life has been shown to be significantly influenced by tensile mean stresses (Bannantine et al. 1990, Koenigs et al. 2003). The addition of member PT will surely change the dynamic characteristics of steel traffic supporting structures, by increasing damping. Further, the use of additional damping elements, such as elastomeric pads or Belleville washers, will also be considered for use in the connection. An increased level of damping will lead to reduced vibration amplitudes, lessening the fatigue demand placed on the connections. PT concepts are very promising for the fatigue retrofit of traffic signal and other overhead sign structures.

1.3 Research Objectives

The proposed research has six primary research objectives. These primary objectives of the research are to:

i. Construct a full-scale cantilevered steel traffic signal support and develop an experimental plan capable of providing the necessary data to form relationships necessary to complete all tasks and studies.

ii. Determine the dominant mechanisms that result in mast arm vibrations, their role in the accumulation of fatigue damage in cantilevered traffic signal structure connections, and identify potential remedies.

iii. Present a probabilistic methodology that may be used to: (a) assess the statistical risk of fatigue failure of steel traffic supporting structures; and (b) rapidly assess damage accumulated by similar structures following extreme natural wind events.

iv. Design, install, and experimentally evaluate the effectiveness of PT device(s) aimed to mitigate fatigue and fracture of traffic signal structure connections based on DAD principles by increasing fatigue capacity and decreasing wind-induced demands.

v. Use the developed risk assessment model to: (a) assess the effectiveness of the developed fatigue mitigation device(s) to justify their installation by comparing the estimated service life with and without mitigation; and (b) develop a relationship between the characteristics of a natural wind environment and dependable service life to determine locations where fatigue mitigation measures must be taken.

vi. Investigate the validity of using simplified (AASHTO-type) connection fatigue models during probabilistic fatigue. Strain-life (crack initiation) and linear elastic fracture mechanics (crack propagation) principles will be used to develop fatigue

strength (S-N) curves. The effect that mean stress has on connection fatigue resistance shall be investigated and corroborated with past fatigue test results.

vii. When applicable, regional fatigue assessments shall be performed to relate historical local wind conditions to the expected service life of traffic signal structures.

1.4 New Contributions in Dissertation

Several contributions will be made as a result of the proposed research. The expected contributions are associated with the following:

i. The role that various identified excitation mechanisms have on cantilevered traffic signal structure vibrations and fatigue damage accumulation is appraised. This information offers insight on which fatigue mitigation strategies are most appropriate.

ii. A target-less computer vision technique is developed and implemented to measure/monitor traffic signal structure displacements and determine modal parameters. Access-limited structures can be analyzed from a distance.

iii. Annual average wind speeds are related to the risk of wind-induced fatigue failure in an effort to identify regions where the risk of fatigue failure justifies the installation of the proposed fatigue mitigation devices.

iv. A probabilistic fatigue risk assessment model is extended: (a) for the assessment of steel traffic support structures under natural winds, and (b) as a means to evaluate the performance/effectiveness of fatigue mitigation measures. The

framework may also be used during the rapid assessment of damage suffered (or accumulated) during extreme natural wind events.

v. PT DAD prototypes for traffic signal structure connection fatigue and fracture mitigation are installed and experimentally evaluated to study changes in wind-induced response, allowing their effectiveness to be probabilistically evaluated. Such mitigation measures offer a low-cost, long-term alternative to more costly fatigue design/remediation techniques.

vi. The vibration reduction associated with using: (a) an internal steel tendon within the horizontal arm and (b) a concentric rod within the vertical pole of a wind-excited steel support structure will be assessed experimentally.

vii. The effect of tensile dead load (mean) stress has on the fatigue performance of the fatigue-critical tube-to-transverse base plate welded connections is revisited using a total life (initiation-propagation) approach. The validity of simplified connection fatigue capacity modeling is investigated.

1.5 Research Significance

The significance of this work stems from the impact that it will have when added to the existing knowledge on the fatigue behavior of traffic signal structures. The proposed research focuses on the gaps in current knowledge or practice in the management or design of lightweight traffic support structures. The work primarily concentrates on the development, application, and assessment of a low-cost, PT DAD fatigue mitigation methodology for new and existing signal structures, as well as the introduction of a probabilistic risk assessment model for the wind-induced fatigue of structures. It also aims

to study the behavior of the structure in the natural wind environment and identify primary excitation mechanisms.

To aid in maintaining the nation's aging infrastructure, fatigue and fracture prevention for lightweight steel traffic support structures must be more effective and available at a low cost. When such options are found to be viable, many more of these structures can be rehabilitated for continued use, rather than being replaced, allowing for reallocation of public resources. Further, traffic signal structures are not the only light steel structures used in utility infrastructure. With common connections used in many facets of the country's infrastructure, transformative solutions for fatigue elimination could be applied to many structures with similar detailing, regardless of application. For instance, DAD solutions have the ability to be implemented on traffic light poles, overhead traffic sign structures, communication and electrical towers, and large wind turbines; such free-standing cantilever type structures having commonality across several engineering fields.

Connection types that have the potential to entirely eliminate the possibility of fatigue are promising concepts for new design, but the application for mitigation and repair could also prove invaluable. Additionally, in recognition of the need for intellectual expanse, such connections can be designed to introduce energy dissipation (damping) into the structural system to help reduce the number of cycles and amplitude of vibrations. If a reliable connection could not only eliminate fatigue, but also introduce additional damping to the system without damaging the connection, the uses of such a system could show promise of widespread use in structural engineering. This idea is not new as research currently focuses on seismic application where connections are being developed for

energy dissipation to occur through low-cycle inelastic material deformation. For use on traffic signal structures, a transformative solution must advance current knowledge to improve high-cycle fatigue life by dissipating energy without dampers and negligible inelastic material deformation.

Current fatigue life evaluation methodologies are based on fatigue strength or stress-life (S-N) curves and behavior models that are appropriately conservative. An easy-to-implement, probabilistic risk assessment model is developed as past and current fatigue life estimation strategies do not conform to concepts seen in reliability theory and new design. The introduction of a straight-forward probabilistic methodology allows a quantitative risk assessment on the population of traffic signal structures to be made. Assigning service life estimates to a prescribed probability is possible using available wind data, field measured strain data, and fatigue test results. This methodology is shown effective for fatigue assessment of lightweight infrastructure support structures, but may be used for rapid damage assessment and replacement prioritization following extreme wind events. The implementation of such a model will aid in infrastructure management, specifically in scheduling inspections, replacement planning, and rapid population assessments.

Many studies have been conducted to determine the excitation mechanisms that affect typical Texas traffic signal structures, as well as such structures nationwide. An assessment of pertinent large amplitude vibration events during full-scale testing of the unmodified structure sheds light on the excitation mechanisms involved for the typical traffic signal configurations under observation. As a result, excitation mechanism-targeted

vibration mitigation measures may be considered. The installation of helical strakes to the horizontal tapered arm provides further evidence to support claims on the excitation of these structures. The role of the tapered arm cannot be ignored as it contributes to vortex shedding about the signal clusters and thus large amplitude vibrations. Despite being effective for use in certain environments, properly designed and installed helical strakes are not a panacea for preventing wind-induced fatigue. This assessment also highlights the benefit of incorporating PT DAD concepts.

Regional risk assessments are enabled once relationships between wind environment and connection fatigue are established. Given wind maps or other forms of regional weather data, the risk of traffic signal connection fatigue are able to be assessed. As a result, locations can be identified where the risk of fatigue failure necessitates the installation of fatigue mitigation devices (preferably those proposed, tested, and studied herein). Not only do the results of this research serve as notification to traffic signal owners of potential traffic signal fatigue issues, but the developed tools may be used by local governments and stakeholders to assess their structure population given their local (specific) wind characteristics.

A target-less computer vision system is developed and implemented measure/monitor traffic signal structure displacements and determine modal parameters. Experimental analysis of structural response is often difficult or costly to employ because current methods generally require large arrays of instrumentation. Further, as is the case for several types of wind-excited structures, physical access is limited and installing instrumentation presents a risk for injury. The benefit of a computer vision-based

technique is the inherently non-contact approach. Short term studies or analyses of hard-to-access structures can be performed in situations where traditional instrumentation would be infeasible.

In summary, this work aims to develop and test PT DAD fatigue mitigation prototypes for lightweight steel traffic supporting structure. Using results from full scale experimentation, both done as part of this and previous works, a probabilistic risk assessment model is implemented to: (i) assess the effectiveness of the developed mitigation measures in extending the fatigue life of traffic signal structures; and (ii) identify regions where such structures are fatigue prone and where fatigue mitigation measures should be taken. Resulting from experimental work done, further insight into excitation mechanisms is gained. A fatigue mitigation procedure will be developed and validated for use not only for steel traffic signal structures, but also on a wide variety of lightweight, tubular steel structures used beyond transportation infrastructure. A fatigue assessment methodology is extended to: (i) rapidly assess the statistical risk of fatigue failure based on local wind parameters; and (ii) evaluate the performance/effectiveness of fatigue mitigation measures.

1.6 Dissertation Organization

This dissertation is divided into 10 sections. Following this introductory section, Section 2 presents a literature review which first covers the natural wind excitation of cantilevered traffic signal structures. Next, general fatigue considerations are discussed, followed by an in-depth review of past work on tube-to-transverse base plate connection fatigue. Past wind-induced fatigue mitigation strategies are reviewed, leading to a

discussion about DAD and its application in earthquake engineering. Finally, past probabilistic risk assessment techniques developed to quantify wind-induced fatigue damage are reviewed alongside another used in the assessment of financial risk related to natural hazards.

Section 3 commences the new work in this dissertation where the natural wind response of a full-scale prototype traffic signal structure is studied. In Section 3, the instrumented prototype traffic signal structure is described along with observed fatigue-inducing stress range results. The nature of dynamic wind-induced response variability is identified and quantified in terms of the central tendency and dispersion parameters. To further investigate the role of across-wind effects, the dynamic response results are compared without and with the installation of helical strakes to the mast arm. Findings/trends are compared against the results of past research.

Section 4 presents the development of a target-less computer vision technique to measure/monitor traffic signal structure displacements and modal parameters. Details pertaining to the experiments and program development are given. The validity of MQD-based computer vision is analyzed for structural displacement measurements and stress inference (when used in conjunction with an analytical model). With video from a consumer-grade camcorder, the methods is applied to determine the dynamics properties of the prototype structure, including mode shapes. Stresses inferred from wind-induced, ambient vibration monitoring are compared against those obtained from strain gage readings.

Section 5 presents a study conducted to assess the effectiveness of mast arm strake installation as a fatigue mitigation measure. Experimental results without and with low-cost helical strakes are summarized and presented. A fatigue damage analysis framework is introduced that is based on an industry-accepted, code-based technique. To quantify the potential benefit of arm strake installation, the fatigue life of the prototype structure is then estimated considering any changes in natural wind response for several distinct wind environments.

In Section 6, a four-step methodology previously outlined in Mander et al. (2012) for probabilistic loss modeling for seismically damage structures is extended to estimate the fatigue life of lightweight, wind-excited steel structures. The approach relates: (a) the recurrence of wind speeds (hazard analysis); (b) the cyclic stress response amplitudes due to varying wind speeds (structural response); (c) cyclic stress response; and (d) fatigue damage accumulation at a given detail. Natural wind response of a representative structure is characterized in a similar manner as in Section 3, while connection fatigue capacity is described using results of past fatigue testing programs. The proposed probabilistic framework is successfully demonstrated to calculate accumulated wind-induced fatigue damage, then fatigue life, following comparison with field observations.

Section 7 presents the as-tested, low-cost PT DAD solution for steel traffic support structures to: (i) provide alternative load path redundancy (fail-safe mechanism); and (ii) alleviate wind-induced fatigue. To justify the merit of the PT system, the effect of tensile mean stresses on tube-to-transverse base plate connection's fatigue resistance is investigated. Then, prototype testing is detailed that uses the full-scale structure in various

phases to investigate the effect that PT installation has on natural wind response. To quantify the benefit of the PT DAD, dependable service live is determined for the prototype structure using the industry-accepted technique from Section 5 using experimental observations and a mean stress-dependent nominal stress-life relationship model. Comparative evaluations of fatigue performance are made for two contrasting wind environments to assess the efficacy of PT mitigation and to identify any caveats related to the implementation of the proposed DAD technique.

Section 8 presents a modified, more implementation-ready version of the PT DAD solution for steel traffic support structures. Its advantages are discussed and quantified using the four-step probabilistic framework introduced in Section 6. To serve as input and statistically describe structural response, results of the monitoring program in Section 7 are presented and characterized statistically as in Section 3. Results from past fatigue testing programs are used to describe and characterize mean stress-dependent fatigue capacity. Using the developed framework, the effectiveness of the PT DAD concept is evaluated as if installed in several distinct wind environments, taking into account: (i) a fully PT structure relieving the largest expected dead load; and (ii) change/no change in observed natural wind response.

Section 9 presents work done to explore the ramifications of using simplified connection fatigue models during probabilistic assessments in Sections 6 and 8. A fracture mechanics-based, total life (initiation-propagation) model is developed to create fatigue strength curves for tube-to-transverse base plate connections common to traffic signal structures. Developed relationships are verified against experimental test results.

Following detailed refinement, the model is used to demonstrate/justify the detrimental effect mean stress has on tube-to-transverse base plate fatigue resistance. Using fatigue strength curves derived from total life analyses, probabilistic analyses are repeated to quantify the ramifications of using simplified damage models during probabilistic assessment. In closing, a parameter sensitivity analysis is conducted.

Finally, Section 10 presents a summary of the dual experimental and analytical program and the key findings from this study. Major conclusions from each section are presented, and recommendations for future work are made.

2 LITERATURE REVIEW OF PREVIOUS WORK

This section presents an overview of topics and past studies pertaining to the conducted research. To begin, the natural wind excitation of cantilevered traffic signal structures is covered from a description of the physical mechanisms to a review of specific works conducted. Next, general fatigue considerations are discussed, followed by a review of past works on tube-to-transverse base plate connections and related components. Previous works on fatigue mitigation are then be reviewed, starting with methods to reduce demand by reducing mast arm vibrations, then moving to approaches to improve the fatigue capacity of the structure-specific components. Following, the concept of DAD will be introduced and reviewed. Finally, several proposed wind-induced fatigue risk assessment techniques will be reviewed alongside another previously used in the financial risk assessment of structures subject to natural hazards.

2.1 Vibration of Cantilevered Traffic Signal Structures

In this section, the mechanisms that induce traffic signal structure vibrations are first introduced and explained. Following, past works on mechanism identification and demand quantification are summarized as appropriate for the research conducted herein.

2.1.1 Excitation Mechanisms

Kaczinski et al. (1998) identified multiple excitation mechanisms as responsible for wind-induced vibration; they are galloping, vortex shedding, natural wind gust, and traffic induced gust. Galloping is a form of aerodynamic instability caused by negative

aerodynamic damping that results in large amplitude vibrations perpendicular to the mean wind direction (across-wind) due to periodic changes in lift forces due to the oscillation of a body in a constant flow regime. Vortex shedding, like galloping, leads to vibrations perpendicular to the approaching wind. The vortex shedding mechanism occurs due to variations in pressure on the leeward side of a bluff body caused by the periodic detachment of low-pressure vortices from alternating sides of the body subjected to a flow regime, thus resulting in structural vibration. Traffic induced gusts are loads due to vehicle turbulence that lead to vibration of traffic support structures produced by trucks passing beneath or beside the structure. It has been determined that for traffic signal structures, vibrations from traffic induced gusts are not a significant contributor to fatigue failure (Chen et al. 2001; Albert et al. 2007). Vibration due to natural wind gust also occurs due to turbulence (Patel and Freathy 1984); however, in this case it is initiated by changing wind speed and direction, which changes randomly with time. Because gusts are related to turbulence, the resulting motions can be two-dimensional, these motions are also known as buffeting. In lightweight structures with little damping, the response is variable and random, just as are natural wind gusts. Unlike the other types of response in natural winds (galloping and vortex shedding), the response due to natural wind gusts are considered largest along-wind.

2.1.2 Excitation Mechanism Identification and Fatigue Demand

Pulipaka et al. (1995) observed that cantilevered traffic signal structures used by the Texas Department of Transportation (TxDOT) can often exhibit large amplitude, across-wind vibrations at wind speeds near 4.5 m/s. McDonald et al. (1995) conducted

water-table, tow-tank, and wind tunnel experiments, but their work also included field testing. Reflecting regional preferences, the signal clusters were horizontally oriented in all tests. Resulting from their water-table and tow-tank experiments, they concluded that vortex shedding was unlikely the cause of the large amplitude vibration of traffic signal structures. During tow-tank experiments, through the relation to vertical forces, force coefficient as a function of angle of attack was found. It was determined that signal clusters, based on their orientation with respect to the horizontal arm, could be susceptible to galloping. As a result, it was concluded that galloping, not vortex shedding, occurred when wind approached from the backside of the signals when the signals were configured to hang below the mast arm.

Kaczinski et al. (1998) conducted research in response to deadly collapses of traffic signals structures in Michigan (Ocel et al. 2006). Their study encompassed traffic signal support structures, but also other types of sign and signal supports; the conducted research resulted in the fatigue design section in the AASHTO specifications (2001). From literature review, they identified galloping, vortex shedding, natural wind gusts and truck-induced gusts as potential fatigue inducing excitation mechanisms. Similar wind tunnel testing as done by McDonald et al. (1995) was conducted with scaled structures with vertically hung signal clusters. Only one, non-repeatable instance of galloping-like behavior was observed; no vortex shedding vibrations were observed. Based on the literature and their wind tunnel testing, finite element models were used to estimate the magnitude of equivalent static fatigue loads based on each of the four identified excitations for multiple types of traffic support structures. One finding of their multi-faceted work

was that passing trucks caused in-plane arm displacements larger than out-of-plane arm displacements. Because researchers concluded vortex shedding was not responsible for vibrations on cantilevered traffic signal structures, no equivalent static load was specified to account for vortex shedding during fatigue design.

Gray et al. (1999) conducted research following a significant number of traffic signal structure failures in the state of Wyoming. They reported that fatigue cracking occurred at the weld connecting the mast arm to its base plate. By analysis, it was suggested that out-of-plane bending may have a larger role in fatigue cracking than in-plane bending. They found that out-of-plane vibrations result in larger stress ranges than those caused by in-plane vibrations.

Hartnagel and Barker (1999) and Chen et al. (2001, 2002, 2003) conducted research in Missouri after the state had over 12 cantilevered traffic signal structures fail at the arm-mast connection. Hartnagel and Barker (1999) instrumented full-scale structures to study the effects of truck-induced gusts on cantilevered traffic signals. Resulting from their analysis, the gusting caused by passing trucks caused much greater out-of-plane stresses than in-plane, contradicting the findings and recommendations made by Kaczinski et al. (1998). Chen et al. (2001) reported that overstressing, poor fatigue strength and poor weld quality all played a role in the large number of structure failures in Missouri. Two in-service traffic signals were instrumented with strain gages near the base and midspan of both arms to monitor vibrations due to truck-induced and natural wind gusts. To measure the speed of wind gusts, an anemometer was used. Based on their results, it was concluded that the stresses caused by in-plane vibrations were less than one-third of the

stresses caused by the out-of-plane vibrations associated with natural wind gusts. In a later examination of multiple failed arm-base plate specimens, it was found that the cracks on nearly all the failed welded connections initiated at the top of the arms, which would be associated to in-plane vibrations (Chen et al. 2002). Due to the large variability in the age of failed structures, it was concluded that fatigue failures were due to poor weld quality (Chen et al. 2002, 2003).

Dexter and Ricker (2002) continued and expanded on the work done by Kaczinski et al. (1998) on steel cantilever signal, sign and light supporting structures. Their focus was primarily on loads resulting from wind effects on variable-message sign structures, mitigating galloping effects, identifying structures susceptible to galloping and the development of design importance factors. Included in this work is a guide for the design, installation, and inspection and maintenance of cantilevered traffic support structures, where the inspection interval was suggested to be every four years.

Florea et al. (2007) and Albert et al. (2007) conducted studies on the fatigue demand on cantilevered traffic signal structures, including full-scale experiments to study the loading effects of galloping and truck-induced gusts. Florea et al. (2007) instrumented and monitored three signal structures for a total of 9 months to aid in determining the magnitude of galloping forces experienced. Although large amplitude displacements were measured, sustained galloping was never observed. In addition, an analytical model was used in a parametric study for predicting the propensity of galloping for structures with various properties. The model suggested that modifying the aerodynamic properties of the sign and signal attachments may be the most effective way to handle galloping. Albert et

al. (2007) conducted testing of cantilevered traffic signal structures to verify the design recommendations in the 2001 AASHTO specifications. Two cantilevered structures were monitored in the field to determine the effects of truck-induced loads. Over 400 truck passing events were observed, but fewer than 5 percent produced a detectable effect. It was found that passing trucks caused a larger out-of-plane response than in-plane response, agreeing with Missouri researchers and contradicting the AASHTO specifications (2001). Observations made it clear that natural wind gusts produce larger responses in cantilevered traffic signal structures than truck-induced gusts.

Letchford et al. (2008), and later Cruzado et al. 2013, aimed to: (i) determine the mechanisms that lead to mast arm vibrations and determine the size of their role in fatigue failure; (ii) provide a method for estimating the fatigue life; and (iii) provide guidelines to performing life-cycle cost analysis for cantilevered traffic signal structures. Both wind tunnel and full-scale testing were used to accomplish the first objective. As a result of field monitoring the vibrations due to natural winds, and the properties of the natural winds themselves, it was stated that, "having large vibrations at a certain wind speed and direction ranges reflect the typical behavior of vibrations induced by vortex shedding." This finding contradicted previous works that accepted that galloping, not vortex shedding, caused the significant vibrations that lead to fatigue failure. From field testing, it was seen that higher amplitude vertical vibrations occur when backplates are installed on the signal clusters and most often when the wind is between 2.2 m/s to 6.7 m/s and approaching from the backside of the signal clusters. Regardless of the low number of observed large amplitude vibration cases, vibrations collected one day during testing

indicated vortex shedding. Wind tunnel experiments on a scaled specimen were carried out to investigate the vibration behavior under several combinations of wind speed and direction. As a result of identifying vortex shedding as an excitation mechanism, both galloping and vortex shedding were later accounted for in the fatigue provisions of the 2009 Standard Specifications (AASHTO 2009). Subsequently, the latest specifications (AADSHTO 2013) no longer directly take vortex shedding-induced response into direct consideration during fatigue design of cantilevered TSS.

Zou and Letchford (2010), in a parallel, and later subsequent study, continuously monitored an installed traffic signal structure. During the final stage of the study, the signals were removed from the structure and the vibrations of the bare cantilever arms were monitored. Structural vibrations with the signals attached were closely related to the vibrations occurring without the signals. Thus, it was concluded that the wind-induced vibrations were due to the aerodynamic instability of the tapered cantilever cylinders. By comparing the vibrations with and without traffic signal clusters, it was suggested that the observed vibrations were a result of vortex shedding. It was also mentioned that traffic signal supporting structures with larger diameter arms were more susceptible to such wind excitations.

2.2 Fatigue Considerations

Fatigue is well described as an accumulation of damage from repeated cycling in a structure of component from fluctuating loads or vibration (Ocel 2006). Damage becomes visible in the form of crack formation (initiation, nucleation, etc.), then propagation. Crack propagation often can result in component failure in the form of ductile

rupture or brittle fracture. There are several approaches used to determine component fatigue resistance and remaining life. Each incorporate classifying component fatigue-proneness and loading. These methods vary from straightforward design to more complicated, time-intensive analyses.

2.2.1 Fatigue Design Approaches

There are three common means to determine the fatigue resistance of structural components for design and life assessment. Each of which can be classified by the level of refinement necessary to determine the amplitude of fluctuating stresses at a connection of interest.

The first approach utilizes the nominal stress at the region of interest. Nominal stress is the uniform stress away from any geometric discontinuity that can be determined using simple solid mechanics formulas. Stress intensifies when nearing an attachment due to two separate causes; each source of stress concentration requires an additional degree of refinement in analysis. Second, geometrical discontinuities produce elevated stress levels from the nominal. Geometric stress concentration ratios have been studied both experimentally and through the use of finite element modeling. Finally, further stress concentration results due to the local discontinuities present. For welded connections, the local geometry of the weld toe is referred to as the notch stress, which depends not only component detailing, but also random parameters that describe local notch properties that are not commonly quantified by analyses.

Nominal Stress Approach

The nominal stress approach is the simplest manner to determine the fatigue resistance of a detail and is the recommended AASHTO design approach. The stress range determined in this approach is based on the nominal stress near a welded attachment or joint using simple mechanics of materials relationships and equations.

Fatigue life using fatigue strength (S-N) curves based on constant amplitude stress range fatigue tests is typically defined (Keating and Fisher 1986) in the form

$$N_f = A\left(S_r\right)^{-3} \tag{2-1}$$

where $A =$ the double amplitude (peak to trough) stress range amplitude and $S_r =$ the AASHTO fatigue category coefficient. Utilizing that form of the equation, Frank (1980) and Keating and Fisher (1986) have made recommendations for calibrating A for welded steel structures, where six categories exist, A to E and E' where higher letter categories represent an increasingly inferior fatigue life due to the type and geometry of welded details.

In most civil engineering design applications, service-life strains are kept within the elastic range, therefore Eq. (2-1) is a contraction of a more general Manson-Coffin strain-life equation (Manson 1953; Coffin 1954) which states

$$\varepsilon_{ar} = \underbrace{\frac{\sigma'_f}{E}\left(2N_f\right)^b}_{\textit{Elastic term}} + \underbrace{\varepsilon'_f\left(2N_f\right)^c}_{\textit{Plastic term}} \tag{2-2}$$

where $\varepsilon_{ar} =$ the amplitude of the fully reversed strain range; $\sigma'_f =$ the fatigue strength coefficient (approximately equal to the true fracture strength); $E =$ the modulus of

elasticity; $2N_f =$ the number of constant amplitude cycles that leads to the first observable fatigue crack; $b =$ the fatigue strength exponent; $\varepsilon'_f =$ the fatigue ductility coefficient (approximately equal to the true fracture ductility); and $c =$ the fatigue ductility exponent. The first part of Eq. (2-2) represents high-cycle fatigue where strains are elastic, while the second part is the low-cycle fatigue component where strains exceed yield.

Recommendations for AASHTO fatigue category coefficients are typically based on full-scale fatigue testing of unique detail geometries, where strain are measured away from the local effects of weld and connection geometry and stress is inferred. In the past, failure of tube-to-base plate connections has been categorized by several definitions. During full-scale testing, failure has been defined by a specified loss in capacity, a resulting change in applied stress range, or by the length of visually detected cracks. The development of a through-thickness crack is essentially ensured for all preceding failure definitions.

Test data is presented by relating stress range S_r (nominal) to the number of cycles to failure N_f. Because residual and notch stresses can be highly variable, there is considerable randomness in fatigue test results described using nominal stress ranges. AASHTO fatigue category coefficients are conservatively selected to represent the lower bound of the 95 percent confidence interval, equivalent to the 97.5 percent survival rate (exceedance probability).

As indicated previously, there are six design, or fatigue strength or stress-life (S-N), curves that are used during the design of welded details depending on the

connection geometry. Figure 2-1(a) depicts the AASHTO fatigue strength curves, and Table 2-1 provides the corresponding parameters from Eq. (2-1) alongside the stress range corresponding to a fatigue life of one million cycles $S_{r,m}$. Each S-N curve represents the lower bound for details with similar fatigue resistances, therefore are placed into the same category. The nominal stress approach includes the effect of detail geometry and local notch stress concentrations because they are derived from full-scale testing. As a result, the different detail categories reflect different levels of local stress concentration. Because common details may be suggested, detail geometry and local notch stress effects are not directly considered by the designer.

Each detail category has a constant-amplitude fatigue limit (CAFL), defined as the nominal stress range in which no fatigue damage is expected to occur under constant-amplitude loading. As a result, if design stress ranges no not exceed the CAFL for a given welded detail, no fatigue damage/failure is expected. Kaczinski et al. (1998) recommended an infinite-life approach for fatigue design. Infinite life design is a design approach that designers utilize that ensures if design stress ranges are below the CAFL, then no fatigue failure (or cracking) is expected to occur. Design stress ranges are related to loads not expected to exceed the 10^{-4} occurrence probability (Fisher et al. 1993). That is, if 10^{-4} or fewer of the stress ranges exceed the specified CAFL for a welded detail, an "infinite" life results (Kaczinski et al. 1998). Therefore, if over 1-in-10,000 nominal stress ranges exceed the CAFL, a more detailed analysis using Miner's (1945) linear damage rule can be used to determine fatigue life.

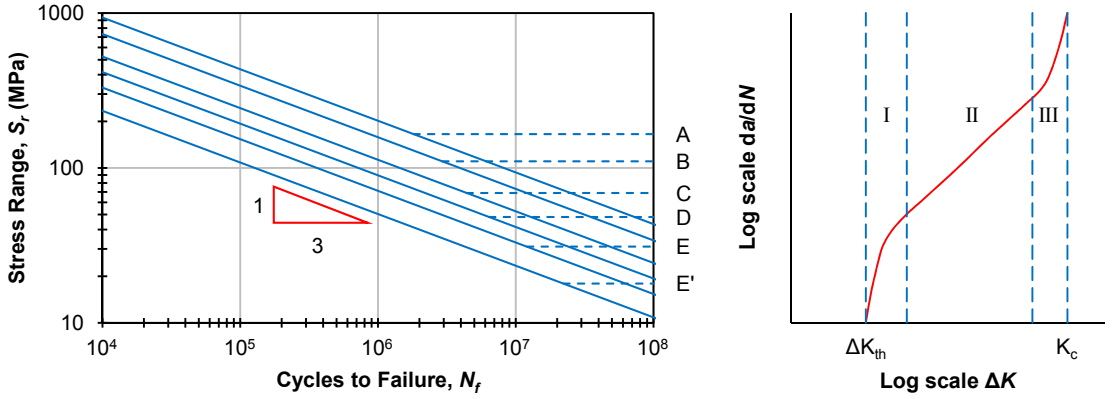

(a) AASHTO fatigue strength (S-N) curves based on nominal stress *(b) Crack growth rate curve*

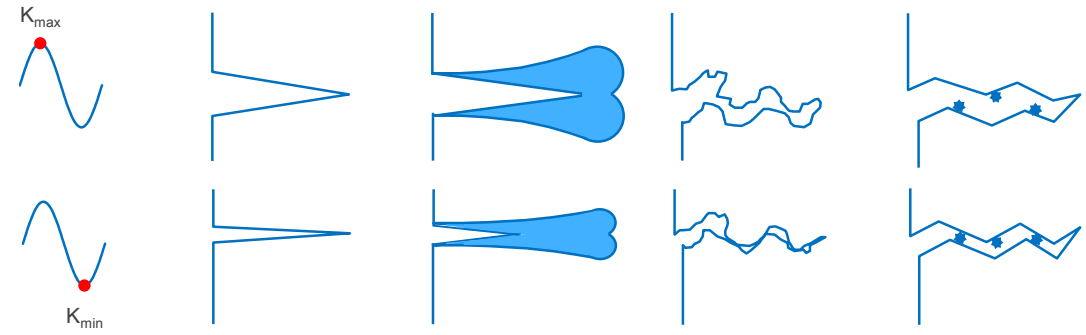

(c) Illustration of crack closure mechanisms

Figure 2-1. Related to fatigue design approaches.

Table 2-1. AASHTO nominal stress S-N curve parameters

AASHTO Category	Fatigue Constant, A ($\times 10^9$ MPa^3)	Constant Amplitude Fatigue Limit, CAFL (MPa)	$S_{r,m}$ (MPa)
A	8200	165.5	201.6
B	3930	110.3	157.9
C	1440	69.0	113.0
D	721	48.3	89.7
E	361	31.0	71.2
E'	128	17.9	50.4

The CAFL is convenient for use in design, however analysis of existing structures with a previously unknown loading history or structures having suffered overstressing require extension past the CAFL for fatigue analyses. Codes conservatively recommend a straight-line extension of the fatigue strength curve below the CAFL (Roy et al. 2011). There have been several recommendations as to what slope the straight-line extension should take, varying from -3 to -5 or more (Crudele and Yen 2006; Sonsino 2007; Yen et al. 2013). Although practical for design, the concept of CAFL or endurance limit is misleading as many design engineers assume "that a structural element will not fail as long as the so-called fatigue limit is not exceeded" (Sonsino 2007).

Hot-Spot Stress Approach

The hot-spot stress approach is quite similar to the nominal stress approach, however the S-N curves in this approach are based on geometric stress range, commonly referred to as "hot-spot" stress. During full-scale fatigue testing, strain is measured in locations expected to have the largest stress concentrations. Then, hot spot stresses are directly inferred from measured strains. As a result, the primary difference between the

nominal stress approach and the hot-spot stress approach is that geometric stress concentrations are now induced during stress analysis (demand side), not fatigue resistance (capacity side). As a result, there is need for a single S-N curve, eliminating the complexity from determining fatigue resistance. However, a more detailed analysis is necessary to include the geometrical effects on stress range, as design would include finite element analysis to determine the magnitude of hot-spot stresses. Notch effects are still considered on the fatigue capacity side through full-scale testing and curve fitting.

Fracture Mechanics Crack Growth Approach

The growth of fatigue cracks can be described using fracture mechanics principles, while the initiation (formation, or nucleation) of the fatigue crack is often determined using strain-life principles noted in Eq. (2-2). The growth rate of fatigue crack length a with respect to cycles N, da/dN, versus stress intensity factor range ΔK has been traditionally described by the three regions as indicated in Figure 2-1(b). Region I behavior is associated with threshold ΔK_{th} effects, where it is understood that intensities must exceed a given threshold to advance a fatigue crack.

The second stage of fatigue crack propagation, Region II, is approximated as linear and is accepted to follow the Paris equation (Paris and Erdogan 1963). The Paris equation relates crack length a and cycles N to stress intensity factor K by

$$\frac{da}{dN} = C\left(\Delta K\right)^m \tag{2-3}$$

where $da/dN =$ the crack growth rate, $C =$ material constant, $\Delta K =$ the stress intensity range, and $m =$ material constant approximately equal to 3.0 for most carbon steels. The

equation can then be solved to obtain crack length as a function of cycles or the number of cycles necessary to propagate a crack a given amount. The stress intensity factor range ΔK is a function of crack length, stress range and geometry such that

$$\Delta K = \alpha S_r \sqrt{\pi a} \tag{2-4}$$

where $\alpha =$ the stress correction factor; $S_r =$ the nominal stress range; and $a =$ the crack length. Specifically, the stress correction factor is given by

$$\alpha = F_c F_s F_w F_g \tag{2-5}$$

where $F_c =$ the crack shape correction factor; $F_s =$ the (front) free surface correction factor; $F_w =$ the finite width correction factor; and $F_g =$ the stress gradient correction factor associated with the non-uniform stresses due to detail geometry.

Solutions depend on loading condition and crack shape, however all require, and are sensitive to, initial crack (or defect) size. For design, this is not practical. Previous studies have found that assuming an initial crack depth and an elliptical crack front have correlated well against tube-to-base plate connections (Zettlemoyer and Fisher 1977; Fisher et al. 1983; Chen et al. 2003; Azzam 2006).

Finally, Region III denotes where rapid crack growth occurs. In most (practical) analysis situations, this region is ignored because it does not significantly affect the total propagation life, i.e. N_f, due to the limited number of cycles undergone prior to ductile rupture or brittle fracture (Bannantine et al. 1990).

2.2.2 Causes for Reduced Fatigue Life

Based on the preceding discussion on fatigue design approaches, there are several factors that affect fatigue life of a welded component, besides those effected by material properties.

Specimen Detailing

First, and most importantly, detailing affects the geometric stress concentration ratio, where base plate thickness and weld dimensions have the greatest influence. Further, local notch properties further add to the local stress concentration found at the notch tip of a component, unfortunately these are more difficult to quantify. AASHTO fatigue categories are assigned to connection details with similar total stress concentrations.

Magnitude of Loading

Applied stress reversal magnitudes obviously affect component fatigue life. Large stress reversals result in shorter fatigue lives where small stress ranges cause little fatigue damage, or no damage at all (depending on 10^{-4} stress range), if CAFL concepts are being considered. Per Eq. (2-1), component life determined using AASHTO guidelines relates to the cube of applied stress range, thus loading magnitude is highly influential.

Mean Stress Effects

AASHTO provisions are based on the nominal stress approach and do not consider mean stress levels as past research demonstrated that mean stress has little influence on fatigue resistance of specific welded structural components (Keating and Fisher 1986). However, as later detailed in this work, researchers have postulated and presented

evidence that mean stress levels may influence the fatigue resistance of tube-to-base plate connections (Koenigs et al. 2003; Ocel 2006). Theory states that elevated (or mean) stresses affect component fatigue performance, where fatigue crack initiation and propagation are each affected. Although it was suggested that the influence of mean stress is negligible for all welded structural components, AASHTO fatigue classifications for tube-to-base plate connections common to traffic signal structures are based on and validated using cyclic loads about an elevated mean to mimic dead load conditions (Miki et al. 1981; Alderson 1999; Koenigs et al. 2003; Ocel 2006; Roy et al. 2011). Simply put, connections typically exposed to high tensile mean stresses are tested at representative elevated stress levels, thus category assignments directly take mean stress effects into consideration.

Mean stresses have been observed to have a significant effect on the fatigue life of some components; this effect is primarily seen at longer lives (Bannantine et al. 1990). Tensile mean stresses have a negative impact on the fatigue life of a component, while compressive mean stresses are typically beneficial, however this behavior is material dependent. Although designers need not directly consider the detrimental effects that tensile mean stresses may have on a welded connection, it does not indicate the decreased fatigue resistance caused by tensile mean stresses. Thus, for cantilevered steel traffic supporting structures, where relatively large mean stresses are common, the fatigue life is influenced by mean stresses (Koenigs et al. 2003).

As example, several modifications to the Coffin-Manson strain-life equation have been proposed to account for mean stress effects (Morrow 1968; Manson and Halford

1981; Smith, Watson and Topper 1970; Walker 1970). Additionally, these modifications have been altered for improved correlation to a wider variety of metal alloys (Walker 1970; Ince and Glinka 2011).

In terms of fracture mechanics, the influence of mean stress can be related directly to the fatigue threshold, which is influenced by stress ratio $R = \sigma_{\min} / \sigma_{\max}$, the ratio of minimum and maximum stress (Bannantine et al. 1990). It has been shown that tensile mean stresses lower the fatigue threshold, the stress intensity range at which fatigue cracks form and begin to propagate (Region I). Crack growth rate da/dN is also influenced, where increased crack growth rates have been observed under tensile mean stresses. Typically, the influence of stress ratio has been observed to decrease as $R \to 0$. Although it is material independent, it is typically the case that growth rates related to $R = 0$ are similar to those occurring while $R < 0$.

Crack closure principles have been used to justify the influence of both stress ratio R (related to mean stress) and other environmental effects on fatigue threshold and growth rates (Elber 1971). Elber discussed that fatigue crack surfaces interfere with crack closure. The three most related to tube-to-base plate connections are: plasticity-induced, roughness-induced, and oxide-induced closures, shown in Figure 2-1(c). As shown, plastic strains occur as yield stress is exceeded at a crack tip. Therefore, as a crack propagates, plastically deformed material comprises both edges of the crack, however remains immersed in an elastic body. During unloading, the plastically deformed material causes a crack to close prior to complete unloading. Roughness- and oxide-induced closures both

pertain to crack surface debris leading to incomplete crack closure, albeit caused by two separate mechanisms.

If a specific value of stress intensity theoretically causes a crack to fully open and propagate a crack, then that value decreases due to incomplete crack closures. As a result, the effective stress intensity range $\Delta K_{eff} < \Delta K$. The effective stress intensity range has been used to account for stress ratio effects on crack growth. High stress ratios (high tensile mean stress) lead to incomplete crack closure, thus $\Delta K_{eff} \rightarrow \Delta K$, exposing the crack to greater stress intensity factor ranges.

2.3 Previous Work on Tube-to-Transverse Plate Connection Fatigue

Present is a wealth of previous work done my other researchers dedicated to studying the fatigue resistance of tube-to-transverse base plate connections common to traffic signal structures. The section introduces and summarizes the critical findings from the studies most pertinent to the study conducted herein. Results stemming from full-scale fatigue testing are presented.

2.3.1 Fatigue Resistance and Capacity

Miki et al. (1981) performed fatigue testing of steel tube-to-transverse plate connections. Figure 2-2(a) depicts the results for all specimens; run outs are not included. A total of 12, 255 mm diameter socket connection specimens were fabricated and tested. Six specimens were fabricated using A283 Grade D tube (thickness = 7.94 mm) attached to a 44.5 mm thick base plate using 45°, equal leg fillet welds. The remaining six specimens consisted to A595 Grade D tube steel (thickness = 6.07 mm) with unequal leg

fillet welds connecting the tube to the 44.5 mm thick base plates. Fisher et al. (1983) may be consulted for a schematic of the testing arrangement. Not common in current practice, the base plate of each mast arm specimen was welded to the box connection on the pole, so no bolts were used. This boundary condition could influence the fatigue resistance of the socket connection, where the additional fixity of the pipe-base plate connection is likely to restrain the detail and elevate the stress field in the pipe wall. The pole connection was bolted to the floor during testing. The specimens were cycled about an elevated mean stress, and failure was defined as a crack larger than 101.6 mm.

Alderson (1999) conducted five fatigue tests as part of a more detailed study. Figure 2-2(b) depicts the results for the four circular specimens tested. Five mast arm connections consisting of a 254 mm diameter, 4.55 mm thick tube were tested about a 96.5 MPa mean stress at a stress range of 55.2 MPa. Three specimens were manufactured by Valmont and labeled as "fatigue resistant", however performed similarly to other pole-to-transverse plate connections. The remaining two specimens were produced by other manufacturers, however one was a polygonal section that cracked prematurely (previously in service) and was excluded from the data set.

Kashar (1999) did not conduct physical, full-scale fatigue tests. Instead, a finite element study was conducted to determine the stresses present in a variable message sign structure that had failed and landed on a passing vehicle. The failed socket connection consisted of a 457.2 mm diameter, 12.7 mm thick, pipe attached to a 69.9 mm thick base plate by 12.7 mm fillet welds on both sides of the plate. Failure was attributed to high cycle fatigue and fracture of the fillet weld connecting the tube steel to the high cycle

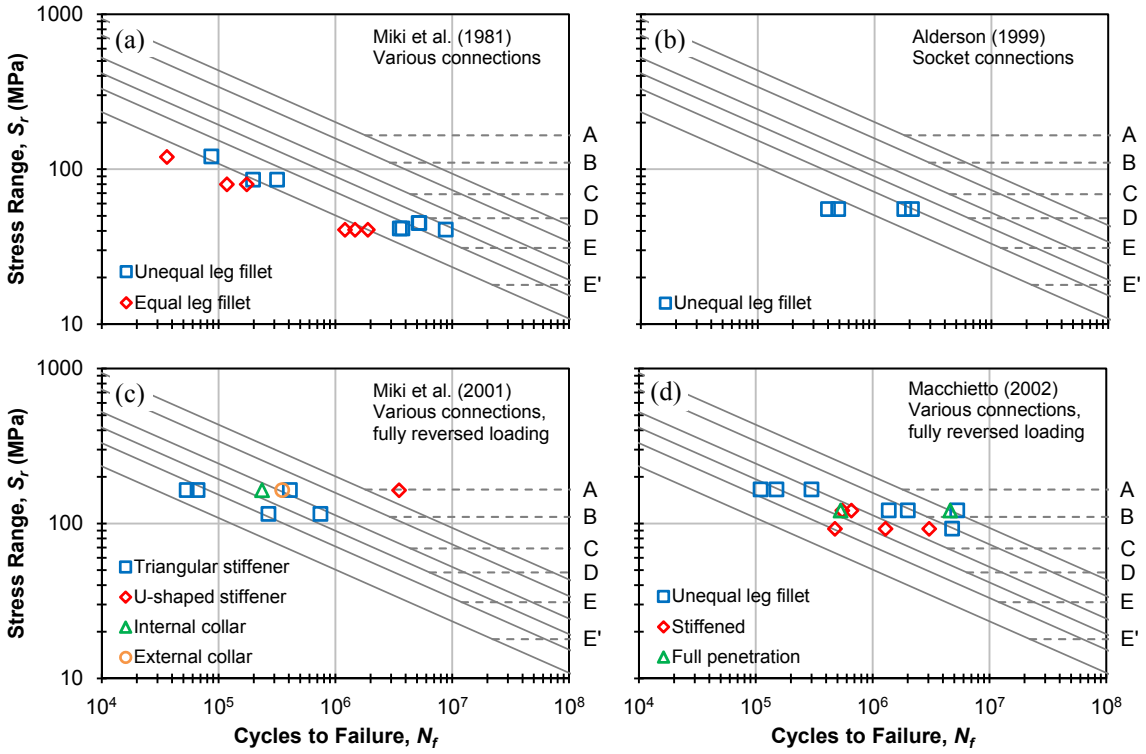

Figure 2-2. Fatigue test results from several past works for a variety of common tube-to-transverse base plate connection types.

fatigue and fracture of the fillet weld connecting the tube steel to the transverse base plate. Of primary importance, Kashar (1999) concluded that the stress concentration factor of the welded socket connection was between 4.5 and 6.0 and fillet weld size had little effect on local stress.

Miki et al. (2001) conducted multiple full-scale fatigue tests focusing on testing of stiffened socket connections using triangular, U-shaped, internal collar, and external collar stiffeners. Figure 2-2(c) presents the results of the fatigue testing by stiffener type. Specimens included in this study had tube diameters of 180 mm, with thicknesses of 4.5 mm or 6 mm. Results indicated a noteworthy improvement in fatigue life when a U-shaped stiffener was used. Fully reversed cyclic loading was applied to each specimen, therefore the mean load applied was zero. As a result, the fatigue capacity of the connections (and the effectiveness of the stiffeners) are believed to be inflated (Koenigs et al. 2003; Ocel 2006).

Macchietto (2002) of Valmont Industries conducted full-scale fatigue testing of their manufactured details to compare the performance of their connections against the 2001 AASHTO specifications (AASHTO 2001). Figure 2-2(d) presents the results of the fatigue testing conducted by Valmont Industries. The tested specimens tested consisted of three general details, all tube-to-transverse base plate connections: unequal leg, fillet-welded socket, stiffened fillet-welded socket, and full-penetration with fillet-welded backing ring. Here, it is inferred that the tube specimens were 254 mm diameter. The test set-up consisted of two mast arms, connected back-to-back, rotating to load the specimens. This configuration did not account for dead load, because the loading was fully reversed

($R = -1$). As a result, the fatigue capacity of the connections may be overstated (Koenigs et al. 2003; Ocel 2006). Here, it was shown that the unstiffened socket specimens demonstrated better performance than the stiffened specimens.

Koenigs et al. (2003) set to investigate whether mast arm-to-transverse base plate connections introduced in the 2001 AASHTO specifications should be classified as Category E' for fatigue. Results of the fatigue tests performed are presented in Figure 2-3(a,b,c). The research investigated a variety of connection details common to traffic signal tube-to-transverse base plate connections. Of the 59 full-size connection specimens fatigue tested, most were unstiffened, fillet-welded socket connections, while most of the remaining were gusset-stiffened socket connections. Few other details were included. Some details were galvanized, while others were not. All test specimens were comprised of a 254 mm diameter mast arm steel attached a 38.1 mm thick transverse base plate using unequal leg fillet welds, unless otherwise noted in this report. Two wall thicknesses were studied: 4.55 mm and 6.07 mm. The stiffened socket connections studied used three different gusset sizes, using two different arrangements. Other socket connections included: four internal and external collar details, along with a few specimens that underwent ultrasonic impact treatment. To best present the results from fatigue testing performed by Koenigs et al. (2003), additional plots are arranged by detail: unstiffened socket connections (Figure 2-3(a)), stiffened socket connections (Figure 2-3(b)), and other specimens of interest (Figure 2-3(c)).

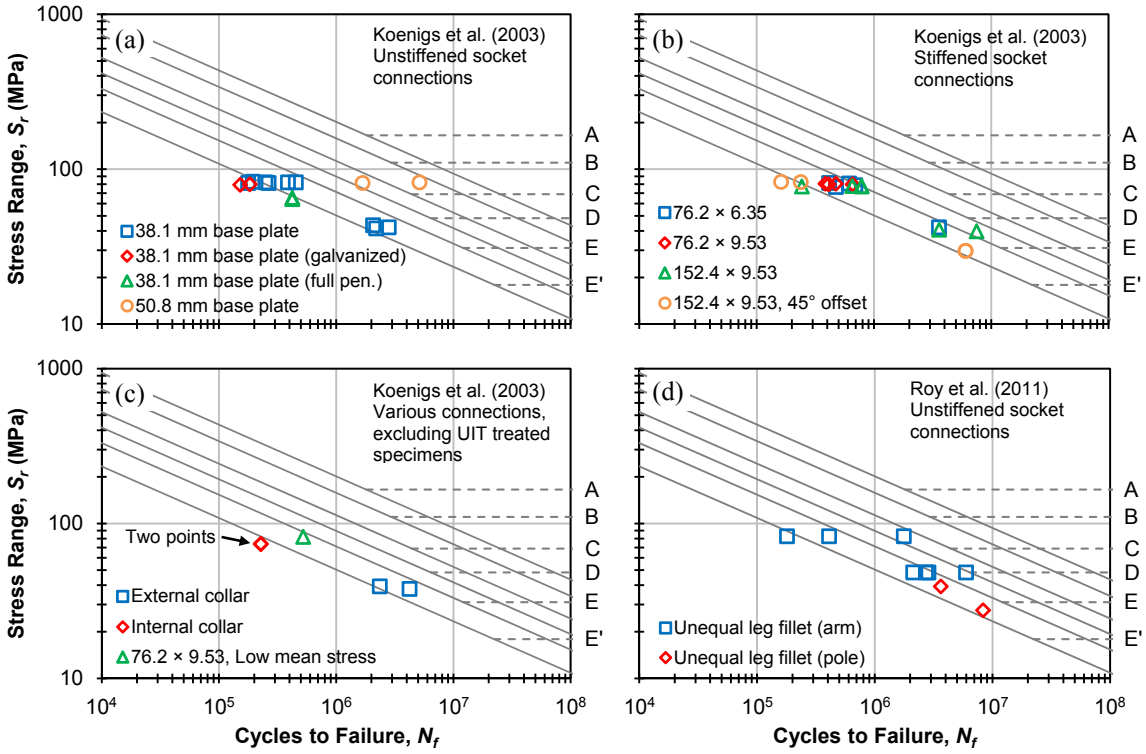

Figure 2-3. Additional fatigue test results from recent works for a variety of common tube-to-transverse base plate connections.

Testing conducted in Koenigs et al. (2003) took into account dead load stresses. As a result, fatigue testing was conducted about an elevated mean stress repetitive of expected dead load effects at a frequency of 3 Hz to 5 Hz. Specimen failure was defined by the first occurrence of three limits: (i) a 5 percent decrease in load required to meet minimum and maximum displacements; (ii) at least a 10 percent decrease in measured strain at near the connection specimen; or (iii) the detection of visible cracking. A failure crack was defined as "a crack that had propagated a significant distance around a socket weld connection, or had branched out into the pole [section] on a stiffened connection." Because there was not one single failure definition, an increased randomness associated with connection fatigue capacity may result.

Results in Koenigs et al. (2003) showed that specifications overestimated the fatigue capacity of stiffened connections. It also affirmed previous findings that resulted in unequal leg fillet welded socket connections being classified as an E' category detail. It was observed that galvanized socket connection specimens exhibited worse fatigue performance when compared to similar non-galvanized specimens, leading to later studies (Goyal et al. 2012). When all available test results (including those by other researchers) were plotted, the scatter was described as "overwhelming". This can be seen in Figure 2-4.

Upon review of Figure 2-4, one relationship was easily identified by the authors; the low mean stress tests (hollow markers) resulted in longer fatigue lives compared to results conducted at a high mean mimicking dead load stresses (filled markers). Koenigs et al. (2003) stated that "the mean stress influences the fatigue life of the specimen," adding that "it is apparent that the tests performed under low mean stress conditions

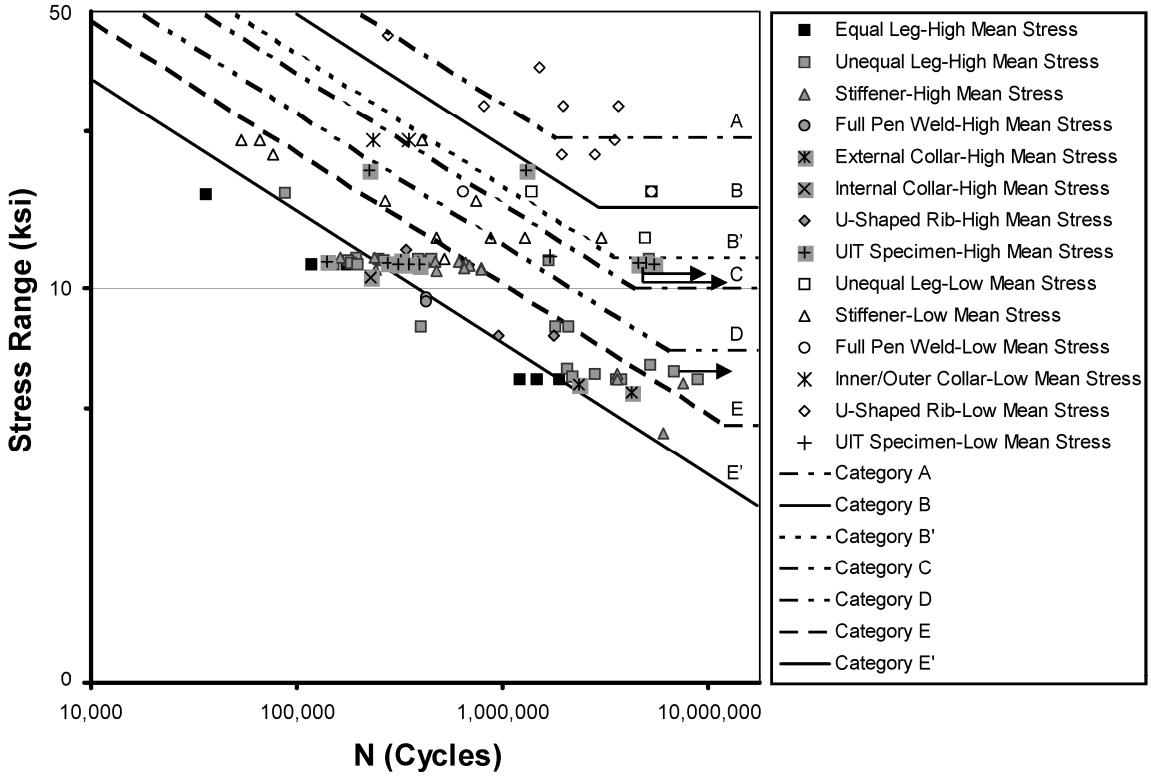

Figure 2-4. S-N plot of all available test results, including those performed by Koenigs et al. (2003) and others compiled from previous research (Koenigs et al. 2003).

produced longer fatigue lives." This work specifically acknowledges that mean stress effects may be significant in the fatigue resistance of tube-to-base plate connections, regardless of detailing.

Ocel (2006) tested the fatigue resistance of multiple Minnesota-specific connections in a laboratory as part of an in-depth fatigue investigation that included a detailed finite element study. In this work, eight pole and mast arm specimens were studied. The pole specimens consisted of eight-sided tube-to-transverse plate connections. Each specimen was made of A588 sheet steel with a thickness of 7.94 mm bent such that the corner-to-corner dimension was 355.6 mm. Base plates were 31.8 mm thick, reinforced with side plates. For each pole specimen, a mast arm specimen was paired. Two different socket connections were fabricated for the mast arm specimens: four were stiffened, fillet-welded socket connections, the other four used a full-penetration weld to connect the base plate. Mast arm specimens were made of A588 steel, 7.94 mm thick, with a corner-to-corner dimension of 294.6 mm. Because the specimens were not circular, the results of this work are not included herein. However, results showed that the eight-sided socket connections had a fatigue resistance around AASHTO Category K_2 (less that E'). Findings also suggested that doubling the base plate thickness for such connections would to attach a fatigue resistance as described by Category E'.

Other findings in Ocel (2006) were enlightening. It was noted that for some connections, the fatigue resistance was less than expected. An important conclusion from the resulting data was that there was not a single "all encompassing fatigue strength classification that works for all tube-to-transverse plate connections, whether they use

fillet-welded socket connection detailing, or full penetration welds." More experimental and analytical research into the fatigue of such connections was called for with a focus on a variety of connection geometries, including base plate thickness, tube diameter, tube thickness, tube shape and anchor rod size and placement. Ocel (2006) stated that there still remained great uncertainty in the fatigue classification of traffic structure connections by referencing Dexter and Ricker (2002). Agreeing with Koenigs et al. (2003), Ocel (2006) also noted that previously tested specimens loaded neglecting the presence of a dead load effects resulted in "artificially high" fatigue resistance.

Roy et al. (2011) documents the results of a comprehensive experimental and analytical study that evaluated the fatigue performance of various connection details common to highway sign, signal, and high-level luminaire support structures. The study demonstrated that tube-to-transverse base plate connections are most fatigue critical. In the study, several optimized tube-to-transverse base plate connection details were experimentally tested, namely: unstiffened, fillet-welded connections; unstiffened, full-penetration groove-welded connections; and stiffened, fillet-welded connections. Figure 2-3(d) presents the fatigue test results pertaining to the unstiffened fillet-welded tube-to-transverse base plate connections tested, run outs not included. Each specimen had a 254 mm tube diameter and a 50.8 mm base plate (optimized thickness). Results pertaining to full-penetration groove-welded and stiffened, fillet-welded connections are not presented as specimens with optimized geometrical properties were tested. Roy et al. (2010, 2012) concisely document the work related to groove-welded and stiffened, fillet-welded connections, respectively.

2.3.2 Summary of Observations

Past work done by multiple researchers has contributed to a pool of full-scale fatigue test results for a multitude of various types of tube-to-transverse base plate socket connections. Standard, unstiffened socket connections typically used for traffic signal structures are most commonly considered AASHTO Category E', although it is seen that several fatigue tests conducted show less resistance (tests performed at representative levels of high mean stress). Regardless, for the family of socket connections used for traffic signal supporting structures, whether unequal leg fillet-welded, equal leg fillet-welded, unstiffened, stiffened, collared or full penetration, it can been that there is considerable randomness in the fatigue resistance of these connections.

Various options have been studied to increase the fatigue resistance, from increasing the transverse plate thickness, to geometrically optimizing the dimensions of stiffeners. Despite the randomness in the data due to the multitude of connections tested, or the fatigue and fracture mechanism itself, one trend remains clear. Mean stress effects have been experimentally shown to affect the fatigue resistance of common tube-to-transverse base plate connections. Specimens tested under fully reversed loading exhibited greater lives than their counterparts tested under elevated mean stress levels, beyond what would have been expected by detail improvement/optimization alone.

Figure 2-5 presents a compilation of results of fatigue tests previously performed separated into four categories: tests performed under elevated levels of mean stress (separated into unstiffened, fillet-welded socket connections and all other socket connections), and those test performed under mean stresses that were little to none

(separated into unstiffened, fillet-welded socket connections and all other socket connections). It is clearly seen that the specimens tested without the presence of dead load effects (no elevated mean stress) require a greater applied stress range to achieve similar fatigue lives, indicating an increased fatigue capacity over tests performed under elevated levels of mean stress. From this, it can be seen that the magnitude of and scatter in fatigue resistance decreases in the presence of an imposed mean stress representative of dead load effects. Elevated (nominal) mean stress levels can be attributed to decreased fatigue capacity because it is reasonable that residual stress levels are similar between the connections.

2.4 Wind-Induced Fatigue Mitigation

Past works have set out to improve the fatigue life of cantilevered steel traffic signal support structures using two distinct methodologies. The first approach to be discussed is to improve fatigue life by reducing demand—that is, by mitigating mast arm vibrations. The second approach, to be discussed later, is to enhance or increase the fatigue capacity of the structure.

2.4.1 Past Demand Reduction Strategies

Pulipaka (1995) and Pulipaka et al. (1998) conducted an investigation where an aerodynamic device was developed to counteract the negative damping effects due to galloping. Wind tunnel testing of a scaled model allowed for the development of the aerodynamic damping device. Damping wings were tested and results were compared against each other as well as against results from the structure without the wing. Pulipaka

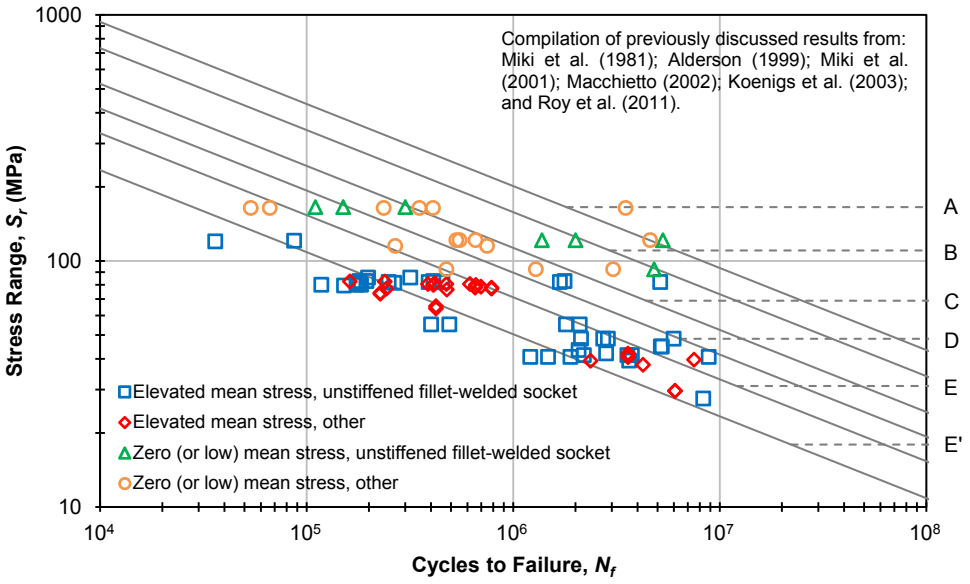

Figure 2-5. Compilation of full-scale fatigue test results indicating the detrimental effect of elevated tensile mean stresses on the fatigue performance of tube-to-transverse base plate connections.

(1995) conducted field tests on two full-scale cantilever traffic signals. As a result, a damping wing was recommended to mitigate large amplitude vibrations due to galloping (McDonald et al. 1995).

Hamilton et al. (2000) instrumented a long-arm signal structure (15.2 m) and determined its dynamic characteristics experimentally. They operated under the thought that galloping and gust-induced motions contribute to fatigue damage. Various damping strategies were investigated to help improve the fatigue performance of the structure. The free vibration response was used to determine the in- and out-of-plane damping of the structure with and without installed dampers. They tested dampers including elastomeric pads, impact dampers, tuned mass dampers and a strut with a built-in mechanical shock absorber. They concluded that combined systems showed the most promise: where elastomeric pads could be applied at the base to increase out-of-plane damping and struts to dampen in-plane vibrations. Although novel, the installation of elastomeric pads require lifting the structure off its foundation and the use of in-plane struts requires the mast pole of the structure to extend well past the arm-pole connection.

Cook et al. (2001) was also involved in the development of damping devices to attenuate vibrations in mast arm traffic signal structures. Over eight types of devices, including multiple versions of each type, were developed and tested. Following successful laboratory tests, selected devices were then tested in the field. The preferred damping device was described as a "spring/mass impact friction damper" and was found to be relatively insensitive to the natural frequency of typical mast arm structures. However, this recommended damper was nearly 1 m long. Because the damper was intended for

installation near the end of the mast arm, it will not work for all signal cluster orientations and arrangements.

Recently, a signal head vibration absorber that utilizes the mass of the signal cluster as part of a tuned mass damper has been developed (Christenson 2011; Christenson and Hoque 2011). For vertically hung signal heads, an internal spring and damper, was tuned to lessen mast arm vibrations. Although effective for a wide range of cantilevered signal structures, is effectiveness is optimized for a small range of structural masses and frequencies.

2.4.2 Past Strategies to Improve Fatigue Capacity

Koenigs et al. (2003) also tested the effectiveness of ultrasonic impact treatment (UIT) on the welds of several full-size connection specimens. To study the effect of the galvanizing process, specimens were subject to UIT before and after galvanizing. The technology had previously been shown to improve the fatigue life of plate girders for bridge applications; the benefits were primarily due to imposed compressive stresses and improved weld profiles. The samples were fatigue tested under two conditions, high and low mean stresses. Under what was defined as a "high mean stress", the UIT did not have the desired effect of improving the fatigue life. However, this high mean stress was intended to approximate the mean stress level at a typical connection due to the dead load from the mast arm and signal attachments. It was believed that the high mean stress was eliminating the imposed local residual compressive stresses resulting from UIT. To test this hypothesis, the remaining specimens were tested under a "low mean stress" (approximately 14 MPa). As a result, the UIT specimens showed a significant fatigue life

improvement when compared to non-treated specimens under the same level of mean stress. Although UIT was shown to be effective for socket connections at low levels of tensile mean stress, it was not proven effective for standard socket connections under typical tensile mean stresses due to dead loads.

Roy et al. (2011) was an extensive, well-rounded study that involved full-scale fatigue testing and a finite element study to conduct a parametric study to optimize tube-to-transverse base plate connections. In effort to improve the fatigue capacity of various connection types, several recommendation were made regarding the geometry of connections. It was found that increasing the plate thickness for fillet-welded tube-to-plate connections was the most cost-effective means to improve fatigue performance, mirroring the previous findings of Duraisamy (2005). To reduce the significant scatter observed in the performance of fillet-welded connections, it was recommended to tightly control weld geometry. Through geometrical optimization, findings suggested the full-penetration, groove-welded connections can provide a CAFL value common to AASHTO Category C, while optimized stiffened, fillet-welded connections can provide a CAFL value common to AASHTO Category D. Based on this research, recommendations were proposed for revision of the 2009 specifications (AASHTO 2009), maintaining infinite life design for new structures and introducing considerations for weld configuration, connection geometric parameters and cross sectional shape. These improvements were implemented in the 2013 AASHTO specifications (AASHTO 2013).

2.5 Damage Avoidance Design

Mander and Cheng (1997) started research on reinforced concrete base foundation connections in the mid 1990's by removing the damage-prone plastic hinge zone from bridge piers and replacing them with post-tensioned (PT) rocking connections. Removing the potential of damage from damage-prone regions, while providing other avenues for energy dissipation, lies at the core of damage avoidance design (DAD). Mander and his colleagues have continued to use this technique, and have developed damage-free solutions for wall-to-foundation connections for industrial buildings, and beam-column connections in concrete moment frame buildings (Mander 2003; Ajab et al. 2004; Rodgers et al. 2007; Li et al. 2008; Solberg et al. 2008a; Rodgers et al. 2008; Solberg et al. 2009; Hamid and Mander 2010; Rodgers et al. 2010, 2012a, 2012b).

In recent years, researchers have also been seeking ways to mitigate the potential for weld fractures in steel moment frame structures, especially during seismic events (Ricles et al. 2001; Christopoulos et al. 2002; Garlock et al. 2005; Rojas et al. 2005; Garlock et al. 2007; Kim and Christopoulos 2008; Christopoulos et al. 2008; Wolski et al. 2009; Lin et al. 2013). Dampers can be used along with PT prestress, thus reducing response demand and increasing capacity at the same time. Practically all above referenced works do this, by using either viscoelastic dampers or by designing plastic hinges where they may be easily repaired; again, these have been intended for seismic environments. Figure 2-6 shows an example of a damped PT self-centering steel moment resisting frame and its corresponding cyclic response. Clearly this is a case for a beneficial transfer of technology from a seismic environment to a wind environment.

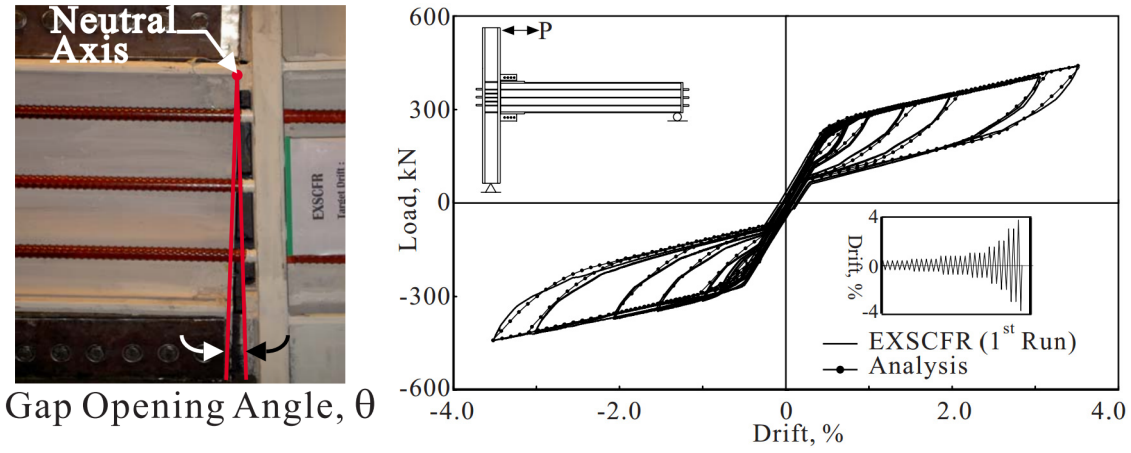

Figure 2-6. Damped post-tensioned self-centering moment resisting steel frame (left) and corresponding cyclic response (right) (Kim and Christopoulos, 2008).

2.6 Quantitative Risk Assessment Techniques

Patel and Freathy (1984) were some of the first to set out to develop a simplified method to quantify wind-induced fatigue damage. At the time, it was common practice to employ a stress-cycle counting algorithm to a constructed stress time history based on loads caused simulated wind environment based on a given wind spectrum. Miner's rule (1945) would then be used to sum accumulated damages suffered by the structure; thus, fatigue life was inferred. The simplified approach, as proposed by Patel and Freathy uses the same general procedure; however, each step is normalized. When deriving normalized damage curves for non-resonant and resonant responses, a denormalization factor was accumulated for each. Total damage was related to the summation of the products of the denormalizing factor and normalized damage incurred by the non-resonant and resonant responses, respectively. As a result, it is only necessary to compute denormalizing factors that are dependent on parameters found from wind data and structural analyses. The primary limitations of this method are associated with approximations made during formulation of the model, in particular: (i) linear fatigue strength relationships are used; (ii) resonance effects are accounted for by through the use of a modulation factor that may be unable to describe resonance for all structural systems; and (iii) extensive calculation is required.

Mander et al. (1992) and Shah (1993) describe work in the early 1990's for Erie County, NY, the owner of the now Ralph Wilson Stadium. During a routine inspection of their six, 46 m tall, stadium light poles, ultrasonic testing revealed the presence of fatigue crack "indications", but the size and magnitude of these cracks could not be ascertained.

The owner engaged researchers study of the cause, extent of fatigue cracking and recommend retrofit measures. An experimental field investigation and instrumented one particular pole using various instruments including an anemometer, strain gauges and accelerometers. Field observations of wind speed and direction were related to pole acceleration and anchor bolt strains. Mathematical models, based on well-known relationship between wind speed, response and bolt strains, were able to explain the results of testing. Based on the (i) fitted lognormal relationship from historical meteorological observations; (ii) fitted RMS response based on experimental observations; and (iii) anchor bolt fatigue classification, a damage density function (DDF) was formed relating mean hourly wind speed to damage. A cumulative damage density is derived by numerically integrating the DDF for each bolt of interest. With that, the 50th percentile wind speed ($V_{50\%}$) is determined; this is the wind speed at which 50 percent of the fatigue damage is accumulated at speeds greater and 50 percent at speeds lower. Also, an equivalent constant amplitude stress range is derived using the RMS response. Then, using the fit parameters for fatigue Category C, the natural frequency of the structure, and the calculated response, the bolt-life to first fatigue crack is assessed.

South (1994) conducted research to combine wind loading and vibration information, fatigue damage theory and experimental data. In doing so, he developed a simple fatigue analysis method for steel traffic support structures, referencing the lack of fatigue provisions in what were the current specifications. After collecting wind speeds for over a year, full-scale testing was performed on a cantilevered traffic signal structure. The structure was excited using a blower aimed at the front of the signal cluster mounted

at the tip of the arm. Although this loading is not seen in the field, observations were used for fatigue analysis. After blower testing, the structure was installed in a location where it could be excited by natural winds. Strain data was collected for four months, then histograms of stress ranges under ambient winds were formed. Wind speeds were not recorded during ambient tests. It was determined that fatigue life was controlled by out-of-plane response, then estimated using two very similar methods. The more robust method involved finding the vortex shedding frequency, drag forces, and then applied stresses at the detail of interest at each wind speed. Next, using a wind speed histogram, an estimate of the number of annual cycles at each wind speed was found. Finally, by creating a histogram of expected number of annual cycles per stress range and using a fatigue strength (S-N) curve, Miner's rule (1945) was implemented for a fatigue life estimation. To compare, South used the stress range histogram from the four months of full-scale measurements. Using this more direct methodology, he calculated a similar fatigue life.

Chen et al. (2001) recommended the following procedure to estimate the number of out-of-plane stress cycles at various levels due to natural wind gusts and to predict the fatigue life of an instrumented signal structure: (Step 1) determine the statistical distribution (lognormal) of the historical wind records in the vicinity of the structure, (Step 2) create a histogram of cycles at various stress levels (normalized by the square of corresponding wind gust speed) from the field test data, (Step 3) extrapolate the relationship in Step 2 for stresses at higher wind speeds, (Step 4) calculate the amount of annual cycles corresponding to different stress ranges by using the developed relationships

in Steps 1-3, (Step 5) find the number of cycles that the connection can endure before a fatigue failure occurs under constant-amplitude stress ranges corresponding to those in Step 4, and (Step 6) using Miner's rule (1945), divide the results of Step 4 by those of Step 5 and sum to calculate the predicted yearly damage, then inverse to obtain the fatigue life (in years) of the signal structure. Chen et al. (2001) concluded that the two studied structures were not expected to crack during their service life due to fatigue incurred due to natural wind gust effects.

Holmes (2002) developed closed-form expressions for upper and lower limits on the fatigue life of a structural element due to loadings as a result of along-wind response. The closed-form formulation considers narrow and broad band fatigue loadings separately. Starting with narrow banded vibrations, the number of stress cycles with specified amplitude is related to the probability density of wind speed. The number of stress cycles at the specified amplitudes is then related to damage fraction, where Miner's rule (1945) is used to sum over all response amplitudes. Assigning a normal probability density for narrow band peaks, total fractional damage can be written in terms of only wind probability density. For broad banded loadings, the damage fraction is assumed as a function of the narrow banded damage fraction. For wind direction independent fatigue life estimates, Holmes assumed a Weibull mean wind speed probability distribution into the formulation of narrow and broad band damage fractions. As a result, an upper and lower fatigue life is defined as the reciprocal of the broad and narrow banded damage fractions, respectively. In Robertson et al. (2004), this method was verified through the full scale testing of two tubular steel light poles with different foundations. The

experimentally determined damage fractions, as a function of wind speed, correlated very well to the upper and lower damage bounds when using the "shallower part" or the elastic portion of the bi-linear S-N curve associated with the connection of interest. Estimates of fatigue life were calculated based on the less exposed (actual) conditions, but also at a location that is prone to higher winds; the model predicted decreased upper and lower bound fatigue lives for the area that is more exposed to higher daily winds.

Robertson et al. (2001), prior to validating the Holmes (2002) model in Robertson et al. (2004), proposed their own method to determine the fatigue life of the two installed steel light poles. After monitoring the wind and structural response of the two structures, stress data was placed into 30 minute time histories, grouped by wind speed range. For each time series, Rainflow counting took place to determine the stress ranges undergone. Using a bi-linear S-N curve associated with the connection of interest, the damage fraction per unit time (hour) was determined for each wind speed range. This relationship was extrapolated for higher wind speeds. Using a Weibull probability distribution for hourly wind speeds, the estimated fatigue life is calculated by taking the reciprocal of the estimated year damage fraction (accumulated). The fatigue life of each pole studied was found to be less than 10 years.

Peil and Behrens (2002) also evaluated the fatigue of tubular steel light structures under wind loads. In particular, the study focused on the effect of handhole openings on the fatigue performance of the pole. Of importance to the proposed research, a methodology was proposed to determine the fatigue life of the studied structures. Consult the publication to view a flow chart related to the proposed method. For the first part of

the formulation (action), the distribution of the mean wind speeds are known. Next, the distribution is subdivided into six or more classes of wind speed. Here, "the contribution of a small number of high wind speeds to the damage accumulation is by far smaller than that of the enormous number of small and medium wind speeds." For the next portion (response), the mean response to the different wind speeds results from static analysis. The RMS of the response is determined using random vibration theory or another method, where modeled stress concentration factors and damping values are used. This is possible as the excitation mechanism is well understood for the circular sections studied. Because the dynamic response of lighting columns are classified as a narrow band process, the number of stress sign changes is directly associated with natural frequency and the peak stress distribution is described by the Rayleigh distribution. This allows a "stress collective" to be formed, where stress cycles are defined by their probability; lower levels of stress occur far more frequently than large stress fluctuations. Finally, fatigue life calculation (assessment) involves using a fitted S-N relationship and summing damage fractions using Miner's rule (1945). Uncertainties were considered in the fatigue life calculation in the form of partial safety factors.

Letchford et al. (2008) proposed a fatigue life prediction methodology for traffic signal support structures. The proposed methodology has similarities to the procedures presented by South (1994) and Chen et al. (2001); however, the method takes into account the effects of wind direction and estimates damage due to in-plane, not out-of-plane, vibrations. The estimate of fatigue life is based on local wind records and wind tunnel results. The proposed methodology is simplified into the following steps: (Step 1) using

wind records, create a matrix such that each element is the probability that the wind will blow at a certain speed and direction, (Step 2) using the matrix created in (Step 1) form another matrix corresponding to the number of vibrations experienced in a specific time period using the fundamental frequency of the structure, (Step 3) use wind tunnel results to form a similar matrix containing the standard deviation of the scaled vibrations at each combination of wind speed and direction, (Step 4) transform the matrix in (Step 3) to provide average peak-to-peak amplitudes of vertical vibrations in a full-scale structure, (Step 5) using the peak-to-peak displacement amplitudes in (Step 4) determine the stress ranges experienced in the connection of interest, (Step 6) using the S-N curve related to the connection of interest, replace the elements in the stress range matrix in (Step 5) with their corresponding points on the S-N curve, and (Step 7) using the matrix from (Step 2) describing the number of vibration cycles expected at each wind speed and direction combination and the matrix from (Step 6) describing the number of such cycles can be withstood before fatigue crack formation, divide each element in (Step 2) by its corresponding element in (Step 6) and sum. This sum equals the damage accumulated in the time interval related to the wind records. Due to the use of wind tunnel test results, a factor had to be used to account for differences between the full-scale and model behavior. Unfortunately, this factor was chosen to obtain a reasonable fatigue life estimate.

Repetto and Solari (2008) proposed a "complete" procedure for the wind-induced fatigue analysis of slender structures (most applicable to light poles) for general wind conditions. This model considers along and across-wind excitation, including vibrations due to vortex shedding. The authors worked to formulate and calibrate the general

procedure for determining the mean fatigue damage and mean fatigue life (Repetto and Solari 2001, 2002, 2004, 2006, 2007; Repetto 2005). In Repetto and Solari (2008), the incoming wind field is dealt with as a vector whose components are the mean wind velocity, elevated at a specific height above the ground, wind direction, and inverse of the Monin-Obukhov length (related to the turbulence intensity near the surface). A loading condition is characterized by a probability, linked to the location, site properties and thermal atmospheric stratification. The loading conditions (along- and cross-wind) are then modeled as a stochastic stationary Gaussian process separated into mean and fluctuating values. As a result, a stress resulting from this complicated loading may then also be modeled as a mean and fluctuating value. After mathematical manipulation, the variance and expected frequency of the wind-induced stress due to each combination of loading is determined. The damage induced by all the wind loading conditions is evaluated collecting the wind loading cycles into a discrete cycle histogram as specified in (Repetto 2005). Using Miner's rule (1945), the mean damage induced by each individual combination of wind conditions is determined. Using the loading condition probability for a given site (location, site conditions, etc.) the combination of damage fractions may be summed over the time frame described by the probability specified. The inverse of the summed damage fractions is the mean fatigue life. The model was then used to analyze the collapses of two real slender structures: a 10 m pole and a 30 m antenna tower. The comparison between the predicted and exhibited fatigue life confirmed the reliability of the proposed model. Although comparisons were favorable, this model requires an extensive amount of information describing the wind conditions, as an extensive amount

of calculations are made. This model also requires that the wind-structure interaction be well known, leading to accurate predictions for wind loading. The examples presented in the Repetto and Solari (2008) work are of circular poles; where wind-structure interaction has been well documented and understood. Finally, this procedure yields only the mean fatigue life estimate. Uncertainties in the model need to be taken into account.

2.7 Manders's Rapid Analysis Methods in Earthquake Engineering

A primary role of performance-based earthquake engineering is to predict the seismic performance of structures within a level of confidence at various levels of earthquake excitation. An engineer must be able to communicate risk in a way understood by stakeholders and managers. The Pacific Earthquake Engineering Research (PEER) Center developed a probability framework equation to be used to estimate a mean annual frequency of a decision variable. Deierlein et al. (2003) presented an early adaptation outlining the PEER framework known as the triple integral equation

$$P_a\left(DV\right) = \iiint G\left(DV \middle| DM\right) dG\left(DM \middle| EDP\right) dG\left(EDP \middle| IM\right) dP_a\left(IM\right) \qquad (2\text{-}6)$$

where $P_a =$ the annual probability of exceedance; $IM =$ the ground motion intensity measure; $EDP =$ an engineering demand parameter (deformations, accelerations, etc.); $DM =$ a damage measure (physical condition); $DV =$ a decision variable that translates DM into quantifiable risk management parameter(s); and $G\left(x \mid y\right) =$ conditional probabilities relating one quantity x to another y. This quantifies the rate of exceeding a level of ground motion; inter-relating ground motion to structural response, and structural response with damage; thus quantifying the likelihood of a decision variable given a

certain damage level. The triple integral equation can be broken into four steps: (Step 1) seismic hazard-recurrence assessment; (Step 2) deriving structural response (demand); (Step 3) estimating damage probability; and (Step 4) interpreting damage in terms of a decision variable (Dhakal and Mander 2006; Solberg et al. 2008b).

Dhakal and Mander (2006) added an additional dimension, time, to the PEER triple integral formula when using financial loss as the decision variable. By quantifying losses over time, the non-engineering community has better tools for decision making. As a result of considering an additional dimension (time), a fourth integral is necessary

$$EAL = \int \iiint L_r \, dP\left(L_r \middle| DM\right) dP\left(DM \middle| EDP\right) dP\left(EDP \middle| IM\right) dP_a\left(IM\right) \qquad (2\text{-}7)$$

where $EAL =$ the expected annual loss; and $L_r =$ the loss ratio (decision variable). Here the additional integral over the annual probability of exceedance sums probable losses annually, providing non-engineering decision makers an understanding of the annual cost related to damages due to regional seismic probability. Further, uncertainties related to each step in formulation may be inter-related and applied prior to integrating with respect of the annual frequency. To aid in describing the procedure involved in the development of the quadruple integral equation, a diagram is presented in Figure 2-7. To demonstrate the described process, Dhakal and Mander (2006) assessed the financial risk of a reinforced concrete highway bridge pier due to seismic hazard.

Mander et al. (2007) and Solberg et al. (2008b) expanded upon the implementation of this engineering loss model. To expedite the implementation of the method, numerical integration, along with the use of incremental dynamic analysis, was incorporated. Mander et al. (2007) used this model to study the financial risk associated to reinforced concrete

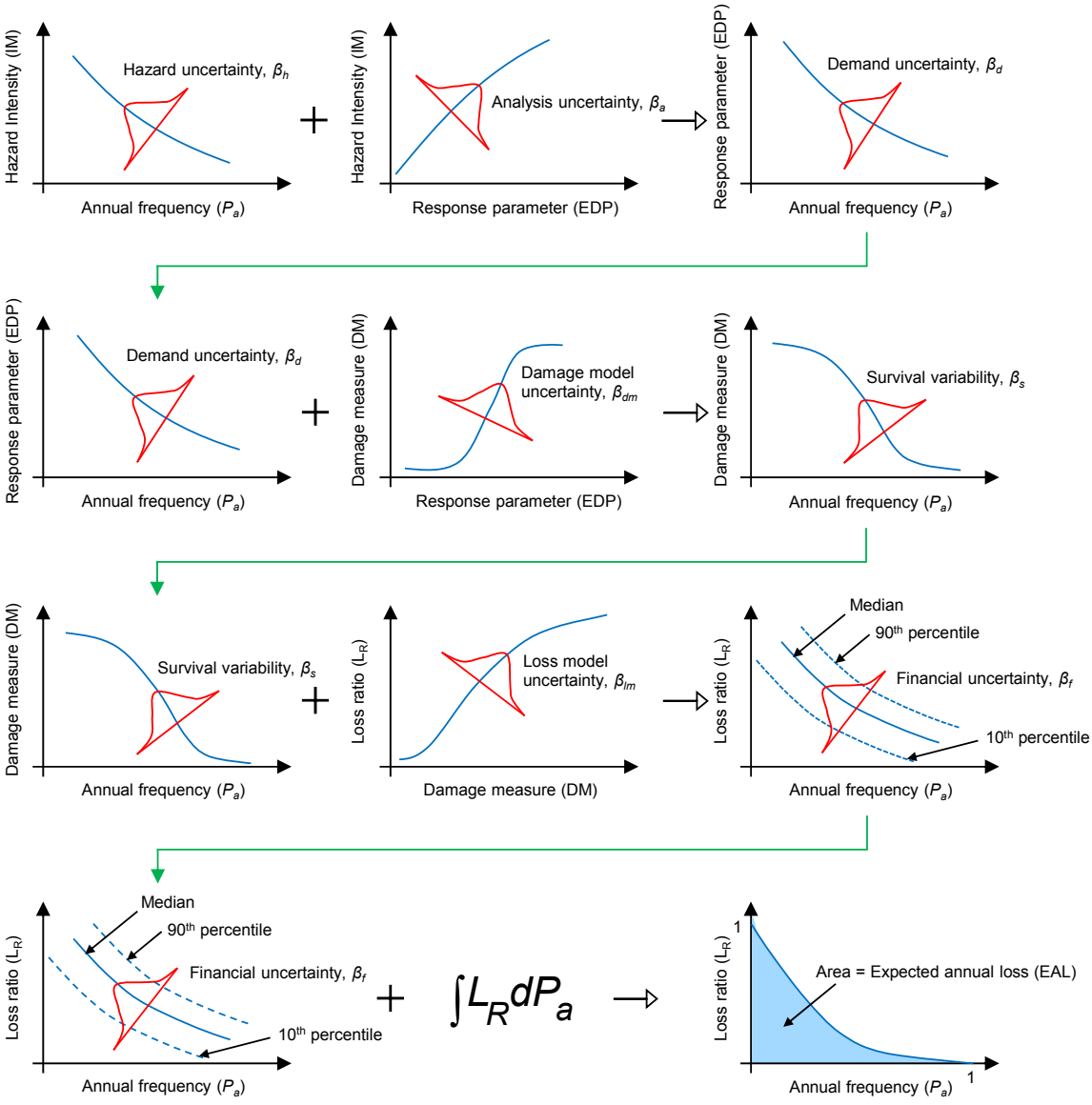

Figure 2-7. Depiction of concepts for the quadruple integral equation.

bridge piers designed three differing specifications. Most importantly, the expected annual loss (in dollars) was given for each pier design; allowing for a simple comparison of the financial risk related to each design type. Solberg et al. (2008b) did a similar study, however the case study involved two very different reinforced concrete bridge pier designs: a conventional ductile pier and the other designed according to the principles of DAD (Mander and Cheng 1997). Although both piers have a similar design basis, the DAD design resulted in an annual risk of only 16 percent of that of the ductile system. This large difference was attributed to the rocking concept as incorporated in the DAD pier.

Mander et al. (2012) introduced a rapid risk analysis framework using a four-step probabilistic engineering loss model. The intent of this new approach was to circumvent the quadruple integral when estimating financial losses related to seismically damaged structures. The work led to the development of a concise closed-form loss estimation framework relating hazard to response to damage and thus to losses without the need for extensive computations. This process included the linearization of models used in the quadruple integral, and a visualization scheme inter-relating the models used. The damage and loss models were calibrated for welded steel moment frame connections to assess the estimated annual loss relating to connections designed before (brittle) and after (ductile) the Northridge earthquake. The improved behavior of the ductile connections led to a large decrease in assumed financial risk.

The four-step approach of Mander et al. (2012) involves: (a) hazard analysis; (b) structural analysis; (c) damage and repair-cost analysis; and (d) loss estimation. As

shown in Figure 2-8, the primary objective of the direct four-step approach in computing financial loss is still to relate the estimated damage to seismic event severity and structural capacity measures. Figure 2-8 visually demonstrates how the four-steps, (a) to (d), are inter-related when plotted using log-log scales. The mathematical expression governing the four-step model, which represents the mutual relation between the four plots in Figure 2-8 is:

$$\frac{L_{i+1}}{L_i} = \left|\frac{\theta_{i+1}}{\theta_i}\right|^{c} = \left|\frac{IM_{i+1}}{IM_i}\right|^{bc} = \left|\frac{f_{i+1}}{f_i}\right|^{d} \tag{2-8}$$

where $L =$ the loss parameter; $\theta =$ interstory drift; $IM =$ intensity measure; $f =$ the annual frequency of an event. The parameters k, b, and c are exponents defined by the slopes of the curves in Figure 2-8 (a), Figure 2-8(b), and Figure 2-8(c), respectively, such that $d = bc/(-k)$.

To this point, median parameters or curves had been used to introduce the four-step loss approximation framework. However, the median curves are transformed to other fractiles (percent non-exceedance probabilities) during the probabilistic risk analysis (Mander et al. 2012). The uncertainties are quantified and allowed to propagate throughout calculations using a similar approach (Dhakal and Mander 2006; Mander et al. 2007; Solberg et al. 2008b; Mander and Sircar 2009; Mander et al. 2012). This formulation procedure is illustrated in Figure 2-9. Due to the multiplicative (power) nature of the loss model, the lognormal distribution was assumed as being an appropriate representation of variability. As a result, if the lognormal standard deviation β represents the dispersion of a variable y, then the relationship between the mean $\bar{y}$ and median $\tilde{y}$ is given by

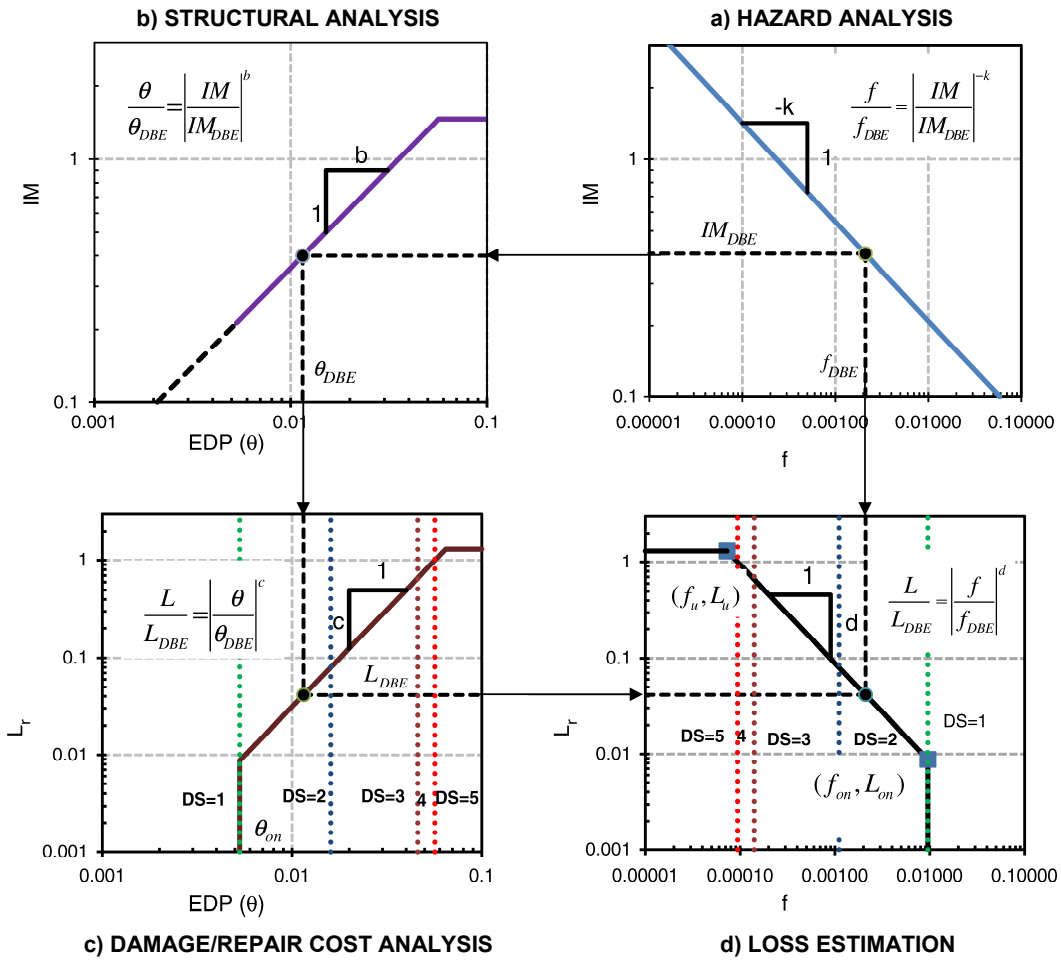

Figure 2-8. Illustration of the four-step approach to estimate annual losses including the: (a) hazard model, (b) structural response, (c) damage and repair cost analysis, and (d) loss estimation (Mander et al. 2012).

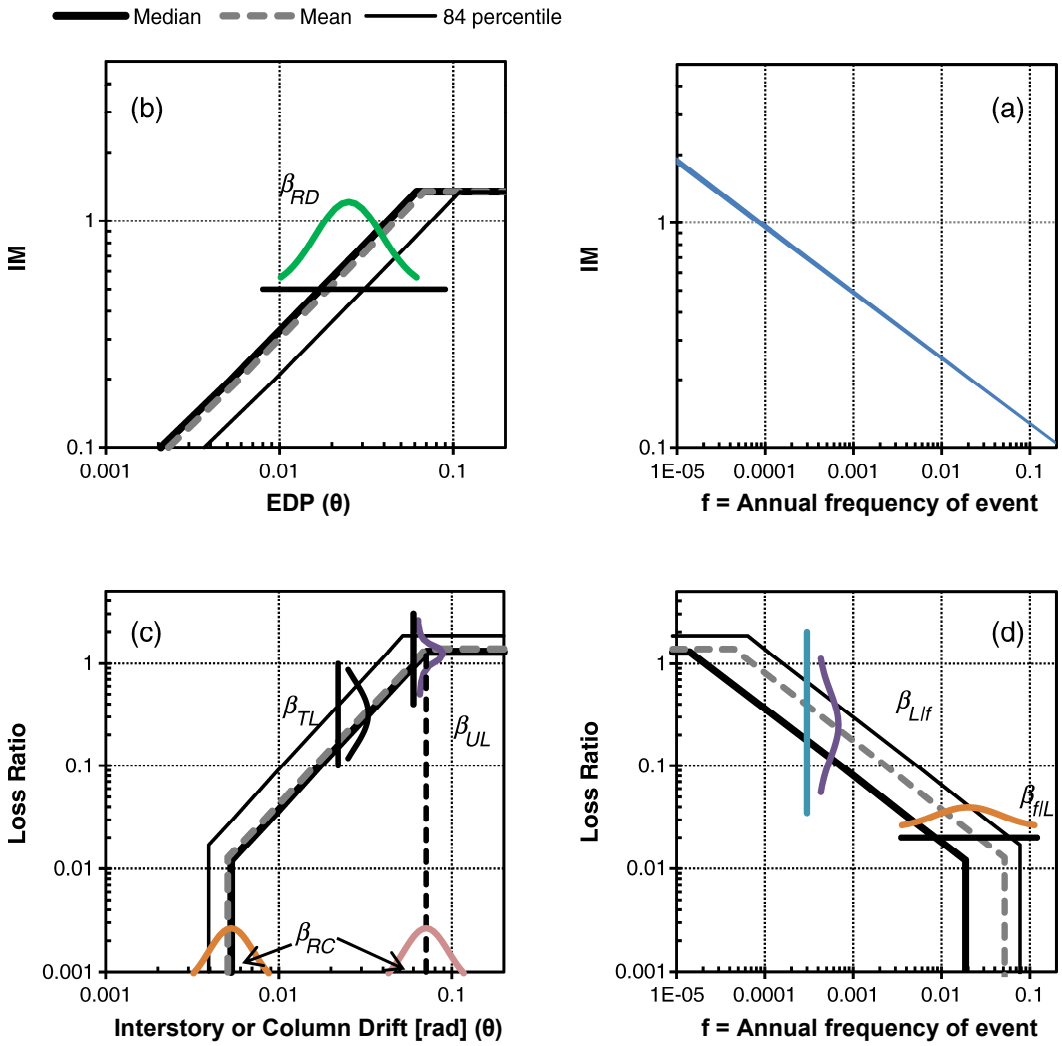

Figure 2-9. **Four-step approach summary after incorporating of uncertainties in the: (a) hazard model, (b) structural response, (c) damage and repair cost analysis, and (d) loss estimation (Mander et al. 2012).**

$$\bar{y} = \tilde{y}\ \exp\left(\frac{1}{2}\beta^2\right) \tag{2-9}$$

For other fractiles $z\%$,

$$y_{z\%} = \tilde{y}\ \exp\left(Z\beta\right) \tag{2-10}$$

where $Z =$ the standard normal variable of a Gaussian distribution with a mean (expected) value of zero and a standard deviation of one. The constructed curve in Figure 2-9(d) is powerful; the expected annual loss is calculated by determining the area beneath the expected loss curve. This probabilistic risk analysis methodology has the potential for application in other areas, including the present proposed research.

3 WIND-INDUCED TRAFFIC SIGNAL STRUCTURE RESPONSE: EXPERIMENTS AND REDUCTION VIA HELICAL ARM STRAKES*

3.1 Overview

Traffic signal structures are prone to fatigue failures due to a combination of along- and across-wind dynamic response. Stress reversal magnitudes with respect to wind speed and direction are experimentally investigated in a natural wind environment for a typical cantilevered mast arm traffic signal structure. Results show a prevalence of in-plane response induced stresses due to vortex shedding for wind speeds in the range of 4 m/s to 6 m/s. To better study the role of the tapered arm in the wind-induced response, the mast arm is retrofitted with helical strakes. Although the diameter of the mast arm is not directly related to the adverse stress reversals observed, arm strake installation significantly reduces the across-wind response attributed to vortex shedding. Results indicate that the slender mast arm section is critical in flow separation and vortex formation on the back side of the signal cluster backplates. As a result of the findings herein, properly designed helical arm strakes can be considered for reducing vibrations that can be attributed to vortex shedding, thus have the potential to reduce fatigue-induced damage in critical wind environments.

* This section is reprinted with permission from Wieghaus, K. T., Hurlebaus, S., Mander, J. B., and Fry, G. T. (2014a). "Wind-induced traffic signal structure response: Experiments and reduction via helical arm strakes." Engineering Structures, 76, 245-254. Copyright 2014 Elsevier Ltd.

3.2 Introduction

Traffic signal structures consisting of a horizontal steel arm and vertical tubular pole are commonly used to support traffic signals over roadways. Traffic signal clusters are attached either horizontally or vertically at various locations along the length of the mast arm. Such a traffic signal support structure may often exhibit large-amplitude wind-induced vibrations that over time can result in reduced service life of these structures.

Multiple mechanisms have been identified as responsible for the large-amplitude vibrations undergone by cantilevered traffic signal structures, but the cause of in-plane motion induced by across-wind effects remains under dispute. Based on past experimental findings, the mechanism behind observed large-amplitude vibrations had been identified as wind-induced galloping of the signal clusters (McDonald et al. 1995; Kaczinski et al. 1998). Galloping is a form of aerodynamic instability that leads to the large-amplitude vibration of long structures perpendicular to the mean wind direction. Initiated by small structural motions, the wind approach angle changes when flowing past a specific geometrical shape. When in a constant flow regime, periodic changes in lift and drag force magnitude results, leading to negative aerodynamic damping and large structural vibrations. As a result, fatigue design loads were specified to account for natural wind gust, truck-induced gusts, and galloping in the 2001 AASHTO specifications (AASHTO 2001).

To better understand the excitation mechanism, recent full-scale (Letchford et al. 2008) and wind tunnel (Cruzado et al. 2013) tests have found that vibrations with signals attached closely resembled vibrations due to vortex shedding, and related the vibrations

to the height of the attached signal clusters. Vortex shedding, like galloping, results in structural oscillations perpendicular to wind direction. Oscillations result due to the creation of vortices with alternating rotation on alternating sides of a bluff body as the wind flow around it. The vortices result in areas of alternating reduced pressure, resulting in alternating across-wind vibrations. Despite vortex shedding being reported as an excitation mechanism, vortex shedding remains unaccounted for in the fatigue provisions of the current AASHTO specifications (AASHTO 2013) for cantilevered traffic signal design. More recently, large-amplitude vibrations have been attributed to the aerodynamic instability of the cantilevered mast arm following other full-scale observations (Zuo and Letchford 2010). Regardless of the excitation source, whether galloping or vortex shedding, both produce across-wind effects.

There is a need to study excitation mechanisms using a new approach to verify previous findings and reach a consensus to improve fatigue design. Considerations must be made to take into account for structure specificity. After previous long-term monitoring programs, observations have been made as general trends; little attention has been paid to describing response in more detailed terms such as central tendency and uncertainty. Such concepts are utilized in reliability theory and modern design codes, and are a necessary requirement in developing comprehensive probabilistic fatigue damage assessments.

Various types of mitigation devices and measures, such as aerodynamic damper plates, have been developed based on the understanding that galloping is the primary excitation mechanism responsible for causing large-amplitude vibrations (Pulipaka et al. 1998). However, the effectiveness of this mitigation device has been limited, indicating

improper installation or a potential inadequacy in the current understanding of the problem. Others devices, such as impact (Cook et al. 2001), viscous (Hamilton et al. 2000; McManus et al. 2003), or integrated tuned-mass dampers (Christenson and Hoque 2011) have been developed to increase the inherent mechanical damping as an excitation-independent solution. Recently, to mitigate response due to signal cluster vortex shedding, visual backplates were removed from the signal cluster housing (Letchford et al. 2008; Cruzado et al. 2013), however this may hinder traffic light visibility. Unfortunately, most mitigation measures are either inefficient or impractical due to: (i) the large variability in the configuration of these structures or (ii) developed under the assumption that galloping is the major cause of damaging large-amplitude vibrations.

There are two main reasons to revisit conventional aerodynamic techniques for mitigation. First, Zuo and Letchford (2010) recently identified mast arm vortex shedding as a primary excitation mechanism for a traffic signal structure with a large-diameter mast arm. Second, wind tunnel tests (Cruzado et al. 2013) of a slender mast arm structure lead to findings that perhaps do not consider the importance of upstream interaction with the mast arm section, focusing on downwind visor interaction. Therefore, this section seeks to address four research questions: (i) Can the nature of the structural response due to the natural wind excitation be adequately represented statistically using a measure of central tendency and dispersion? (ii) Can previously identified excitation mechanism(s) be validated as responsible for the large-amplitude response of traffic signal structures? (iii) If traditionally effective helical strakes were affixed to the cantilevered mast arm of a signal structure, will a reduction in large-amplitude vibrations result? (iv) What new findings

related to excitation would result from monitoring a structure with helical arm strakes installed?

In the following, an instrumented prototype traffic signal structure is described along with observed fatigue-inducing stress range results. The nature of dynamic wind-induced response variability is identified and quantified in terms of the central tendency and dispersion parameters. To further investigate the role of across-wind effects, the dynamic response results are compared without and with the installation of helical strakes to the mast arm. Results of the present investigation may be used as a basis for future work concerning excitation mechanism, response reduction and response characterization.

3.3 Field Experiments in a Natural Wind Environment

To study the response of a traffic signal structure under realistic ambient conditions, field experiments were conducted in a natural wind environment. A traffic signal structure was installed on a drilled shaft foundation at the Texas A&M University Riverside Campus for continuous observation. Figure 3-1 depicts the installed structure and the location of installed instrumentation. The photograph in Figure 3-1(a) shows the traffic signal structure that consists of two tapered cylindrical members. As dimensioned in Figure 3-1(b), the pole tapers from a diameter 372 mm to 262 mm at the top over the 9.14 m height, while the arm tapers from a diameter of 279 mm to 127 mm over the 13.23 m length. The wall thicknesses of the pole and arm are 6.4 mm and 6.1 mm, respectively. An arm of this length is typically used to support three signal clusters.

Figure 3-1(e) depicts the placement of several strain gages in regions where significant dynamic response and fatigue-inducing stress reversals are known to occur.

Strain gages were installed near the arm-pole and pole-base connections located 320 and 394 mm from the welded transverse base plates attached to each member, respectively. This distance is greater than the diameter of each section to eliminate local stress effects. Weldable strain gages (type AWC-8B-11-3LT manufactured by Sokki Kenkyujo Co., Ltd.) were used within full-bridge Wheatstone bridge configurations to measure axial, in-plane bending, and out-of-plane bending strains allowing for temperature compensation and the exclusion of secondary strain effects.

To ensure that the response of the structure was captured over a wide variety of wind conditions, sensors were left on the structure over a period of time. Data was continuously acquired by the data acquisition system consisting of a strain gage measurement system (IOtech Strainbook/616) and a laptop. All channels were continuously sampled at 100 Hz and recorded.

To measure wind speed and direction, a weather station (Davis Instruments Vantage Pro2^{TM}) that included an anemometer was installed on the traffic support structure pole as indicated in Figure 3-1(b) The included sensor suite was connected to a laptop via USB and controlled by proprietary (Weatherlink^{TM}) software. The archived wind speed and direction information, with resolutions of 0.447 m/s and 22.5° (corresponding to a 16-point compass rose), is representative to the conditions directly affecting the cantilevered structure. The dynamic response of the standard structure was observed for a period of 4.5 months, from April 24 to September 9, 2012. Following this time, strakes were affixed to the mast arm to investigate their efficacy in mitigating in-plane response for a month, from September 13 to October 13, 2012.

(a) Full-scale prototype structure

(d) Helical strake installation on the mast arm

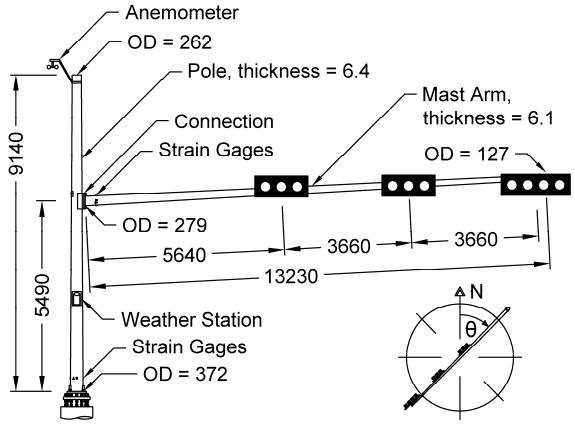

(b) Northeast to Southwest elevation and orientation

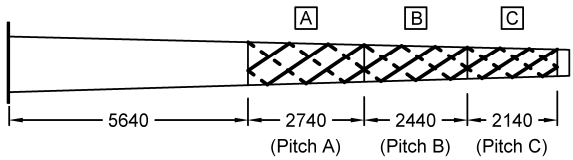

(e) Mast arm strake application schematic

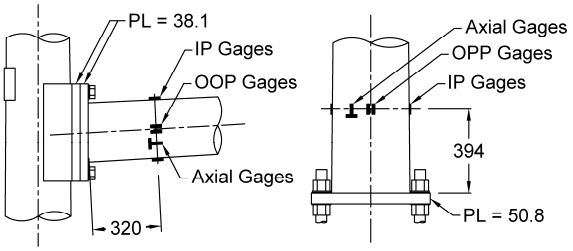

(c) Strain gage location at the arm-pole and pole-base connections

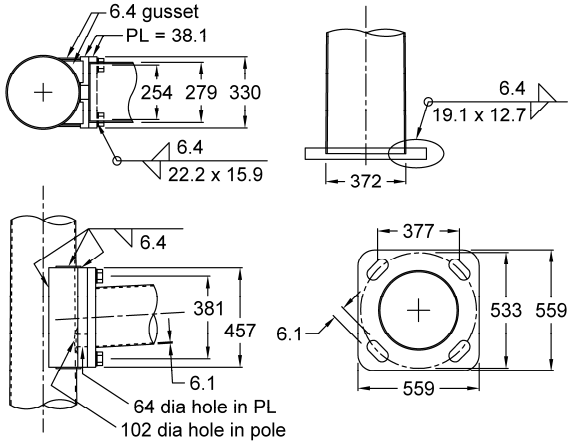

(f) Measured arm-pole and pole-base connection details

Figure 3-1. Experimental traffic signal structure at Texas A&M University's Riverside Campus in Bryan, TX (dimensions in mm).

The photograph in Figure 3-1(d) shows the triple-helix strake configuration as installed on the mast arm of the structure. Each segment denoted in Figure 3-1(e) represents one complete revolution of the installed strakes; each segment is of different length to achieve a pitch of 15 arm diameters, while maintaining a near optimal strake height equal to 10 percent of the arm diameter (Warpinski 2006). Braided polypropylene rope with a diameter of 16 mm was installed on the existing structure between the installed signal clusters by wrapping it around the exterior of the mast arm in a helical pattern as shown in Figure 3-1(d).

The orientation of the structure was positioned with respect to the prevailing wind; the mast arm projected from the northeast to the southwest away from the pole, as shown in Figure 3-1(b). Figure 3-2 presents the observed wind direction distribution and the proportion of recorded wind speeds that occurred out of each direction over the course of three time periods. Analysis of the available 40-year wind history for the region is shown in Figure 3-2(a). The greatest proportion of the wind is derived from the South (180°). Thus, nearly 55 percent of winds approach the rear face of the signal clusters from 90° to 180°. Figure 3-2(b) shows the distribution of winds observed while monitoring the behavior of the standard traffic signal structure. It is evident that the short-term observed wind at the Riverside test site is similar to the historical record at the nearby Easterwood Airport, located 11 km from Riverside Campus. The measured wind environment while testing the structure with arm strakes installed is shown in Figure 3-2(c). Although the test duration was limited, the record depicted in Figure 3-2(c) is considered sufficient to establish similarity to Figure 3-2(a,b).

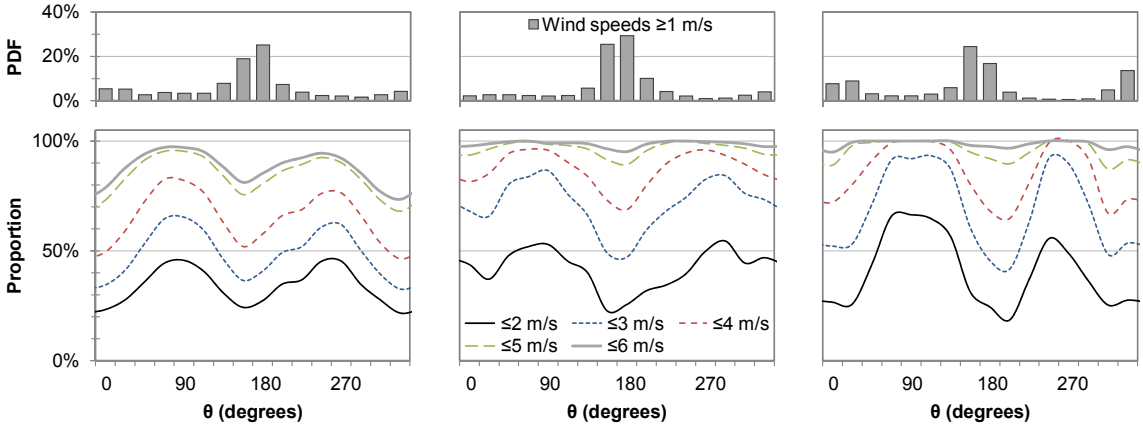

(a) Jan. 1, 1973 to Jan. 1, 2013 Easterwood Airport

(b) Apr. 24, to Sept. 9, 2012 Standard Structure

(c) Sept. 13, to Oct. 13, 2012 Structure with Straked Arm

Figure 3-2. Wind direction distribution (top row) and proportion of wind speeds by direction (bottom row) for the (a) regional and (b,c) local wind environments.

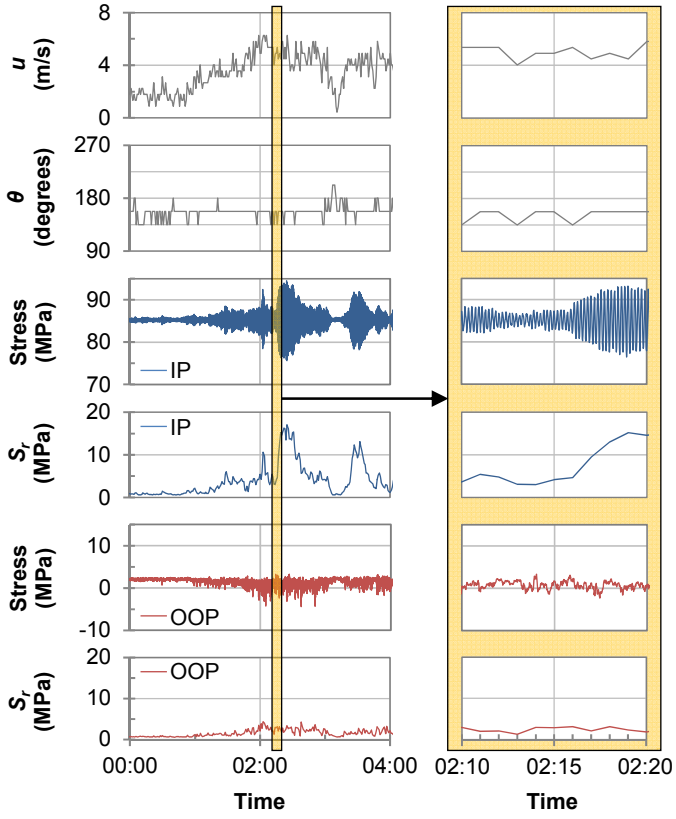

Figure 3-3. Sample measurement of in-plane (IP) and out-of-plane (OOP) time series and calculated one-minute stress ranges.

Figure 3-3 presents an example showing the recorded one-minute wind speed information, along with the related stress time history and calculated one-minute stress range. Post-processing of the recorded voltage time histories was done in MATLAB after field collection. In accordance with previous studies (Zuo and Letchford 2010; Bartilson et al. 2015), statistics of one-minute intervals were analyzed to describe the behavior of the structure under ambient wind excitation. The weather station was set to record one-minute weather statistics, downloaded hourly. Aligning with this time interval, stress ranges were described, as opposed to tip deflection. Although connection stress and arm tip deflection are related for an elastic structure, this study considers the stress response as the primary engineering demand parameter as it relates directly to the damage rate and hence the dependable service life of the structure.

The equivalent one-minute stress range was calculated based on the assumption that the stresses on the structure were sinusoidal. As a simple and convenient alternative to algorithms (Downing and Socie 1982) that incorporate Rainflow counting (Matsuishi and Endo 1968) to form a set of stress reversals over an observation period, intrinsic functions were used (Mander et al. 1992; Shah 1993; Letchford et al. 2008; Wieghaus et al. 2014c; Bartilson et al. 2015) to describe response as a single, one-minute equivalent. Since all points in the time history, rather than just the peaks, were used in the analysis, the one-minute constant amplitude stress range S_r was calculated by:

$$S_r = 2\sqrt{2}\sigma_{std} \tag{3-1}$$

where $\sigma_{std} =$ the standard deviation is taken over a one-minute moving window. Resulting from the analysis are one-minute statistics for archived wind (speed and direction) and

structural response in terms of stress range. Results of this analysis are depicted in Figure 3-3 for the in- and out-of-plane readings at the arm-pole welded connection, over broad (4 hour) and narrow (10 minute) time ranges.

During field tests, only wind-induced vibrations were captured, as the test site location is not near an active roadway. Although vibrations of such structures have been attributed to both natural wind-induced phenomena and traffic gusts, it has been reported that traffic effects are significantly lower than those due to natural winds (Chen et al. 2001; Albert et al. 2007). As a result, natural wind response has been logically assumed to be the primary cause of fatigue damage accumulation when performing fatigue assessments (Shah 1993; Letchford et al. 2008).

To compare with experimental results, an analytical model was developed to simulate the in- and out-of-plane natural frequencies of the traffic signal structure. Only the first natural frequency of the structure is considered in each direction as the vast majority of exhibited vibrations occurred in its first in- and out-of-plane modes. Representative masses were used to simulate traffic signal clusters, the arm-pole connection, arm-tip details, and the polypropylene rope. The modeled frequencies are presented in Table 3-1. Snap-back tests were performed before and after strake installation to experimentally determine the dominant frequencies and damping of the prototype test structure. As expected for such a structure, the experimentally observed frequencies showed good agreement with those determined analytically. Results shown in Table 3-1 indicate there was no appreciable change in structural damping.

Table 3-1. Dynamic properties of the prototype test structure.

Displacement	Field Test (Analytical Model)			
	Standard structure		Structure with straked arm	
	Natural frequency (Hz)	Damping ratio (%)	Natural frequency (Hz)	Damping ratio (%)
In-plane	1.093 (1.092)	0.25	1.086 (1.088)	0.22
Out-of-plane	0.995 (0.989)	0.62	0.989 (0.985)	0.64

3.4 Monitored Response of Standard Structure

Figure 3-4 presents the one-minute stress range S_r results as a function of wind speed u for the standard structure. Similar in- and out-of-plane responses are evident for the arm-pole and pole-base connections. When comparing the in- and out-of-plane response at the arm-pole connection, it is clear that the medians are similar, while the dispersions vary significantly depending on the degree of across-wind response. Across-wind response, which primarily affects the in-plane behavior, is quite pronounced for wind speeds in the range of 3 m/s to 7 m/s.

The second and fourth rows of the graphs in Figure 3-4 present the stress range response with respect to the wind direction. Four percentiles (50^{th}, 84^{th}, 95^{th}, and 99^{th}) are used to indicate the inherent randomness in response given one-minute wind speed and direction. The largest in-plane responses occurred when winds approached from 112.5° and 180°. However, the out-of-plane response also showed this tendency to some extent, along with an additional susceptibility to winds approaching from the opposite direction. When studying the central tendency of the in- and out-of-plane responses, two points are clear: (i) the typical response is quite small; and (ii) the in-plane response is more

dependent on the direction of approaching winds. Thus, based on the results presented in Figure 3-4 for the standard structure, the contribution of the vortex shedding mechanism is clearly evident.

Figure 3-5 further breaks down the response of the structure as measured at the arm-pole connection. Figure 3-5(a) shows the response of the structure by wind direction by separating wind direction into 16 sectors (each 22.5°) centered at the indicated azimuths. The largest in-plane responses occurred as winds approach between 112.5° and 180°. Response dispersion is also greatest in this range. Figure 3-5(a) also shows the out-of-plane response, in which the dispersion is depicted to be relatively similar regardless of approaching wind direction.

Figure 3-6 corresponds to analysis of response related to the component of the wind speed perpendicular to the orientation of the mast arm. Indicative of vortex shedding, the response of the monitored structure varies with both wind speed and direction. Figure 3-6(a) presents the response at the arm-pole connection as a function of the wind speed's perpendicular component. Positive speeds result when winds approach from the back side of the signal clusters. To further study the wind conditions related to the large-amplitude response observations, Figure 3-6(b) presents a histogram of the perpendicular speeds while the in-plane stress responses were greater than 10 MPa. Over three quarters of these events occurred between 4 m/s and 6 m/s, where nearly half occurred at 5 m/s.

The presented information makes a compelling case that vortex shedding is responsible for the large-amplitude responses of the monitored cantilevered traffic signal structure. The perpendicular velocity in Figure 3-6 will be used to determine the Strouhal

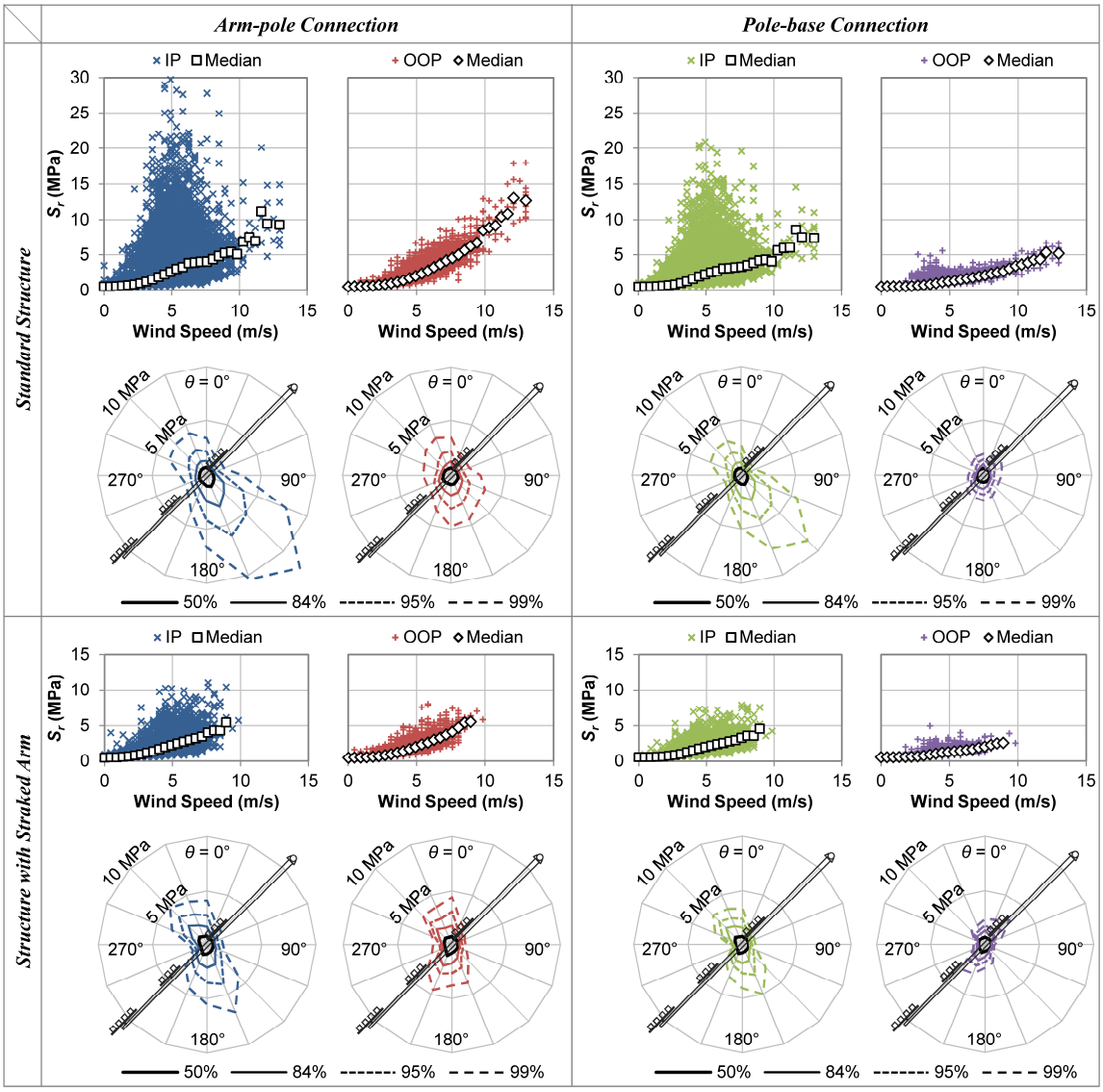

Figure 3-4. Measured in-plane (IP) and out-of-plane (OOP) structural response vs. total wind speed and wind direction.

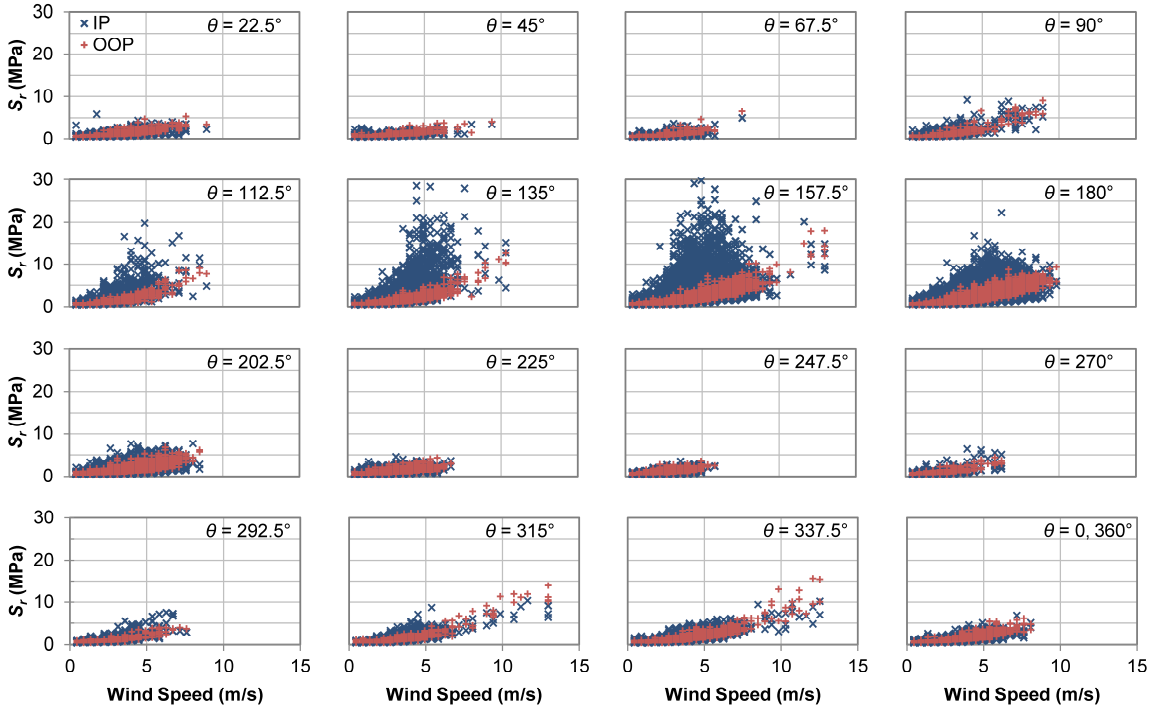

(a) Response of standard structure

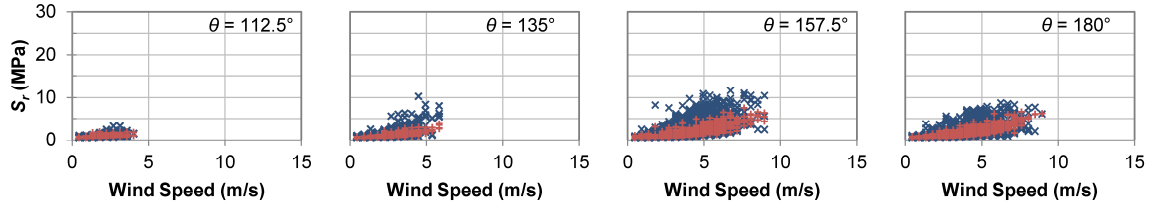

(b) Response of structure with straked arm

Figure 3-5. Wind direction dependence of in-plane (IP) structural response at the arm-pole connection compared against out-of-plane (OOP) response.

number related to the signal clusters and the horizontal mast arm itself. The vortex shedding frequency is often described by the non-dimensional Strouhal relationship (Letchford et al. 2008)

$$St = \frac{f_{vs} D}{\overline{u}_{perp}} \tag{3-2}$$

where $St =$ Strouhal number, $f_{vs} =$ the vortex shedding frequency, $D =$ cross-wind (characteristic) body dimension, and $\overline{u}_{perp} =$ mean speed of the oncoming flow.

The occurrence of vortex shedding "lock-in" is typically referred to as the synchronization between the vortex shedding frequency and the in-plane natural frequency of the structure over a period of time, where vibrations may enhance vortex strength, leading to large (and damaging) vibrations. Given the largest across-wind effects occurred at the first in-plane natural frequency of 1.09 Hz (the first in-plane natural frequency of the structure) and the height of the signal clusters is 600 mm, the Strouhal number when the wind was perpendicular to the signal clusters is 0.131. This corresponds well with the literature where it has been shown that the Strouhal number for a rectangular object with a small depth-to-height ratio is approximately 0.15 (Blevins 1977; Yu et al. 2013). If the average diameter of the mast arm (203 mm) was used as the characteristic dimension, the Strouhal number is 0.045, which shows no resemblance to the Strouhal number related to a circular cylinder of 0.20 (Walshe and Wooton 1970). If mast arm vortex shedding was a primary excitation mechanism, the expected lock-in wind speed would be approximately 1 m/s; clearly, no instances of amplified across-wind response were observed at this speed.

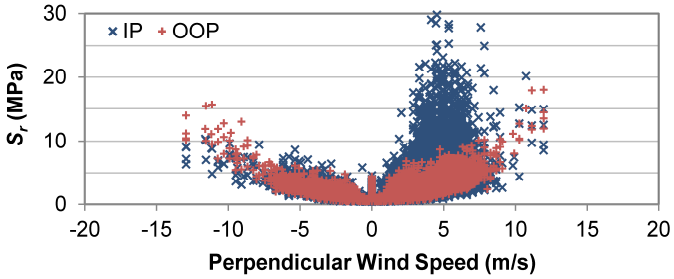

(a) In-plane (IP) and out-of-plane (OOP) response vs. perpendicular wind component

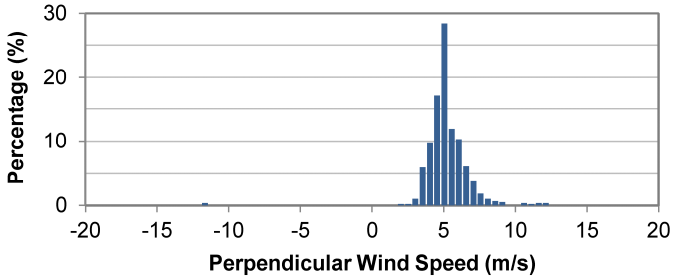

(b) Distribution of winds resulting in $S_r > 10$ MPa

Figure 3-6. Conditions responsible for the large in-plane (IP) response of the standard traffic signal structure.

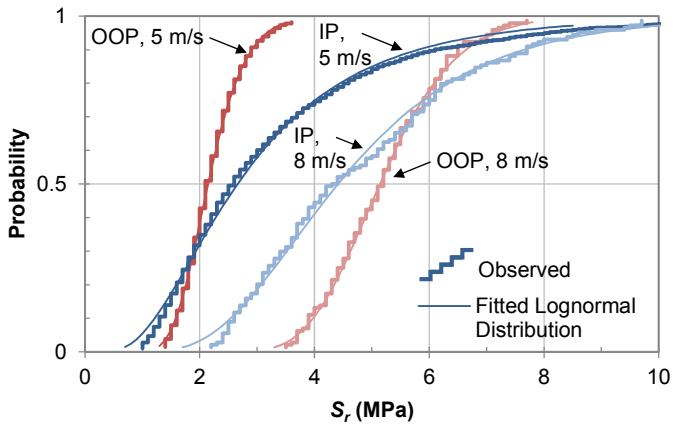

Figure 3-7. Variability in the in-plane (IP) and out-of-plane (OOP) stress responses using the Lognormal distribution.

Thus, the reasonable conclusion is that the large-amplitude observations occurred due to signal cluster vortex shedding.

Figure 3-7 presents the cumulative distribution of observed stress ranges for two specific wind speeds, 5 m/s and 8 m/s. As expected, the 50^{th} percentile (median) in- and out-of-plane stress responses increase as a function of wind speed, as indicated in Figure 3-4. Also depicted in Figure 3-7 is the increased dispersion (randomness) in in-plane response at 5 m/s, the wind speed in which the vortex shedding mechanism is influences response. As seen, uncertainty in in-plane response decreases at 8 m/s, as the observed distribution function narrows. Stress response dispersion was observed to increase until 5 m/s, then decreased thereafter, again influenced by the vortex shedding mechanism.

Resulting from the observed trends, the two parameter lognormal distribution is fitted to the observed results as specified by the median stress range, and the lognormal standard deviation for stress at a given wind speed condition $\beta_{\mathrm{Sr}|u}$. Findings demonstrate satisfactory agreement between the observations and the corresponding fitted lognormal distributions. It should be noted that the observations were within the confidence band as defined by the critical value of the Kolmogorov-Smirnov goodness-of-fit test at the five percent significance level (Smirnov 1948). As a result of this finding, the response of a wind-excited traffic signal structure in a natural wind environment can be characterized statistically by a lognormal distribution, given wind speed and direction.

Now that signal cluster vortex shedding has been related to the large stress ranges observed, the influence that excitation mechanism has on the median and dispersion of the

response can be quantified. Figure 3-8(a) presents a log-log plot of the one-minute response as a function of wind speed independent of direction. As seen for the standard structure, the median of the total in- and out-of-plane responses is extrapolated as a function of wind speed squared, in agreement with theory and standards (AASHTO 2013). The median in-plane response is evidently affected by the tendency of the signal clusters to shed vortices. As a result, the median response varies with wind direction; Figure 3-8(b) illustrates this dependence. When wind approaches from the back side of the structure $(90° < \theta < 180°)$ and the wind speed is near 5 m/s, there is an apparent increase in in-plane median response; whereas this is not the case for all other approaching winds. With increasing wind speed, the median in-plane response increases with the square of wind speed and is relatively direction independent. These in-plane vibrational effects arise from the unsteady nature of the along-wind response (buffeting). Likewise, the analysis demonstrates that the out-of-plane response is direction independent and also attributed to buffeting.

Figure 3-8(c) indicates that the uncertainty in response varies with wind speed and direction by presenting the lognormal standard deviation parameter (dispersion), $\beta_{Sr|u}$. Dispersion values for both the in- and out-of-plane response at higher wind speeds appear scattered; this is attributed to the relatively small number of data points used in relation to those at lower speeds. Despite the mostly invariant nature of the out-of-plane median response to wind direction, the dispersion parameter appears somewhat dependent on wind direction, and in particular the degree of across-wind response. Accounting for the

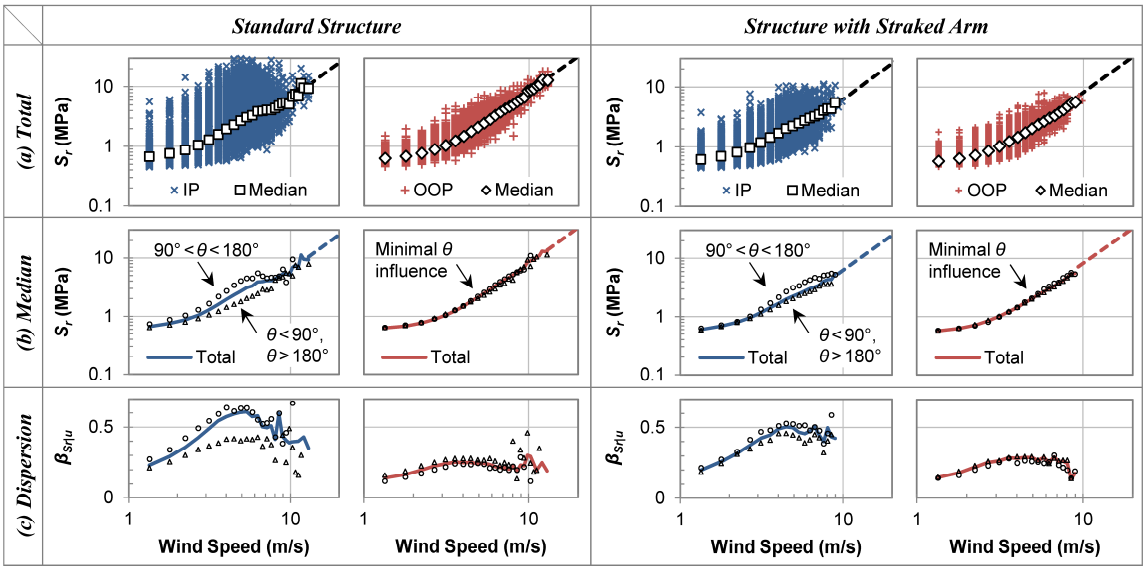

Figure 3-8. Wind-induced one-minute in-plane (IP) and out-of-plane (OOP) stress response at the arm-pole connection characterized by the: (a) total response and calculated median, (b) median response and influence of vortex-induced vibrations, and (c) lognormal standard deviation and influence of vortex-induced vibrations.

propensity of signal cluster vortex shedding, the in-plane dispersion parameter associated with winds approaching from the back side of the attachments increases linearly to a maximum of 0.64 at 5 m/s. From that point, the dispersion decreases. The dispersion of in-plane response while winds approached from the other directions reached a maximum of $\beta_{\mathrm{Sr}|u} = 0.42$ and decreased thereafter. For conservatism, a value of $\beta_b = 0.30$ would describe the in-plane response due to buffeting (occurs at lower and higher wind speeds). Because the variability of the total response at a specified wind speed is described with the lognormal distribution, it may be described as a function of the variability of its components:

$$\beta_t = \sqrt{\beta_b^2 + \beta_{aw}^2} \tag{3-3}$$

where β_b and $\beta_{aw} =$ the dispersion parameters associated with buffeting and across-wind effects (including vortex shedding), respectively. Using the dispersion value of $\beta_t = 0.64$ to describe the total response when winds approach from the back side of the structure and the value assigned to buffeting, the dispersion related to across-wind effects is $\beta_{aw} = 0.57$. When winds do not approach from the back side of the attachments, the across-wind contribution is reduced.

3.5 Monitored Response with Strakes Installed to the Mast Arm

Several strategies and devices have been used on high-mast light structures to alleviate vortex-induced vibrations (Ahearn and Puckett 2010). The most common add-on aerodynamic damping device for cylindrical structures is helical strakes (Warpinski 2006). Helical strakes have been shown to significantly disrupt the formation of a shear layer,

along with vortex formation and shedding (Scruton and Walshe 1973). Optimal strake sizes and installation geometry have been well documented (Kumar et al. 2008). Despite their demonstrated effectiveness, helical strakes have not yet been considered for application on traffic signal structures because vibrations have only recently been associated with vortex shedding, and vortex shedding it not considered in the current AASHTO fatigue provisions.

Similar to previous observations (Letchford et al. 2008; Zuo and Letchford 2010; Cruzado et al. 2013), the presented results demonstrate that an ordinary traffic signal structure is prone to increased dynamic response due to across-wind effects. Previous observations of a traffic signal structure without attached signal clusters (Zuo and Letchford 2010) showed several relatively significant responses while winds approached the front of the structure (as opposed to only the back side). Because their structure had a large-diameter mast arm, large-amplitude vibrations were attributed to vortex shedding of the mast arm, not the attached signal clusters.

In an attempt to mitigate the adverse effects of across-wind response, helical strakes were installed on the mast arm of the structure: (i) to study the effect of the tapered mast arm on the response of the structure; and (ii) to appraise the viability of strakes as a response mitigation measure. Helical strakes or ribs are a body surface modification that has long been shown to significantly reduce vortex-induced vibrations and are widely used, particularly on the likes of industrial chimneys, high-mast illumination poles, mooring cables, etc. Typically, three equi-angularly spaced strakes with a height of 0.1 and a pitch of 15 arm diameters are optimal. Helical strakes effectively disrupt the

formation of a boundary layer, adversely affecting shear layer roll up, to prevent vortex formation and shedding (Kumar et al. 2008). As depicted in Figure 3-1(d), braided rope was used to form helical strakes on the mast arm at an optimal arrangement utilizing three separate pitch lengths. Winds of primary interest were captured, allowing ample opportunity to complete the desired studies.

The lower row of results presented in Figure 3-4 shows the response of the structure with mast arm strakes installed. With strakes installed, the structure experienced no one-minute in-plane stress ranges over 12 MPa. With the vast majority under 10 MPa, the structure displays less tendency to exhibit large across-wind vibrations. Installing strakes also decreased the median in-plane stress response; nearly eliminating the influence of vortex-induced vibrations. When comparing the out-of-plane response at the arm-pole connection with and without arm strakes, the median and dispersion of the response appears relatively unchanged.

Figure 3-5(b) depicts a selected subset of the modified structure's stress response related to the wind directions in Figure 3-5(a) that resulted in the largest response. By comparing Figure 3-5(b) against the second row of Figure 3-5(a), it is evident that the installed arm strakes mitigated all occurrences of large-amplitude response observed in the standard structure.

Figure 3-8 depicts a more detailed analysis of the response before and after arm strake installation. The addition of arm strakes is clearly seen to reduce the occurrence of large, sustained in-plane stress cycles at the arm-pole connection. Figure 3-8(a) indicates that the presence of arm strakes reduces the in-plane median response by reducing the

influence of vortex-induced vibrations. The modification does not lead to significant changes that justifies changing the extrapolation of the in- or out-of-plane median response. In Figure 3-8(b), the in-plane median response when winds approached from the back side $\left(90° < \theta < 180°\right)$ shows little change, showing a slight decrease near "lock-in"; the median response when approached from the other directions shows little change. Observations demonstrate that the median out-of-plane response remains direction independent; the added drag assumed with strake installation had no effect on the typical response. Figure 3-8(c) further demonstrates the effectiveness of the helical arm strakes by showing a significant decrease in the dispersion of the in-plane response. While winds approach from certain directions that promote vortex induced vibrations, the maximum in-plane lognormal standard deviation $\beta_{Sr|u} = 0.53$, decreased from 0.64. As a result, the dispersion related to across-wind effects $\beta_{aw} = 0.43$, significantly down from 0.57. The dispersion related to remaining winds remains virtually unchanged. Most importantly, the dispersion of the total in-plane response showed a significant decrease as a result of eliminating the influence of vortex-induced vibrations.

Figure 3-9 displays the wind-induced stress response at the arm-pole connection characterized by various percentiles. As indicated previously, the dispersion in the in-plane response is far greater than in the out-of-plane for the standard structure. This is clearly shown by the intervals formed by the 16th and 84th percentiles (±1 standard deviation $\beta_{Sr|u}$). The effectiveness of the installed arm strakes can also be clearly seen in Figure 3-9. Aimed to reduce the in-plane response, strake installation did just that by

reducing the 50th percentile (median) response and response variability $\beta_{Sr|u}$. Although the out-of-plane median response was practically unaffected by the addition of arm strakes, the variability in response slightly increased. However, as seen in Figure 3-9, this increase can be attributed to a decreased 16th percentile response, not an increase of the 84th percentile.

3.6 Comparisons with Other Results

Some observations made while monitoring the installed traffic signal structure in a natural wind environment were similar to previous studies, while others differed. Overall, the monitored structure was observed to be quite lively when compared to a similarly tested structure (Letchford et al. 2008; Cruzado et al. 2013), where signal cluster vortex shedding was also suspected. Although the amplified across-wind response observed in this investigation over a restricted range of wind speeds (4 m/s to 6 m/s), the range was not originally as apparent as that exhibited by the structure studied in Zuo and Letchford (2010), where mast arm vortex shedding was studied and related to large-amplitude vibrations at low wind speeds. Only after further analysis (Figure 3-6) did the range became more clearly defined. This was most likely the result of a differing dominant excitation mechanism; their structure was found to experience mast arm vortex shedding, as opposed to signal cluster vortex shedding. The largest in-plane responses were observed when winds approached from 112.5° to 180°, showing good agreement with each of the aforementioned studies.

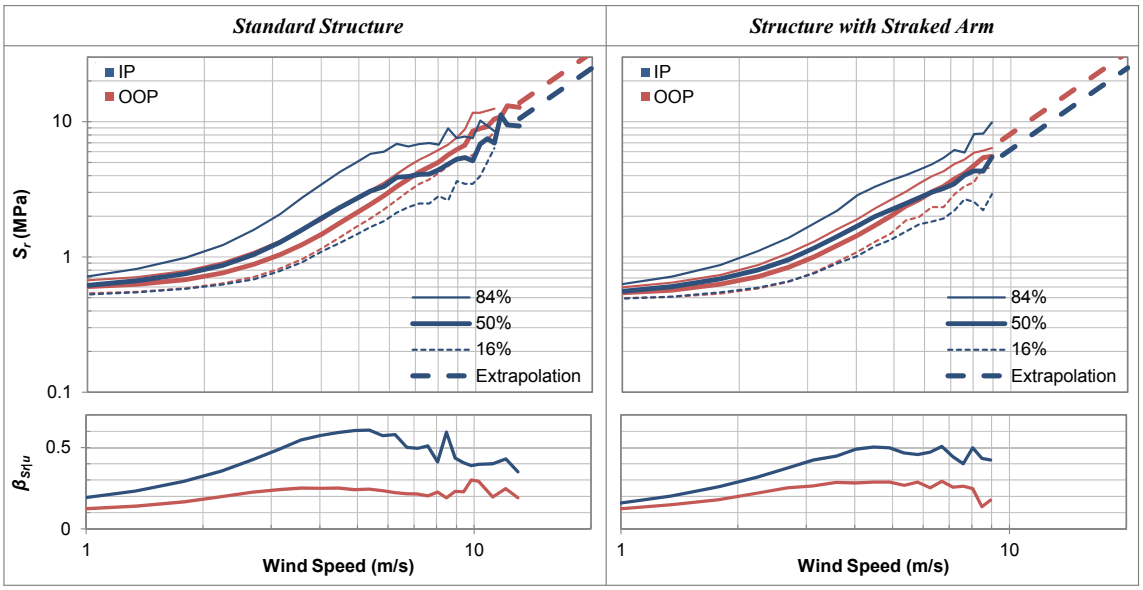

Figure 3-9. In-plane (IP) and out-of-plane (OOP) wind-induced stress response at the arm-pole connection characterized at various percentiles, and lognormal standard deviation.

After studying the Strouhal relation pertaining to the large-amplitude responses, the reasonable conclusion is to attribute those observations to signal cluster vortex shedding. Further, the in-plane response variability peaks at a wind speed of 5 m/s and decreases thereafter. This peak in dispersion can also be seen via visual inspection of the results presented in Letchford et al. (2008). This clearly demonstrates the influence of the vortex shedding mechanism on response. Identifying signal cluster vortex shedding as a significant excitation mechanism is in agreement with previous work (Letchford et al. 2008; Cruzado et al. 2013). However, observations show that the influence of signal cluster vortex shedding appears greater than previously indicated, although previous research did not study the response in such detail.

3.7 Discussion of Findings

The monitored response of the standard structure studied shares similarities with the previous work, where signal cluster vortex shedding, then mast arm vortex shedding was identified as responsible for large-amplitude vibrations (Letchford et al. 2008; Zuo and Letchford 2010; Cruzado et al. 2013). Helical strakes were then installed on the mast arm of the structure to: (i) study the effect of the mast arm on the response of the structure to better understand the excitation mechanism; and (ii) appraise the viability of strakes as an aerodynamic response mitigation measure.

The installation of helical strakes to the mast arm of the full-scale test structure directly resulted in a significant decrease in response as indicated by the elimination of all large stress responses within the wind speed range associated with signal cluster vortex shedding, indicating interaction between the mast arm section and the attached signal

clusters. Strake installation reduced the influence of vortex shedding on the in-plane median response and reduced dispersion; the strakes did not significantly change the typical out-of-plane (along-wind) response. The results indicate that although the diameter of the mast arm is not large enough to drive vibrations (i.e. leading to mast arm vortex shedding), the section is critical in flow separation and vortex formation on the back side of the signal cluster backplates. Based on these and the results of the previous work of others, if a mast arm is of large diameter to shed vortices near the structure's natural frequency and there is little difference between the characteristic dimension of the mast arm and installed attachments, the mast arm controls response. Alternatively, if the characteristic dimension of the mast arm is significantly smaller than the signal clusters, it should be viewed that the mast arm separates the approaching flow toward the back side of the attachment with little disruption, further enabling signal cluster vortex formation and shedding.

Optimally sized and spaced arm strakes disorganize flow separation, hindering vortex formation on the back side of the attached signals. Although the mechanism is well reasoned, the effectiveness of strakes to mitigate mast arm vibrations and structural response for structures with slender mast arms was relatively unexpected. Because (i) mast arm vortex shedding has been observed in structures with large-diameter arms and (ii) strakes have been shown effective even for slender-armed structures, then helical arm strakes (optimally sized and spaced based on mast arm dimensions) should be a considered vibration mitigation measure for traffic signal structures susceptible to large-amplitude, vortex-induced vibrations. Based on the studies discussed herein, the installation of arm

strakes appears a viable, and potentially a more consistent, passive means to mitigate the vertical, across-wind vibration of cantilevered traffic signal structures due to vortex shedding.

Notwithstanding the aforementioned findings, to overcome certain obvious limitations of the present study and to advance the state of knowledge, further work remains to be carried out. Although accomplished through more full-scale testing, controlled laboratory testing and/or computational modeling could assist in: (i) validating the findings of the presented research and enable extrapolation of the response at higher wind speeds; (ii) determining how representative the presented results are over a demonstrative variety of structural dimensions and attachment configurations; and (iii) investigating the benefits of disaggregating flow around circular section at or near attachments.

3.8 Closure and Key Findings

The following key findings are drawn based on the research described and performed herein:

i. Stress reversals in traffic signal structures occur due to a combination of along-wind buffeting leading to two-dimensional vibrations, and across-wind vortex shedding that primarily result at low to moderate wind speeds. Both in- and out-of-plane responses in a natural wind environment result in highly variable behavior, but such behavior can be characterized statistically by a lognormal distribution. Observations show that the lognormal standard deviation (dispersion)

for the total in-plane response may vary from 0.2 to 0.6, but can be as high as 0.64 when across-wind effects are prevalent.

ii. Two excitation mechanisms were found to primarily provoke in-plane vibrations: vortex shedding and buffeting. The occurrence of large stress reversals correlate with a specific wind condition and the characteristic dimension (height) of the attachments, so signal cluster vortex shedding is identified. Cantilevered traffic signal structures with slender mast arms and horizontally oriented signal clusters are most susceptible to signal cluster vortex shedding. However, as the diameter of the mast arm increases, the mast arm will begin to control response.

iii. Optimally sized and spaced arm strakes may be used to mitigate the detrimental effects of low-speed vortex shedding by reducing the median and dispersion of the in-plane response. As a result of the research performed herein, it is shown that even small-diameter mast arm sections are critical as they contribute toward flow separation and vortex formation on the back side of signal cluster backplates.

4 TARGET-LESS COMPUTER VISION FOR TRAFFIC SIGNAL STRUCTURE VIBRATION STUDIES*

4.1 Overview

The presented computer vision method allows for the non-contact, target-less determination of traffic signal structure displacement and modal parameters, including mode shapes. Using an analytical model to relate displacement to stress, it is possible to utilize a rapid set-up and take-down computer vision-based system to infer structural stresses to a high degree of precision. Using this computer vision method, natural frequencies of the structure are determined with accuracy similar to strain gage and string potentiometer instrumentation. Even with structural displacements measured at less than 0.5 pixel, excellent mode shape results are obtained. Finally, one-minute equivalent stress ranges from ambient wind excitation are found to have excellent agreement between the inferred stress from strain gage data and stresses calculated from computer vision tied to an analytical stress model. This demonstrates the ability of this method and system to develop fatigue life estimates using wind velocity data and modest technical means.

4.2 Introduction

Structural vibrations from live and environmental loads constitute a mechanism for fatigue failure due to cyclic stresses developed within the excited structure. Vibrating

* This section is reprinted with permission from Bartilson, D. T., Wieghaus, K. T., and Hurlebaus, S. (2015). "Target-less computer vision for traffic signal structure vibration studies." Mechanical Systems and Signal Processing, 60-61, 571-582. Copyright 2015 Elsevier Ltd.

structures generally exhibit multiple natural frequencies and shapes of deformation corresponding to each frequency. Traffic signal structures are excellent examples of ambient wind-excited, flexible structures, and have been extensively studied (McDonald et al. 1995; Kaczinski et al. 1998; Cook et al. 2000; Hamilton et al. 2000; McManus et al. 2003; Letchford et al. 2008; Zuo and Letchford 2008; Zuo and Letchford 2010; Wieghaus et al. 2014a,b). Cyclic strains are observed at the connections of traffic signal structures due to wind-induced excitation. Such vibrations occur both vertically and horizontally as a result of vortex shedding, natural gusts, truck-induced gusts, and other effects (Kaczinski et al. 1998; Letchford et al. 2008; Zuo and Letchford 2008; Zuo and Letchford 2010; Wieghaus et al. 2014a,b). As a result of these repetitive strains, connections within the structure often exhibit a reduced fatigue life. While the fatigue failure of traffic signal structures does not realize a significant portion of traffic accidents or deaths, concern is highlighted due to the apparent unpredictability of this hazard to motorists and the economics of replacing fatigued traffic signal structures (Kaczinski et al. 1998). Unfortunately, experimental analysis of structural response is often difficult or costly to employ because current methods generally require large arrays of instrumentation (Ren et al. 2004; Teughels and De Roeck 2004; Cunha and Caetano 2006; Gaul et al. 2008; Whelan et al. 2009; Magenes 2011; Reyer et al. 2011; Rice et al. 2012). For structures such as high mast illumination poles (Magenes 2011), application of instrumentation presents a risk for injury. Current technology available to monitor traffic signal structure response includes infrared camera-emitter systems, fixed linear displacement sensors, accelerometers, and strain gages (McDonald et al. 1995; Cook et al. 2000; Hamilton et al.

2000; McManus et al. 2003; Letchford et al. 2008; Zuo and Letchford 2008; Zuo and Letchford 2010; Wieghaus et al. 2014a,b,c).

Computer vision-based techniques offer an alternative experimental analysis method and have been used for the analysis of structural motion for many years (Olaszek 1999; Patsias and Staszewski 2002; Paulsen et al. 2011; Busca et al. 2013). Computer vision is based on research into artificial intelligence and is closely related to pattern recognition (Gagvani 2009). The main benefit of a computer vision-based technique is the inherently non-contact approach. Short term studies or analyses of hard-to-access structures can be performed in situations where traditional instrumentation would be infeasible.

One prominent example of a computer vision-based analysis of a bridge measured the static and dynamic response due to car traffic (Olaszek 1999). This experiment provided a strong proof-of-concept for computer vision methods of analysis for civil engineering structures. However, the non-contact benefits of computer vision techniques were negated by the necessity of installing targets, where the accuracy of the analysis was noted to be highly dependent upon the target geometry.

Target-less analysis of bridge dynamic responses using consumer-grade cameras has been performed (Busca et al. 2013). This approach utilized edge detection and pattern matching algorithms in combination, initially on specialized targets, but noted that without a target, measurement reliability was strongly influenced by the contrast at the point of analysis (Busca et al. 2013). Edge detection and cross-correlation algorithms have been more commonly used due to their relatively low computational demand. However, these

algorithms are generally less robust than pattern recognition algorithms (Mori and Chang 2003; Busca et al. 2013). A robust algorithm is denoted by its broad applicability and lack of dependence on well- or pre-defined geometry for a target.

While edge detection algorithms are usually not robust enough to permit tracking of any given target geometry, researchers have been able to analyze damage in structures by determination of bridge mode shapes using a wavelet-based edge detection technique (Patsias and Staszewski 2002). This presented a novel use of an algorithm for determination of mode shapes to a high degree of accuracy. More importantly, this technique did not require the placement of targets on the structure of interest. The researchers noted, however, that the presence of any edges in the image background, such as separated clouds, tended to distort the mode shape obtained by edge detection.

Computer vision-based measurement has also been successfully applied to wind turbines, resulting in effective determination of mode shapes. This approach utilized a packaged, point-tracking software with specialized cameras (Paulsen et al. 2011). While this presented an example of the general application of a computer vision method for modal analysis, the need to attach specialized targets negated the non-contact benefits associated with a computer vision-based approach.

In order to generalize a computer vision method for broader application to experimental analysis of structures, it is necessary to develop an approach which does not require specialized targets or geometry. Through utilization of a robust pattern recognition algorithm, the application of computer vision-based techniques will not be limited to analysis at structural points amenable to the attachment of targets. The minimum quadratic

difference (MQD) algorithm presents a robust method of analysis for determining dynamic characteristics and displacement time series of flexible structures.

Using a non-contact, target-less computer vision based on the MQD algorithm, the objectives of this research are to: (i) develop and validate a method to determine structural displacements; (ii) develop and validate a method to infer structural stresses; (iii) validate a method to determine the dynamic characteristics of a structure; and (iv) apply the developed method to infer stresses due to ambient wind-induced excitation.

This section details the traffic signal structure of interest and the methods for obtaining data (Section 4.3). The validity of MQD-based computer vision is then analyzed for structural displacement measurements and stress inference (Section 4.4). This method is then applied to determine the dynamic properties of the structure (Section 4.5). Using the developed stress inference method, MQD-based computer vision is used to relate structural response to wind speed during wind excitation (Section 4.6). The findings are then discussed and concluding remarks are made (Sections 4.7 and 4.8).

4.3 Experimental Structure and Measurement Techniques

The combination of a wealth of previous research into traffic signal structure dynamic responses and the relatively large displacements realized during vibration makes traffic signal structures excellent candidates for dynamic response analysis using a computer vision-based method. As examples of flexible structures which are excited by ambient wind, traffic signal structures easily undergo vibration, with damping ratios generally less than one percent and fundamental frequencies of approximately 1 Hz (Letchford et al. 2008).

Traffic signals are generally supported by a vertical pole and horizontal mast arm which jointly constitute a cantilevered traffic signal structure. The vibrations of these structures are categorized as in-plane for vertical vibrations and out-of-plane for vibrations parallel to the direction of vehicles passing under. Section 3 describes the full-scale traffic signal structure of interest that was installed at Texas A&M University's Riverside Campus (Wieghaus et al. 2014a).

A Firstmark Controls 160-0963-S6SS string potentiometer was used to directly measure mast arm tip displacement. The string potentiometer was powered by an Agilent A3611A power supply, and output voltage was recorded using a Tektronix TDS3034B oscilloscope at a sampling frequency of 100 Hz. In-plane bending stresses inferred from strain gages installed near the pole-base connection were of primary interest for the study herein. Section 3 (Wieghaus et al. 2014a) should be consulted for details pertaining to gage installation/placement and sampling rate.

Video was captured with a SONY HDR-CX220 consumer-grade video camera with a 1280×720 pixel resolution and a sampling rate of 29.97 Hz. Note that the 30 Hz sampling rate effectively limited this setup to capture modes of 15 Hz or less due to the Nyquist frequency criterion. The camera was situated at a ground distance of 41.3 m from the closest point on the structure. For every test except ambient excitation, a scale factor of 13.2 mm/pixel was chosen based upon the measurement of five geometries in the field of view shown in Figure 4-1(a). This factor was used to scale measured displacements from pixels to physical dimensions. For simplicity, the line-of-sight of the camera was set up with a perpendicular orientation to the plane of the traffic signal structure. A strictly

(a) Representative video capture field of view for artificial excitations

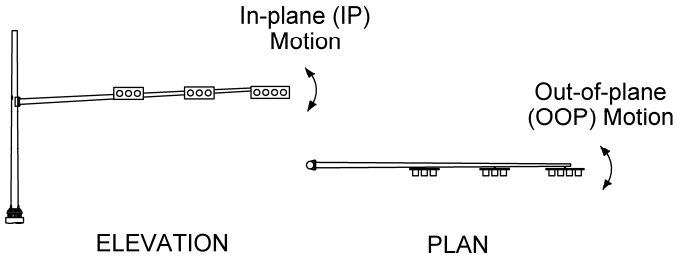

(b) Displacement/motion nomenclature

Figure 4-1. Experimental traffic signal structure for computer vision study.

perpendicular orientation is not necessary to this approach, but tends to simplify the field-of-view calculations. Out-of-plane motion may be observed by motion toward or away from the camera, therefore as a relatively miniscule change in size of an object. This approach could be more properly adapted to the analysis of 3D-motion by utilizing one or more cameras situated in perpendicular fields of view.

For reminder, a Davis Instruments Vantage Pro2 weather station was installed the top of the pole of the structure to determine wind velocity during ambient wind excitation test (Wieghaus et al. 2014a).

4.3.1 Scale Factor Estimation

Figure 4-2 provides a schematic describing camera field of view relative to a plane of interest. Simple geometric relationships can be developed from this figure to describe the scale factor.

The scale factor SF (in dimensions of distance/px) may be estimated by

$$SF = \frac{1}{n_{px}}\left(\frac{l_G}{\cos^2(\beta)}\frac{d_i}{f_i}\right) \tag{4-1}$$

where $d_i =$ the size of the sensor (generally in film equivalent); $f_i =$ the focal length; $n_{px} =$ the pixel resolution in the measured direction; $l_G =$ is the ground distance; and $\beta =$ the angle between a line perpendicular to the plane of the traffic signal structure and the camera line of sight. In an existing setup, the scale factor can be measured by

$$SF = \frac{h_{known}}{h_{obs,px}} \tag{4-2}$$

where h_{known} = the known dimension of physical geometry and $h_{obs,px}$ = the observed dimension of the imaged geometry in pixels.

4.3.2 MQD-based Computer Vision Measurement

For displacement measurement between two images captured during motion, a computer was used to perform comparisons between one sub-window of the initial image and multiple sub-windows of the succeeding image. Based on the notation in (Gui and Merzkirch 2000), the sub-window of the initial image $\mathbf{g_1}$ can be defined as a $N \times M$ matrix of pixels with elements given by $g^a_{k,l}$

$$\mathbf{g_1} = \left\{ g^a_{k,l} \right\} = \begin{Bmatrix} g^a_{11} & \cdots & g^a_{M1} \\ \vdots & \ddots & \vdots \\ g^a_{1N} & \cdots & g^a_{MN} \end{Bmatrix} \tag{4-3}$$

where the superscript a denotes the initial image, and the subscripts k and l give element locations.

A sub-window of the succeeding image, located (m,n) from the sub-window of the initial image, has elements given by $g^b_{k,l}$, and must also be of size $N \times M$,

$$\mathbf{g}_2 = \left\{ g^b_{k,l} \right\} = \begin{Bmatrix} g^b_{11} & \cdots & g^b_{M1} \\ \vdots & \ddots & \vdots \\ g^b_{1N} & \cdots & g^b_{MN} \end{Bmatrix} \tag{4-4}$$

where the *b* superscript denotes the succeeding image, and the subscripts *k* and *l* give element locations.

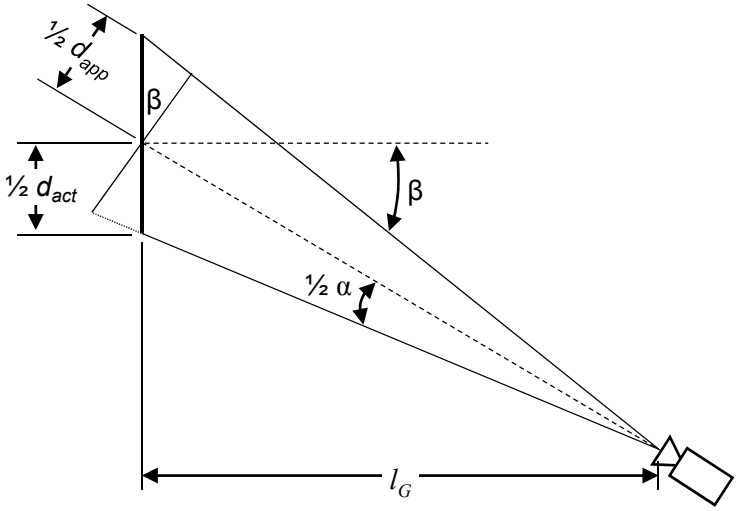

Figure 4-2. Schematic of camera field of view relative to region of interest.

One algorithm which computes displacements based on least-square determination of pattern movements between images the MQD algorithm (Gui and Merzkirch 2000)

$$D(m,n) = \frac{1}{M \cdot N} \sum_{i=0}^{M-1} \sum_{j=0}^{N-1} \left[g_1(i,j) - g_2(i+m, j+n) \right]^2 \tag{4-5}$$

The MQD algorithm seeks the location (m^*, n^*) of displaced sub-window which yields the minimum sum of the squared gray value difference D relative to the initial image sub-window. The MQD algorithm allows for uses that extend beyond its original application to fluid motion analysis due to the ability of the algorithm to analyze pattern movement. However, the robustness of the MQD algorithm comes at the cost of generally greater computation time than the more common, less robust cross-correlation algorithm utilized in other computer vision-based structural studies (Chang and Ji 2007; Kim and Kim 2013). Mori and Chang (2003) developed the code for applying the MQD algorithm. The code was modified to read in sequential frames from a video file and perform displacement comparisons relative to a user-defined sub-window.

Computer vision-based measurement error is generally compared on the basis of root mean square error (RMSE) of measured versus known displacements. The MQD algorithm provides some inherent error. Based on the work of Gui and Merzkirch (2000), higher RMSE is associated with displacements in the sub-pixel range, though maximum error is quantified at less than 0.05 pixel. The MQD algorithm is thus said to have sub-pixel accuracy (Gui and Merzkirch 2000; Mori and Chang 2003).

Any computer vision-based displacement measurements are sensitive to even small changes in the field of view, as may be caused by camera base motion. In the

presented setup, for example, a vertical camera rotation of one-hundredth ($1/100^{th}$) of a degree corresponded to several millimeters of displacement measurement error. Pure translations of the camera would cause measurement errors of the same magnitude as the applied translation. For measurement of periodic motion, application of digital filtering can effectively remove any disturbance that is caused by base motion. This relies, however, on the base motion of the camera being non-periodic or periodic with a frequency sufficiently different from the modes of interest. While this presents a simple, cost-effective method for countering base motion, active control base systems (Hurlebaus and Gaul 2006; Kerber et al. 2007) may provide a more robust method for avoiding disturbance from base motion.

4.3.3 Mode Shape Determination

In many image processing applications, a region of interest is defined for the processing tasks. For displacement analysis, a sub-window is defined in the initial image for comparison and encloses the geometry of interest. To determine structural displacements, damping ratios, or natural frequencies, the single region of interest exemplified in Figure 4-3(a) may suffice, while mode shape determination requires quantifying displacements at multiple points along the structure, as shown in Figure 4-3(b). The benefit of a computer vision-based approach is the large number of pixels available as discrete points of analysis while only requiring a single video capture device (Patsias and Staszewski 2002).

(a) Single region of interest

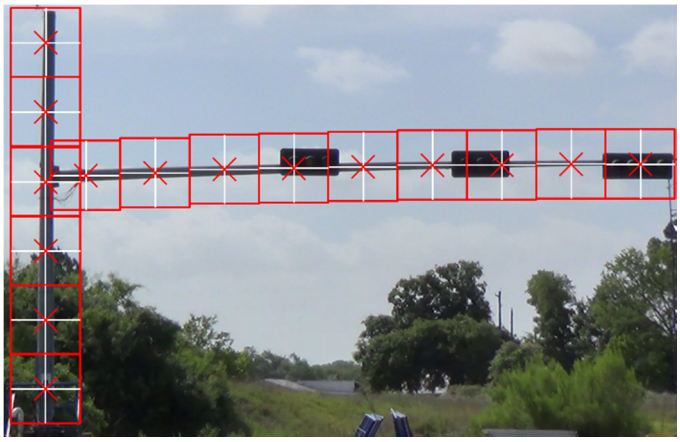

(b) Multiple regions of interest

Figure 4-3. Sample region(s) of interest for performed study.

For mode shape determination, each point of analysis on the structure had a corresponding displacement time series which was filtered for each desired mode. To realize a valid time series for points of analysis along simple geometry, such as the bare pole or mast arm, digital gridlines were applied in the direction of motion for analysis. This forced the MQD algorithm to recognize a higher degree of correlation between sub-windows aligned with the gridlines. Thus, for analysis along the horizontal mast arm, gridlines were digitally superimposed at the boundaries of each sub-window in the vertical direction; for pole analysis, horizontal gridlines were digitally superimposed. The RMS displacement was used to quantify displacement associated with each point of analysis. The relative direction of the RMS displacement was inferred by the sign of the average displacement for each point. While the average displacements were near zero, a small bias towards a negative or positive mean was introduced by the decrease in consecutive peak and trough amplitudes due to damping. RMS modal displacements were then normalized.

4.3.4 Ambient Wind Response Measurement

To demonstrate the use of computer vision for analysis of ambient wind-induced vibrations, four hours of traffic signal vibrations were captured with scale factors between 0.9 mm/pixel and 1.1 mm/pixel. The camera was situated at a ground distance between 5.2 m and 6.8 m from the mast arm tip and raised to a height of 1.8 m. Wind speeds ranged between 2 m/s and 9 m/s and predominantly approached the structure from its back side, between 90° and 180° (Wieghaus et al. 2014a). Figure 4-4 displays the field of view for the camera for ambient wind excitation tests. For ambient wind excitation analysis, only in-plane displacements and bending stresses were studied.

4.3.5 Analytical Model

A SAP2000 model was developed to form an analytical stress-displacement relationship and for modal analysis. Representative masses were used to simulate the traffic signal clusters, arm-pole connection, and end-plate detail at the extent of the arm. A relationship between in-plane base bending moment and in-plane tip displacement was developed. Since the first in-plane mode dominates dynamic response of the structure (McDonald et al. 1995; Letchford et al. 2008; Zuo and Letchford 2008; Zuo and Letchford 2010; Wieghaus et al. 2014a,b), only first in-plane mode displacements and moments were considered. As a result, in-plane bending stress was inferred as a function of in-plane arm displacement using section properties of the structure.

4.4 Computer Vision Vibration Measurement

A snapback excitation was applied to the structure and the mast arm tip displacement was measured using both a string potentiometer (direct vibration measurement) and computer vision. The stress at the base of the pole was inferred from the strain gage output during the same test. The snapback excitation involved applying an initial displacement at the tip of the traffic signal structure mast arm, then releasing the structure, allowing it to vibrate freely. This primarily induced first in-plane mode vibrations.

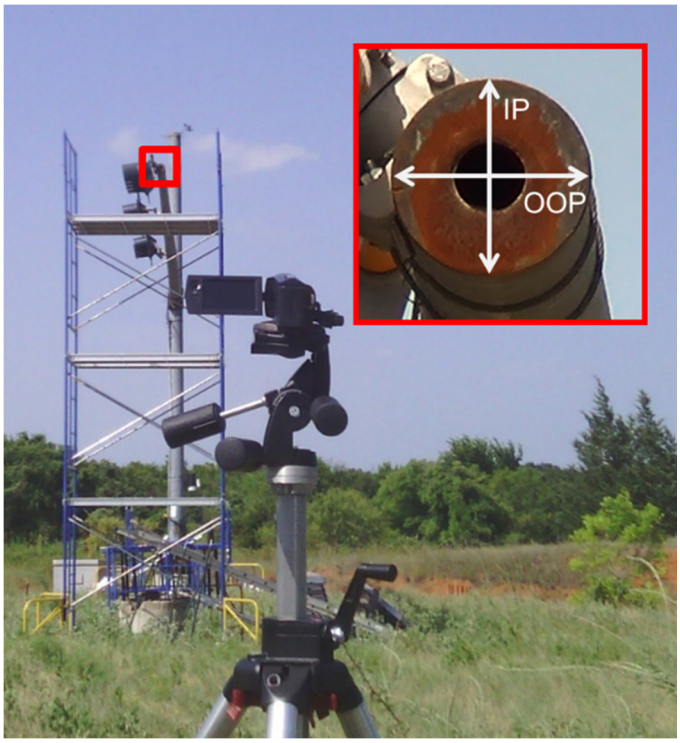

Figure 4-4. Ambient wind excitation video capture setup (IP = in-plane, OOP = out-of-plane).

4.4.1 Displacement Measurement

The resulting in-plane arm tip displacement time histories were analyzed, as shown in Figure 4-5. As can be seen from Figure 4-4, the frequency of the direct vibration measurement and computer vision signals are alike, while the amplitudes are similar. The RMS of the direct vibration measurement signal was 43.8 mm, while the computer vision result was 44.4 mm. This corresponds to 1.3 percent difference in RMS with respect to the direct vibration measurement result. Direct comparison between signals is shown in Figure 4-5.

4.4.2 Stress Analysis

With agreement between the analytical and computer vision-based stress-displacement models, the inferred stress time histories were directly compared, as shown in Figure 4-6. The RMS of the strain gage signal was 8.90 MPa, while the computer vision result was 9.09 MPa. This corresponds to only 2.1 percent difference in signal RMS with respect to the strain gage RMS. The time signals show the same features, which suggests that the computer vision-based method provides inferred stresses at approximately the same accuracy as strain gage instrumentation.

There is an initial discrepancy between the signals presented in Figure 4-6(c), likely due to the greater contribution of second in-plane mode motion to base stress than to tip displacement. Compared to the first in-plane mode, second in-plane mode tip displacement corresponds to a much larger base bending stress. The presented analysis considered only the stress contribution from first in-plane mode motion, so a discrepancy between stress signals was expected at the initial time of excitation, before the higher

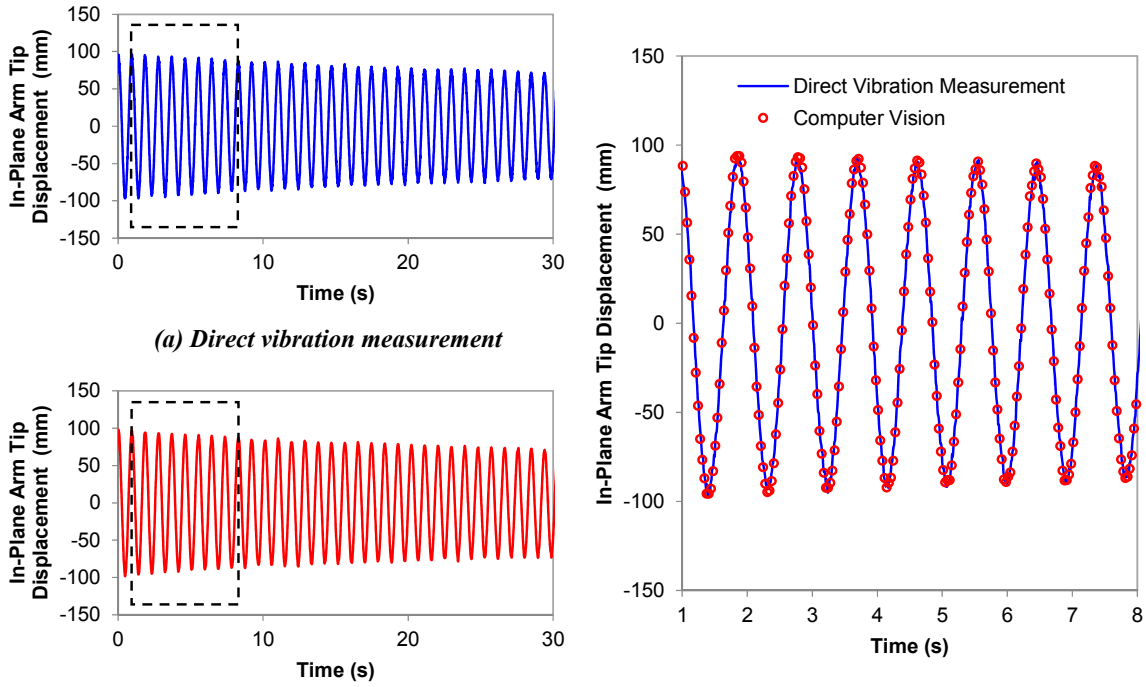

(a) Direct vibration measurement

(b) Computer vision

(c) Overlaid results for direct comparison

Figure 4-5. Sample arm tip displacement time series during computer vision study.

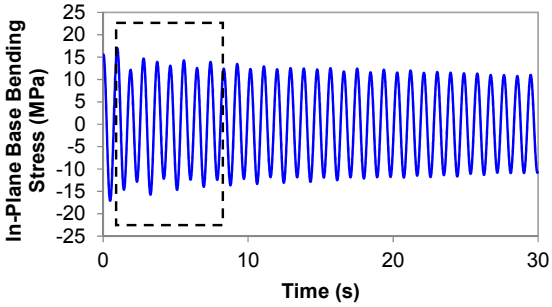

(a) Strain gage

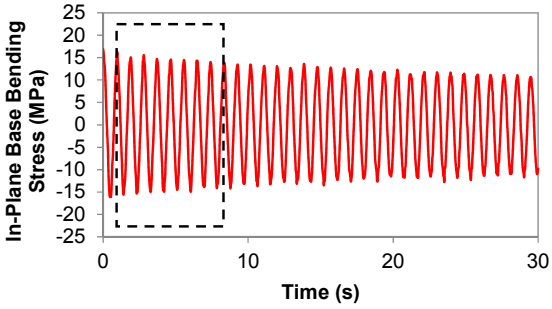

(b) Computer vision to stresses using analytical stress-displacement relationship

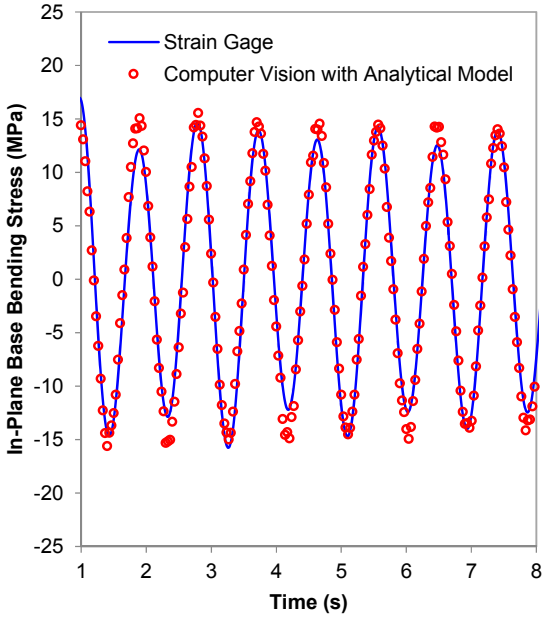

(c) Overlaid results for direct comparison

Figure 4-6. Sample inferred stress time series during computer vision study.

modes have been sufficiently damped. More detailed analyses could be performed by filtering the displacements from each mode and developing stress-deflection relationships for each mode. Due to the rapid damping of higher modes, this was not implemented for this study.

4.5 Dynamic Property Determination

Building upon the MQD-based computer vision method for determining traffic signal structure displacement, the method was used to determine dynamic properties. Three types of excitation were applied to the full-scale traffic signal structure: snapback, forced (in the first and second in-plane modes), and broadband. For each excitation type, three trials were performed and analyzed using computer vision, direct vibration measurement, and strain gages. The snapback excitations were performed as previously described and allowed for the determination of natural frequencies, modal damping ratios, and mode shapes. Forced excitations involved the manual application of a periodic force at a rate coinciding with a natural frequency of the structure. This excitation reduced the influence of other modes while producing larger vibration amplitudes in the excited mode. Broadband excitation simultaneously induced the excitation of multiple modes and was accomplished by impacting the end of the mast arm. This allowed for the determination of first and second in-plane natural frequencies and mode shapes using only one impact.

4.5.1 Natural Frequency Determination

The in-plane natural frequencies f were obtained from instrumentation time signals. Fast Fourier transforms (FFTs) of the experimental results from a single snapback

test in Figure 4-7. The computer vision and direction vibration measurements at the mast arm tip showed a second in-plane mode amplitude approximately 3 percent of the first in-plane mode amplitude. The strain gage, located at the base of the pole, produced an FFT which shows the second in-plane mode amplitude as nearly 15 percent of the first in-plane mode amplitude. This higher contribution of the second mode is due to the greater contribution of second in-plane mode motion to base bending stress than to tip displacement.

The analytical and average experimental natural frequency results are given in Table 4-1. The experimental results exhibited minimal variance in natural frequencies, with small disagreement between the analytical and experimentally determined second in-plane natural frequency. This suggests that the analytical model did not completely account for the boundary condition, though this did not affect the stress-displacement relationships.

Table 4-1. In-plane natural frequency results from analytical modeling and average experimental results.

	Analytical	Computer Vision	Direct Vibration Measurement	Strain Gage
f_1 (Hz)	1.092	1.088	1.090	1.088
Error (%)	---	-0.34	-0.09	-0.33
f_2 (Hz)	3.324	3.227	3.227	3.231
Error (%)	---	-2.91	-2.92	-2.81

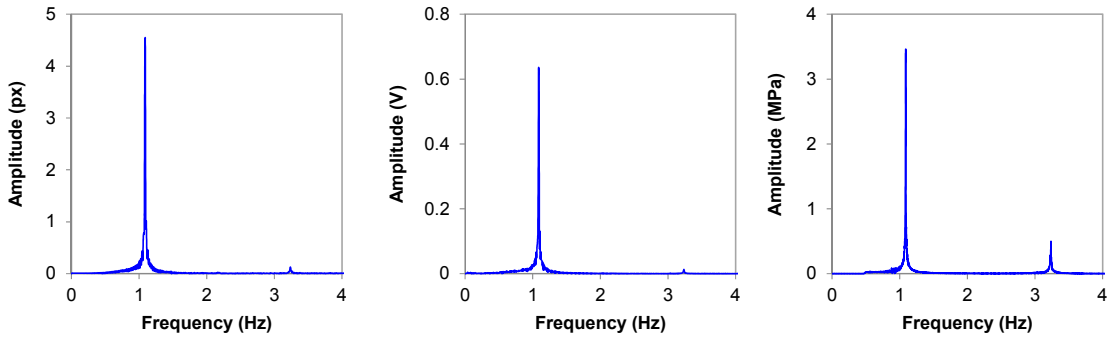

(a) Computer vision *(b) Direct displacement measurement* *(c) Strain gage*

Figure 4-7. Sample in-plane frequency analysis during computer vision study.

4.5.2 Damping Ratio Determination

To determine damping ratios, each snapback time series was filtered through bandpass filters for first and second in-plane mode motion. A sample total signal with filtered first and second mode signals are included in Figure 4-8.

Modal damping ratio ζ was determined by measuring the logarithmic decrement (Chopra 2007) of the signal of interest over 30 seconds. The determined damping ratios are included in Table 4-2, with agreement between the average for first and second in-plane mode damping ratios from each measurement instrument. The variability in modal damping ratios was largest for the second in-plane mode when determined using computer vision. This was caused by greater effect of the MQD algorithm RMSE in the measurement of low amplitude peak heights, where the second in-plane mode vibration amplitudes were approximately one order-of-magnitude smaller than the first in-plane mode vibration amplitudes. Despite the variability, computer vision was able to determine the modal damping ratios to a high accuracy.

Table 4-2. Average damping ratio results from experimental measurement.

	Computer Vision	Direct Vibration Measurement	Strain Gage
ζ_1 (%)	0.216	0.241	0.222
ζ_2 (%)	0.150	0.124	0.157

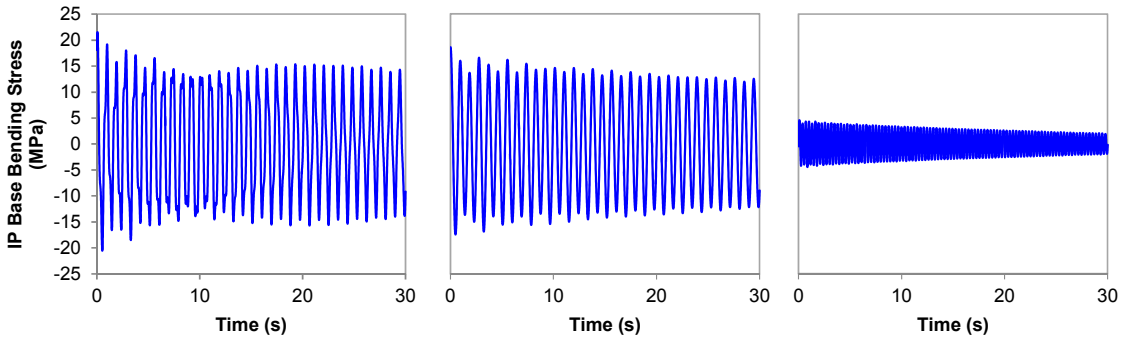

(a) Total signal *(b) Filtered first IP mode* *(c) Filtered second IP mode*

Figure 4-8. Sample free vibration time series, representative of the signals used for damping ratio analysis (IP = in-plane).

4.5.3 Mode Shape Determination

To determine mode shapes, tighter bandpass filter parameters were used. The last half of each time series was used to ensure that the resulting RMS modal displacements would not be affected by the zero displacements preceding excitation. The normalized mode shapes were scaled such that the largest displayed displacement in each mode shape was 1000 mm. The resulting mode shapes from three trials were then averaged for each excitation type, as shown in Figure 4-9. The modal assurance criterion (MAC) (Pastor et al. 2012) was utilized as a numerical comparison of consistency between the computer vision-determined mode shape vectors ϕ_X and the analytical mode shape vectors ϕ_A:

$$\mathrm{MAC}(X, A) = \frac{\left|\{\phi_X\}^T \{\phi_A\}\right|^2}{\left(\{\phi_X\}^T \{\phi_X\}\right)\left(\{\phi_A\}^T \{\phi_A\}\right)} \tag{4-6}$$

MAC values range between 0 and 1, where values above 0.9 generally indicate consistency between similar mode shapes if mode shape orthogonality can be shown. Orthogonality was shown between the analytical mode shapes using the procedure in (Allemang 2003). From this, orthogonality was assumed in the experimental mode shapes which were consistent with the analytical mode shapes. Alternatively, a MAC value near zero, which was observed between first and second in-plane mode shapes, may be used as an approximation of an orthogonality check (Pastor et al. 2012). This suggests that the exhibited mode shapes were indeed orthogonal.

Each excitation type allowed for determination of the first in-plane mode shape, as shown in in Figure 4-9(a). Each determined mode shape compared favorably with respect to the analytical mode shape, as shown by the high average MAC values. The second in-

plane mode shapes, shown in Figure 4-9(b), displayed slightly lower average MAC values, indicating a marginally lower consistency between the experimental and analytical mode shapes. As in the damping ratio analysis, the second in-plane mode displacements were at least an order-of-magnitude smaller than the first in-plane mode displacements, which caused the RMSE associated with MQD algorithm to become significant. Despite this, all experimentally determined second in-plane mode shapes exhibited acceptable MAC values for consistency except for one broadband excitation trial.

Figure 4-10 provides the relationship between maximum RMS displacement of the measured mode shape and the MAC value. This relationship suggests that valid mode shapes can be determined using MQD-based computer vision for modal displacements which exhibit a maximum RMS displacement of 0.5 pixel. The relationship between MAC value and average RMS modal displacement is also included, but it provides essentially the same information as the maximum RMS displacement. This occurred because the original mode shape can be obtained by multiplying the normalized mode shape by the maximum displacement. Since each normalized mode shape was approximately the same, differences in average modal displacement predominantly occurred due to differences in maximum modal displacement. The average normalized modal displacement was approximately 0.25 for each mode, thus an average RMS modal displacement of 0.25 pixel is approximately equivalent to a maximum RMS modal displacement of 1 pixel.

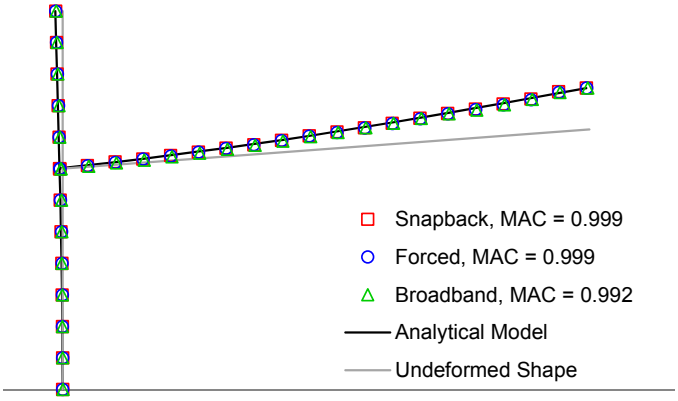

(a) First IP mode

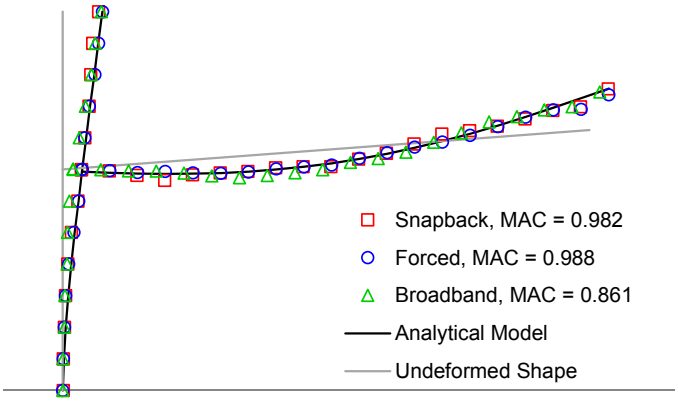

(b) Second IP mode

Figure 4-9. Average mode shape and modal assurance criterion (MAC) results.

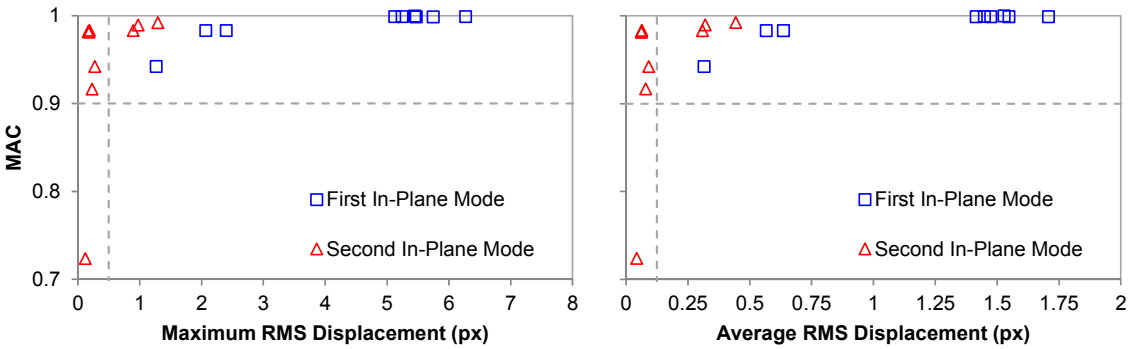

(a) Maximum RMS modal displacement *(b) Average RMS modal displacement*

Figure 4-10. Modal assurance criterion (MAC) versus computer vision RMS displacement.

4.6 Ambient Wind Response Analysis

The presented research has shown that MQD-based computer vision coupled to an analytical stress-displacement model offers a non-contact, target-less method for inferring stresses in traffic signal structures. This technique was then used to infer stresses resulting from ambient wind excitation. Since all points in the time series may be used for analysis rather than only the peak stresses, an equivalent one-minute constant amplitude stress range S_r may be calculated by

$$S_r = 2\sqrt{2}\sigma_{std} \tag{4-7}$$

where the standard deviation of stress σ_{std} is taken over a one-minute moving window (Letchford et al. 2008, Zuo and Letchford 2010, Wieghaus et al. 2014a-c). Acquiring stress and wind velocity data concurrently allowed for the development of a structural response model which could be used for fatigue and other analyses.

Both the computer vision-measured displacement and the strain gage-inferred stress time histories were filtered through a highpass filter. This process removed the mean of the signal and allowed for alignment of time histories. Using the analytical deflection-stress relationship, the computer vision-measured displacements were then converted to stresses for first in-plane mode motion. The results of this analysis using both strain gage and computer vision-inferred responses are shown in Figure 4-11. The results show excellent correspondence on the time series features.

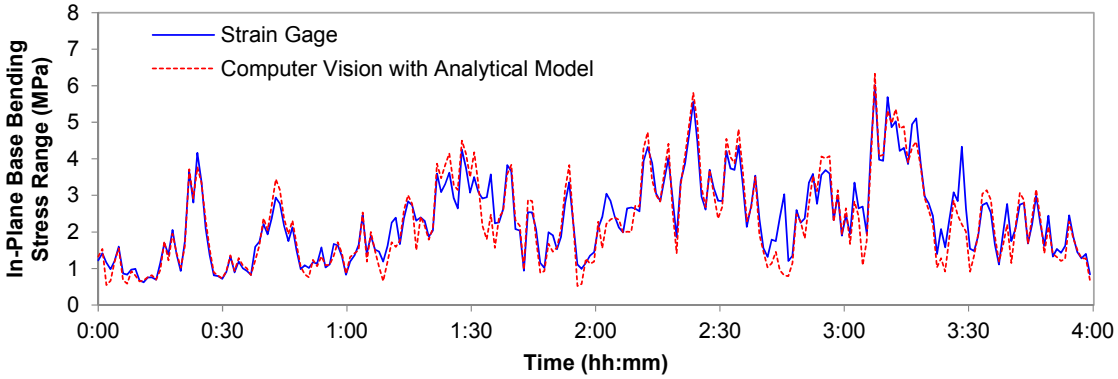

Figure 4-11. One-minute equivalent stress range time history of the full-scale traffic signal structure under ambient wind-induced vibrations.

Using the wind speed data, relationships were then developed between in-plane stress range and wind speed based on the strain gage data and the computer vision inferred stresses. As shown in Figure 4-12, the statistics based on computer vision observation are comparable to those inferred from strain gage instrumentation.

4.7 Discussion

MQD-based computer vision using a consumer-grade camera was shown effective in determining traffic signal displacements. This method was shown to have excellent agreement to direct vibration measurement using a string potentiometer.

Computer vision-measured displacement coupled with an analytical stress-displacement model allowed for accurate determination of stress time series, with results comparable to strain gage output. For higher accuracy, a greater number of pixels may be used to represent the displacement by using a higher resolution video capture device (Patsias and Staszewski 2002). Similarly, to obtain a smoother time series, a higher frame rate video capture device may be utilized.

Natural frequencies were well agreed upon by the results of the various excitation types and instrumentation, which demonstrates the validity of MQD-based computer vision for determination of structural natural frequencies. As expected, damping ratio values showed greater dependence on modal displacement. The order-of-magnitude smaller amplitude of the second in-plane mode vibrations led to a much greater effect of the inherent MQD algorithm RMSE. While this may explain some of the variance, the obtained small damping ratios (less than 0.5 percent) are excellent results for the observed low pixel amplitude vibrations.

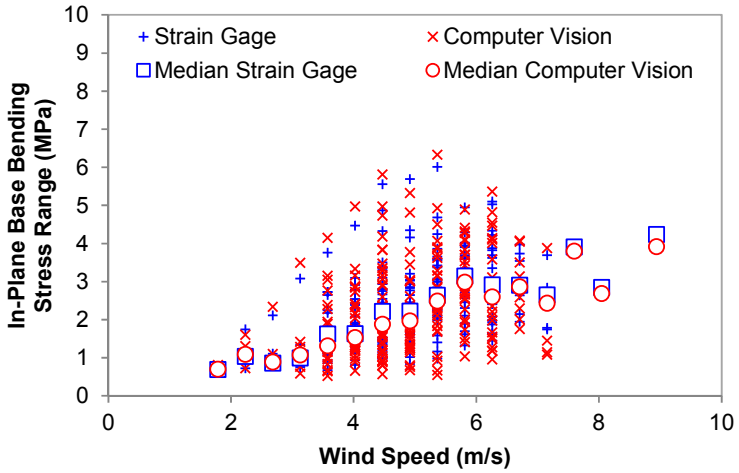

Figure 4-12. One-minute equivalent stress range versus wind speed from computer vision and strain gage.

All three types of excitation performed were shown to provide mode shapes which satisfy the MAC criterion for correspondence to the analytical mode shapes. Indeed, most of the MAC values for the first in-plane mode shapes were near unity, and only one of the second in-plane mode shapes did not compare favorably with the analytical mode shape. For this structure, it was noted that a maximum RMS modal displacement of 0.5 pixel or higher leads to excellent results, with near unity MAC results obtained for any mode shapes with a 1 pixel or greater maximum RMS modal displacement. An average RMS modal displacement of 0.125 pixel yielded the same results as a maximum RMS modal displacement of 0.5 pixel because the average normalized RMS displacement of each mode shape was approximately 0.25.

By comparison of the wind-induced one-minute equivalent stresses in Figure 4-11, it was shown that the computer vision-derived stress ranges provide excellent agreement with strain gage output. Deviation between the strain gage and computer vision results may be explained by the greater influence of the second in-plane mode at the base of the pole, which is the point of measurement for the strain gage. The relationship developed for base bending stress as a function of tip displacement considered only the first in-plane mode because the response of the structure is typically assumed to be dominated by this mode (McDonald et al. 1995; Letchford et al. 2008; Zuo and Letchford 2008; Zuo and Letchford 2010; Wieghaus et al. 2014a,b).

The median stress response from computer vision was marginally lower than the median stress response from the strain gage for the same wind speed. Despite the apparent

bias towards a slightly lower inferred response when inferred using computer vision, the median response of the traffic signal structure was effectively characterized.

4.8 Closure and Key Findings

The presented MQD-based computer vision method allows for non-contact, target-less determination of traffic signal structure displacements and modal parameters. Unlike similar non-contact computer vision-based approaches, the MQD-based approach showed high accuracy results with no dependence on well-defined target geometry or background pattern. This establishes MQD-based computer vision as a novel method for enacting truly non-contact methods for determination of modal parameters and displacement time histories. By using the analytical model to correspond computer vision-measured structural displacements to stresses during vibrations, an efficient, non-contact method for inference of stress time histories was validated.

Using computer vision to measure displacements, it was shown possible to accurately determine natural frequencies of a full-scale traffic signal structure, with accuracy similar to strain gage and string potentiometer output. Utilization of time series filtering allowed for accurate determination of modal damping ratios. Even with the maximum observed RMS displacement of the mode shapes reaching only 0.5 pixel, excellent MAC results were obtained, proving that modal displacements on the order of a pixel have the potential to provide excellent experimental mode shape results. This establishes MQD-based computer vision using consumer-grade cameras as a viable method for determining mode shapes of traffic signal structures, where the resulting quality is dependent upon RMS pixel displacement magnitude.

For this structure, the highest amplitude mode occurred around 1 Hz. The lower measurement accuracy encountered with higher modes most likely occurred due to lower modal displacements, and likely not due to frame capture rate limitations. Thus, this approach should only be limited only by pixel displacement associated with the mode of interest. The frame capture rate should satisfy the Nyquist frequency criterion for the highest mode of interest, or the rate of input excitation, whichever is higher.

One-minute inferred stress ranges during ambient wind excitation were found to have high agreement between strain gage and computer vision coupled to an analytical stress-displacement model. The developed relationships agreed favorably, suggesting that computer vision is a viable method to measure the response of flexible, wind-excited structures using modest technical means.

The benefits of this method are the inherent non-contact approach and the low-complexity, low-cost instrumentation. Hard-to-access structures such as high mast illumination poles, high span bridges, and wind turbines can be analyzed. Similar benefits apply in situations where the dynamic study of the structure is short term and the costs associated with application of traditional instrumentation would make the study infeasible. This study obtained excellent results using a low-cost, consumer-grade camera, which suggests that the accuracy of results may be increased further by the utilization of higher resolution cameras.

5 EFFECTIVENESS OF STRAKE INSTALLATION FOR TRAFFIC SIGNAL STRUCTURE FATIGUE MITIGATION (DETERMINISTIC SERVICE LIFE ASSESSMENT)*

5.1 Overview

Across-wind response is often the cause of significant structural vibrations that in turn cause fatigue damage to welded and other connections. The efficacy of low-cost helical strakes to mitigate such adverse response is presented for a traffic signal structure. Field observations are made on a prototype structure in a natural wind environment without and with helical strakes installed on the cantilevered arm. Through continuous monitoring, the strakes were found to be effective in reducing across-wind response at wind speeds less than 10 m/s. Estimates of service life are made for four different geographical locations and wind environments. Results for the class of traffic signal structure show that helical arm strakes are most effective in locations with benign wind environments where the average annual wind speed is not more than the vortex shedding wind speed, which for this investigation is 5 m/s. It is concluded that while strakes may be effective, it is not the panacea to mitigating connection fatigue at all locations.

* This section is reprinted with permission from Wieghaus, K. T., Hurlebaus, S., Mander, J. B. (2014b). "Effectiveness of strake installation for traffic signal structure fatigue mitigation." Structural Monitoring and Maintenance, an International Journal, 1(4), 393-409. Copyright 2014 Techno Press.

5.2 Introduction

The persistent excitation of cantilevered traffic signal structures result stress reversals that can lead to fatigue, particularly in welded connections. Multiple mechanisms have been identified to cause the large-amplitude vibrations undergone by cantilevered traffic signal structures, but the reason for certain common characteristics, particularly the in-plane motion induced by across-wind effects, remains under dispute. Galloping (McDonald et al. 1995; Kaczinski et al. 1998), signal cluster vortex shedding (Letchford et al. 2008; Cruzado et al. 2013), and mast arm vortex shedding (Zuo and Letchford 2010) have all been previously linked to large amplitude vibrations, while natural wind and traffic-induced gusts contribute to the most persistent vibrations.

This section seeks to evaluate a low-cost, aerodynamic vibration suppression device for cantilevered traffic signal support structures. The approach involves the use of helical strakes in the form of a braided rope wound around the arm in a triple helix formation. Ropes/strakes have been successfully used by other researchers for mitigating vortex shedding induced vibration in high mast structures (Blevins 1977; Kaczinski et al. 1998; Ahearn and Puckett 2010; Ahearn 2010; Connor et al. 2012). The simple solution may be used as a retrofit and is intended to improve the fatigue life of certain existing fatigue prone systems. However, strakes could potentially be used in new construction for structures installed in suitable locations. As a means to determine the effectiveness of helical strake installation, the stress response at the pole-to-arm connection is observed in a natural wind environment before and after strake installation. To quantify the potential benefit of arm strake installation (in Section 3), the fatigue life of the structure is then

estimated using a deterministic framework considering any changes in natural wind response for several distinct wind environments.

5.3 Experiments on a Prototype Traffic Signal Structure

To investigate the response of a traffic signal structure under realistic ambient conditions, field experiments were conducted in a natural wind environment. Section 3 should be consulted for information pertaining to structural dimensions, instrumentation, and data acquisition (Wieghaus et al. 2014a). Field monitoring (Section 3) of the standard structure took place from April 24 to September 9, 2012, and the structure with arm strakes installed from September 13 to October 13, 2012. These observations are used here in Section 5.

The helical strakes were attached to the arm using flexible bands (at minimum 3 per strake revolution) adhered to the strake and arm section using a heavy adhesive. Each segment (pitch length) denoted in Figure 3-1(e) represents one complete revolution of the installed strakes. Additional information (dimensions) pertaining to strake installation is presented in Table 5-1, where d_{avg} refers to the average diameter of each tapered arm segment, as denoted in Figure 3-1. The selected configuration was intended to achieve recommended strake size and pitch using a constant diameter strake.

As described in Section 3, one-minute statistics were used to describe the ambient behavior (structural response and weather statistics). Only wind-induced stress responses are included as the structure's location is not near an active roadway. Although response has been attributed to natural wind and traffic gusts, the response due to traffic effects are significantly lower than those due to natural winds (Chen et al. 2001; Albert et al. 2007).

Consequently, it has been assumed that the monitored response is primarily responsible for the fatigue damage to these structures.

Table 5-1. Design parameters for arm strake installation.

Segment	Pitch Length, L_p (mm)	Average Diameter, d_{avg} (mm)	d_{rope} / d_{avg}	L_p / d_{avg}
A	2740	195	0.08	14
B	2445	165	0.10	15
C	2130	140	0.11	15

5.4 Deterministic Fatigue Analysis Methods

Fatigue life using a constant amplitude stress range is typically defined in the form

$$N = A\left(S_r\right)^{-3} \tag{5-1}$$

where S_r = double amplitude (peak-to-trough) stress range amplitude and A = AASHTO fatigue category coefficient as recommended from physical experiments (Frank 1980; Keating and Fisher 1986). The arm-to-base plate welded connection at the arm-pole connection has traditionally been compared against AASHTO Category E' (Fisher et al. 1983). Figure 5-1 presents a comparison of relatively recent traffic signal connection fatigue tests of common traffic signal connections (Koenigs et al. 2003; Roy et al. 2011) against their AASHTO fatigue classification, where $A = 128 \times 10^9$ MPa^3. In the case that the 1-in-10,000 observed stress range exceeds the constant amplitude fatigue limit for infinite life analyses, a straight line extension of the fatigue strength (S-N) curve is to be used in fatigue analyses (Roy et al. 2011).

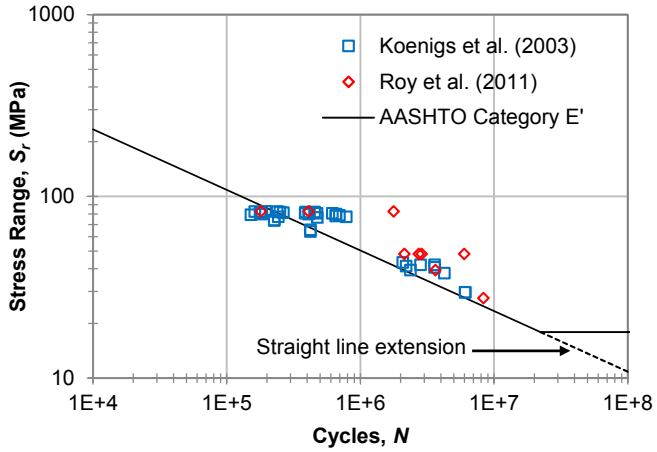

Figure 5-1. Fatigue performance of mast arm-to-base plate connection (cycled about elevated mean stress).

Following calculation of the one-minute responses over the observation period, a measure of fatigue equivalent stress range S_{re} may be used to account for the variability in response at each incremental wind speed. The root mean cube stress range is an equivalent stress range that can be used for fatigue life estimation under variable amplitude stress ranges when using the governing AASHTO fatigue strength (S-N) curves above and below the constant amplitude fatigue limit (Yen et al. 2013). The fatigue equivalent response may be appropriately extrapolated for wind speeds higher than those observed.

The number of stress cycles undergone by the structure per year can be determined as a function of wind speed. Using historical wind records attained from the National Oceanographic and Atmospheric Administration (NOAA) at select locations of interest, probability distribution functions for wind speed may be empirically generated. These functions, along with the first in- and out-of-plane natural frequencies of the structure (1.09 Hz and 0.99 Hz, respectively), may be used to determine the number of cycles n_U for a given wind speed U as

$$n_U = t\, p_U\, f_n \tag{5-2}$$

where $t =$ the period of time under consideration in seconds; $p_U =$ the probability associated with wind speed U; and $f_n =$ the response frequency of the structure in Hertz.

Incorporating the fatigue equivalent stress range response as a function of wind speed, as well as the number of stress cycles expected to occur annually, the distribution of fatigue damage annually accumulated at the arm-pole connection may be found applying Miner's rule (Miner 1945). For the case of traffic signal structure connections,

this damage relationship is evaluated using the AASHTO Category E' fatigue classification. For which case, the total annual damage accumulated may be shown

$$D = \sum_{U} \frac{n_U}{N} = \sum_{U} p_U f_n \left(\frac{S_r}{16} \right)^3 \tag{5-3}$$

where N = the fatigue life (cycles) corresponding to the fatigue equivalent constant amplitude stress range amplitude at each wind speed; and S_r has units of MPa. The inverse of annual fatigue damage is the fatigue or service life as determined using the deterministic means set fourth using AASHTO analysis concepts. Utilizing this procedure allows the effect of natural wind response to be visually related to fatigue damage and thus dependable service life.

5.5 Experimental Observations

The following includes a synopsis and further analysis of the observed one-minute inferred stress response and wind statistics obtained stemming from structural monitoring detailed in Section 3.

5.5.1 Response of Standard (As-Built) Prototype Structure

Figure 5-2 presents the inferred stress range results as a function of wind speed for the standard structure based on experimental observations. As seen in Figure 5-2(a), roughly one-half of all winds approached from a southerly direction. As previously mentioned, a measure of fatigue equivalent stress range was used to account for the variability in response at each incremental wind speed.

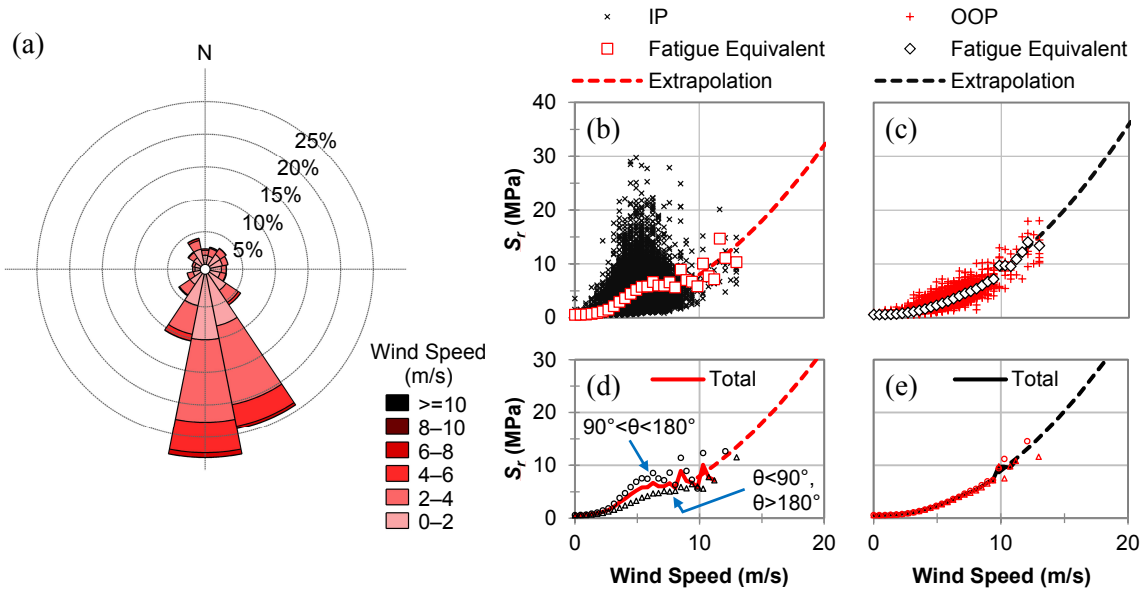

Figure 5-2. **Standard (unmodified) structure: (a) Measured wind conditions, total (b) in-plane (IP) and (c) out-of-plane (OOP) stress responses at the arm-pole connection, (d) IP and (e) OOP fatigue equivalent response as a function of wind speed and direction.**

When comparing the total in- and out-of-plane response at the arm-pole connection as depicted in Figure 5-2(b) and Figure 5-2(c), respectively, it is clear that although the equivalent stress ranges begin similarly, the large dispersion in the across-wind response causes the equivalent response to vary significantly between 3 m/s and 7 m/s. Despite a lack of observed wind speeds greater than 13.5 m/s, fitted trends indicate that out-of-plane response is greater than the in-plane response. This is typically the case with a response that arises due to the unsteady nature of natural winds (buffeting). Because the largest in-plane responses occur when winds approach from the back side of the structure $(90° < \theta < 180°)$, the stress response is greater than when winds approach from the other directions. This variation in low-speed response is depicted in Figure 5-2(d), where the equivalent stress range is shown to vary with wind direction. In contrast, the out-of-plane response appears wind direction invariant in Figure 5-2(e). When studying the fatigue equivalent in- and out-of-plane response, two observations were clear: (i) the response is typically small; and (ii) the in-plane response is more dependent on wind direction at lower wind speeds.

Recall that it was concluded that large-amplitude in-plane observations were influenced by the propensity of signal cluster vortex shedding at lower wind speeds (Wieghaus et al. 2014a). The overall in-plane response is attributed to a combination of vortex shedding, galloping, and natural wind gusts.

As depicted in Figure 5-2, the fatigue equivalent in- and out-of-plane responses were observed to increase with the square of wind speed when not influenced by across-wind effects, thus the extrapolations follow this relation. This response arises due to the

unsteady nature of the along-wind response (buffeting). In a similar fashion, the observations clearly demonstrate that the out-of-plane, fatigue equivalent response is direction independent due to its association with the buffeting.

5.5.2 Response of Structure with Arm Modified with Helical Strakes

Figure 5-3 depicts a summary of the structural response with mast arm strakes installed. As seen in Figure 5-3(a), it was seen that almost one-half of the observed winds approached the structure from the backside. Therefore, a similar proportion of winds found to cause an increased low-speed in-plane response (direction dependent) were measured over the two observation periods. It was thus deemed appropriate to compare results obtained without and with arm strakes installed.

Figure 5-3(b) indicates that the structure's arm-pole connection experienced no inferred one-minute in-plane stress ranges over 12 MPa. With the vast majority of observations being smaller, the structure displayed no tendency to exhibit large across-wind lock-in vibrations. Arm strake installation decreased the in-plane fatigue equivalent stress response, nearly eliminating the influence of vortex-induced vibrations. When comparing the out-of-plane response at the arm-pole connection without and with strakes, the response appears unchanged. The fatigue equivalent in-and out-of-plane responses was extrapolated using the same relationship as used for extrapolating the response of the standard structure as the buffeting response remained similar. The additional drag assumed with strake installation showed no appreciable effect during observation.

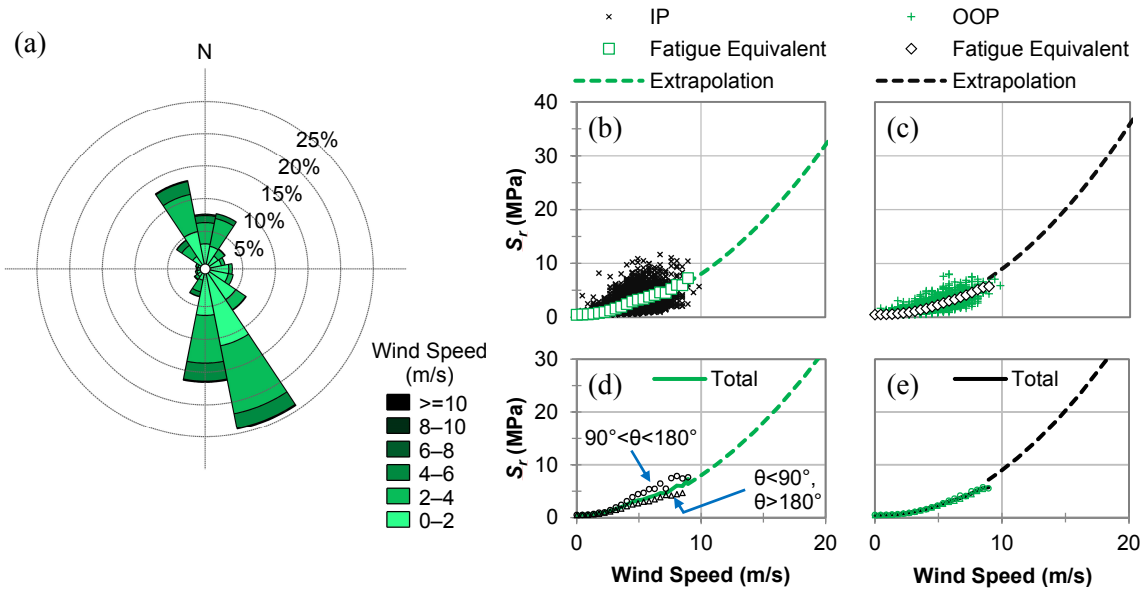

Figure 5-3. Structure with arm strakes: (a) Measured wind conditions, total (b) in-plane (IP) and (c) out-of-plane (OOP) stress responses at the arm-pole connection, (d) IP and (e) OOP fatigue equivalent response as a function of wind speed and direction.

5.6 Fatigue Analysis and Implications

The fatigue life of the structure is estimated considering changes in natural wind response as a result of arm strake installation for several distinct wind environments to assess: (i) the role of vortex shedding on fatigue damage accumulation; and (ii) the effectiveness of helical strake installation to extend the fatigue life. Based on the observed stress response at the pole-to-arm connection before and after strake installation, the fatigue life was estimated based on changes in natural wind response for four distinct wind environments: College Station, TX; Chicago, IL; Corpus Christi, TX; and Cheyenne, WY.

Figure 5-4 not only depicts the process used to characterize the fatigue performance and fatigue life under several distinct wind environments, but more importantly depicts this analysis to determine in-plane fatigue for the standard and straked structure (Figure 5-4(a) and Figure 5-4(b), respectively). The first row depicts the in-plane stress range as a function of wind speed for the responses calculated and extrapolated using the individual one-minute observations at each incremental wind speed reflects the reduction of low-speed across-wind effects. Correlating with the information presented in Figure 5-2 and Figure 5-3, it is evident that the in-plane across-wind fatigue equivalent response below 10 m/s is quite small in comparison to the response above 10 m/s, although it was observed that large, low-speed across-wind responses occur. It should be noted that each response above 10 m/s is based on extrapolation of stress range made previously based on experimental observations, where response extrapolation before and after strake installation is similar.

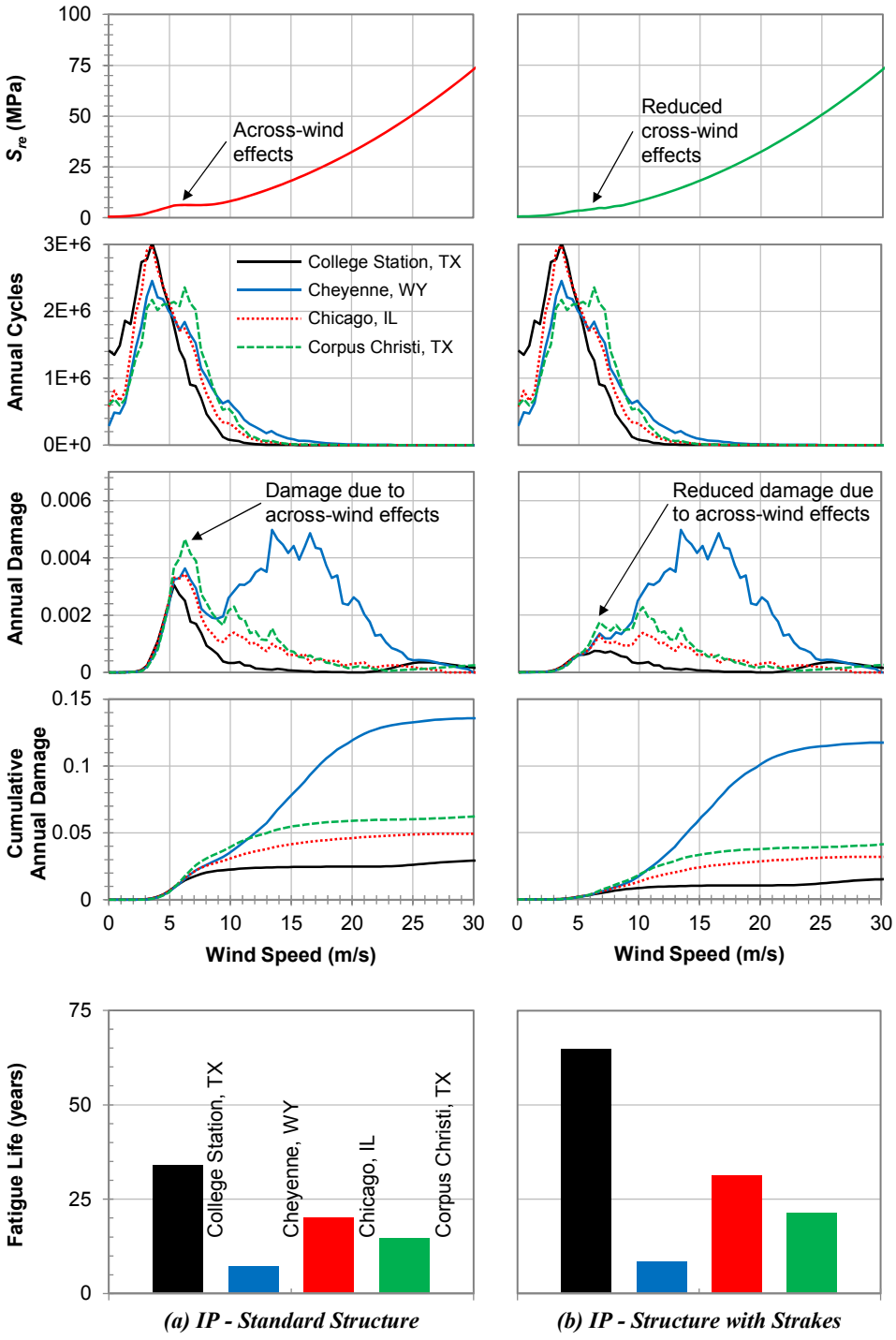

Figure 5-4. The in-plane (IP) fatigue assessment for the (a) standard structure and (b) structure with helical arm strakes installed.

The second row of Figure 5-4 represents the annual number of stress cycles undergone as a function of wind speed, whose shapes resemble the empirical probability distribution at each of the selected locations. The third row depicts the fatigue damage annually incurred as a function of wind speed, where the following row depicts the cumulative fatigue damage incurred over ranging wind speeds, whose sum is the inverse of service life.

As seen in the first column of the presented damage plots in Figure 5-4, a fair amount of fatigue damage occurs atop the arm-pole connection at speeds related to lock-in across-wind effects for the standard traffic signal structure observed. This is apparent in all assessed wind environments. Through visual inspection of the damage plots without and with strakes installed, it is evident that the reduction in in-plane low-speed fatigue equivalent response nearly eliminates all amplified fatigue damage occurring at speeds below 10 m/s. This, however, has little impact on dependable service life unless the structure is located in a rather benign wind environment such as College Station, TX. As evidence, in Cheyenne, WY, where the probability of wind speeds above 10 m/s is quite high, significant fatigue damage is accumulated annually. As a result, for both the standard and straked arm structure in non-benign wind environments, a significant amount of accumulated fatigue damage is attributed to wind speeds over 10 m/s and is thus sensitive to the prevalence of winds above this threshold, as reflected in the service life estimates depicted in the final row of Figure 5-4.

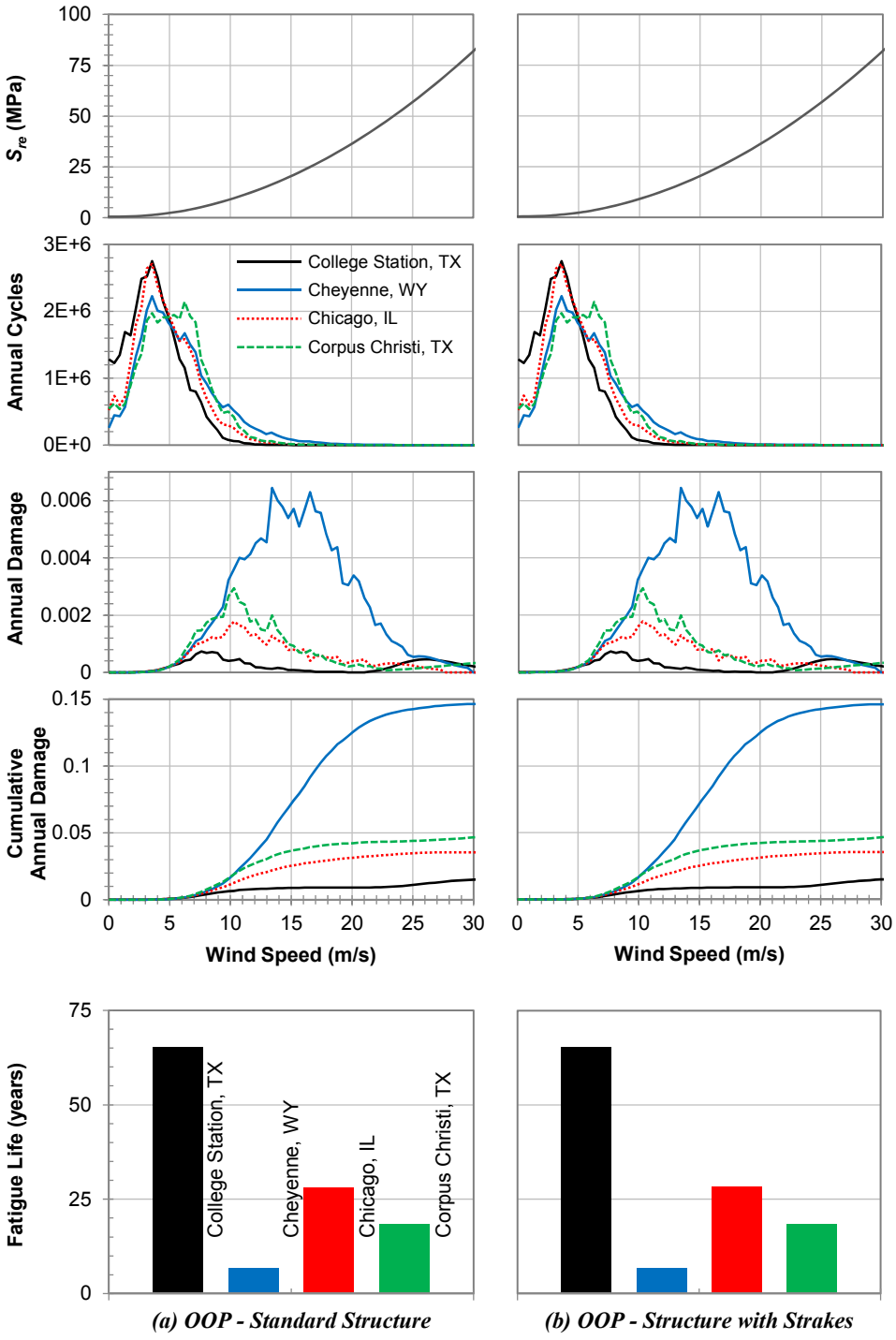

Figure 5-5. The out-of-plane (OOP) fatigue assessment for the (a) standard structure and (b) structure with helical arm strakes installed.

Figure 5-5 presents fatigue analyses to characterize the out-of-plane (along-wind) performance and dependable fatigue life of the traffic signal structure without and with arm strakes installed. Since the out-of-plane behavior of the structure showed little change with the addition of helical arm strakes, the out-of-plane fatigue performance showed little to no change. Further, extrapolated out-of-plane buffeting response is greater than the in-plane buffeting response, thus out-of-plane fatigue may control in certain wind environments. As was previously the case for in-plane fatigue, most out-of-plane fatigue damage accumulated is attributed to wind speeds over 10 m/s, and is thus sensitive to the proportion of winds that occur over this threshold.

5.7 Discussion

Following months of ambient response observations, change in the natural wind response of the structure was studied and quantified using fatigue equivalent parameters. Arm strakes nearly eliminated the influence of vortex-induced vibrations on the stress response. Using inferred one-minute statistics, the fatigue equivalent response was then extrapolated for higher wind speeds, where strake installation was not observed to change the expected response of the structure at high wind speeds. Using historical wind records from four distinct locations in the United States, the fatigue life of the structure was estimated considering any changes in natural wind response for several distinct wind environments to assess: (i) the role of vortex shedding on fatigue damage accumulation; and (ii) the effectiveness of helical strake installation to extend the fatigue life of cantilevered traffic signal structures. Table 5-2 presents service life estimates related to

in- and out-of-plane excitation, as each separately results in damaging stress reversals at different locations along the welded connection detail.

Table 5-2. Location-based service life estimates based on historical wind records and inferred structural response.

Location	Mean Annual Wind Speed (m/s)	Configuration	In-plane Service Life (years)	Out-of-plane Service Life (years)
College Station, TX	3.6	Standard	**33.9**	65.1
		Arm Strakes	**64.8**	65.3
Chicago, IL	4.6	Standard	**20.2**	28.1
		Arm Strakes	**31.4**	28.2
Corpus Christi, TX	5.3	Standard	**14.6**	18.5
		Arm Strakes	21.3	**18.5**
Cheyenne, WY	5.7	Standard	7.3	**6.8**
		Arm Strakes	8.5	**6.8**

*Critical case is in bold typeface

To relate these results against inspection records, Cheyenne, WY, was used for comparison. Based on the analyses performed, the predicted fatigue life in that wind environment is approximately 7 years (using Category E' extended). Previously compiled inspection records (Price et al. 2008) for 172 similar traffic signal structures in Cheyenne, WY, were statistically analyzed assuming random, right-sided censoring. Based on this analysis, the 2.5 percent non-exceedance probability corresponding to fatigue crack formation and/or detection relates to a life of approximately 8 years (Wieghaus et al. 2014d). Given the uncertainty in the fatigue resistance of these connections and that the fatigue category E' is assigned somewhat conservatively (Keating and Fisher 1986), it is

not unreasonable that this AASHTO-type analysis would yield a dependable service life of some 7 years in that wind environment.

Based on the findings of the performed research as presented in Table 5-2, it is clear that the effectiveness of helical arm strakes as a service life mitigation strategy depends greatly on wind environment. Figure 5-6 depicts the impact of regional wind environment on the effectiveness of helical strake installation. Figure 5-6(a) graphically depicts the results of the preceding fatigue analysis, fit with respect to wind speed. Additionally, regions are identified depicting the benefit of arm strake installation. As seen, the effectiveness of helical strake installation increases with decreasing mean annual wind speed. To further categorize wind environment, Figure 5-6(b) relates the portion of commonly occurring winds below 10 m/s to damage accumulation. It can be seen that the corresponding fatigue life estimates directly coincide with this wind speed portion, where Cheyenne, WY, has the least expected life and College Station, TX, has the greatest. The effectiveness of mast arm strakes is related to the portion of winds that occur below 10 m/s, a measure to quantify the severity of the wind environment, whereas Figure 5-4 and Figure 5-5 demonstrate the influence of winds above 10 m/s on the fatigue service life of traffic signal structures.

During fatigue assessments, empirical distributions based on wind records attained from NOAA were used to describe wind speed distribution; extreme wind climatology was not incorporated into the analysis. Taking into account the probability of large windstorm events lessens the effectiveness of arm strakes in extending dependable life, however not significantly as it has been shown that more prominent winds are responsible

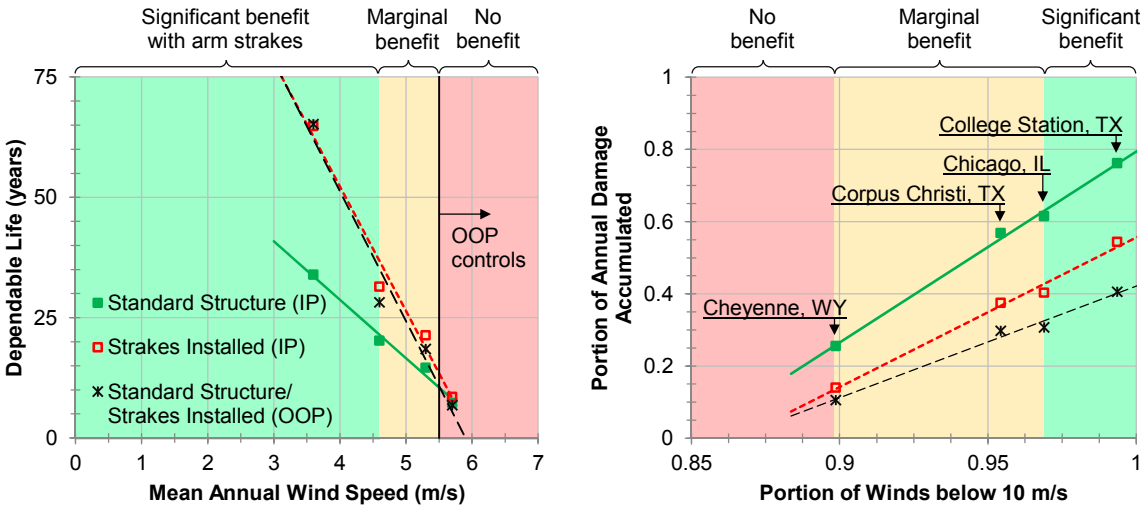

(a) Dependable life with mean wind speed

(b) Common wind influence on damage accumulation

Figure 5-6. Influence of local wind environment on arm strake mitigation viability.

for most fatigue damage accumulation. During an extreme wind event, however, the effectiveness of helical arm strakes in vibration and fatigue mitigation diminishes. Since arm strake installation only reduces the influence of across-wind effects at low wind speeds, it does not reduce the fatigue damage accumulated during high wind speed events where significant damage occurs. For this reason, the structure remains susceptible to large decreases in service life due to extreme events.

In addition to the work presented herein, further natural wind testing in conjunction with computational modeling should be conducted to further investigate the efficacy of helical mast arm strakes for a broader variety of traffic signal structure dimensions and attachment configurations. It may be possible for future developments to further improve strake effectiveness with the potential for in-plane dependable life to surpass the life related to out-of-plane excitation. Therefore, it is also important to strive for improved performance for out-of-plane motion. One possibility may be to use louvered signal cluster (visual) backplates or other damping devices (tuned mass or viscous) to further reduce out-of-plane response. While these methods reduce the fatigue demand, it is considered more important to improve the fatigue resistance capacity.

5.8 Closure and Key Findings

Based on recent findings that identify vortex shedding as a significant excitation mechanism responsible for amplified across-wind traffic signal structure responses at low wind speeds, helical strakes were installed to reduce wind-induced response. To investigate the response of a traffic signal structure without and with helical arm strakes, field experiments were conducted in a natural wind environment. The installation of

traditionally-effective helical arm strakes to the cantilevered traffic signal structure mast arm significantly reduced the large amplitude response associated with vortex shedding of the signal clusters. This demonstrates that helical strakes can effectively disrupt the formation of a boundary layer and vortex formation on the back side of the signal clusters. Consequently, helical arm strakes are effective in reducing across-wind response at low wind speeds.

The following findings are drawn based on the experiments and analyses described herein:

i. The effectiveness of helical arm strake installation in improving the service life of cantilevered traffic signal structures greatly depends on the role of across-wind effects, and in particular vortex shedding, on fatigue damage accumulation. Arm strake installation has been shown to be very effective at reducing in-plane across-wind effects at low wind speeds, thus greatly reducing fatigue damage accumulated at those speeds. As a result, the practical benefit of helical arm strake installation on service life depends on local wind environment, where over 90 percent of all winds should be below 10 m/s.

ii. Because helical arm strakes did little to change the out-of-plane response of the cantilevered traffic signal structure, their installation is of little benefit, if any, in increasing the out-of-plane service life as assessed in this work. Unfortunately, the installation of helical arm strakes is not a panacea for mitigating connection fatigue.

iii. Although strakes were shown to be effective at reducing in-plane fatigue damage accumulation for existing structures in mild wind environments, alternative fatigue mitigation measures should be sought in an effort to find a single mitigation solution effective across all wind environments. Instead of attempting to mitigate fatigue by reducing the demand, new methods are emerging whereby the improved fatigue resistance (capacity) is achieved through connection PT.

6 PROBABILISTIC FATIGUE (FRAGILITY) ANALYSIS OF WIND-EXCITED TRAFFIC SIGNAL STRUCTURES (WITHOUT HELICAL ARM STRAKES)

6.1 Overview

Traffic signal structures are prone to fatigue failure due to wind-induced excitation that is often difficult to characterize due to the variable response arising from a combinations of along- and across-wind effects and the uncertainties associated with the fatigue and fracture phenomena. A probabilistic framework is proposed to predict structure component fatigue life. To solve the problem of wind-induced fatigue, the model is introduced to inter-relate wind hazard to structural response and hence fatigue damage. Stress range demand variabilities are considered separately from the randomness associated with the fatigue capacity. To characterize the natural wind response of a representative structure, full-scale structural monitoring is conducted, and the data were incorporated into an example application of the framework. To successfully demonstrate the efficacy of the proposed framework, resulting wind-induced fatigue life distributions are compared against compiled inspection records for a large traffic signal structure population in Wyoming.

6.2 Introduction

Traffic signal structures of the type studied in this dissertation are commonly used at intersections and other locations. Due to the lack of redundancy and increasing span

length of these structures, connection fatigue, particularly at the arm-to-pole joint, is increasingly becoming of concern, especially for existing, aging structures.

In this section, the viability of modeling wind-induced fatigue damage and hence the fatigue life of a steel structure using a direct probabilistic approach is investigated. The accumulation of fatigue damage in lightweight, wind-excited structures can be estimated by modifying the four-step direct approach of (Mander et al. 2012), which builds upon the developments of previous work in seismic risk assessment (Dhakal and Mander 2006; Mander et al. 2007; Solberg et al. 2008). Specific to the work presented herein, the framework is divided into four subtasks, namely: (a) wind hazard analysis which defines the hazard intensity (wind speed) at a particular location; (b) the observed structural response that relates cyclic stress amplitudes to wind speed excitation for a structure; (c) the fatigue damage analysis which is related to cyclic stress amplitudes for as-built structural details; and (d) probable fatigue-life estimation, from which the annual rate of damage and hence fatigue life (fragility) can be assessed.

One underlying problem related in determining the fatigue life of lightweight steel traffic signal structures due to wind excitation has been the lack of consensus in determining the excitation mechanism responsible for large amplitude vibrations (McDonald et al. 1995; Letchford et al. 2008; Zuo and Letchford 2010; Cruzado et al. 2013; Wieghaus et al. 2014a). To this point, several advanced quantitative assessment techniques have been proposed to determine the fatigue life of wind-excited steel pole structures (Robertson et al. 2001; Holmes 2002; Peil and Behrens 2002; Robertson et al. 2004; Goode and van de Lindt 2007; Repetto and Solari 2008, 2012), but each requires a

good understanding of the excitation mechanisms for modeling purposes. Such techniques can be computationally intensive. Works specifically oriented to assess the fatigue life of cantilevered signal structures have also had shortcomings. The response of these structures have been based on the full-scale response of a structure excited by a single blower (South 1994), the brief response following natural wind gusts (Chen et al. 2001), or scaled wind tunnel results where the scale factor was not precisely known (Letchford et al. 2008). If fatigue is to be fully addressed in a probabilistic fashion, the structural response demands due to natural wind must also, where such demands are compared with the probabilistic fatigue capacity of the critical fatigue-prone connections.

Unlike past works (South 1994; Chen et al. 2001; Letchford et al. 2008), or recently recommended deterministic methods (Roy et al. 2011), to estimate the fatigue life of steel support structures, aleatoric and epistemic uncertainties present in the analysis must be considered. The research described herein modifies and expands upon the approach presented in (Mander et al. 2012) to quantify fatigue damage accumulated by lightweight steel traffic support structures under natural wind excitation. This information, along with quantified uncertainties, is used to form probability-based fatigue life fragility curves for these wind-excited structures. Thus, dependable service life may be specified at a given level of non-exceedance.

As a result, this section first explains the four-step methodology specifically cast to predict the fatigue life of lightweight wind-excited steel structures in a probabilistic (fragility) manner. To illustrate the application of the proposed method, each step in the framework is detailed to enable the determination of fatigue damage accumulation in

cantilevered signal structures due to natural wind excitations. Differing from previous works, structural response is based on long-term field observations of stress range versus wind speed of a prototype structure in Bryan, TX, depicted in Figure 3-1(a) with dimensions given in Figure 3-1(b). To successfully demonstrate the efficacy of the proposed framework, resulting wind-induced fatigue life distributions are compared to analysis performed on compiled inspection records for a large population of structures in southern Wyoming. Based on ease of implementation and the quality of results derived from the analyses performed herein, the proposed risk assessment methodology demonstrates promise for application in other areas.

6.3 Theoretical Direct Damage Estimation Framework

The four-step approach is introduced to estimate the fatigue damage accumulated in fatigue-prone connections of wind-excited structures by relating damage levels to recurrence rate. Each step in the framework is based on the central tendency, or median, of each involved variable. Shown in Figure 6-1, the primary objective of the direct four-step approach in computing fatigue life is to relate the estimated damage to (local wind) demands and structural capacity measures. Figure 6-1 visually demonstrates the interaction of the four plots, from (a) to (d), when plotted using log-log scales. These inter-relationships are best described using piecewise power functions and are described in the following paragraphs.

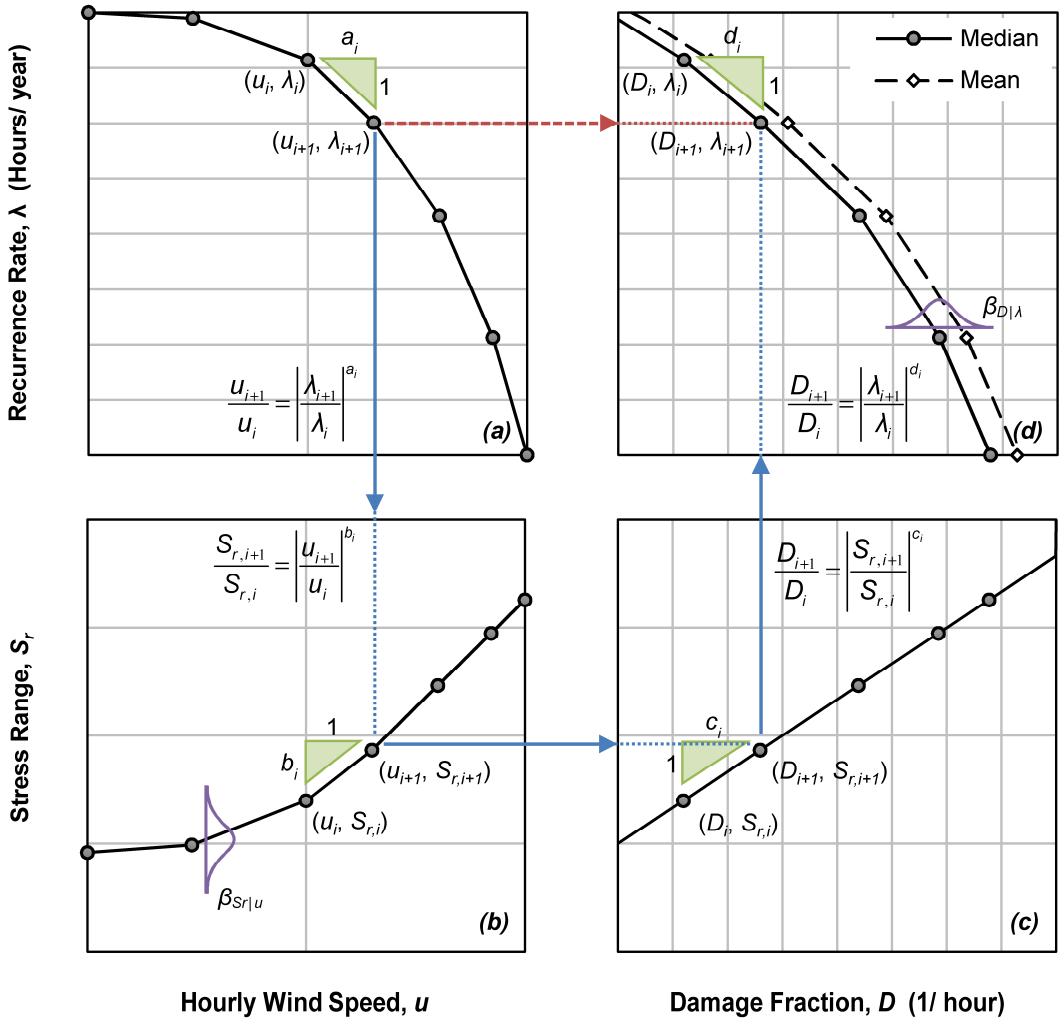

Figure 6-1. **Quantitative risk assessment of fatigue damage: (a) wind hazard recurrence rate for a given wind speed, (b) imposed stress range vs. wind speed, (c) damage arising from the imposed range, (d) damage fraction vs. its recurrence rate.**

Power functions may be used based on the observation that most of the relationships represented in Figure 6-1 can be simplified as linear segments in log-log space. The interaction of the four-step damage estimation approach may be consolidated to a single compound equation

$$\frac{D_{i+1}}{D_i} = \left|\frac{S_{r,i+1}}{S_{r,i}}\right|^{c_i} = \left|\frac{u_{i+1}}{u_i}\right|^{b_i c_i} = \left|\frac{\lambda_{i+1}}{\lambda_i}\right|^{a_i b_i c_i} \tag{6-1}$$

where $D =$ damage fraction; $S_r =$ stress range; $u =$ wind speed; and $\lambda =$ recurrence rate for a given wind speed. The alphabetically related exponents are equal to the slopes in log-log space of graphs a, b, c, and d of Figure 6-1 between points i and $i+1$, respectively. The relationships presented in Eq. (6-1) and the graphical representation hold true because the scales of two neighboring plots (one beside and one above/below) have similarly scaled axes.

6.3.1 Local Hazard Model

The first subtask in the proposed methodology involves analyzing the wind hazard at a particular location. Beginning with Figure 6-1(a), the local wind hazard is represented by relating a wind intensity measure, the hourly mean wind speed u, to the recurrence rate λ of events $U > u$ in hours per year. When discretized, the power function for each linear segment relates wind speed to recurrence rate by

$$\frac{u}{u_i} = \left|\frac{\lambda}{\lambda_i}\right|^{a_i} \tag{6-2}$$

over the interval $u_i < u < u_{i+1}$ where a_i is determined between consecutive points.

For example, the local wind environment is characterized by the wind hazard model at a specific location. As exemplified in Figure 6-2(a), historical hourly wind records near the test site in Bryan, TX (Easterwood Airport, College Station, TX, 11 km from the installed test structure) are attained from the National Oceanic and Atmospheric Administration (NOAA) and analyzed independent of wind direction. An empirical probability distribution function of hour-averaged wind speeds may be generated from the historical records. Extreme wind climatology is taken into account to evaluate the stress response that may occur during the life of a traffic support structure. If wind records are over 20 years in length, it is reasonable to extrapolate the probability density for winds with a recurrence rate $\lambda < 1$ hour/year (return period for hourly wind speed greater than one year). Thus, an Extreme Type I (Gumbel) distribution may be used to fit to the extreme data from the attained records (Simiu and Scanlan 1996). Recurrence rates are then determined using the composite cumulative distribution of wind speed.

6.3.2 Structural Response Model

The second subtask in the proposed framework involves structural response analysis relating stress response to a given level of wind excitation for a particular structure. Following the arrow downward from the point in Figure 6-1(a) to a correlating point on the curve shown in Figure 6-1(b), it is shown that the structural response, represented here as a double amplitude (peak-to-trough) stress range S_r, results from the selected wind speed with a specific recurrence rate λ. A piecewise power function is also used to relate consecutive points along the structural response model, as indicated in Figure 6-1(b).

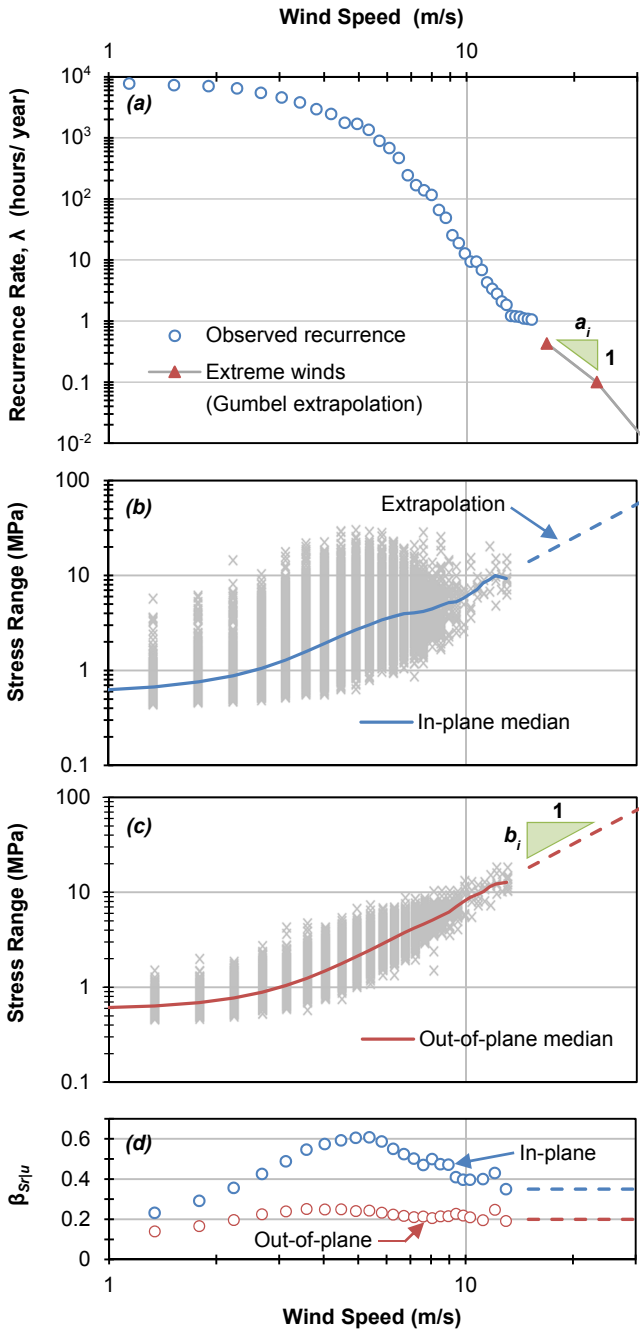

Figure 6-2. **Natural wind (a) hazard recurrence based on observations and extrapolation for extreme events, (b,c) nominal wind-induced response and (d) dispersion at the fillet weld of the arm-to-end plate connection.**

When conducting fatigue life analyses, demand-side uncertainty is related to structural response where the variabilities that exist between wind speed and response are due to directional and dynamic (random) effects due to the spatially unsteady nature of most common natural wind fields (Wieghaus et al. 2014a). Instead of using a response model based on upper bound design curves founded on effective static pressures, scaled wind tunnel results, or the results of numerical simulation, where each would require additional uncertainty quantification, the proposed framework herein incorporates the median and dispersion of the observed stress range response. At each discrete wind speed, a statistical analysis is performed on the response. Since concurrent analysis has shown that both in-plane and out-of-plane response components can be characterized statistically by a lognormal distribution (Wieghaus et al. 2014a), the lognormal standard deviation $\beta_{Sr|u}$ is used to describe the randomness in response due to variations in wind speed and direction.

Results from full-scale structural monitoring may be (but not necessarily) observationally (empirically) derived, extrapolated if necessary, and implemented within the proposed framework to eliminate the epistemic uncertainty associated with modeling assumptions. However, a full scale experimental approach has the disadvantage related to the need to instrument and observe response for a certain time. Alternative approaches may be considered to model natural wind-induced structural response and its associated uncertainty.

Both the in-plane and out-of-plane structure response to natural winds need to be considered. In-plane and out-of-plane stresses refer to stresses at the connection due to

vertical and horizontal arm deflections, respectively. Because in-plane vibrations refer to the vertical motions caused by across-wind effects or the component of along-wind buffeting that takes place in the plane of the structure, these cyclic stresses result in fatigue damage accumulation at the top and bottom of the welded arm-to-end plate connection. Conversely, out-of-plane vibrations refer to horizontal arm motions resulting from along-wind drag effects, thus the induced stresses and fatigue accumulation occurs at the sides of the connection.

Figure 6-2 also presents experimental observations for the stress range versus wind speed to characterize response for the test structure in Bryan, TX. Figure 6-2(b) and Figure 6-2(c) present the one-minute in- and out-of-plane stress responses, respectively, plotted independent of wind direction with respect to the structure. As shown in Figure 6-2, the median monitored response (graphs b and c) and dispersion parameter $\beta_{Sr|u}$ (graph d) are determined at each wind speed increment. At higher wind speeds, the median in- and out-of-plane responses are expected to increase with the square of wind speed, as indicated by well-known theory and design standard specifications (AASHTO 2013). As a result, the exponent $b = 2$ is assumed for extrapolating the response for wind speeds higher than observed.

6.3.3 Damage Model

When moving right from Figure 6-1(b) to Figure 6-1(c), the structural response is related to an hourly fatigue damage fraction. Thus, the third subtask involves performing a fatigue damage analysis derived from past fatigue test results for a given connection detail, or for the case of traffic signal structures, a family of similar connections. The

damage model shown in Figure 6-1(c) does not indicate randomness in the fatigue resistance of the connection, because capacity-side uncertainty is quantified and aggregated separately—this is discussed later herein.

Figure 6-3 depicts the calibration and uncertainty quantification related to the damage model for several details related to tube-to-transverse base plate connections common to traffic signal structures. Fatigue test results presented in past works (Miki et al. 1981; Alderson 1999; Koenigs et al. 2003; Roy et al. 2011) were selected to calibrate the damage model, and are inclusive of a variety of representative materials and common arm-pole connection details used in the field. Common practice utilizes AASHTO (2013) fatigue strength (S-N) curves to relate the number of constant amplitude cycles N that leads to fatigue cracking as

$$N = A\left(S_r\right)^{-3} \tag{6-3}$$

where $S_r =$ the peak-to-trough stress range amplitude and $A =$ the AASHTO fatigue category coefficient determined from physical experiments. In practice, designers neglect the influence of mean stress, thus it shall too be during analysis in this section. To be consistent with notation utilized in the proposed framework, the traditional form of the design equation is recast in terms of damage per cycle $D = \left(N\right)^{-1}$ for a given stress range S_r by

$$\frac{D_{i+1}}{D_i} = \left|\frac{N_{i+1}}{N_i}\right|^{-1} = \left|\frac{S_{r,i+1}}{S_{r,i}}\right|^{3} \tag{6-4}$$

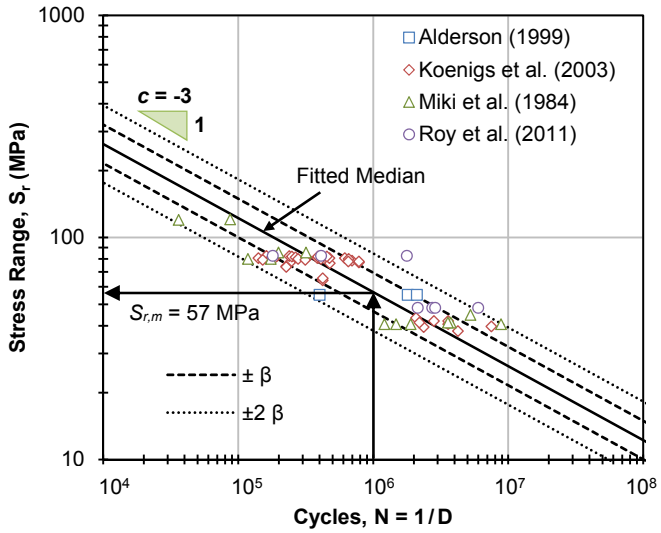

(a) Fatigue life test results from various investigators

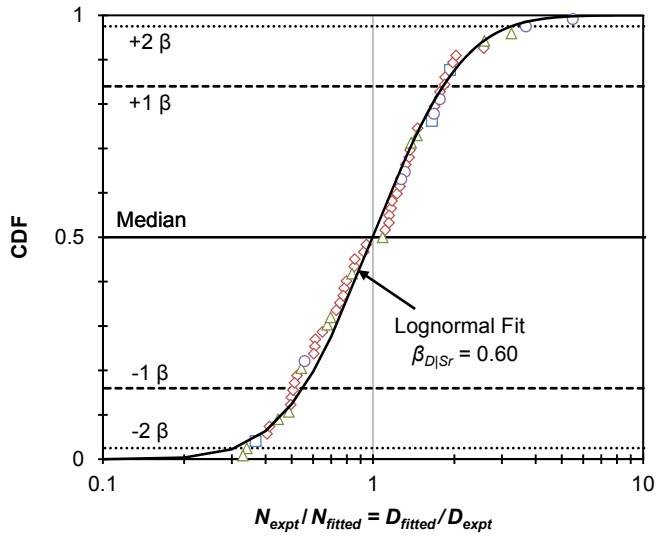

(b) Variability in fatigue test data

Figure 6-3. Fatigue performance of common arm-to-end plate connection.

as shown in Figure 6-1(c). The hourly fatigue damage incurred by a connected part may be found from the number of cycles per hour by

$$D_{hr} = \frac{0.0036}{T_n}\left|\frac{S_r}{S_{r,m}}\right|^3 \tag{6-5}$$

where $T_n =$ the natural period of the structure in seconds and $S_{r,m} =$ the calibrated stress range that would lead to failure at one million cycles as shown in Figure 6-3(a).

The lognormal standard deviation $\beta_{D|Sr}$ is used to represent the variability in the observed damage per cycle. As shown for the specific test results in Figure 6-3, a best fit to the two-parameter lognormal distribution is given by $S_{r,m} = 57\,\text{MPa}$ and $\beta_{D|Sr} = 0.60$. The lognormal standard deviation $\beta_{D|Sr}$ is synonymous to the randomness in connection fatigue resistance (or capacity) β_{FR} based on their inverse relationship, thus $\beta_{FR} = \beta_{D|Sr}$.

6.3.4 Relating Hazard to Damage

The final and fourth subtask, which leads to estimation of probable fatigue life, relates the hazard rate to the incurred damage fraction as shown in Figure 6-1(d) where Eq. (6-1) is contracted to

$$\frac{D_{i+1}}{D_i} = \left|\frac{\lambda_{i+1}}{\lambda_i}\right|^{d_i} \tag{6-6}$$

where $d_i = a_i b_i c_i$ between points i and $i+1$.

6.3.5 Accounting for Demand-Side Variabilities in Damage Estimation

It should be noted that the variability for a given stress range response given wind speed $\beta_{Sr|u}$, propagates through Eq. (6-1) and consequently affects the damage outcome as a function of the powers a, b, c, and hence d.

Variabilities correspond to both uncertainty and randomness involved in estimating the demand and capacity of the structure (Kennedy et al. 1980). To this point, median parameters or curves have been used to introduce the four-step fatigue damage framework in an effort to describe central tendency. In the present context, demand-side variability is attributed to randomness in wind-induced response (Wieghaus et al. 2014a). Each point on the developed curves may be described as a lognormal random variable; the central limit theorem states that a distribution of a random variable that depends on numerous external factors tends to be lognormal. The median damage-rate curve formed in Figure 6-1(d) is transformed into an expected value (mean) damage-rate relationship derived from the arithmetic moments of the lognormal distribution after quantifying degree of uncertainty in the response model $\beta_{Sr|u}$.

Because capacity-side randomness of fatigue resistance at the connection is considered separately; the damage model remains crisp. Therefore, an implication of using the lognormal distribution to describe dispersion in accumulated damage given recurrence rate may be expressed as a function of the inter-relation (slopes) of the four plots as

$$\beta_{D|\lambda,i} = \frac{d_i}{a_i}\left(\frac{\beta_{Sr|u,i}}{b_i}\right) = c_i \beta_{Sr|u,i} \tag{6-7}$$

The expected damage-rate curve is then formed where the expected value of the damage fraction is piecewise related to dispersion in structural response, as shown in Figure 6-1(d).

6.3.6 Computing Expected Annual Damage Rate and Fatigue Service Life

Following the incremental formation of the expected damage-rate curve as shown in Figure 6-1(d), expected annual damage accumulation can be determined. By applying Miner's hypothesis (Miner 1945), the area beneath the expected damage-recurrence curve represents the expected annual damage rate (EADR) and is calculated via integration of the expected annual damage-rate curve with respect to recurrence rate by

$$\text{EADR} = \int \bar{D}(\lambda)\,\mathrm{d}\lambda = \sum_{i=1}^{M} \frac{1}{\bar{d}_i + 1}\left(\bar{D}_i \lambda_i - \bar{D}_{i+1}\lambda_{i+1}\right) \tag{6-8}$$

in which $M =$ the number of discretizations used during integration; $\bar{D} =$ mean damage fraction which for a lognormal distribution is connected to the median $\tilde{D}$ via the relationship

$$\bar{D} = \tilde{D}\exp\left(\frac{1}{2}\beta_{D|\lambda}^2\right) = \tilde{D}\exp\left(\frac{1}{2}c^2\beta_{Sr|u}^2\right) \tag{6-9}$$

The formulation of Eq. (6-8) takes into account not only the probabilistic recurrence rate associated with possible wind conditions, but also the variability in structural stress response. Because this formulation incorporates a well-described response variability at incremental wind speeds while performing a piece-wise integration of damage over all wind hazard recurrence rates (based on long historical records), this value may be viewed as nearly-deterministic. That is, EADR is not expected to vary significantly from year-to-

year while considered for a single location. Therefore, the inverse of the EADR is the expected fatigue life of the structure in years, thus $T_f = \left(\bar{D}\right)^{-1}$.

Given the negligible variation in EADR (and thus T_f), fatigue life is assumed herein to behave as a lognormally distributed random variable modeled using the parameter assigned to randomness in connection fatigue resistance (or capacity) β_{FR}. This approach is consistent with that proposed and implemented by Goode and van de Lindt (2007). As a result, service life T_s related to a specified non-exceedance probability of failure p_f, is calculated as

$$T_s = T_f \exp\left(\Phi^{-1}\left(p_f\right)\beta_{FR}\right) \tag{6-10}$$

where $\Phi^{-1} =$ the inverse of the standard normal cumulative probability function.

6.4 Application: Test Structure in Bryan/College Station, Texas

To demonstrate application of the proposed probabilistic fatigue risk framework, a fatigue study for the test structure located at Texas A&M University's Riverside Campus in Bryan, TX is presented. The following section details: quantifying the location's wind hazard-rate relationships, determining wind-induced response for the representative test structure, quantifying connection fatigue resistance, and calculating the service life of the structure.

Figure 6-2(a) depicts the formation of the wind hazard at Easterwood Airport in neighboring College Station, TX, located 11 km from the installed test structure, derived using wind data obtained from NOAA. As described in Section 6.3.1, recurrence rates

based on an empirical probability distribution function are used for hourly winds with a return period of a year or less, whereas the Gumbel distribution are used for winds with a return period greater than a year.

To directly determine the median and dispersion in the response of the structure under realistic ambient conditions, results from field experiments conducted in Section 3 were consulted (Wieghaus et al. 2014a,b). The traffic signal depicted in Figure 3-1 was oriented to achieve maximum response to the local wind environment by allowing prevailing winds to approach the structure from the back side of the attached signal clusters (the reverse side of the structure from that depicted in Figure 3-1). Such approaching winds have been shown to lead to an amplified response (McDonald et al. 1995; Kaczinski et al. 1998; Letchford et al. 2008; Zuo and Letchford 2010; Cruzado et al. 2013; Wieghaus et al. 2014a,b).

As depicted in Figure 3-1(c), strain gages were placed on the horizontal mast arm section near the arm-pole connection and on the vertical pole section near the pole-base connection to measure in- and out-of-plane bending strains at each location. Section 3 (Wieghaus et al. 2014a) should be consulted for information pertaining to structural dimensions, strain gage/anemometer instrumentation, data acquisition, and data post-processing.

One-minute statistics were used to describe wind (speed and direction) and structural response in terms of stress range; experimentally determined in- and out-of-plane natural periods of the signal support structure were 0.92 s and 1.01 s, respectively, with field measured damping ratios of 0.25 percent and 0.62 percent.

Although response has been attributed to natural wind effects and traffic gusts, the response due to traffic effects is significantly lower than those due to natural winds (Chen et al. 2001; Albert et al. 2007). It is thus assumed that the monitored response is primarily responsible for the fatigue damage to these structures.

Figure 6-2 summarizes the resulting one-minute in- and out-of-plane stress responses inferred at the arm-pole connection plotted as a function of wind speed, independent of wind direction with respect to the structure. Details of the arm-pole connection are most commonly the critical location for fatigue failure, as the arm-pole connection experiences the largest strain-reversals. In-plane response at low wind speeds is influenced by across-wind affects, leading to a slight amplification in median response. As a result of concurrent findings, the median and lognormal standard deviation of the response are determined for each incremental wind speed (Wieghaus et al. 2014a). Figure 6-2(d) presents the observed variability in the in- and out-of-plane responses. High wind speed response is attributed to two-dimensional buffeting behavior and the variability is extrapolated as shown in Figure 6-2(d).

Previous work has studied the directional dependence of response and its effect on fatigue life estimates (Wieghaus et al. 2014a,b). The in-plane median response and its dispersion was found to be relatively dependent on the proportion of winds approaching the backside of the signal clusters ($\pm 45°$ from perpendicular). During observation, roughly half of all winds approached from the backside of the structure. Thus, the resulting in-plane response model is best paired only with natural wind environments with similar

wind distributions. Conversely, out-of-plane structural response was independent of wind direction.

Formulation of the damage model is presented in Eq. (6-5) where $S_{r,m} = 57\,\text{MPa}$. The dispersion parameter used to represent randomness in fatigue test results also describes randomness in fatigue life, thus $\beta_{N|Sr} = \beta_{FL} = 0.60$.

6.4.1 Fatigue Evaluation of Traffic Support Structure

The proposed approach is implemented to create the damage-rate relationship curve as summarized in Eqs. (6-1) and (6-6). Figure 6-4 depicts implementation of the four-step approach for the structure in Bryan/College Station, TX. Figure 6-4(a) depicts the local wind hazard model, Figure 6-4(b) depicts the description of the natural wind in-plane stress response, and Figure 6-4(c) is the typical traffic signal structure connection damage model representing the median of the fatigue test results. Shown in Figure 6-4(d) is the median and expected (mean) damage curves, where the latter is derived from the former using Eq. (6-9). As depicted by the shaded region in Figure 6-4(d), implementation of Eq. (6-8) indicates that the determined EADR for the monitored structure in its current location is 0.0091/year, thus the expected fatigue life is $T_f = 109$ years. The fatigue service life of the structure may then be related to a specified non-exceedance probability after considering randomness in fatigue resistance via Eq. (6-10). For example, if dependable service life is defined by the 2.5 percent target non-exceedence probability and $\beta_{FL} = 0.60$, then using Eq. (6-10) yields a dependable service life of $T_s = 33$ years.

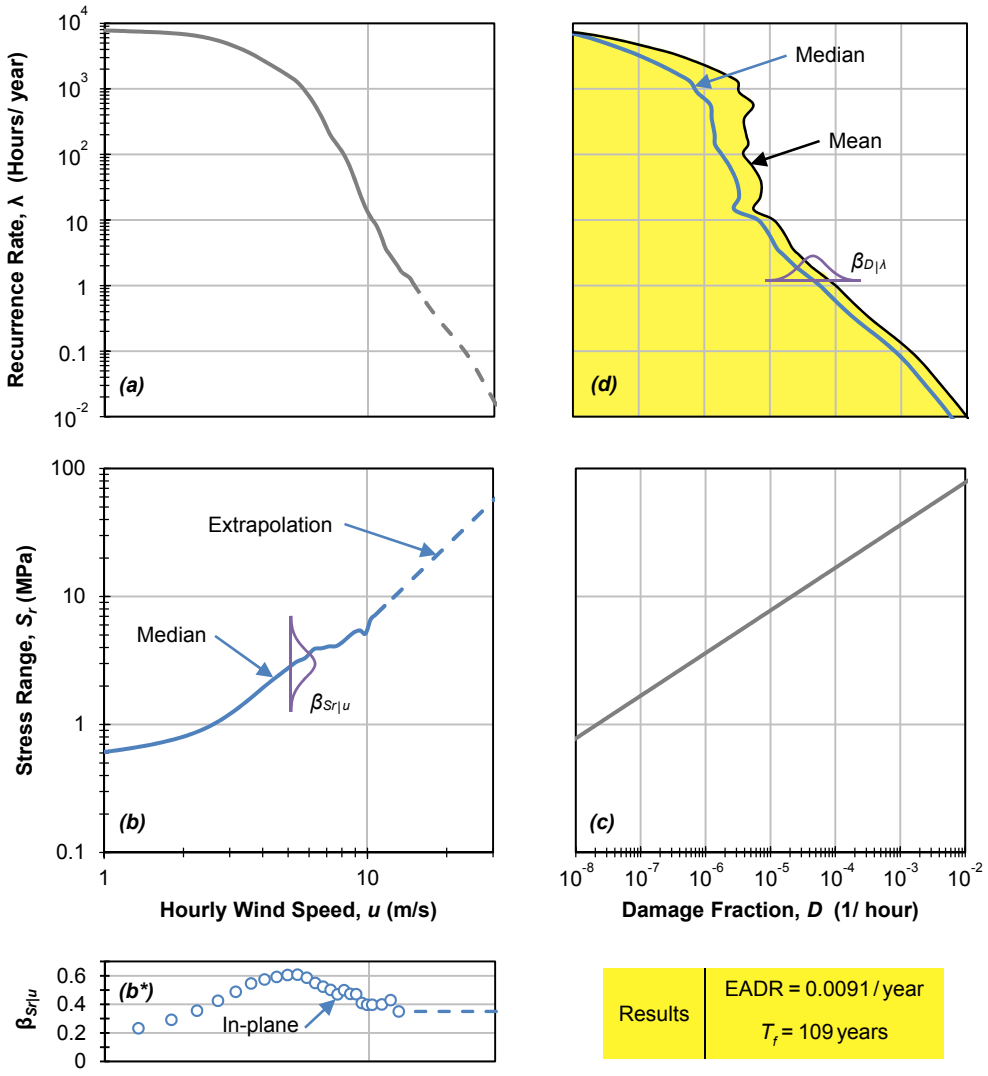

Figure 6-4. **Four-plot assembly for the studied traffic signal structure in Bryan/College Station, TX, incorporating the uncertainties to predict the annual fatigue damage rate and hence expected life. The process starts with (a) defining the wind hazard at the site, (b,b*) the measured (in-plane) stress range response and dispersion, (c) calibrated damage model, and (d) annual damage rate analysis, as represented by the shaded area.**

As indicated by the probabilistic fatigue analysis for the test structure located in Bryan/College Station, TX, the resulting expected fatigue life is rather high due to the relatively benign local winds. To demonstrate the utility of the proposed quantitative risk framework, the effect of wind hazard exposure on fatigue life is now investigated for harsher environments where traffic signal structure fatigue has been of noted concern.

6.5 Effect of Wind Hazard Exposure on Fatigue Life

A comprehensive regional study was conducted by Price et al. (2008) who investigated fatigue failures in traffic signal structures in several states. Of particular interest is southern Wyoming where the integrity of numerous traffic signal support structures was reported along with observed fatigue life failure statistics. Herein, the results for the Wyoming cities of Cheyenne, Laramie, and Rock Springs were selected. The top two rows of Figure 6-5 present the wind direction (rose plot) and wind hazard for each location. Each wind hazard model was substituted into the previously used framework. Although signal clusters in southern Wyoming may be hung vertically, the current response model was deemed valid due to the large dispersion observed. Regardless of signal cluster orientation, similarly sized vertical and horizontal signal clusters are expected to cause a similar buffeting response, along with slight variations due to the vortex shedding mechanism. Given the severity of the wind environment in southern Wyoming, the influence of vortex shedding is reduced (Wieghaus et al. 2014b). As seen, prevailing winds in each location constitute between approximately 45 percent and 60 percent of the total when a 90° azimuth range is considered.

Figure 6-5 presents the results for the Wyoming regional fatigue analyses and compares with the Bryan/College Station, TX case. The third row of Figure 6-5 presents the annual damage distribution function (DDF/yr) with respect to wind speed for each wind environment. Each relates the piecewise accumulated damage fraction in Eq. (6-8) back to wind speed. Essentially all in-plane fatigue damage occurs due to winds under 25 m/s; therefore, common winds (particularly in the 5 m/s to 15 m/s range) are most responsible for the fatigue of traffic signal structures, not extremes. This does not mean that severe fatigue damage does not occur during high wind speed (storm) events, it merely reflects the low occurrence rate related to those events. It can also be seen that for the representative structure, more in-plane fatigue damage is accumulated at wind speeds under 9 m/s for the representative structure, while more out-of-plane damage occurs after. This indicates the point in which the greater out-of-plane response overcomes its lower response frequency to cause more damage accumulation.

The final row of Figure 6-5, presents the expected in- and out-of-plane fatigue damage-rate curves for the representative structure in each specified wind environment. Note that in each location the in-plane case is critical. The additional locations experience higher wind speeds at greater rates, so more damage is expected. As seen at greater recurrence rates, the slight amplification in median in-plane response, along with the increased uncertainty in response due to low-speed, across-wind effects, is responsible for an increased damage accumulation. However, as recurrence rate diminishes (with higher wind speeds) out-of-plane damage accumulation is greater. The effect of the local wind

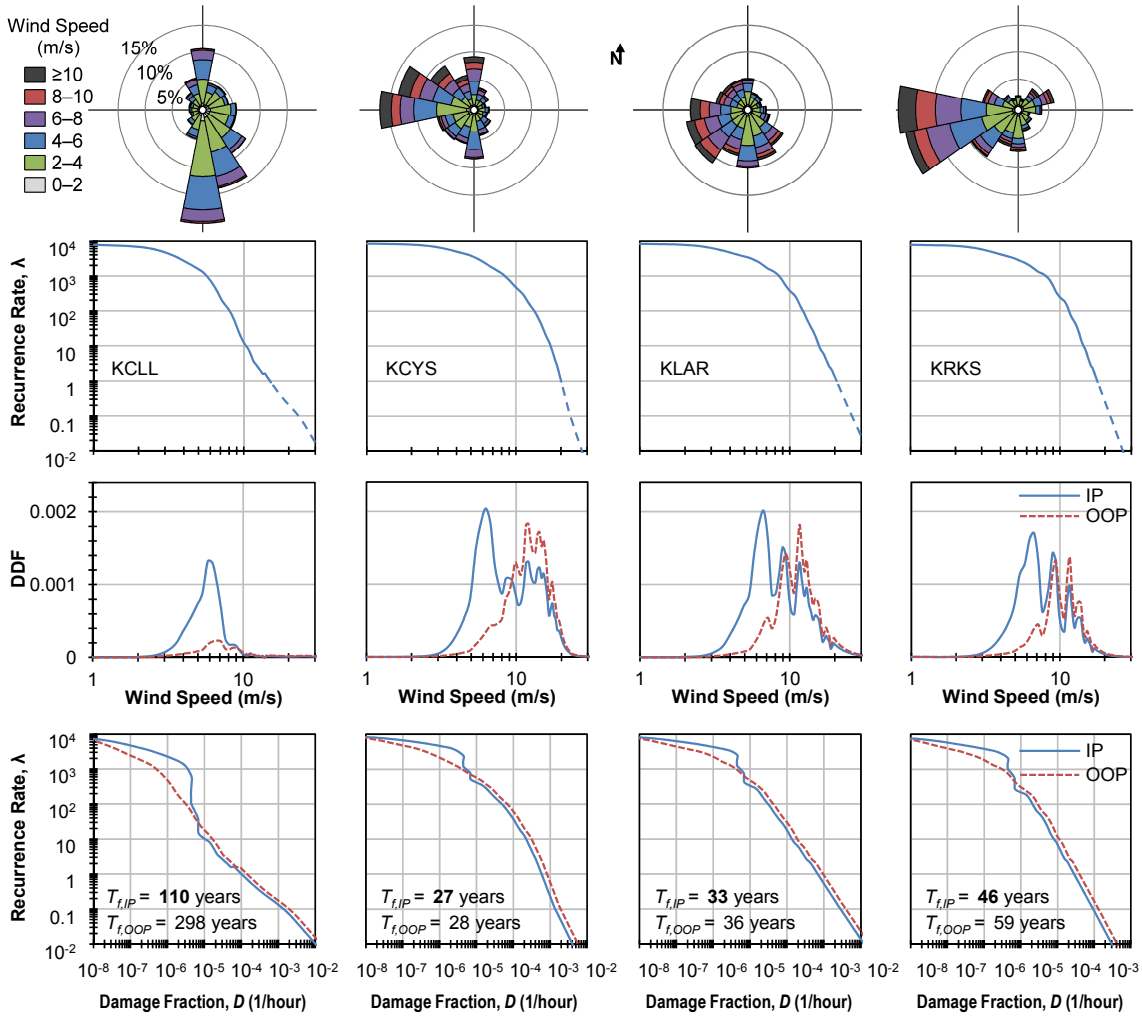

(a) Bryan/College Station, TX *(b) Cheyenne, WY* *(c) Laramie, WY* *(d) Rock Springs, WY*

Figure 6-5. Results for the representative traffic signal support structure by location showing: (top row) wind roses, (second row) wind hazard-rate models, (third row) in-plane (IP) and out-of-plane (OOP) expected annual damage distribution functions, and (final row) expected fatigue damage-rate relationships including expected fatigue lives.

environment is best seen for wind speeds that occur more than 10 times annually. The in- and out-of-plane expected life T_f, where $T_f = \left(\bar{D}\right)^{-1}$, at each location is included in Figure 6-5.

As Figure 6-5 indicates, the in-plane response controls the fatigue life of the structure. However, where wind speeds greater than 9 m/s have an increased occurrence rate, out-of-plane fatigue damage becomes more significant. When a location has a preponderance of winds above this threshold, fatigue crack formation may occur at either the top or sides of the connection within a similar timeframe.

6.6 Model Corroboration Using Observed Damage in Wyoming

To further verify the proposed probabilistic approach, results of observed fatigue crack observations for a large family of similar structures in Wyoming are used (Price et al. 2008). The study examined the relation between traffic signal fatigue failures to location by use of wind power maps. As inferred from the report, compiled inspections from locations in southern Wyoming shared similarity because each were wind-swept environments with similar topologies and wind speed distributions. Based on the relative number of inspections performed in each location, the composite distribution has an expected life of 32 years with dispersion for spatial distribution and fatigue randomness $\beta_{FR} = 0.63$. Because a single value of expected life was used to describe life over a wide region in southern Wyoming, additional uncertainty is considered. An epistemic uncertainty $\beta_{FU} = 0.30$ is adopted to account for additional fatigue modeling uncertainty arising from differences in regional topology, wind speed distribution, and traffic signal

configuration; this uncertainty quantification is based on similar estimates across several allied applications (Kennedy et al. 1980; Wirsching 1984; Ronold et al. 1999). As a result, for a regional assessment, $\beta_{FL,region} = \sqrt{\beta_{FR}^2 + \beta_{FU}^2} = 0.70$. When the AASHTO fatigue category-defined, 2.5% non-exceedance probability (AASHTO 2013) is adopted to serve as the basis for a dependable service life given the preceding formulation of T_f , then an approximate 75% reduction in the expected fatigue life results according to Eq. (6-10). The regional service life may thus be estimated at 8 years.

Figure 6-6 compares the empirical distribution function (Kaplan and Meier 1958) describing the field observations compiled by Price et al. (2008) against the modeled prediction stemming from application of the proposed framework. Also depicted is the 95 percent confidence bounds on the random, right censored dataset according to Greenwood (1926). The tail of the predicted distribution compares quite favorably with observations and falls well within the confidence bounds, demonstrating that the proposed framework may be used to appropriately quantify fatigue service life, which occurs at low levels of non-exceedance. This finding remains practically true for $0.20 \le \beta_{FU} \le 0.40$, as the generally large value of randomness in fatigue capacity of the connection $\beta_{FR} = 0.63$ dominates the total randomness assigned for regional assessments $\beta_{FL,region}$. Dependable life estimates change by less than 10% from 8 years over this range of β_{FU}.

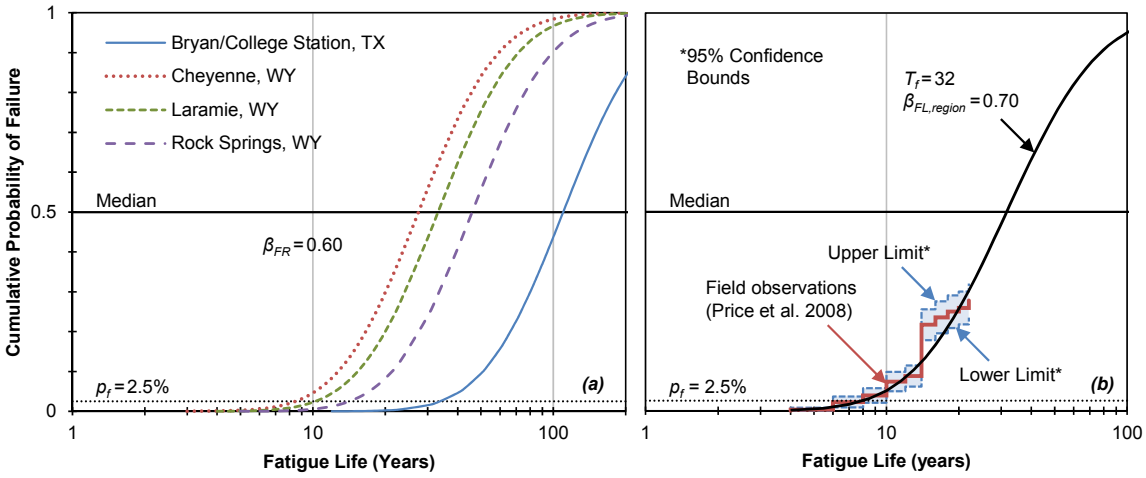

(a) Fatigue fragility curves *(b) Comparison*

Figure 6-6. Traffic signal structure fatigue life fragility curves for: (a) select locations, and (b) comparison between predicted and observed distributions of fatigue cracking.

6.7 Closure and Key Findings

A four-step methodology previously developed in (Mander et al. 2012) for probabilistic seismic loss modeling has been extended to estimate the fatigue life of lightweight, wind-excited steel structures. This approach inter-relates the close interaction between: (a) the recurrence of wind speeds (hazard analysis); (b) the cyclic stress response amplitudes due to varying wind speeds (structural response); (c) cyclic stress response; and (d) fatigue damage accumulation at a given detail (damage analysis). The proposed probabilistic framework was successfully demonstrated to calculate accumulated wind-induced fatigue damage, then fatigue life, upon comparison with field observations. As a result of the work performed herein, it can be seen that the presented methodology lends itself quite useful for comparative studies, as the incorporated models may be easily reformed or substituted, then implemented. Requiring minimal modification, the presented framework has promise for application in a variety risk-related areas.

Based on the research presented herein, the key findings may be summarized as follows:

i. A probabilistic methodology has been proposed and successfully demonstrated for the prediction of fatigue damage of wind-excited structures. By accounting for randomness and uncertainties, the analysis yields a fatigue life fragility function; dependable service life can thus be inferred with respect to a specified non-exceedance probability. Subsequent studies may follow by varying characteristics pertaining to: wind environment, structural response, and/or fatigue resistance. The method could easily be adapted for the probabilistic assessment of other high-

cycle fatigue prone structures or for applications with similar hazard-response-damage model interactions.

ii. It is the common wind environment (with return periods of less than one year) that is mostly responsible for the fatigue damage accumulation of traffic signal structures, while the strength of the structure is governed by design gust speeds associated with a 50 year mean recurrence interval (per basic wind speed ratings). This finding, however, does not indicate that severe fatigue damage does not occur during high wind speed (storm) events, it merely reflects the low occurrence rate of those events. Event duration (and the wind speed variability) has much effect on damage incurred.

iii. Findings suggest that fatigue is generally controlled by across-wind components that influence in-plane response at modest wind speeds in the range of 4 m/s to 10 m/s. When in- and out-of-plane fatigue resistance is considered similar for the structure of interest, therein lies a threshold wind speed (≈9 m/s) beyond which more damage is expected to accumulate due to out-of-plane response. This occurs when the magnitude of the out-of-plane response overcomes its smaller response frequency (when compared to in-plane response). As a result, out-of-plane fatigue is of greater concern in locations with higher typical wind speeds, such as Cheyenne and Laramie, WY.

iv. Traffic signal support structure fatigue varies greatly and is largely dependent on the local wind environment. Locations with higher prevailing wind speeds are particularly susceptible to wind-induced traffic signal structure fatigue. The

prevalence of low wind speeds coupled with across-wind dominated response is primarily responsible for the early fatigue failures of mast arm-to-pole connections found in cantilevered traffic signal support structures.

7 POST-TENSIONED TRAFFIC SIGNAL STRUCTURE: EXPERIMENTAL NATURAL WIND RESPONSE AND (DETERMINISTIC) FATIGUE ASSESSMENT

7.1 Overview

Cantilevered traffic signal structures undergo wind-induced vibrations causing persistent stress cycles that result in welded connection fatigue and fracture. A low-cost damage avoidance system is proposed to apply post-tensioned (PT) prestress to eradicate the detrimental tensile stresses found in the tube-to-transverse end plate welded connections. A supplementary load path is introduced to balance the moments arising from the significant dead load associated with the cantilevered arm spanning the roadway, while offering a fail-safe mechanism. Field observations are made on a full-scale prototype structure in a natural wind environment without and with the proposed mitigation system installed; changes in the structure's stress response are studied. To quantify the benefit of the proposed system, the fatigue life is estimated using a deterministic framework considering the expected change in fatigue resistance, as well as observed changes in natural wind response for two contrasting wind environments. Test results and companion analyses show that there is potential to markedly extend the dependable fatigue life of the traffic signal structure of subject in this study well beyond its expected service life. The proposed concept shows potential to reduce detrimental mean stress effects for a variety of fatigue-critical, lightweight steel infrastructure components.

7.2 Introduction

Non-redundant traffic signal support structures are constantly subject to wind-induced vibrations which result in stress reversals that can lead to fatigue and fracture in welded connections. Spans continue to increase to accommodate additional lanes or to reduce roadside hazards, however so does the number of observed connection failures. At the turn of the 21st century, 60 percent of states surveyed reported excessive cantilever vibrations or fatigue cracking of overhead support structures (Dexter and Ricker 2002).

Two approaches may be taken to enhance or extend the fatigue life: (i) demand reduction by decreasing response such as increasing damping; or (ii) via fatigue capacity improvement. Mast arm or attachment aerodynamics have been modified to reduce excitation (Pulipaka et al. 1998; Letchford et al. 2008; Cruzado et al. 2013; Wieghaus et al. 2014a); however the effectiveness has been limited due to inconsistent installations or targeting a mechanism with limited influence (Wieghaus et al. 2014b,c). Viscous (Hamilton et al. 2000; McManus et al. 2003), impact (Cook et al. 2001), and signal-integrated tuned-mass dampers (Christenson 2011; Christenson et al. 2011) have been shown to increase system damping, and thus reduce vibrations.

Alternatively, fatigue capacity improvement has been accomplished by investigating weld treatment techniques or studying the effect of detail geometry (Koenigs et al. 2003; Ocel 2006; Roy et al. 2011). Unfortunately, the effectiveness of these various strategies remains subject to the occurrence of potentially poor weld quality (Chen et al. 2001), the negative impacts of galvanizing (Goyal et al. 2012), and the adverse effects of high tensile mean stresses. In practice, designers have countered by using larger sections

and heavily stiffened connections to eliminate vibrations and increase connection fatigue capacity—at the expense of increased material, production, and installation costs.

Safety concerns remain despite previous research. Non-redundant, cantilevered sign structures justifiably remain in favor over portal-type structures due to the reduced cost and roadside collision risk. Structural redundancy in cantilevered structures is typically of little concern because common practice considers the fatigue life of weldments to be independent of mean stress (Kaczinski et al. 1998). Despite this practice, when assigning AASHTO (2013) fatigue classifications notable testing programs have applied cyclic loads about an elevated mean to simulate the tensile mean stress present in tube-to-transverse base plate connections to replicate dead load effects (Miki et al. 1981; Koenigs et al. 2003, Ocel 2006; Roy et al. 2011). When these results have been compared to those subjected to fully reversed loading conditions (zero mean stress) (Miki et al. 2001; Macchietto 2002) researchers have acknowledged one clear and potentially contentious trend. That is, the determined fatigue resistance of tube-to-base plate connections is overstated when not accounting for the effects of dead load (Koenigs et al. 2003; Ocel 2006). More discussion on these test results will follow.

Damage avoidance design (DAD) incorporates aspects of rocking, structural flexibility and prestressing (Mander and Cheng 1997). Several post-tensioned (PT) DAD solutions have been developed for wall-to-foundation connections (Hamid and Mander 2010), concrete beam-column connections (Rodgers et al. 2012a,b), and total-structure re-centering systems (Pekcan et al. 2000). In parallel, researchers have developed ways to mitigate the weld fracture potential in steel moment-resisting frame structures during

seismic events (Pekcan et al. 2000; Ricles et al. 2001; Christopoulos et al. 2002; Garlock et al. 2005; Rojas et al. 2005; Garlock et al. 2007; Kim and Christopoulos 2008; Christopoulos et al. 2008; Wolski et al. 2009; Lin et al. 2013). Practically all the above referenced works that used PT achieved response reduction and increased capacity. Dampers have also been used with PT components to simultaneously increase capacity and reduce response (Pekcan et al. 2000; Rojas et al. 2005; Kim and Christopoulos 2008; Christopoulos et al. 2008; Wolski 2009; Rodgers et al. 2012a,b; Lin et al. 2013). Clearly this is a case for a beneficial transfer of concept from seismic- to wind-related disciplines.

This section proposes a low-cost supplemental system aimed to increase the fatigue resistance by introducing a load-balancing redundancy not only to cantilevered traffic signal structures, but also a variety of lightweight, tubular structures that use welded or bolted connections found across several engineering fields. The system incorporates concepts of PT and load-balancing—with favorable applications implemented in structural concrete (Pekcan et al. 2000; Hamid and Mander 2010; Rodgers et al. 2012a,b) and steel (Pekcan et al. 2000; Ricles et al. 2001; Christopoulos et al. 2002; Garlock et al. 2005; Rojas et al. 2005; Garlock et al. 2007; Kim and Christopoulos 2008; Christopoulos et al. 2008; Wolski et al. 2009; Lin et al. 2013). To increase structural safety by adding redundancy while increasing fatigue capacity, the PT system (Hurlebaus and Mander 2014) presented herein is an excitation-independent solution to connection fatigue available for the retrofit of in-service and integration into current and future structures.

The detrimental dead load tensile stresses found in tube-to-transverse end plate connections are relieved. Via PT, an alternative load path is introduced to balance the

moments arising from the significant dead load associated with the cantilevered arm spanning several traffic lanes. Components of the prototype fail-safe system are installed to a full-scale traffic signal structure and field testing/monitoring is conducted to study changes in the wind-excited behavior of the structure before and after each installation.

In this section, a DAD system is introduced for steel traffic support structures to provide a dual action: (i) provide alternative load path redundancy; and (ii) alleviate wind-induced fatigue. To justify the merit of the PT system, the effect of tensile mean stresses on tube-to-transverse base plate connection's fatigue resistance is investigated. Then, prototype testing is described that uses a full-scale, decommissioned traffic signal structure in various phases to investigate the effect that PT installation has on natural wind response. Using the experimentally observed response and mean stress-dependent fatigue relationships, the dependable service live of the traffic signal structure without and with the proposed DAD system is estimated using a deterministic approach. Two locations are considered: (i) Bryan/College Station, TX, which is generally a quiet and benign wind environment with a low average wind speed of 3.6 m/s; and (ii) Cheyenne, WY, which has a more energetic wind environment with an average wind speed of 5.7 m/s. Comparative evaluations of fatigue performance are made to assess the efficacy of PT mitigation and to identify any caveats related to the implementation of the proposed DAD technique.

7.3 Fatigue Considerations

As discussed in this dissertation, the welded arm-to-transverse base plate connection at the arm-pole connection has traditionally been classified as AASHTO

Category E', where $A = 128 \times 10^9$ MPa^3. In the case of overloading, where 10^{-4} of the stress cycles exceed the constant amplitude fatigue limit, an extension is permitted for analysis (Fisher et al. 1993).

Figure 7-1 illustrates the fatigue performance of past fatigue testing programs and fatigue strength curves assigned under various conditions. Tube-to-transverse end plate connections are appropriately described as Category E' when subjected to larger tensile mean stresses caused by dead loads; this is evident based on the overall satisfactory performance of current designs nationwide. However, if these connections are not subjected to tensile mean stresses, this assigned category is conservative as shown in Figure 7-1(a). Stiffened connections are indicated by filled markers.

Past research has acknowledged that tube-to-transverse base plate connections demonstrate better fatigue performance when tested under zero (or low) mean stress levels when compared against those tested under higher mean stress levels intended to mimic dead load stresses in prototype systems (Koenigs et al. 2003; Ocel 2006). This trend is seen in Figure 7-1(a), where results are separated by mean stresses imposed during testing. Specimens tested about an elevated mean stress were from a family of similar tube-to-transverse base plate connections with either socket or non-optimally stiffened connections, while connections tested about zero mean stress (fully reversed) belong to a similar, but superiorly-detailed family. Thus, the vast improvement in fatigue performance can be attributed to both superior detailing and the lack of tensile mean stress when testing. The median tensile mean stress in the connections was approximately 150 MPa, corresponding to the highest dead load stress expected for a 13.4 m long arm structure

when fully equipped/loaded with metal signals (Koenigs et al. 2003). If these results are considered, the resulting fatigue models herein are inclusive of the variety of connections demonstrated by a broad population of traffic signal support structures.

As such, all results stemming from previous research (Koenigs et al. 2003; Roy et al. 2011) were cast as equivalently tested under 150 MPa mean stresses. The Walker (1970) mean stress correction model was considered of the form

$$S_{rr} = S_r \left(1 + \frac{2\sigma_m}{S_r} \right)^{1-\gamma_w} \tag{7-1}$$

in which $S_{rr} =$ the equivalent completely reversed stress range (zero mean stress); $\sigma_m =$ mean stress about which the double amplitude stress range $\left(S_r\right)$ is cycled; and $\gamma_w =$ the Walker parameter given by $\gamma_w = 0.8818 - 0.0002\sigma_u$, where $\sigma_u =$ the ultimate tensile strength in MPa (Dowling et al. 2009). The Walker correction reduces to the well-known SWT correction when $\gamma_w = 0.50$ (Smith, Watson, and Topper 1970).

Figure 7-1(b) presents the transformation of the previously tested fatigue results, using Eq. (7-1) with $\gamma_w = 0.8$ to represent the results if tested under a common mean stress of $\sigma_m = 150\,\text{MPa}$. As shown, the design fatigue strength remains appropriately described as Category E' for the family of connections considered.

Figure 7-1(c) depicts transformation of AASHTO Category E' using Eq. (7-1) to represent the expected fatigue performance of the connection family if subjected to fully reversed, damage equivalent stress range S_{rr}. The transformed test results from those originally tested about elevated mean stresses are also shown. As seen, the effect of mean

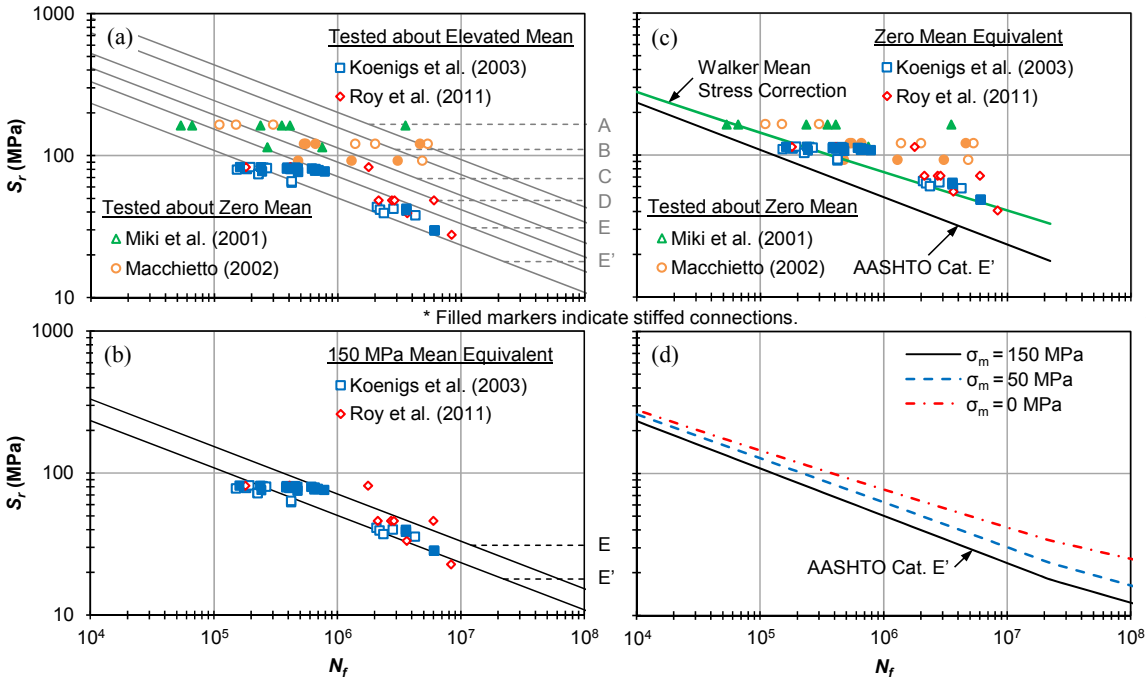

Figure 7-1. Fatigue performance of tube-to-transverse base plate connections: (a) results for specimens subjected to various levels of dead load mean stress; (b) Walker (1970) adjusted 150 MPa mean stress equivalent results; (c) Walker (1970) adjusted zero mean stress equivalent results; and (d) fatigue strength curves representing various levels of tensile mean stress.

stress becomes more apparent with decreasing cyclic stress amplitudes where the fatigue strength curve flattens (and slope c becomes more negative). To justify this shift, the results from fully reversed tests (Miki et al. 2001; Macchietto 2002) are also shown in Figure 7-1(c). These results exhibit higher fatigue capacity, however recall their fatigue performance can be attributed to both superior detailing and the lack of tensile mean stress when testing. Therefore, the remaining difference is attributed to superior detailing and it is thus reasoned that the adjusted relationship using the Walker correction reasonably demonstrates the beneficial effect of tensile mean stress relief for the connection family considered herein.

Multiple fatigue strength curves are depicted in Figure 7-1(d) to illustrate the dependence that fatigue resistance has on mean stress for this family of tube-to-transverse plate connections. As shown the lower portion of the Category E' fatigue strength curve was extended below the well-defined and understood CAFL using a slope of $c = -4$ to reduce conservativism in future analyses (Crudele and Yen 2006; Yen et al. 2013). Fatigue strength curves related to decreased mean stresses were derived using Eq. (7-1) and AASHTO Category E' to describe performance when mean stress is 150 MPa.

7.4 Fatigue Mitigation

As previously demonstrated, tensile mean stresses have been shown to adversely affect the fatigue life of tube-to-transverse plate connections. Therefore, fatigue proneness can be reduced, by design, using stress manipulation. Load-balancing prestress concepts may be used to alleviate or completely reduce detrimental mean stresses by implementing a counteracting compressive state of stress. As a result, component fatigue performance

(capacity) should improve even if there are no changes to the structural dynamic characteristics in a natural wind environment.

Figure 7-2 illustrates the implementation of a DAD system for the traffic signal structure studied herein. To protect the arm-pole connection detail, load-balancing prestress is applied through a PT tendon installed within the confines of the horizontal mast arm and anchored at each end. End anchorages for the PT system include a bearing plate at the free end of the cantilever and a curved bracket is used to evenly distribute the PT force on the backside of the cylindrical pole section. To help evenly distribute the bearing stress, a thin rubber pad may be used between the pole and curved bracket. Vertical PT may similarly be applied to the structure to alleviate stresses at the pole-base connection.

The concept of stress superposition at the arm-to-transverse base plate connection is shown in Figure 7-2. PT may be eccentrically applied to balance (Pekcan et al. 2000) the self-weight of the structure and attached signs/signals. Sharing similarities to a gravity-loaded, prestressed concrete beam, optimal tendon eccentricity for the mast arm would generally conform to the shape of the dead moment. For this application, eccentricity at the connection is of primary interest.

In addition to improved fatigue performance, the PT concept provides additional redundancy, with the additional load path delivering fail-safe performance to the connection in the event of a fatigue/fracture failure during an extreme event or other overloading scenario. The cantilever would remain suspended, held in position by the redundant internal tendon under high PT load. The PT system could also be installed in

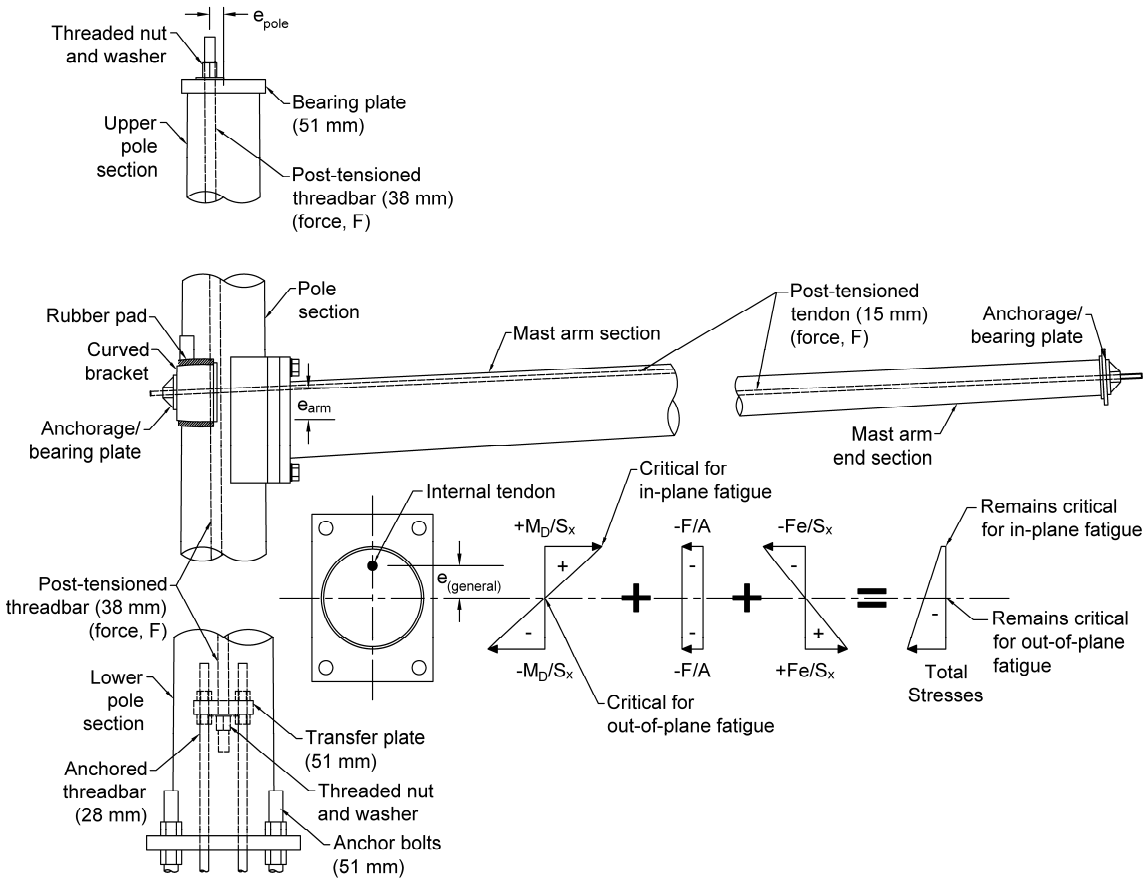

Figure 7-2. Schematic depicting the as-built configuration of proposed mast arm and pole load-balancing systems to alleviate the tensile mean stresses found atop the arm-pole and outside the pole-base connection.

aging structures with existing fatigue cracks to eliminate the tensile component of stress response. Finally, PT concepts can be incorporated to offset increased dead load demands brought about by the necessity for longer cantilever spans (Puckett et al. 2014).

7.5 Experimental Investigation

Field experiments were conducted to investigate the response behavior for a common traffic signal structure (Wieghaus et al. 2014a). The described prototype DAD system was installed and the response re-assessed. Free vibration tests and long-term monitoring under ambient, natural wind conditions were conducted for each configuration considered.

7.5.1 Phase I: Field Test of Standard Structure

Figure 3-1 presented the experimental structure selected for field testing. The decommissioned traffic signal structure was selected for having member dimensions and other attributes found related to large excitation susceptibility. Consult Section 3 for a description of structural dimensions, instrumentation, sampling rate, data acquisition and data post-processing (Wieghaus et al. 2014a).

As stated in Section 3, the ambient natural wind response of the standard structure was observed from April 24, 2012 to September 2, 2012. As shown in Figure 7-3(a), the in-plane tensile mean stresses in the structure were approximately 90 MPa and 50 MPa at the arm and pole connections, respectively. Note that the tensile mean stress atop the arm section near the weld did not equal 150 MPa, as it was not fully loaded with steel signal clusters and electrical wiring. As expected, the out-of-plane means tended toward zero.

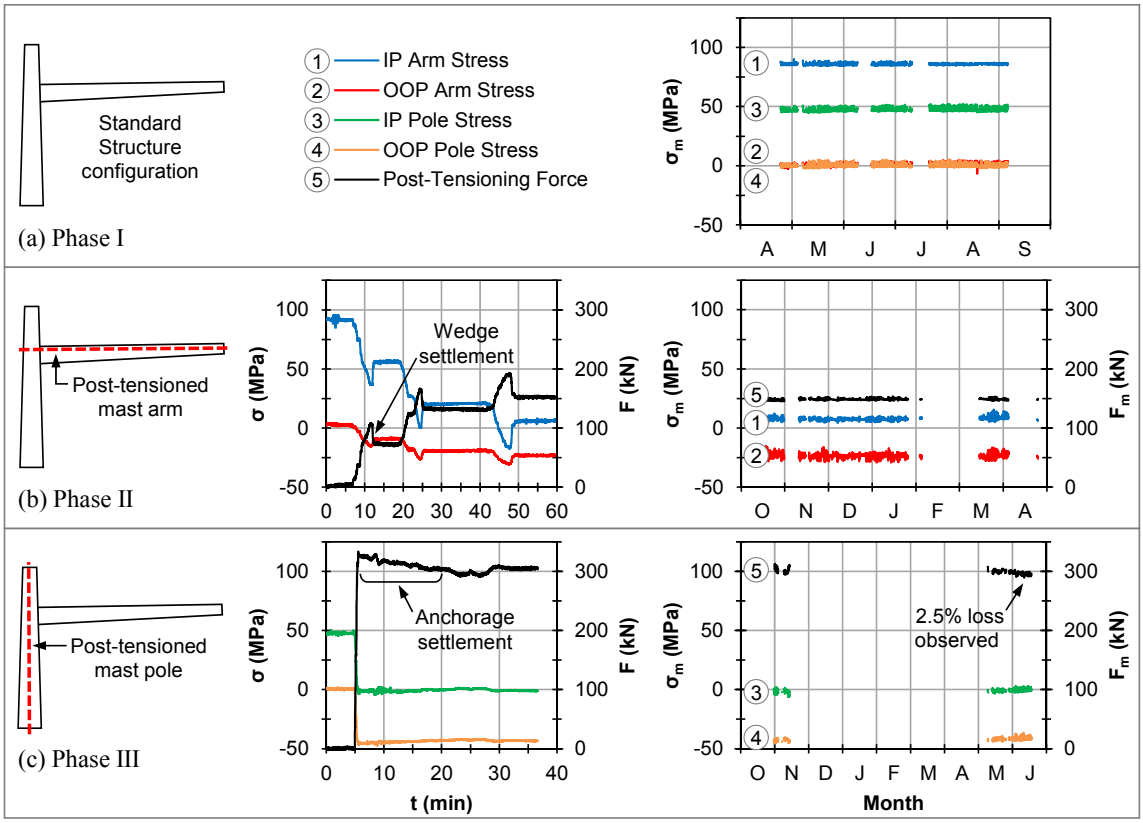

Figure 7-3. Observed in-plane (IP) and out-of-plane (OOP) mean stresses at the critical locations during: (a) Phase I for the standard (as-built) structure, (b) Phase II for the prototype structure with the post-tensioned arm, and (c) Phase III for the prototype structure with the post-tensioned pole.

The dominant in- and out-of-plane response periods were 0.92 s and 1.01 s, respectively. Snap-back tests also indicated damping ratios well under one percent. As shown in Figure 7-3(a), it is as-expected that the mean stress observed at each critical location remained constant during the duration of Phase I.

7.5.2 Phase II: Prototype Structure with PT Mast Arm

Following assembly of the traffic signal structure, Phase II involved the field installation of the prototype PT prestress system to the horizontal arm. As illustrated in Figure 7-2, a 15 mm prestressing strand was used in conjunction with a single-strand anchorage, bearing plate, and rubber pad at the connection end as shown in Figure 7-4(a) and Figure 7-4(b). As depicted in the aforementioned figures, a rubber bearing pad was used to ensure uniform contact between the curved bearing bracket and the circular pole section. Holes were flame cut through the pole section and plate connection to allow for maximum eccentricity adjacent to the welded connection. A center-hole jack was used to apply the PT load, and the wedges were manually set. Figure 7-3(b) presents the stress time history during loading, as well as the long-term monitored mean stress. Due to stroke limitations, the PT was applied in three stages to allow for jack adjustments, and each stage was followed by a loss due to wedge settlement. With a PT force of approximately 150 kN, the in-plane tensile mean stress atop the welded connection was reduced from 90 MPa to 7.5 MPa (92 percent reduction), while the sides of the connection experienced a compressive stress of 25 MPa. The wind-excited response of the prototype structure with arm PT was then observed from October 17, 2011 to April 24, 2012.

Figure 7-4. Photos depicting installation of the proposed arm PT system from the (a) backside of the arm-pole connection and (b) mast arm end, and (c) the pole PT system from atop the pole.

During snap-back testing, the observed in- and out-of-plane response periods were 1.02 s and 1.10 s, respectively. While testing, it was observed that the internal tendon came into contact the inside of the tube wall while the structure underwent large-amplitude vibrations, quickly dissipating the response. An in-plane damping ratio equivalent of approximately 8 percent was observed following impact. This behavior may not occur for all structures and their respective configurations. Following lower amplitude snap-back tests, in- and out-of-plane damping was observed to increase modestly, remaining under one percent. As shown in Figure 7-3(b), the 150 kN axial load (and thus, the mean stresses) stayed constant throughout Phase II, therefore it is reasonable to assume that anchorage losses are most prominent and long-term losses are negligible.

7.5.3 Phase III: Prototype Structure with PT Pole

The pole PT system depicted in Figure 7-2, was later installed during Phase III following the relief and removal of the arm PT. A series of 38 mm ASTM A193 B7 threadbar sections were coupled while being fed downward through the vertical length of the pole through a bottom bearing plate suspended roughly 1 m atop the foundation. This square plate was suspended by four 28 mm threadbars. Shown in Figure 7-4(c), an eccentrically-placed round plate was used atop the pole to distribute the PT into the pole section. Using a large-capacity center-hole jack, a 300 kN PT force was imposed onto the vertical pole. As shown in Figure 7-3(c), this completely relieved the tensile mean stress from the pole-base plate connection. The ambient wind response of the structure during Phase III was observed from October 30, 2012 to November 14, 2012, then the pole alone from May 9, 2013 to June 17, 2013.

Snap-back tests indicated a negligible change in period and damping when compared to that of the standard configuration tested in Phase I. As can be inferred from Figure 7-3(c), monitoring during Phase III was interrupted. Following equipment repair, a slight PT loss was measured eight months after installation, however this loss is unjustified and may be attributed to equipment function.

7.6 Field Experiments: Test Results

Figure 7-5 to Figure 7-7 present the results for each of the three phases of testing the prototype experimental structure. Recall that each phase involved testing of a different configuration described previously. Inferred in- and out-of-plane bending stresses were intermittently confirmed using a computer vision technique coupled with an analytical model (Bartilson et al. 2015).

7.6.1 Phase I: Field Test of Standard Structure

Sections 3 and 5 may be consulted for details concerning observations made during Phase I. Figure 7-5 presents the stress response (now near both the (b) arm-pole and (c) pole-base connections) stemming from observations made during Phase I for which the standard (as-built) structure was studied. Using the traditional means to demonstrate fatigue equivalent response, the root mean cube stress range is depicted to account for observation variability. In accordance with theory and design standards, extrapolation of the fatigue equivalent response follows the square of wind speed. Typical of the buffeting response at higher wind speeds, the along-wind (out-of-plane) response is greater than that of the across-wind (in-plane) component.

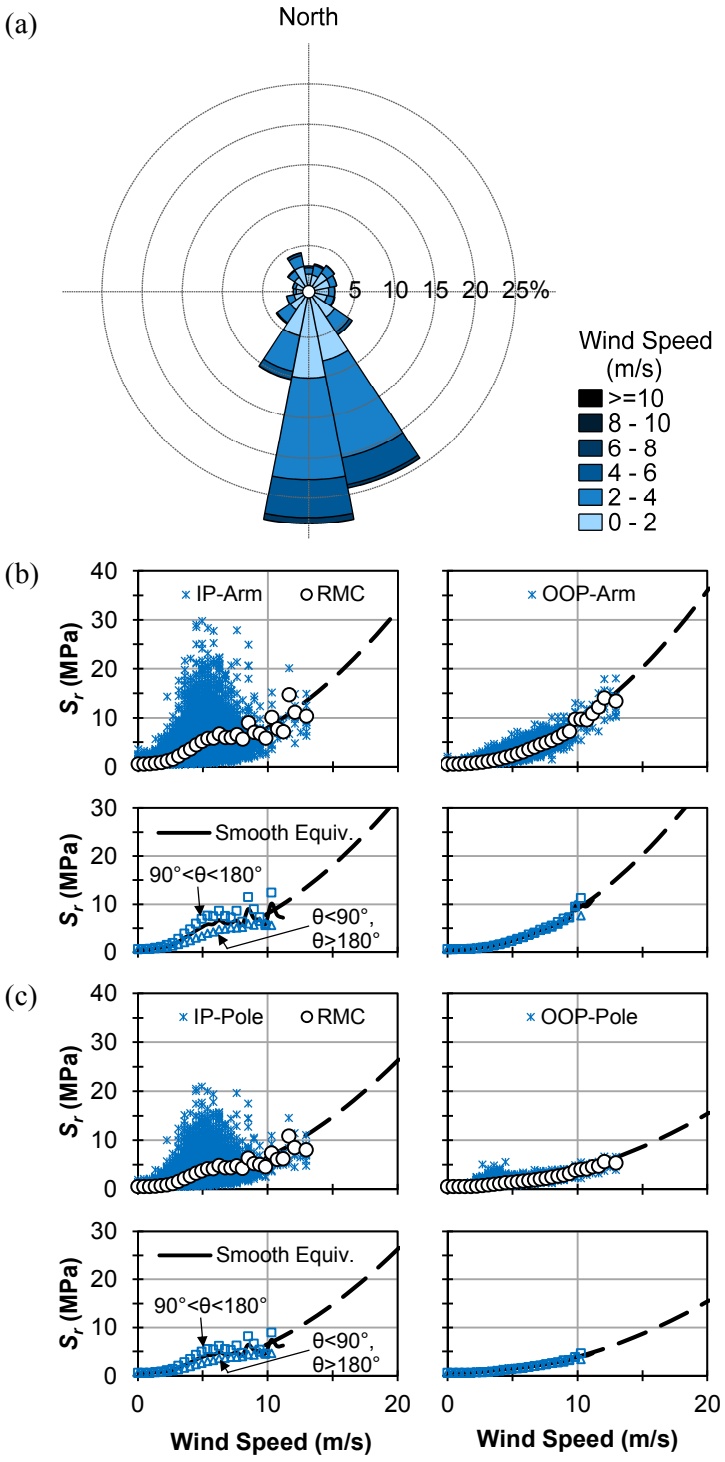

Figure 7-5. Phase I (standard structure): measured (a) wind conditions, total in-plane (IP) and out-of-plane (OOP) stress responses at the (b) arm-pole and (c) pole-base connections as a function of wind speed and direction.

7.6.2 Phase II: Prototype Structure with PT Mast Arm

Figure 7-6 presents the Phase II field experimentation results for the prototype structure following installation of the proposed PT DAD system to the horizontal mast arm. As show in Figure 7-3(b), eccentric PT relieved 92 percent of the original 90 MPa tensile mean stresses atop the arm section at the arm-pole connection. Resembling both historical and previously measured winds, Figure 7-6(a) shows that slightly less than one-half of winds approach from the backside of the signal structure, despite a seasonal weather pattern leading to many winds approaching from the North. Figure 7-6 shows in (b) the in-plane and (c) the out-of-plane stress response near the arm-pole and pole-base connections, respectively.

Observed wind speeds are similar to those observed during Phase I, thus it was deemed appropriate to compare results obtained during Phase II. Examination of the results shown in Figure 7-6(b,c) indicates a clear decrease in in-plane (across-wind) response, whether due to the unexpected strand impacting or the use of rubber bearing pads. Phase II saw decreases of 65 percent and 13 percent in the maximum observed in- and out-of-plane stress response in the arm section. Again, extrapolation of the fatigue equivalent responses followed the square of wind speed. In-plane response was markedly reduced following installation of the proposed PT DAD system, whereas a smaller decrease in out-of-plane response was noted.

7.6.3 Phase III: Prototype Structure with PT Pole

Figure 7-7 presents the Phase III experimental results for field testing the prototype structure with vertical PT applied to the pole using 38 mm diameter threadbar as shown

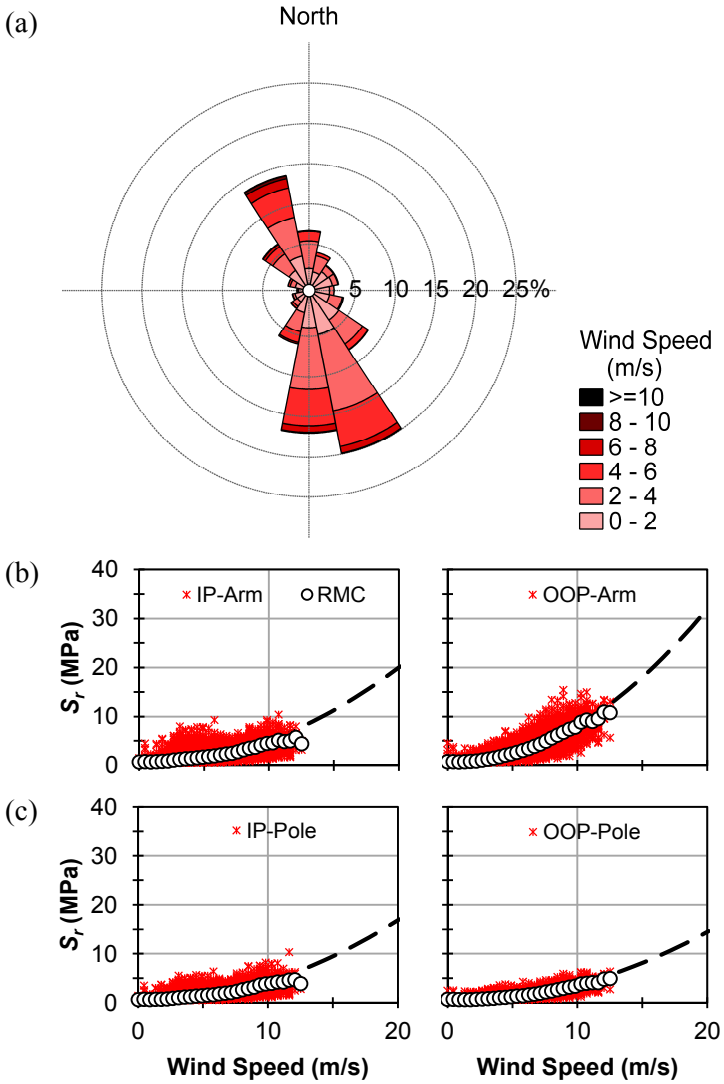

Figure 7-6. Phase II (post-tensioned arm): measured (a) wind conditions, total in-plane (IP) and out-of-plane (OOP) stress responses at the (b) arm-pole and (c) pole-base connections as a function of wind speed.

in Figure 7-2. The applied PT load of 300 kN completely relieved the in-plane tensile mean stress occurring on the outside of the pole's tube-to-transverse base plate connection. As seen in Figure 7-7(a), approximately one-half of all observed winds were again out of the South. The observed natural wind stress response near the arm-pole and pole-base connections is shown in Figure 7-7(b,c), respectively. The observed cyclic stress range response was observed to be similar to Phase I response, brought about by the negligible change in period and damping from Phase I.

7.7 Fatigue Analysis

When the traditional slope $c = -3$ is used in fatigue strength relationships (Keating and Fisher 1986), the root mean cube stress range is an equivalent stress range used for life estimation for components under variable amplitude loadings above and below the constant-amplitude fatigue limit (CAFL). Thus, it may be viewed that the fatigue equivalent stress range S_{re} accounts for variability in measured response.

When a bi-linear fatigue strength curve is utilized and only a small percentage of the stress ranges are described by the upper (steeper) portion, the lower segment of the curve (less steep) can be conservatively used (Yen et al. 2013). Therefore, to determine an equivalent stress range S_{re}

$$S_{re} = \left[\sum_i S_{ri}^{-c_L} \right]^{-1/c_L} \tag{7-2}$$

where $c_L =$ the lower slope of the fatigue strength curve.

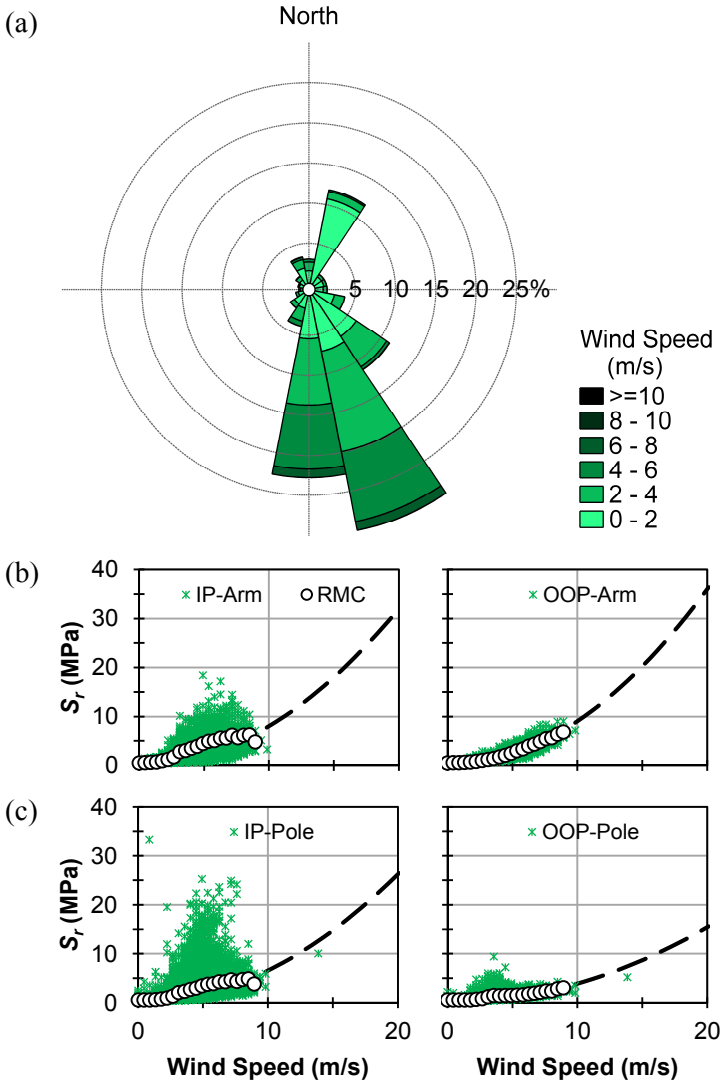

Figure 7-7. Phase III (post-tensioned pole): measured (a) wind conditions, total in-plane (IP) and out-of-plane (OOP) stress responses at the (b) arm-pole and (c) pole-base connections as a function of wind speed.

Using an analysis procedure similar to that described in Section 5, the damage relation may be evaluated using a linearized version of the fatigue strength curve derived using AASHTO Category E' and Eq. (7-1) for the observed mean stress of 90 MPa atop the mast arm-to-transverse base plate connection. As such, the annual damage accumulated may be approximated as a function of wind speed U by

$$d_U = \frac{n_U}{N_U} = \min\left(\frac{p_U}{T_n}\left(\frac{S_{re}}{18.9}\right)^{4.0}, \frac{p_U}{T_n}\left(\frac{S_{re}}{17.7}\right)^{3.0} \right) \tag{7-3}$$

where $N_U =$ the fatigue life (cycles) corresponding to the fatigue equivalent constant amplitude stress range amplitude at each wind speed; and S_{re} has units of MPa and is related to the corresponding lower fatigue strength curve slope $c_L = -4$ in Eq. (7-2). Likewise, to describe connection performance considering that the detrimental dead load was partially balanced using the proposed DAD scheme ($\sigma_m = 7.5\,\text{MPa}$), the annual damage at each incremental wind speed may be expressed as the smaller of

$$d_U = \frac{n_U}{N_U} = \min\left(\frac{p_U}{T_n}\left(\frac{S_{re}}{29.9}\right)^{4.3}, \frac{p_U}{T_n}\left(\frac{S_{re}}{26.8}\right)^{3.4} \right) \tag{7-4}$$

after the fatigue strength curve is linearized. Similar relationships are derived for other mean stress levels between 0 MPa and 150 MPa. Dependable service life T_S can then be determined via

$$T_S = \left[\sum_U d_U \right]^{-1} \tag{7-5}$$

7.7.1 Results for the As-Tested Structure

Figure 7-8 illustrates the effectiveness of the proposed PT DAD system in reducing the rate of in-plane fatigue damage accumulation at the non-redundant arm-pole connection. The relatively benign as-tested wind environment of Bryan/College Station, TX, is shown in Figure 7-8(a). Here, observations made during Phases I and II are considered, namely: (i) the response of the standard structure when $\sigma_m = 90\,\text{MPa}$; and (ii) the reduced response following PT installation where $\sigma_m = 7.5\,\text{MPa}$. As a result, the improved fatigue performance is attributed to improved fatigue capacity via tensile means stress relief combined with the reduction in structure response.

Figure 7-8 not only depicts the process previously described to determine the fatigue performance and service life, but more specifically depicts the expected in-plane performance of the mast arm-to-transverse base plate connection without (solid line) and with (dotted line) the proposed DAD system implemented, based on the observations made herein. As seen in the damage density function (DDF) in Figure 7-8(b), an appreciable amount of damage accumulates atop the connection at wind speed related to vortex-induced vibrations (3 m/s to 7 m/s) for the standard structure tested during Phase I. As indicated in the cumulative damage density function (CDDF) of Figure 7-8(c), mean stress relief, in concert with response reduction, leads to a marked reduction in fatigue damage accumulation by about two orders of magnitude at lower wind speeds and by over an order of magnitude as wind speed increases.

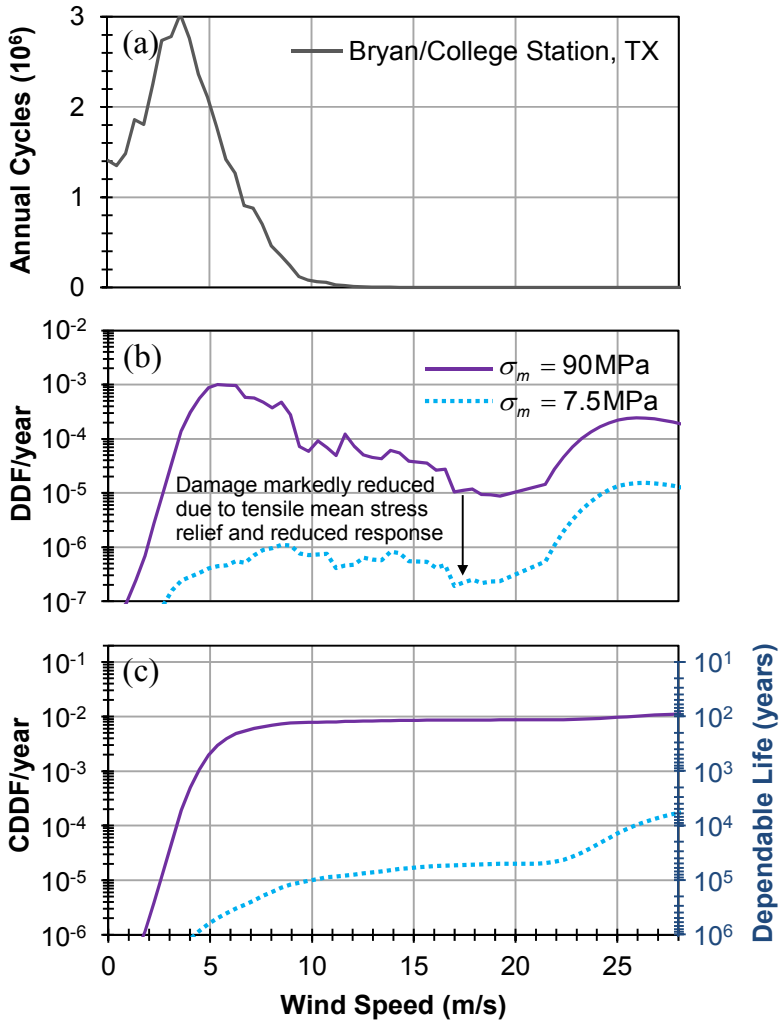

Figure 7-8. **In-plane fatigue assessment of the mast arm-to-transverse base plate connection for Bryan/College Station, TX, considering the experimentally observed shift in mean stress and reduction in wind-induced structural response.**

Not shown in Figure 7-8 is the out-of-plane fatigue analysis conducted for the structure as observed during the first two test phases. Compressive stresses resulting from mast arm PT are not conservatively considered to have additional benefit herein (Bannantine et al. 1990).

In- and out-of-plane fatigue analysis of the connections were conducted, considering the in-plane mean stresses of 90 MPa and 50 MPa at the arm and pole connections, respectively. The expected service life of the standard structure in Bryan/College Station, TX, is $T_S = 83$ years, controlled by the in-plane fatigue at the mast arm connection. For the structure as observed during Phase II, out-of-plane fatigue controls, but the associated service life is over an order of magnitude greater, which is well beyond the expected service life of the structure. Again, this marked improvement may be attributed to both mean stress relief and response reduction observed following arm PT installation. Although focus is not placed on fatigue at the non-critical pole-base connection, pole PT increased the in-plane fatigue life of the connection by a factor of five.

7.8 Discussion

The structure in this study supported three lightweight composite signal clusters and was not wired for operation, thus the observed in-plane mean stresses in the arm and pole were 90 MPa and 50 MPa, respectively. If fully equipped with heavier (steel) signal clusters and appropriately wired, past research indicates an in-plane mean stress of 150 MPa in the arm connection, which would lead to an 80 MPa mean stress at the pole-base connection (Koenigs et al. 2003). If this was the case, the PT loads applied herein

would leave remaining in-plane mean stresses of 67.5 MPa and 30 MPa at the arm and pole connections, respectively. To consider this case, additional in-plane analysis was conducted accounting for changes in the related fatigue strength curves. When subjected to these larger stresses, the dependable service life of the standard structure in Bryan/College Station, TX, decreases to $T_S = 51$ years, still controlled by the in-plane fatigue at the mast arm connection. As expected, the dependable service life decreases when related to higher levels of detrimental tensile mean stresses, and the improvement in dependable service life is not as marked when only partial load-balancing (partial PT) is conducted.

The aforementioned analyses have considered the experimentally observed change in wind-induced structural response following the installation of arm PT. To appropriately quantify the ramifications of PT DAD installation, the more realistic (conservative) case in which no change in structural response will occur is now considered. As such, the experimentally observed Phase I response is alone considered for what follows.

Figure 7-9 depicts analyses conducted for the mast arm-to-transverse base plate in which two differing wind environments are considered: (i) Bryan/College Station, TX; and (ii) Cheyenne, WY. The standard structural response is considered alongside two tensile mean stresses in the connection: (i) $\sigma_m = 150\,\text{MPa}$ for the fully-loaded structure; and (ii) $\sigma_m \leq 0\,\text{MPa}$ considering full PT, where there is no detrimental tensile mean stresses resulting from the self-weight of the structure and its attachments.

As seen in Figure 7-9(b), it is clear that mean stress modification (reduction) alone markedly affects the amount of fatigue damage accumulated annually. As expected, the

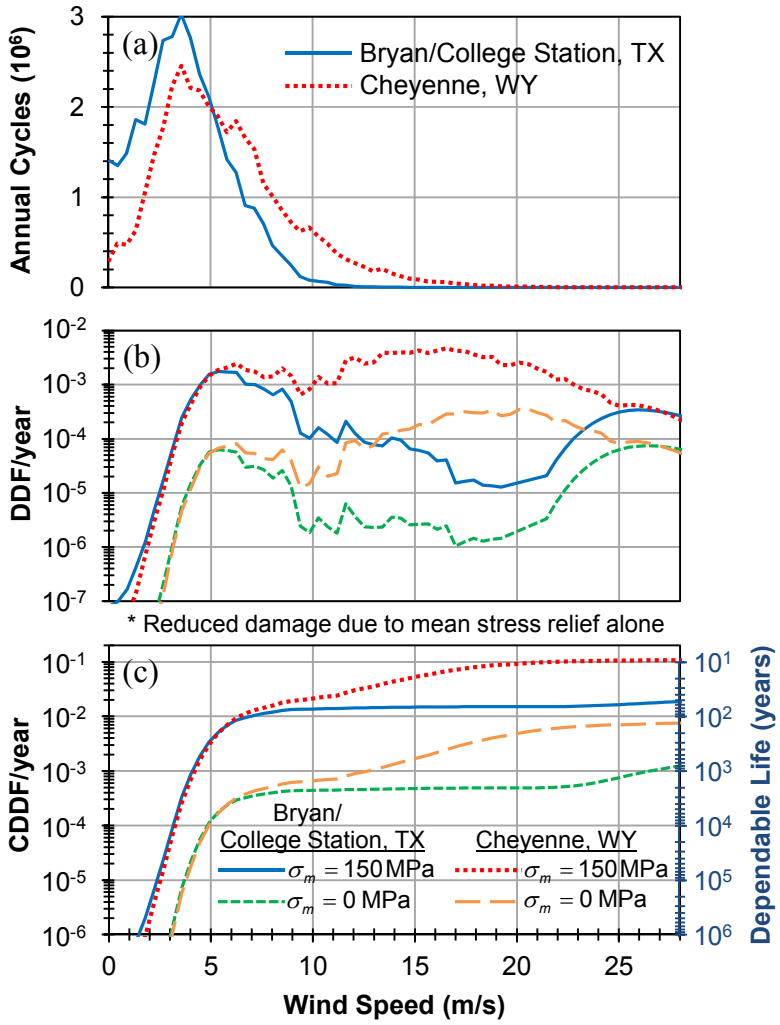

Figure 7-9. **In-plane fatigue assessment of the mast arm-to-transverse base plate connection for contrasting environments: Bryan/College Station, TX, and Cheyenne, WY. The expected as-built performance of a fully-loaded cantilever considers full mast arm PT and no change in wind-induced structural response.**

improved fatigue performance is less pronounced with increasing wind speed, however Figure 7-9(c) indicates that full PT reduces annual fatigue damage accumulation by an order of magnitude when compared to the case of a fully-loaded structure ($\sigma_m = 150\,\text{MPa}$). There, it can be seen that the dependable service lives increase from $T_S = 51$ years and 9 years, to 658 years and 130 years in Bryan/College Station, TX, and Cheyenne, WY, respectively. However, the expected service life of the arm-to-transverse base plate connection is now controlled by the larger out-of-plane (along-wind) response, because compressive mean stresses have not been considered to have additional benefit herein. Thus, the dependable life of the fully stress-relieved structure is $T_S = 645$ years and 92 years in Bryan/College Station, TX, and Cheyenne, WY, respectively. Regardless, analysis of these contrasting environments indicates that the dependable service life of the selected traffic signal structure can be increased by an order of magnitude without a change in structural response, regardless of wind environment.

As approached by other researchers, demand reduction is directed against a specific mechanism or increasing structural damping. Although these alternatives have been found to be effective, the related changes in natural wind response have not been quantified, or presented in a manner that allows the calculation of a fatigue equivalent response from scattered observations. To compare the merits of DAD against an aerodynamic mitigation technique targeted a specific excitation mechanism, results from Wieghaus et al. (2014b) should be consulted. Therein helical strakes were found to effectively reduce the vortex-induced, in-plane response of the prototype structure, however analysis indicated a marginal benefit for locations where connection fatigue

would be of reasonable concern. That is, strake effectiveness depends on wind environment severity, unlike that of the presented DAD approach. Moreover, the proposed system using PT provides a fail-safe performance.

The proposed PT DAD solution increases connection fatigue resistance by providing a load-balancing redundancy for cantilevered, monotube structures common to several engineering fields. Because there is demand to further increase the spans of cantilevered traffic signal structures (Puckett et al. 2014), this supplemental PT system could be used in effort to increase the cantilevered spans associated with today's newer, larger structures. If vibrations would then become of concern, the proposed PT concept could be used in conjunction with viable passive damping systems (Hamilton et al. 2000; McManus et al. 2003; Cook et al. 2001; Christenson 2011; Christenson and Hoque 2011).

Despite the availability of current datasets, the claims made herein should be experimentally substantiated via additional fatigue testing of similarly detailed specimens to allow for direct result comparison. Computational analyses should also be conducted to support the findings from fatigue testing program. As a result, future codes could, ideally, permit designers to incorporate DAD concepts into designs to achieve improved service life. These considerations could potentially dictate more cost efficient designs or allow for the span of longer distances. The proposed concept herein demonstrates the potential to lead to a variety of damage avoidance solutions for other connection types.

7.9 Closure and Key Findings

A low-cost DAD system has been proposed and evaluated to reduce wind-induced fatigue damage accumulation from tube-to-transverse base plate connection in

cantilevered traffic signal structures. Supplemental load-balancing was used to transfer the dead load associated with the cantilevered monotube directly to the supporting member, relieving the detrimental tensile dead load mean stress from the fatigue-prone tube-to-transverse plate connection(s). As a result, the fatigue performance of the connections under a relieved mean stress was enhanced. Prototypes were installed to a full-scale structure to study changes in response, where arm PT was found to increase damping and reduce response. Despite this finding, fatigue analyses performed indicate that response reduction is not necessary to significantly improve the service life of structures similar to that studied herein if dead load tensile stress can be significantly relieved.

The addition of load-balancing redundancy would not only benefit cantilevered traffic signal structure connections, but also a variety of similar connections found throughout infrastructure. The proposed system not only provides a fail-safe mechanism for affected connections, but also reduced fatigue damage accumulation by reducing the detrimental effect of tensile mean stresses. Internal (or external) PT systems could also be used in new designs to increase cantilever spans without increasing connection mean stresses.

The following deductions are drawn based on the experiments and analyses described herein:

i. A low-cost, supplemental PT DAD system was proposed to relieve tensile mean stresses, thus reducing the detriment posed by tensile mean stresses. Load-balancing redundancy is offered and has potential for other applications.

Additionally, the dependable service life of cantilevered traffic signal structures may be potentially increased by eliminating detrimental tensile mean stresses from fatigue-critical tube-to-transverse plate connections.

ii. Established fatigue strength curves can be appropriately modified to extract and eliminate built-in mean stress considerations to assess the dependable fatigue life of PT steel connections.

iii. Full-scale arm PT prototype tests provided an increased mechanical damping when the eccentrically placed PT strand impacted the inner tube wall during large-amplitude vibrations. When not undergoing large-amplitude vibrations, arm PT only marginally increased structural damping. Pole PT installation had a negligible effect on natural wind-induced structural response, but as intended reduced stresses at the pole-to-base connection.

iv. Complete tensile mean stress reduction (full PT) can alone increase the dependable service life of the structure considered herein by an order of magnitude, regardless of wind environment (severity).

8 DAMAGE AVOIDANCE SOLUTION TO MITIGATE WIND-INDUCED FATIGUE IN STEEL TRAFFIC SUPPORT STRUCTURES (PROBABILISTIC ASSESSMENT)

8.1 Overview

Non-redundant, cantilevered traffic signal support structures undergo frequent wind-induced excitation; the subsequent vibrations result in stress reversals that lead to fatigue, and possibly fracture, particularly at the welded connections. To accommodate more lanes and reduce roadside hazards, spans continue to increase—as do the number of connection failures. Presented herein is a practice-ready version of the low-cost damage avoidance approach to mitigate wind-induced fatigue effects for cantilevered traffic support structures. The benefit of the proposed system is quantified using a probabilistic fatigue assessment framework. Full-scale prototype testing is conducted in an ambient wind environment to serve as input and statistically describe response. Fatigue performance is modeled as mean stress dependent from which a dependable service life is derived. The efficacy of the proposed damage avoidance technique is assessed for a variety of wind environments where it is shown the dependable service life can increase by an order of magnitude.

8.2 Introduction

In the following, a practice-ready version of the DAD system is presented to mitigate wind-induced fatigue in steel traffic support structures. Then, its advantages are

discussed and quantified using a probabilistic framework. To serve as input and statistically describe structural response, a full-scale prototype structure is monitored in a natural wind environment under several experimental configurations. Using fatigue performance modeled as dependent on mean stress, dependable service lives are determined for a typical traffic signal structure without and with application of the proposed technique for several distinct wind environments, taking into account both: (i) the modeled change in fatigue resistance; and (ii) any observed changes in natural wind response. The evaluated fatigue performance of the modified structure demonstrates the efficacy of the proposed DAD technique.

8.3 Damage Avoidance Fatigue Mitigation Strategy

As stated herein, tensile mean stress due to dead loads adversely affects the fatigue life of tube-to-transverse plate connections (Koenigs et al. 2003; Ocel 2006). As such, fatigue proneness may be markedly reduced upon design mean stress manipulation. The concept of damage avoidance may be implemented superimposing a compressive state of stress to reduce the detrimental tensile mean stress in connections. Although the structural response may not be reduced, the applied compression action will improve the fatigue resistance of the tube-to-transverse plate connection, thus the fatigue life will increase.

Figure 8-1 depicts a practice-ready presentation on the described concept may be applied to a traffic signal structure to improve the fatigue life of tube-to-transverse plate connections. As reiterated in Figure 8-1(a), a PT tendon may be installed to run the length of the mast arm, being anchored at each end to installed bearing plates. Figure 8-1(b)

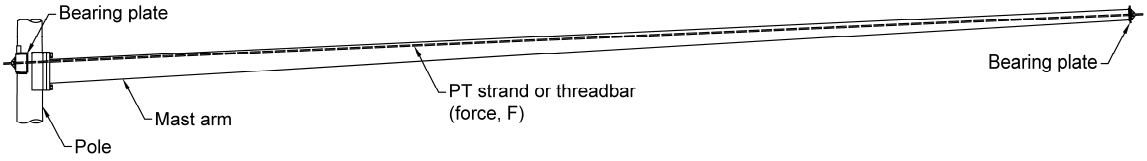

(a) Mast arm PT system

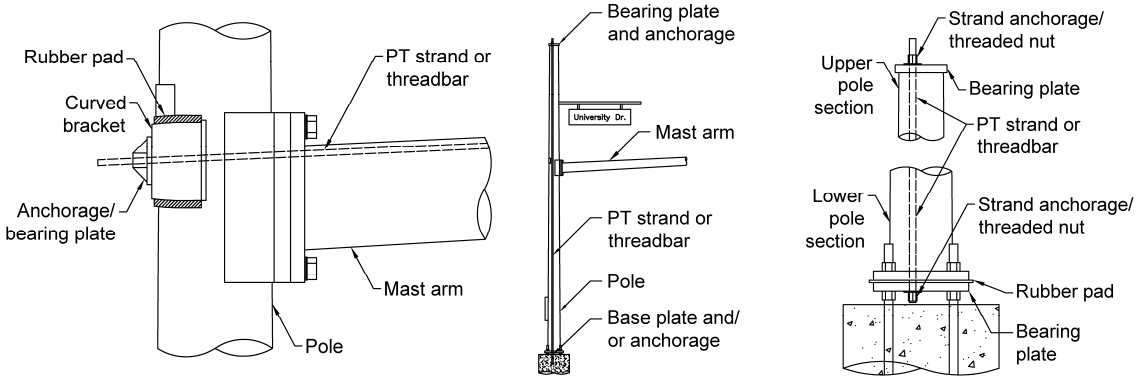

(b) Mast arm PT design detail

(c) Mast (pole) PT system and design detail

Figure 8-1. Proposed (a,b) mast arm and (c) pole fatigue DAD systems and detailing to reduce the detrimental effect of tensile mean stresses in the welded connections.

better depicts the end detailing by showing the bracket on the back side of the arm-pole connection, curved to evenly distribute the PT force over the backside of the pole section back into the arm-pole connection. Differing from the configuration shown in Section 7, Figure 8-1(c) shows a modified application for protecting the vertical pole from fatigue damage, where a bearing plate is used to directly transfer the compressive force into the pole section via the transverse base plate. Despite the applied location, the anchorage at the connections should be to balance (Pekcan et al. 2000) the self-weight of the structure and attached signal clusters, as depicted in Figure 8-1(b). Analogous to a gravity loaded prestressed concrete beam, optimal tendon eccentricity for the mast arm would generally conform to the shape of the dead load moment, increasing toward the mast arm-pole connection.

It should be noted that even if the region around the arm-to-end plate weld were to fail through fatigue and/or fracture during an extreme event or other overloading scenario, the arm would remain suspended, being held in position by the internal tendon under a high PT stress. As a result, the proposed system provides a fail-safe performance strategy, thereby preventing collapse of the mast arm when an unstable fatigue crack develops. Notwithstanding the fail-safe nature of the PT design modifications, the compressive stress on the critical location of the weld also has a beneficial effect by improving the fatigue life of the connection. This is discussed in the following section.

8.3.1 The Influence of Mean Stress on Fatigue Resistance

Tube-to-transverse base plate specimens typical of traffic signal structures fatigue tested under zero (or low) mean stress levels have resulted in longer fatigue lives when

compared to companion specimens tested under higher mean stress conditions that were evidently intended to mimic dead load stresses (Koenigs et al. 2003; Ocel 2006). This trend is evident via comparison of past fatigue test results given in Figure 8-2.

The results presented in Figure 8-2(a) (Koenigs et al. 2003; Roy et al. 2011) stem from fatigue tests conducted on specimens (common to the prototype structure selected later herein) under superimposed loads that led to a typical mean tensile stress of 150 MPa (median value for fatigue tests). This stress corresponds to the expected dead load stress at the arm-to-transverse plate connection for a typical structure with a fully equipped (loaded), 13.4 m mast arm (Koenigs et al. 2003). Thus, this value is adopted herein because the mean stress in the arm-pole connection of the later selected prototype structure is slightly lower due to the lack of wiring, etc., related to a fully-functional structure. Because multiple fatigue studies were considered, the calibrated model is inclusive of a variety of representative materials and common arm-pole connection details used in the field. The superimposed relationships depict the median fit and uncertainty related to the fatigue resistance (and hence damage model) for several details related to tube-to-transverse base plate connections common to traffic signal structures. Figure 8-2(a) depicts that when a customary slope of $c = -3$ is used to describe the median fatigue resistance with an elevated mean stress, variability in fatigue life may be adequately modeled using the well-known, two-parameter lognormal distribution with a one-million cycle median stress of $S_{r,m} = 57\,\text{MPa}$ and a lognormal standard deviation of $\beta_{D|Sr} = 0.55$.

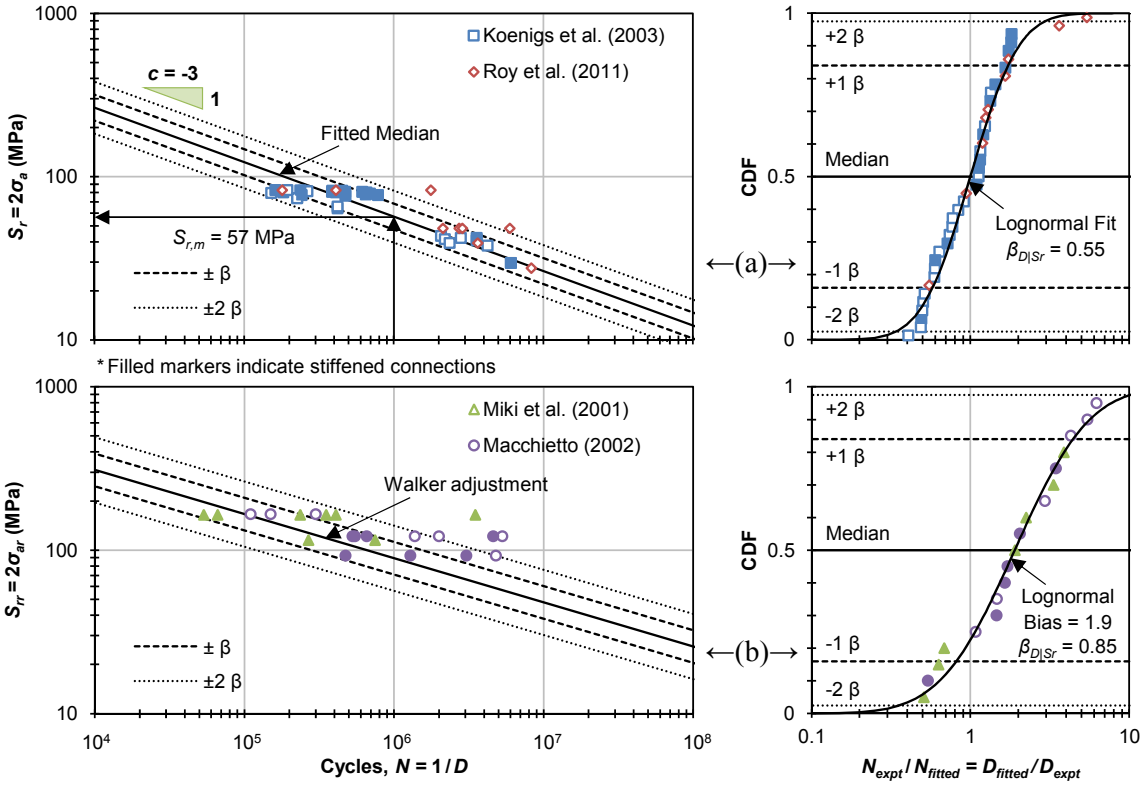

Figure 8-2. Fitted fatigue model results depicting the mean stress-dependent fatigue resistance on tube-to-transverse base plate connections common to traffic signal structures showing comparisons for (a) an elevated tensile mean replicating dead load effects and (b) zero mean (fully reversed loading).

Figure 8-2(b) depicts transformation of the previously fit relationship using the previously-justified Walker (1970) model, converting the nominal stress range (at an elevated mean stress of 150 MPa) to a fatigue damage-equivalent stress range S_{rr} corresponding to fully reversed conditions. This result is shown alongside fatigue test results (Miki et al. 2001; Macchietto 2002) conducted without a superimposed mean stress. Upon review of the Walker (1970) relation, the effect of mean stress becomes more apparent with decreasing nominal stress range. Thus, the equivalent stress range increases more significantly—causing the slope of the fatigue resistance curve to reduce. Figure 8-2(b) shows that the associated dispersion increases, which is in agreement with previous observations (Koenigs et al. 2003). More notable than the increased randomness ($\beta_{D|Sr} = 0.85$) is the evident bias relating to a conservative underestimation in fatigue resistance.

To investigate the reason for the bias depicted in Figure 8-2(b), a further review of the connection test results in Figure 8-2 was conducted. Nearly double the percentage of the connections tested under a zero mean stress were stiffened when compared to those tested under an elevated stress level. Filled markers indicate stiffened connections in Figure 8-2. Upon study of the fit in Figure 8-2(a) for the tests performed about an elevated mean, the ratio of average bias between stiffened and unstiffened connections was 1.25, when excluding the outlier. But as seen in Figure 8-2(b), a greater percentage of specimens subjected to fully reversed loading were stiffened, yet this had little influence on fit bias. However, the (conservative) bias in predicted fatigue resistance is best justified upon review of the large difference in crack tip intensity factors relating to fatigue categories E

and E' (AASHTO 2013). This difference can be represented by a ratio of maximum 1.93, similar to the model bias. Therefore, it can be reasoned that the specimens compiled in Figure 8-2(b) exhibit an increased fatigue resistance due to both a decreased mean stress and improved detailing. Thus, the Walker (1970) adjusted relationship reasonably considers the increased fatigue life expected when under fully reversed loading. This model fit was also found in acceptable agreement when compared against the results of more exacting fracture mechanics initiation-propagation analyses.

8.4 Fragility Analysis Framework

A four-step probabilistic approach modified and expanded from a seismic approach in (Mander et al. 2012) has been adapted for a wind environment in Section 6. Wind-induced fatigue damage accumulated in fatigue-prone connections is related to a wind speed-recurrence rate. Figure 8-3 depicts the piece-wise interaction between submodels that include: (a) wind hazard; (b) wind-induced structural response; (c) fatigue damage analysis; and (d) probabilistic fatigue damage-recurrence rate estimation. See Section 6 for a complete description/derivation.

8.5 Field Test Description

Field experiments were conducted (Section 3) to investigate the statistical response behavior outcomes for a common traffic signal structure (Wieghaus et al. 2014a). As noted in Section 7, a prototype DAD system was installed in phases and the response was observed. Free vibration experiments, as well as long-term monitoring under while under ambient wind excitation, were carried out for each structural configuration considered.

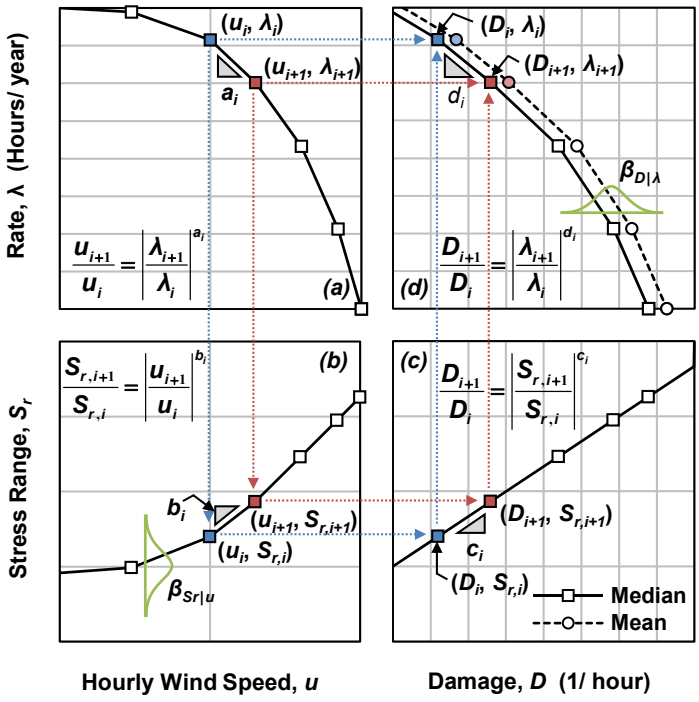

Figure 8-3. Probabilistic fatigue damage assessment: (a) wind hazard; (b) wind-induced structural response; (c) fatigue damage analysis; and (d) fatigue damage-recurrence rate relation.

8.5.1 Standard (Unmodified) Structure

The previously decommissioned traffic signal prototype structure has been detailed throughout this dissertation. Dimensions, connection detailing, instrumentation locations, and the selected orientation relating to the installed structure are depicted in Figure 3-1. Section 3 should be consulted for any further information pertaining to structural dimensions, strain gage/anemometer instrumentation, data acquisition, and data post-processing (Wieghaus et al. 2014a).

8.5.2 Prototype with Post-tensioned Mast Arm

In Section 7, the prototype PT system was field installed to the horizontal mast arm during Phase II. The wind-excited response of the prototype structure with arm PT was observed near each connection from October 17, 2011 to April 24, 2012.

8.5.3 Prototype with Post-tensioned Pole

As described in Section 7, the PT in the arm was removed and then applied in a similar manner to the mast (pole) as depicted in Figure 7-2 (Phase III). While Figure 8-1(c) depicts a suggested configuration for best implementation at the pole-base connection, field installation varied slightly. Unlike that shown in Figure 8-1(c), a square bearing plate was elevated approximately one meter from the pole-base connection anchored to the foundation using four threaded rods. The as-built detail did not require a rubber bearing pad, but was deemed comparable to the proposed system for field testing. The ambient wind dynamic response of the prototype structure with pole PT was observed from October 30, 2012 to November 14, 2012, then the pole alone from May 9, 2013 to June 17, 2013.

8.6 Field Test Results

Figure 8-4 presents the results stemming from the full-scale experimental testing of the installed prototype structure, along with the statistical characterization as necessitated for future probabilistic fatigue analysis. As described herein, three configurations of the prototype structure were tested under both snap-back and ambient wind-excited tests. These configurations involved: (a) the standard (unmodified) prototype structure typical to a majority of in-service structures; (b) the prototype structure with the proposed PT system field installed only to the horizontal mast arm; and (c) the prototype structure with only mast (pole) PT applied. The first row of Figure 8-4 presents a single arm tip displacement time history during free vibration tests for each configuration, inferred from arm bending strains intermittently validated using a computer vision technique (Bartilson et al. 2015). From the results, in- and out-of-plane natural frequencies and damping ratios were determined. The two rows of Figure 8-4 present the across- and along-wind inferred stress range responses at the arm and pole connections as a function of wind speed for each structural configuration.

8.6.1 Standard (Unmodified) Structure

Shown in Figure 8-4(a) are the observations made in Section 3, where in- and out-of-plane natural frequencies of 1.09 and 0.99 Hz were observed, with in-plane damping being less than the out-of-plane damping—each were under one percent and of similar order to those in past studies (McDonald et al. 1995; Letchford et al. 2008). Consult Section 3 for a discussion on characterizing of response of the standard prototype structure.

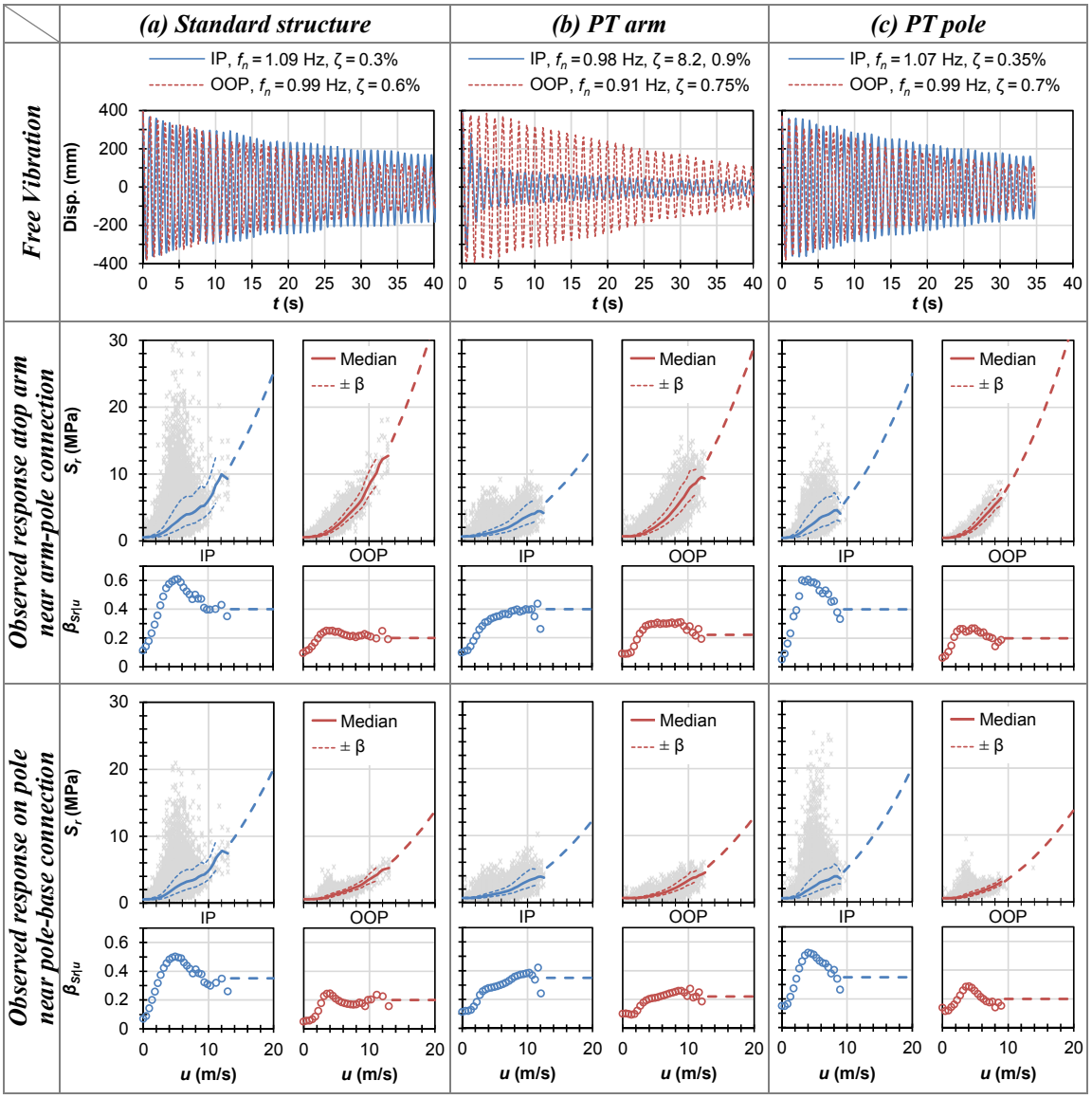

Figure 8-4. In-plane (IP) and out-of-plane (OOP) observations and subsequent statistical characterization following field testing of the prototype traffic signal structure with (a) standard configuration, (b) PT arm, and (c) PT pole.

8.6.2 Structure with Post-Tensioned Horizontal Mast Arm

Figure 8-4(b) depicts the results of field experimentation of the prototype structure following installation of arm PT (Phase II). Decreased in- and out-of-plane natural frequencies of 0.98 Hz and 0.91 Hz, respectively, resulted from increasing the effective mass of the mast arm. As discussed in Section 7, an increased in-plane damping was observed free vibration tests because the eccentrically placed PT strand came into contact with the inner tapered mast arm section. Figure 8-4(b) presents a sample free vibration where the effect of strand 'knocking' is apparent. Immediately following release of the cantilevered mast arm, an equivalent damping ratio of 8.2 percent was observed. Once the impact damping discontinued the observed damping ratio decreased to 0.9 percent. The unforeseen impact damping effect may not occur for all combinations of traffic signal structure and strand configuration. Although damping increased following arm PT installation, damping did not increase beyond one percent unless well-excited. The subtle increase in damping is most likely a result of the rubber pads installed at the bearing locations.

As shown by Figure 8-4(b), observed wind speeds were similar to those measured while observing the ambient wind-induced response of the prototype structure under a standard configuration. Because testing occurred under similar conditions, it was appropriate to compare results obtained without and with the installed arm PT. As shown, continuous monitoring indicated a notable decrease in in-plane (across-wind) response, which is directly related to the unexpected increase in damping, whether due to the impacting strand or the rubber bearing pads. Extrapolation for higher wind speeds again

followed the square of wind speed, where decreases of 44 percent and 12 percent are expected for in- and out-of-plane median response at the arm-pole connection, respectively. Fitted trends again indicate that the along-wind (out-of-plane) response at the arm-pole exceeds the across-wind (in-plane) stress response. The observed stress response at the pole-base connection decreased similarly when compared to the standard configuration; however the magnitudes of the in- and out-of-plane response stresses are relatively similar.

8.6.3 Structure with Post-Tensioned Vertical Pole

Figure 8-4(c) depicts the results of field testing of the prototype under snap-back and ambient excitation, following installation of a PT threaded rod running along the height of the vertical pole (Phase III). Results from free vibration snap back tests indicated negligible change in the frequency or damping of the prototype structure.

Due to the negligible change in system properties, the observed stress response was found similar to that of the prototype structure under standard configuration, as shown in Figure 8-4(c). Thus, the median responses and their dispersions at higher wind speeds are similarly extrapolated.

8.7 Probabilistic Fatigue Analysis and Implications

The presented framework was used to determine the fragility of the wind-excited prototype structure for the three tested configurations subjected to five unique wind environments. The analyses performed consider both in- and out-of-plane fatigue damage accumulation at the arm-pole and pole-base connections. Figure 8-5 offers a sample

application for the prototype subjected to the local wind environment unique to College Station, TX—assessing the in-plane fatigue life of the arm-pole connection without and with arm PT. Presentation of each submodel helps visualize the effect of mean stress on probabilistic connection fatigue damage accumulation.

Figure 8-5(a) depicts the local wind hazard model based on historical wind records. Empirical probabilities used for annual winds, whereas extreme value distribution used to extrapolate the probability density function for winds with recurrence rate less than one hour annually. Figure 8-5(b) is the in-plane response of the prototype structure before (solid) and after (dashed) the installation of arm PT. For the case presented, the stress response inferred from continuous monitoring is used; the reduction in in-plane stress response, along with the uncertainty in response is shown in Figure 8-5(b,b'), respectively. Figure 8-5(c) presents the calculated response-damage relationships determined via using the fit stress-life curves via Eq. (6-5). As shown, reducing the dead load tensile stress decreases fatigue damage accumulation in the connection.

Given the section properties of the prototype structure and the 150 MPa bending stress assumed atop the arm-pole connection, a mean bending stress of approximately 80 MPa would result on the back side of the pole-base connection. As a result, the fatigue resistance of the pole-base connection would be increased with respect to that of the arm-pole connection. As such, the Walker (1970) model was used to transform the relationship shown in Figure 8-2(b) downward to a stress-life related to a dead load mean stress equal to 80 MPa.

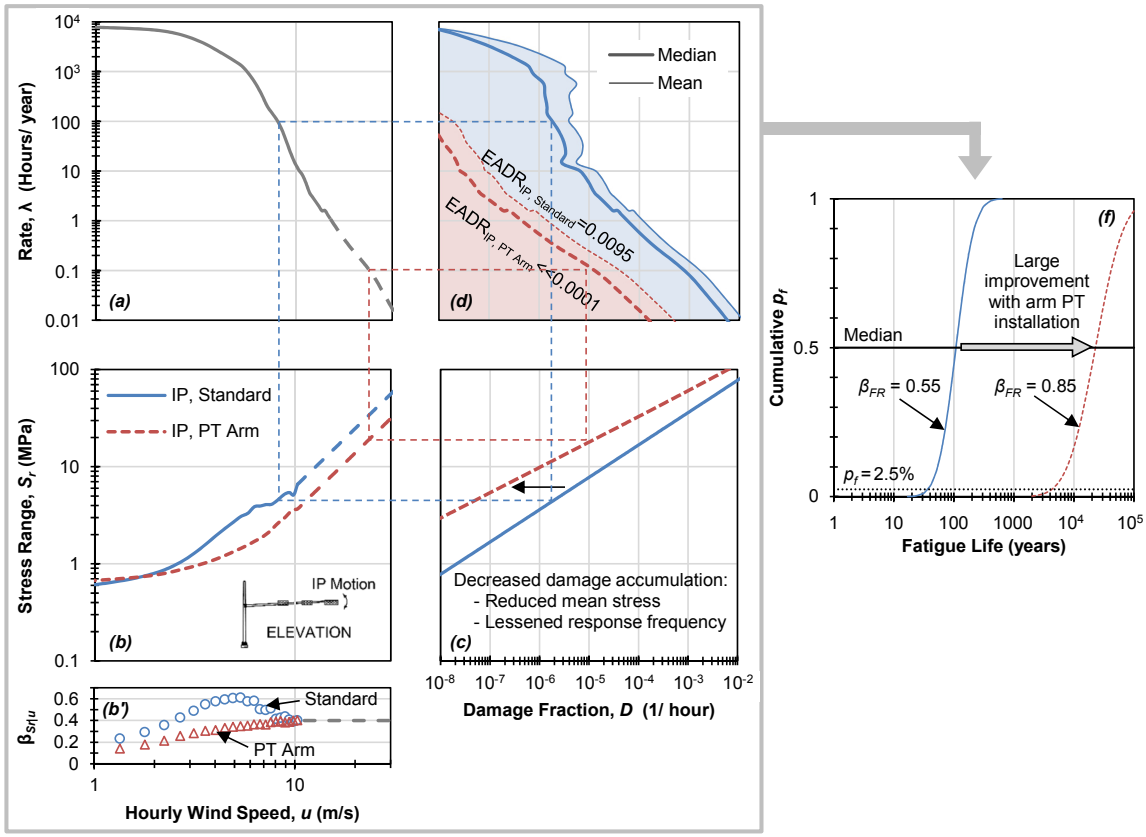

Figure 8-5. Probabilistic fatigue damage analysis for the studied traffic signal structure in (a) Bryan/College Station, TX, depicting the effect that arm PT has on (b,b') in-plane (IP) response and (c) fatigue capacity improvement, followed by the determined (d) damage-recurrence relationship and the resulting (e) fatigue fragility.

Shown in Figure 8-5(d) are the median and expected (mean) damage curves, piece-wise determined using Eq. (6-1) and the relation between the median and expected value of a lognormally distributed variable, respectively. The shaded regions represent the EADR, calculated using Eq. (6-8). Given EADR and the randomness associated with the fatigue resistance, the dependable service life is calculated as defined by the 2.5 percent non-exceedance probability. For the prototype structure, arm PT markedly increases the dependable service life from 35 years to over (theoretically) 1000 years.

Of particular interest in Figure 8-5 are the observed and modeled differences between the prototype without and with the proposed arm PT installed. As previously discussed, the arm PT installation disrupted practically all occurrences of large-amplitude across-wind structural response, albeit inadvertently. This is again shown in Figure 8-5(b,b') and would alone greatly improve the in-plane fatigue life of the structure. Next, Figure 8-5(c) depicts a leftward decrease in fatigue damage accumulated (per hour) given structural stress response after the detrimental tensile mean stress atop the arm section is relieved using PT (load-balancing) concepts. This includes a 10 percent decrease due to the reduction in response frequency alone; however this is quite small when compared to the reduction resulting from the load-balancing which is over an order of magnitude for the most commonly occurring stress cycles. Finally, Figure 8-5 illustrates the interaction of the slope of the damage model c and the uncertainty related to fatigue damage accumulation. From Eq. (6-5), the variability in stress response at a given wind condition is amplified by the magnitude of the power c. Thus as mean stress decreases the uncertainty in response is more heavily weighed when determining the mean damage

fraction and thus EADR. Regardless of this relation, minimizing the mean tensile stress within tube-to-transverse base plate connections significantly reduces the wind-induced fatigue damage incurred by traffic signal support structures.

Figure 8-6 displays the results for the three considered configurations, subjected to five different wind environments of varying severity. For each, in- and out-of-plane fatigue was considered at both the arm-pole and pole-base connections. The results are separated into several categories. The first category (Line 1) describes the lower bound dependable life as a function of mean annual wind speed at a specified location. In which case, it was observed that the dependable life could be reasonably expressed as a function of wind speed cubed, which is related to wind power. As seen for the standard prototype structure, fatigue at the arm-pole connection resulting from in-plane excitation controlled the dependable life. The second category (Line 2) describes the case in which either only arm PT or arm and pole PT is applied to a structure similar to that of the prototype. This relationship was developed assuming that pole PT would be installed if it became critical following arm PT installation. In which case, considering the observed changes in structural response, the dependable life increases over an order of magnitude.

The third category (Line 3) in Figure 8-6 results when it is assumed that neither arm nor pole PT would lead to changes in structural response; the response parameters in Figure 8-4(a) were used and only mean stress was changed. Results show that a combination of arm and pole PT would increase the dependable life of a cantilevered traffic signal structure by nearly an order of magnitude.

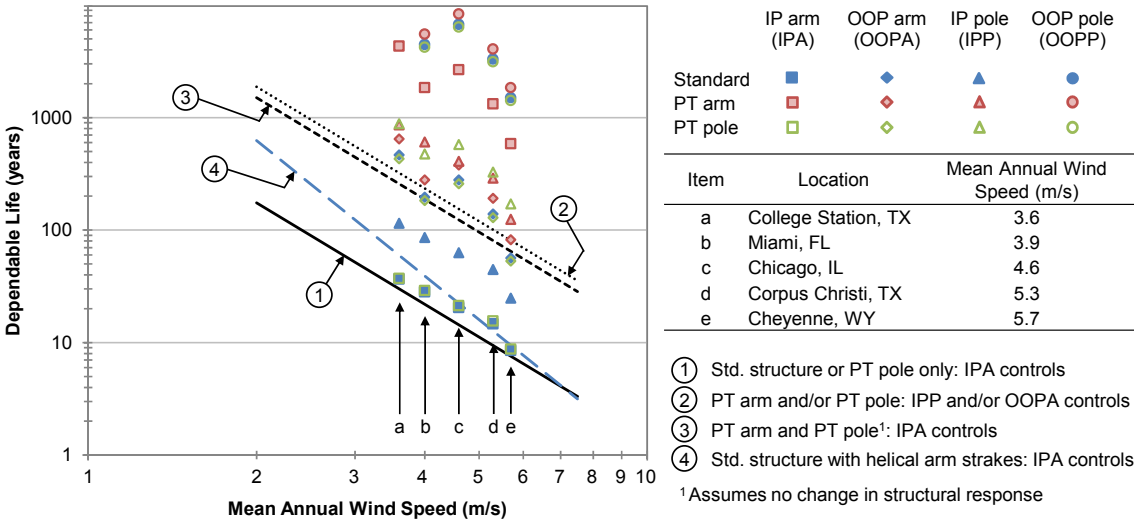

Figure 8-6. Effectiveness of the proposed PT DAD system for traffic signal structure fatigue mitigation despite variability in local wind environment.

8.8 Discussion

A capacity improvement technique has been presented whereby a load-balancing PT solution superimposes compressive stresses to relieve the elevated tensile mean stresses present in tube-to-transverse plate connections. The unintended increase in structural damping may also classify the system as a demand reduction technique, however this cannot be assumed for all structures and configurations.

As previously approached by past researchers, demand reduction may be approached by reducing excitation caused by a specific mechanism or by increasing structural damping. Although effective techniques and/or devices have been developed, the related changes in natural wind response have not been statistically quantified, thus no related probabilistic fatigue assessments have occurred. To compare the merits of DAD against an excitation mechanism-targeted mitigation technique, results found in Section 3 (Wieghaus et al. 2014a) are used. Therein, the response of the prototype traffic signal structure was studied before and after the installation of helical mast arm strakes, designed to reduce the influence of vortex shedding on the across-wind (in-plane) response.

The result stemming from further probabilistic analyses is shown by the fourth category (Line 4) in Figure 8-6. As shown, the effectiveness of helical arm strakes, an aerodynamic measure, is dependent on wind environment severity, where a marginally worthwhile benefit is seen in locations in which the mean annual wind speed is less than 4.5 m/s. This is where a significant benefit of the proposed DAD approach is seen: its effectiveness is independent of wind environment. The PT solution is significantly more effective in increasing the dependable life when compared to an aerodynamic means to

eliminate a specific excitation mechanism. Moreover, the approach provides a fail-safe mechanism.

The proposed PT DAD solution adds a beneficial load-balancing redundancy for cantilevered traffic signal structures, but could do so for a variety of lightweight, tubular structures with welded or bolted connections across several engineering fields. Not only does the PT reduce the effect of dead load stresses to increase fatigue resistance, the system also provides a fail-safe mechanism to prevent total arm collapse following extreme overloads or collisions. As demonstrated, the proposed method may be incorporated for retrofit of existing fatigue-critical structures, but could be easily implemented for new designs.

Despite the availability of current datasets, additional fatigue tests should be conducted to overtly corroborate the effect of elevated tensile mean stresses atop tube-to-transverse base plate connections. Test specimens should be similarly detailed to allow direct result comparisons, and the results should be substantiated using computational analyses. Mean stress-dependent fatigue strength curves could result whereby two classifications could be used for design: (i) capacity considering an elevated mean stress (as current practice does); and (ii) capacity considering a reduced (not necessarily zero) dead load effect for designs implementing DAD systems as presented herein. These considerations could potentially dictate more cost efficient designs. Further refinement of the proposed concept presented herein could lead to damage-free solutions for similar connections.

8.9 Closure and Key Findings

A low-cost DAD solution using PT concepts has been developed to mitigate wind-induced fatigue damage accumulation from tube-to-transverse base plate connections in cantilevered traffic signal structures. Load-balancing is used to transfer the dead load associated with cantilever mast arm directly to the vertical pole, as opposed to transferring the load through the fatigue-prone tube-to-base plate connection. If necessary, this load may then be transferred directly to the back side of the pole-base connection via pole PT. As such, the elevated tensile mean stresses located in the vicinity of the welded connections are eliminated and the fatigue life improved. Full-scale prototypes were installed to a representative traffic signal structure for snap-back and ambient wind testing. Although unexpected, full-scale prototype ambient testing indicated an increase structural damping and reduced natural wind response following mast arm PT. However, subsequent probabilistic fatigue analyses performed indicate that response reduction is unnecessary to significantly improve the dependence service life of these structures.

The following key findings are drawn based on the research described and probabilistic analysis performed herein:

i. Tensile mean stresses are detrimental to the fatigue performance of tube-to-transverse base plate connections. The proposed PT DAD concept is a low-cost solution to reduce the detrimental effects that tensile mean stresses pose. The proposed fail-safe DAD system adds a load-balancing redundancy to cantilevered members with welded and bolted connections and has further potential to other applications.

ii. When testing the prototype structure with eccentric arm PT, it was evident that a mechanical damping mechanism was present as tendon 'knocking' was observed. This source of mechanical damping further reduced response. When not experiencing large-amplitude vibrations, the arm PT system along with the associated bearing pads, increased in-plane damping, while out-of-plane damping was practically unaffected. Applying PT to the pole had little influence on the dynamic, wind-induced response of the prototype structure.

iii. Given the mean stress values presented by past researchers for the prototype structure, a reduction of tensile mean stress alone may increase the dependable service life of the prototype structure by an order of magnitude. In contrast to an aerodynamic vibration mitigation device (helical strakes), the proposed PT solution is effective for all natural wind environments.

9 RIGOROUS VERSUS SIMPLIFIED FATIGUE LIFE MODELING: EXPLORING THE VALIDITY OF SIMPLIFIED CONNECTION FATIGUE MODELING

9.1 Overview

Simplified, cubic-fitted stress-life curves are most commonly used during fatigue life studies. To investigate the ramifications of using connection damage models based on these curves during previously conducted probabilistic analyses, a fracture mechanics-based, total life initiation-propagation model is developed to create alternative stress-life curves for common traffic signal structure connections. Probabilistic assessments are repeated to investigate the validity of simplified connection damage models used previously in this dissertation. The mean stress-dependent total life model is also used to demonstrate and justify the detrimental effect mean stress has on tube-to-transverse base plate fatigue resistance. Simplified damage models are found to yield conservative life expectancy estimates that tend to overestimate the effect of mean stress relief on dependable life. Using total life-based models, it is now predicted that applied prestress may increase dependable life by an order of magnitude in the most severe wind environments, while greatly increasing dependable life for others. Regardless, the use of simplified models is deemed acceptable for use in the probabilistic framework proposed in this dissertation for mean stress-adjusted dependable life estimation.

9.2 Introduction

AASHTO fatigue classifications for tube-to-transverse base plate connections common to traffic signal structures are based on findings from tests conducted using cyclic loads about an elevated mean to mimic the detrimental effect that tensile dead load stresses imposed at the welded connection (Miki et al. 1981; Alderson 1999; Koenigs et al. 2003; Ocel 2006; Roy et al. 2011). Welded tube-to-transverse base plate specimens typical of traffic signal structures fatigue tested under zero (or low) mean stress levels have demonstrated longer fatigue lives when compared to companion specimens tested under higher mean stress conditions that were evidently intended to mimic dead load stresses (Koenigs et al. 2003; Ocel 2006).

Fracture mechanics-based crack propagation modeling has been used to acceptably model the stress-life behavior of tube-to-transverse base plate connections when using crack tip correction factors from past research (Zettlemoyer and Fisher 1977; Fisher et al. 1983). Despite acknowledging the detriment of mean stress effects by testing connections under dead load stresses, crack propagation modeling assumed fully reversed stress cycles (Fisher et al. 1983). Thus, crack propagation modeling alone is not acceptable to model the entirety of the mean stress-dependent nature of tube-to-transverse base plate connection fatigue resistance.

Recent works have implemented total life, or initiation-propagation, models, where it is expected that crack initiation lasts significantly longer than crack propagation for lower levels of structural stress response (Chen et al. 2003, Azzam 2006). Total life

modeling offers a solution to account for effect of dead load mean stresses on both crack initiation and propagation within a fracture mechanics-based analysis approach.

As presented in Sections 6 and 8 of this dissertation, the median stress-life relation corresponding to past fatigue tests results have been fit using a traditional cubic-related slope that conforms to current AASHTO fatigue design strength curves. These sections should be consulted for: (i) a brief summary of the simplified stress-life modeling performed, and (ii) a description of the relationship between stress-life and fatigue damage models implemented in the probabilistic framework used throughout the dissertation. Fatigue life assessments for structures similar to that experimentally observed were made using these simplified models. Use of a mean stress-corrected simplified damage model indicated that applied prestress may increase the dependable service life of traffic signal structures by nearly an order of magnitude over varying levels of wind environment severity.

In this section, a fracture mechanics-based, total life initiation-propagation model is developed to create fatigue stress-life curves that account for mean stress effects and connection geometries common to traffic signal structure tube-to-transverse base plate connections. Using the results of past fatigue testing programs, the model is verified for unstiffened, fillet-welded connections using best-fit parameters. The model is then used to describe the fatigue resistance of the family of common tube-to-transverse base plate traffic signal structure connections tested. Using a total life-based damage model, probabilistic assessments are repeated to investigate the validity of simplified connection damage models used previously in the dissertation. A complementary initiation-

propagation model parameter sensitivity analysis is also conducted. The mean stress-dependent model is also used to demonstrate the detrimental effect mean stress has on tube-to-transverse base plate fatigue resistance. The total life-based model is then used to reassess the effectiveness of mitigating the adverse mean stresses by applying a supplementary post-tensioned prestress. Differing from past analyses, the effect of mean stress relief is not constant with wind environment severity. It is now predicted that the application of prestress may increase dependable life by an order of magnitude in the most severe wind environments, while greatly increasing dependable life for others. Regardless, it is shown that extending the service life well past current expectations.

9.3 Development of a Total Life Initiation-Propagation Model

A total life fracture mechanics approach is considered to more rigorously model the mean stress-dependent fatigue resistance of tube-to-transverse base plate connections common to traffic signal structures. Total life was first introduced as a combination method (Dowling 1979) consisting of a notch root (or local) strain-life approach to predict crack initiation (i.e. formation or nucleation) life, and a fracture mechanics approach to predict crack propagation life. This is referred to as an initiation-propagation approach, where both crack initiation and propagation are essential to capture the fatigue and eventual fracture of such connections (Azzam 2006). Strain-life modeling is used to estimate the crack initiation or early growth from a notch root. A combination approach circumvents the difficulties of using linear elastic fracture mechanics to describe the earliest stages of crack growth (Bannantine et al. 1990). In general, the initiation lasts

significantly longer than propagation (Chen et al. 2003). The lives corresponding to crack initiation and crack propagation are summed to estimate the total fatigue life.

9.3.1 Considerations for Total Life (Initiation-Propagation) Model

As discussed previously, a multitude of processes affect the fatigue resistance of tube-to-end plate socket connections. The following paragraphs introduce aspects of the approach to consider while using a total life framework to form an alternative fatigue resistance model for traffic signal structure connections. Briefly discussed are the strain-life approach (crack initiation), Neuber's (1961) rule to determine notch stresses and strains, fracture mechanics (crack propagation), potential for overloads, and past material/connection fatigue testing.

Strain-life (Crack Initiation)

The fatigue life of a material undergoing loading can be expressed in terms of the well-known Coffin-Manson strain-life equation (Manson 1953; Coffin 1954) as presented in Eq. (2-2). As eluded to by the variable definitions, the first part of Eq. (2-2) represents high-cycle fatigue where strains are elastic, while the second part is the low-cycle fatigue component where strains exceed yield. The Manson-Coffin formulation typically assumes a smooth sample, under fully reversed loading. This, however, does not have to be the case. If the notch root strain history and smooth specimen strain-life parameters are known, fatigue life estimates can be made for notched members. A primary advantage of this method is that one may account for mean stresses (Bannantine et al. 1990; Stephens et al. 2000).

Notch Effects according to Neuber's Rule

Geometry (detailing) and local notch properties are the two primary sources of stress concentration at the notch root of traffic signal-type connections (Ocel 2006; Roy et al. 2011). Expressed in the 2013 specifications (AASHTO 2013) is an expected range of notch tip intensity factors expected for each the most common tube-to-transverse base plate connection categories. Table 9-1 presents the infinite life stress concentration factor K_I related to AASHTO Categories D, E, and E'—these values correspond to the design constant amplitude fatigue limit (CAFL) specified for each category.

Table 9-1. AASHTO infinite life fatigue stress concentration factor values for welded tube-to-transverse plate connections. This concentration factor incorporates the effect of connection geometry and geometric notch effects at the weld toe.

AASHTO Category	K_I	
	Lower Bound	Upper Bound
D	--	4.0
E	4.0	6.5
E'	6.5	7.7

The strain-life method can be used to perform fatigue life evaluations for notched members if notch root strains and smooth specimen strain-life parameters are known. Given nominal stresses or strains, local stress and local strain at the notch root can be obtained by: experimental methods, finite element methods, or analytical models (Stephens et al. 2000). Analytical models are commonly found to be the least time-

consuming and least expensive method to relate nominal stresses and strains to notch values (Bannantine et al. 1990).

Typically, the theoretical stress concentration factor K_t relates nominal stresses S or nominal true strains e to notch (local) values σ and ε. However, following notch yielding the local stress σ and local strain ε are no longer linearly related to their respective nominal values via K_t. Thus, beyond elastic behavior, nominal and notch tip values are related in terms of stress and strain concentration factors, $K_\sigma = \sigma / S$ and $K_\varepsilon = \varepsilon / e$, respectively. As expected, K_σ decreases and K_ε increases following yield.

Neuber (1961) derived the following relation (Neuber's rule) for grooved shafts under torsion

$$K_t^2 = K_\sigma K_\varepsilon \tag{9-1}$$

or

$$\varepsilon\sigma = K_t^2 eS \tag{9-2}$$

According to Eq. (2-1), the geometric mean of the stress and strain concentrations factors under plastic deformations is equal to the constant theoretical stress concentration factor K_t. Despite this method being proven for a single geometry, Neuber's rule has been widely used and holds true for most notch geometries (Bannantine et al. 1990; Stephens et al. 2000).

For nominally elastic behavior $\varepsilon = S/E$, Eq. (9-2) can be expressed as

$$\varepsilon\sigma = \frac{\left(K_t S\right)^2}{E} \tag{9-3}$$

When combined with the Ramberg-Osgood true stress-strain relationship for monotonic loading (Ramberg and Osgood 1943), Eq. (9-3) becomes

$$\frac{\sigma^2}{E}+\sigma\left(\frac{\sigma}{K}\right)^{1/n}=\frac{\left(K_t S\right)^2}{E} \tag{9-4}$$

where $K=$ the strength coefficient and $n=$ the strain hardening exponent. Thus, combining Eqs. (9-3) and (9-4) yields

$$\varepsilon\sigma=\frac{\sigma^2}{E}+\sigma\left(\frac{\sigma}{K}\right)^{1/n} \tag{9-5}$$

For cyclic loading, the hysteresis curve replaces the monotonic stress-strain curve, and stresses and strains are replaced by their ranges. In addition, since small notches have less of an effect as indicated by K_t for fatigue, Topper et al. (1969) suggested the use of a fatigue notch factor K_f when using Neuber's rule in Eq. (9-3). Thus, implementation of Neuber's rule for cyclic loading yields

$$\frac{\left(\Delta\sigma\right)^2}{E}+2\Delta\sigma\left(\frac{\Delta\sigma}{2K'}\right)^{1/n'}=\frac{\left(K_f\Delta S\right)^2}{E} \tag{9-6}$$

and

$$\Delta\varepsilon\,\Delta\sigma=\frac{\left(\Delta\sigma\right)^2}{E}+2\Delta\sigma\left(\frac{\Delta\sigma}{2K'}\right)^{1/n'} \tag{9-7}$$

where $K'=$ the cyclic strength coefficient and $n'=$ the cyclic strain hardening exponent.

Fracture Mechanics (Crack Propagation)

The Paris equation relates crack growth rate da/dN to stress intensity factor range ΔK (Paris and Erdogan 1963) by

$$\frac{\mathrm{d}a}{\mathrm{d}N} = C\left(\Delta K\right)^m \tag{9-8}$$

in which C and m are material constants and

$$\Delta K = \alpha S_r \sqrt{\pi a} \tag{9-9}$$

where $S_r =$ the nominal stress range; $a =$ the crack length (through the tube thickness); and $\alpha =$ the stress correction factor. Specifically, the stress correction factor is given by

$$\alpha = F_c F_s F_w F_g \tag{9-10}$$

where $F_c =$ the crack shape correction factor; $F_s =$ the (front) free surface correction factor; $F_w =$ the finite width correction factor; and $F_g =$ the stress gradient correction factor associated with the non-uniform stresses due to detail geometry.

In this present study, the crack shape correction factor F_c is based on that of a thumbnail surface crack, elliptical in geometry; this model has been used on several instances for tube-to-transverse plate studies (Fisher et al. 1983; Chen et al. 2003; Azzam and Menzemer 2006). The elliptical crack shape correction factor F_e is described by

$$F_e = \frac{1}{E\left(k\right)} \tag{9-11}$$

in which

$$E\left(k\right) = \int_0^{\frac{\pi}{2}} \left(1 - k^2 \sin^2\theta\right) \mathrm{d}\theta \tag{9-12}$$

where $k^2 = 1 - \left(a/d\right)^2$, such that $a =$ the minor radius (length through thickness) and $d =$ the major radius of the elliptical crack.

While these past works assumed the same elliptical thumbnail crack shape, each assumed different crack shape geometries:

- Chen et al. (2003) assumed $a/d = 1/5$,
- Azzam (2006) used $d = 1/2$, and
- Fisher et al. (1983) used $d = 3.355 + 1.29a$ for $a < 4\,\text{mm}$, and $d = 3.549a^{1.133}$ thereafter.

As a result, Azzam (2006) is least conservative and Chen et al. (2003) is most conservative for pole thicknesses common to traffic signal structure connections.

The front free surface or edge crack correction factor F_s accounts for the zero stress condition on the free boundary (crack origin) and is given as

$$F_s = 1 + 0.12\left(1 - \frac{a}{d}\right)^2 \tag{9-13}$$

The finite width correction factor F_w accounts for the effect that the ratio a/t_{FL} (in which t_{FL} = the flange or tube wall thickness) has on the propensity of section bending. Zettlemoyer and Fisher (1977) expressed this as

$$F_w = \sqrt{\sec\left(\frac{\pi a}{2t_{FL}}\right)} \tag{9-14}$$

Barsom and Rolfe (1999) suggests a bilinear formulation whose maximum is 1.6; however this difference has little effect on propagation life.

The stress gradient correction factor F_g accounts for the stress distribution acting on the crack resulting from detail geometry. An early form presented in Zettlemoyer and

Fisher (1977), later used by Fisher et al. (1983) to aid in predicting the fatigue strength of steel tube-to-transverse-plate connections, describes stress gradient as

$$F_g = \frac{K_f}{1 + \frac{1}{g}\left(\frac{a}{t_{FL}}\right)^q} \tag{9-15}$$

where $K_f =$ the fatigue notch factor (namely the local stress concentration factor); $g = 0.1473$; and $q = 0.4348$ (for an average cover plate detail with a 45 degree fillet weld).

Fisher et al. (1983) postulated that this gradient may be overly conservative for welds with profiles less than 45 degrees. It can be inferred from intermediate results in Azzam (2006) that perhaps $g \approx 0.14$ and $q \approx 0.40$ are more appropriate for today's profiles.

Eq. (9-8) may be rearranged and integrated with respect to a from initial crack size a_i to a critical crack size $a_{cr} = t_{FL}$. Substituting Eqs. (9-9) and (9-10) gives

$$N = \int_{a_i}^{a_{cr}=t_{FL}} \frac{\mathrm{d}a}{C\left(F_c F_s F_w F_g S_r \sqrt{\pi a}\right)^m} \tag{9-16}$$

This expression is typically numerically integrated because all stress correction factors are a function of crack size a.

Overloads

If cyclic stress response exceeds the design CAFL over the 10^{-4} occurrence probability, a straight-line extension of the fatigue strength curve below the CAFL and cumulative damage analysis (e.g. Miner's rule) is recommended (Roy et al. 2011). To

determine the finite life of connections, current practices include extending the S-N curve beyond the CAFL using a straight-line extrapolation with ranging slope m ranging from -3 to -5. (Robertson 2001; Crudele and Yen 2006; Sonsino 2007; Yen et al. 2013). When related to fracture mechanics, CAFL is a function of threshold stress intensity ΔK_{th}. Thus, to remain consisted with current practice, a lower bound to crack propagation is not estimated using ΔK_{th}.

Past Material and Specimen Testing

Material tests were performed on samples taken from A595 mast arm steel specimens to obtain strain-life and fracture mechanics parameters for common for tubular steel structures (Chen et al. 2003). Table 9-2 presents the test results.

Table 9-2. Cyclic loading and crack initiation (strain-life) parameters relating to typical unstiffened, fillet-welded socket connections common to traffic signal structures.

Parameter	Mast arm samples	A595
E (MPa)	222600	200000
K' (MPa)	881	793
n'	0.1427	0.1463
σ'_f (MPa)	784	793
ε'_f	1.8256	0.9943
b	-0.0808	-0.0878
c	-0.7	-0.5 – -0.7[1]

[1]Estimated by Chen et al. (2003)

Crack propagation material constants, C and m, specified for tube steel in past works are given in Table 9-3. Total life analyses conducted herein use parameters presented by Chen et al. (2003) as input unless otherwise specified. Compiled fatigue tests referring to a variety of tube-to-transverse base plate connections typical to traffic signal structures are used during model development. If necessary, parameters are selected to best fit the compiled experimental data and reduce uncertainty in the capacity model. Uncertainty in resistance accounts for variability and randomness in: (i) residual stresses; (ii) connection geometry and local notch effects; and (iii) material properties.

Table 9-3. Paris equation crack propagation material constants for common tube steels.

Parameter	Fisher et al. (1983)	Chen et al. (2003)
C[1]	1.2×10^{-13}	9.7×10^{-14}
m	-3	-3.11

[1]In the units of a as mm and K as $\text{MPa}\sqrt{\text{mm}}$

9.4 Total Life Model

Considering the aforementioned items, a total life (initiation-propagation) from fatigue-to-fracture approach is used to assess the overall fatigue resistance of various tube-to-base plate connections common to traffic signal support structures. Corrections are implemented to account for mean stress effects in both crack initiation and crack propagation.

The Manson-Coffin crack initiation model presented in Eq. (2-2) was intended to consider a smooth sample, under fully reversed loading; local notch and mean stress

effects are not accounted for. Slight modification and implementation of Neuber's rule are used consider the local notch strains and mean stress effects. To begin, Eqs. (9-5) to (9-7) are modified to determine the effect of mean stress by substituting the nominal stress range $\Delta S,$ notch stress range $\Delta\sigma,$ and notch strain range $\Delta\varepsilon,$ with the maximums $S_{\max},$ $\sigma_{\max}$ and $\varepsilon_{\max},$ respectively, such that

$$\varepsilon_{\max}\sigma_{\max} = \frac{\left(K_f S_{\max}\right)^2}{E} \tag{9-17}$$

$$\frac{\sigma_{\max}^2}{E} + \sigma_{\max}\left(\frac{\sigma_{\max}}{K'}\right)^{1/n'} = \frac{\left(K_f S_{\max}\right)^2}{E} \tag{9-18}$$

and

$$\varepsilon_{\max}\sigma_{\max} = \frac{\sigma_{\max}^2}{E} + \sigma_{\max}\left(\frac{\sigma_{\max}}{K'}\right)^{1/n'} \tag{9-19}$$

where $S_{\max} = S_m + \Delta S/2,$ in which $S_m =$ the nominal mean. Given $K_f, S_{\max}, E, K'$ and $n',$ the maximum notch root stress $\sigma_{\max}$ may be determined to later be used in mean stress considerations. Following, given $K_f, \Delta S, E, K'$ and $n',$ Eqs. (9-5) to (9-7) are used to determine not only the notch (local) stress range $\Delta\sigma,$ but also the strain range $\Delta\varepsilon.$ Given $\sigma_{\max}$ and $\varepsilon_a = \Delta\varepsilon/2,$ the Walker (1970) mean stress corrected strain-life model is used to determine the number of cycles to crack initiation N

$$\sigma_{\max}^{1-\gamma}\varepsilon_{\mathrm{a}}^{\gamma} = \left[\sigma_f'\left(2N\right)^b\right]^{1-\gamma}\left[\frac{\sigma_f'}{E}\left(2N\right)^b + \varepsilon_f'\left(2N\right)^c\right]^{\gamma} \tag{9-20}$$

where $\gamma_w =$ the Walker parameter.

For steel materials, γ_w linearly correlated with ultimate tensile strength σ_u, such that $\gamma_w = 0.8818 - 0.0002\sigma_u$ (Dowling et al. 2009). The Walker-corrected strain-life formula reduces to the well-known SWT-corrected strain-life formula when $\gamma_w = 0.50$ (Smith, Watson, and Topper 1970).

The preceding implementation of Neuber's rule and strain-life modeling is repeated for multiple nominal stress ranges, then multiple mean stress levels to represent the first part of several S-N diagrams describing the mean stress dependency on the fatigue capacity of traffic signal structure connections.

Next, fracture mechanics principles are used to determine the necessary cycles to propagate a thumbnail crack through the wall (flange) thickness of the tube section constituting the traffic signal connection. Given the material properties necessitated in Eq. (9-8) and terms to determine the stress intensity correction factors related to Eq. (9-10), all that remains is to account for stress ratio (mean stress) effects on crack growth rate $\mathrm{d}a/\mathrm{d}N$. For a constant ΔK, crack growth rates increase with increasing R, however sensitivity is material dependent. A common method (Beden et al. 2009, Dowling et al. 2009) to compensate for mean stress (or stress ratio) effects is the Walker (1970) modification of the stress intensity factor, which an equivalent, fully reversed stress intensity ΔK_r, expressed as

$$\Delta K_r = \frac{\Delta K}{(1-R)^{1-\gamma_w}} \tag{9-21}$$

The equivalent stress intensity ΔK_r is then substituted into crack growth formulas, however ΔK remains dependent on specimen geometry and crack size/shape.

The total life (number of cycles) corresponding to crack initiation and crack propagation are summed to estimate total fatigue life of the component, whose mean stress dependence has been considered.

9.4.1 Initial Model Calibration

The introduced total life framework was first cast to describe a 'typical' tube-to-transverse base plate socket connection. As a starting point, A595 strain-life and crack-propagation parameters in the range of those given in Chen et al. (2003) are used to describe the tube steel. As seen throughout the literature, the geometric stress concentration factor (GSCF) corresponding to the top of the tubular connection is expected to be between 3.0 and 3.5, therefore selected was an approximate fatigue stress intensity factor $K_f \approx 6.5$ (Roy et al. 2011). Table 9-4 resents the cyclic loading and strain-life parameters selected for preliminary analyses based on visual inspection of the fit. Crack initiation life was assumed to represent the time in which it took to form a crack of depth $a = 1$ mm (Chen et al. 2003).

Following crack initiation, growth was modeled assuming an initial crack size $a = 1$ mm (Fisher et al. 1983; Chen et al. 2003) and a critical crack size equal to the tube thickness $t_{FL} = 4.6\,\text{mm}$. The crack front was assumed to be of thumbnail geometry with an elliptical crack front, with dimensional ratio previously specified in Fisher et al. (1983). The crack propagation material constants C and m were set as to those determined by

Chen et al. (2003). To account for mean stress effects, the Walker modification is used to modify stress intensity; given an appropriate ultimate strength of $\sigma_u \approx 450\,\text{MPa}$, $\gamma_w \approx 0.8$. All factors constituting the correction factor in Eq. (9-10) are taken as previously presented, including the stress gradient correction F_g corresponding to today's lower-profile welds.

Table 9-4. Cyclic loading and crack initiation (strain-life) parameters relating to typical unstiffened, fillet-welded socket connections common to traffic signal structures.

Parameter	Input Value
E (MPa)	200000
K' (MPa)	793
n'	0.143
σ'_f (MPa)	780
ε'_f	1.8
b	-0.10
c	-0.6

The preliminary total life model considered a mean stress $\sigma_m = 150\,\text{MPa}$ and is compared to the unstiffened, fillet-welded connection test results found in Koenigs et al. (2003) that were performed at similar mean stress levels. Over 90% of the tested specimens had tube thicknesses $t_{FL} \approx 4.6\,\text{mm}$. The total life model is also used to predict fatigue resistance when $\sigma_m = 0$, then compared against unstiffened, fillet-welded connection fatigue results conducted under fully reversed loading (Macchietto 2002), where all specimens are believed to have similar tube thickness (however unaware of base

plate thickness and weld dimensions). Figure 9-1(a) depicts the results of the total life models given the inputs specified.

As seen in Figure 9-1(a), the total life model closely resembles the previous cubic fitting, except demonstrates a slope related to $m < -3$ for $N_f > 10^7$, bearing some resemblance to recent works (Crudele and Yen 2006; Sonsino 2007; Yen et al. 2013). It can be seen however, that the model corresponding to zero mean stress does not agree well with the compiled fatigue test results. To justify this difference, stress intensity factors were back-calculated using the developed model. The disagreement between the Macchietto (2002) and Koenigs et al. (2003) results shown in Figure 9-1(b) can be hypothesized as due to differences in detailing, as the Macchietto (2002) specimens relate to superior detailing (as postulated during simplified modeling). When a more appropriate $K_f = 3.5$ is used, the developed model appears to more adequately describe the zero mean stress test results. The hypothesis is be revisited when evaluating the complete data set being considered the family of connections common to traffic signal structures.

To investigate the proficiency of the presented framework to model the fatigue behavior demonstrated by the compiled family of unstiffened, fillet-welded socket connection specimens fatigue tested at a similar level of elevated mean stress as by both Koenigs et al. (2003) and Roy et al. (2011) (where the median $\sigma_m = 150\,\text{MPa}$). Figure 9-1(c) depicts the representative S-N diagram derived using the aforementioned total life framework with $\sigma_m = 150\,\text{MPa}$. To minimize bias (acknowledging superior detailing of Roy et al. (2011) specimens) and variability, K_f was increased to 6.7 while

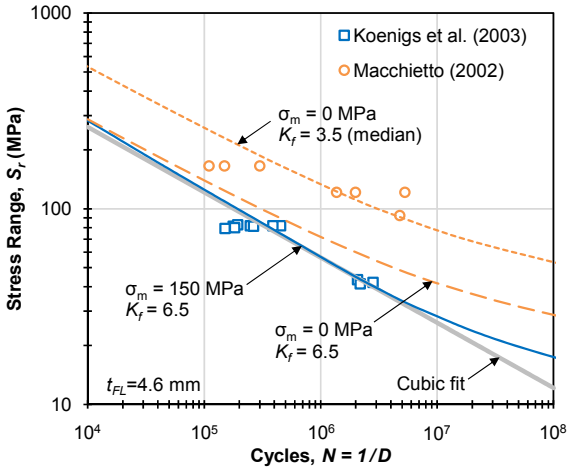

(a) Preliminary total life model with fatigue test results from on unstiffened, fillet-welded connections.

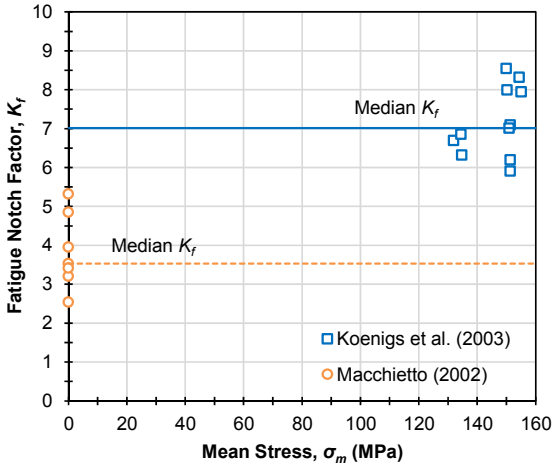

(b) Preliminary fatigue notch factors calculated for the unstiffened, fillet-welded connections that indicate a difference in connection detailing.

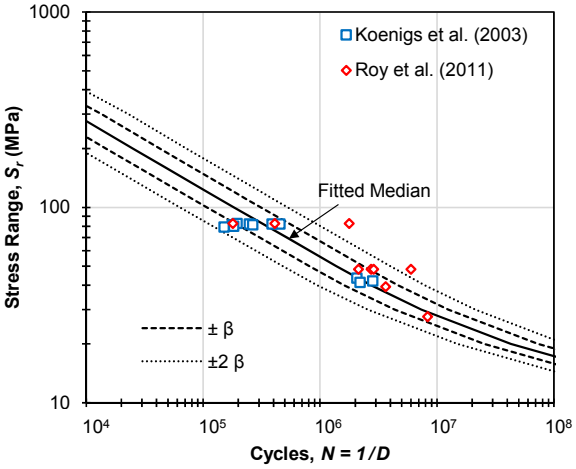

(c) Total life model developed for a broad family of unstiffened, fillet-welded socket connections at a mean stress of 150 MPa with K_f=6.7.

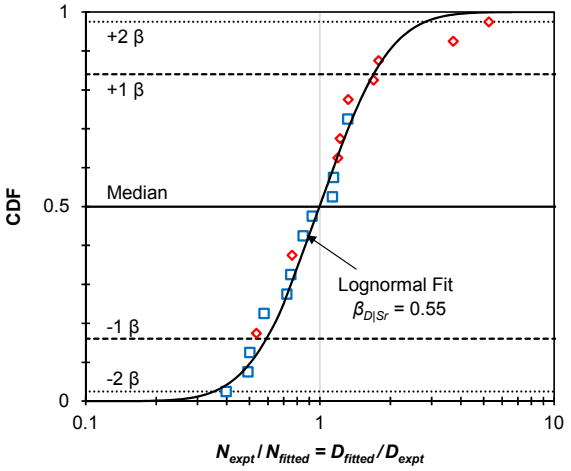

(d) Modeled variability in fatigue test results corresponding to the fit depicted in (c).

Figure 9-1. Total life (initiation-propagation) model development for tube-to-transverse base plate connections.

no change was made to strain-life and cyclic loading parameters. As seen in Figure 9-1(d), the model compares to the test data with lognormal standard deviation $\beta_{D|Sr} = 0.53$.

Due to the limited number of data points associated with unstiffened, fillet-welded socket connections tested at $\sigma_m = 0$ as shown in Figure 9-1(a), similar analysis and uncertainty quantification are not performed. These analyses are carried out when evaluating the effectiveness of the total life framework in predicting the fatigue performance of the aggregated test results for the complete family of connections common to traffic signal structures.

9.4.2 Modeling Fatigue Resistance for Connection Family

The mean stress-dependent total life (initiation-propagation) model must accurately predict the fatigue performance of the multitude of compiled fatigue test results that have been referred to as the family of connections common to most traffic signal structures. For this comparison, all introduced fatigue tests results from Koenigs et al. (2003) and Roy et al. (2011) are used to represent the connection family. As a reminder, Koenigs et al. (2003) tested a multitude of unstiffened to stiffened, and fillet- to groove-welded connections, while the connection tests selected from Roy et al. (2011) are standard, unstiffened fillet-welded connections with improved base plate thicknesses.

Figure 9-2(a) depicts the S-N diagram formed for comparison against the tube-to-transverse base plate connection family common to traffic signal structures. Given the parameters presented in the previous discussions, the model was again used to form a representative S-N diagram with $K_f = 6.6$ and $\sigma_m = 150\,\text{MPa}$. Shown in Figure 9-2(b),

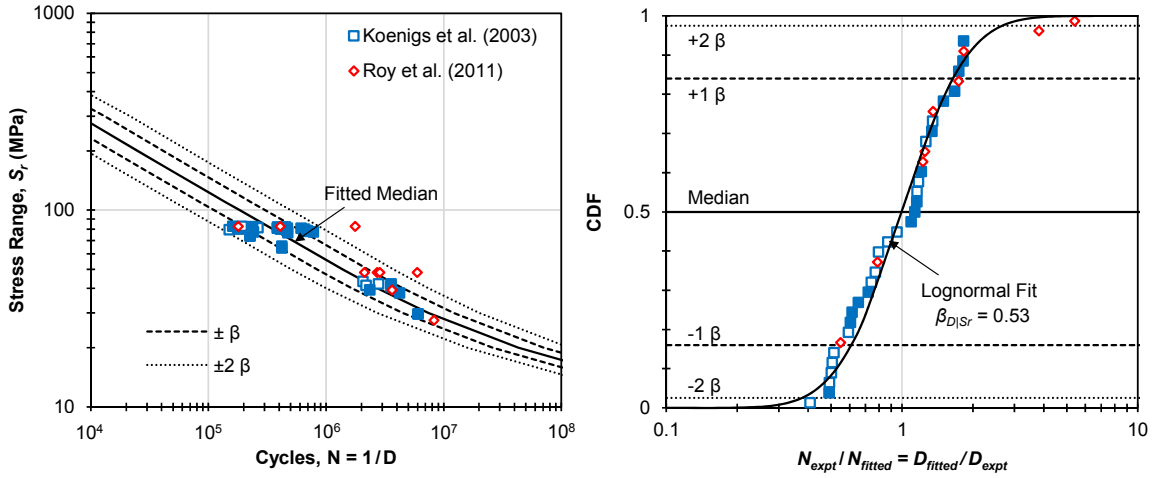

(a) Tube-to-transverse bae plate connection fatigue resistance when subjected to an elevated mean stress of 150 MPa and modeled with K_f=6.6.

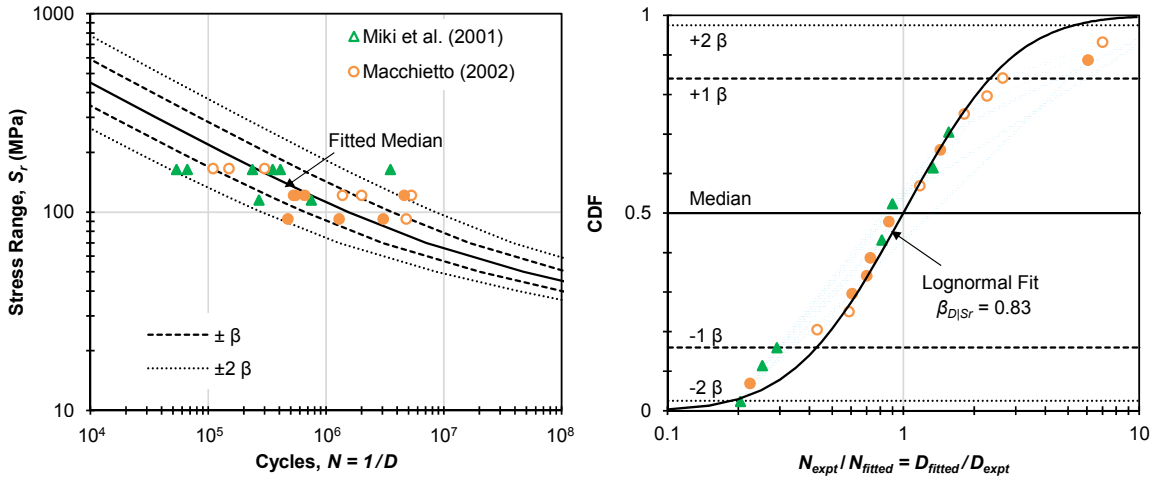

(b) Tube-to-transverse base plate connection fatigue resistance when subjected to fully reversed loading and modeled with K_f=4.1.

Figure 9-2. Fitted total life (initiation-propagation) model results depicting the mean stress-dependent fatigue resistance of the family of tube-to-transverse base plate connections common to traffic signal structures. Note: Filled and open markers indicate stiffened and unstiffened connections, respectively.

the model compares to the test data with slightly decreased lognormal standard deviation $\beta_{D|Sr} = 0.53$.

Figure 9-2(c,d) gives the results of the total life model for $\sigma_m = 0$. Also shown are results from Miki et al. (2001) and Macchietto (2002), representing a variety of socket connection configurations. Recall, the hypothesis that the connection specimens tested under zero mean stress were of superior detail. To demonstrate this, K_f was set to minimize model bias and variability. As indicated, when $K_f = 4.1$ the model well-predicts the fatigue resistance exhibited by past test results. The variability associated with connection fatigue resistance is increased for fully reversed loading ($\beta_{D|Sr} = 0.83$); this is in agreement with observations made by Koenigs et al. (2003).

9.4.3 Model Summary

As presented in the preceding section, the implemented total life model adequately predicts the fatigue resistance for a variety of tube-to-transverse base plate connections common to traffic signal structures. Utilized were strain-life (crack initiation) and fracture mechanics (crack propagation) parameters similar to those determined or used in past research (Zettlemoyer and Fisher 1979; Fisher et al. 1983; Chen et al. 2003; Azzam 2006). Variability in fatigue resistance is slightly reduced with use of the total life model when compared to the simplified model used previously in Sections 6 and 8.

Two fatigue resistance models have now been presented in this dissertation: a simplified stress-life model, and a total life-based model. Figure 9-3 illustrates each to compare/contrast these models. For an elevated mean stress of 150 MPa, the notable

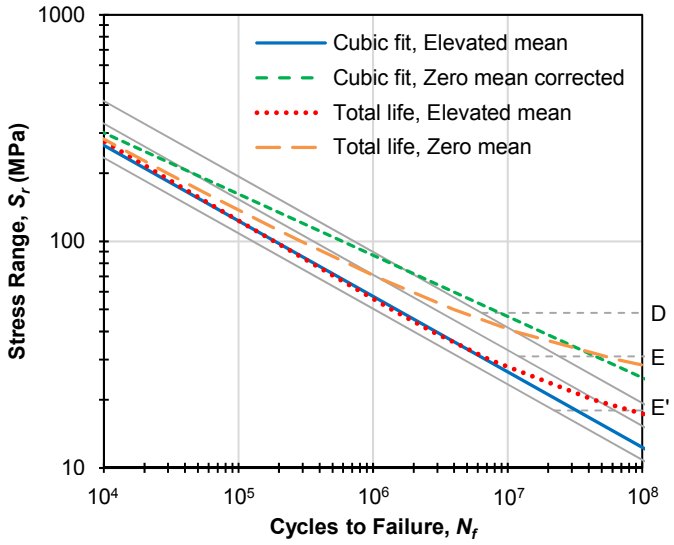

Figure 9-3. Developed total life and previously-fitted cubic-based models relating to the median resistance expected given if cyclic testing is performed about high (150 MPa) and zero nominal mean stress in tube-to-transverse base plate connections common to traffic signal structures.

difference lies at the modeled performance of the connection at longer livers where $N_f > 10^7$. For $10^4 < N_f < 10^7$, it can be seen that the total life model coincides with the simplified model, yet demonstrates a change in slope which is in agreement with recent works (Crudele and Yen 2006; Sonsino 2007; Yen et al. 2013). When modeling the capacity of the connection when subjected to fully reversed loadings (zero mean stress), differences between the simplified and total life models are evident—the total life model demonstrates a varying slope (power) whereas the simplified total life model can be practically described using a single power function. Fatigue assessments are conducted in what follows to investigate the validity of simplified connection fatigue modeling.

9.5 Probabilistic Fatigue Assessment

To investigate the ramification of using a simplified damage model, that is the damage relation based on a simplified, cubic stress-life relationship, probabilistic risk assessments performed in Section 8 are repeated using total life-based models.

9.5.1 Implementation of Total Life Model

The damage model depicted in Figure 9-4 was set using the stress-life relationship depicted in Figure 9-2(a) (and Figure 9-3). As can be inferred via comparison with Figure 8-5, the median damage incurred at low levels of cyclic stress is decreased, along with the associated dispersion in the fatigue or damage resistance of the connection family β_{FR}. In comparison with previous analysis using the simplified damage model, utilizing the total life-based damage model yields a large, 90 percent increase in expected life to 205 years. Dependable service life similarly changes given a slight change in β_{FR}.

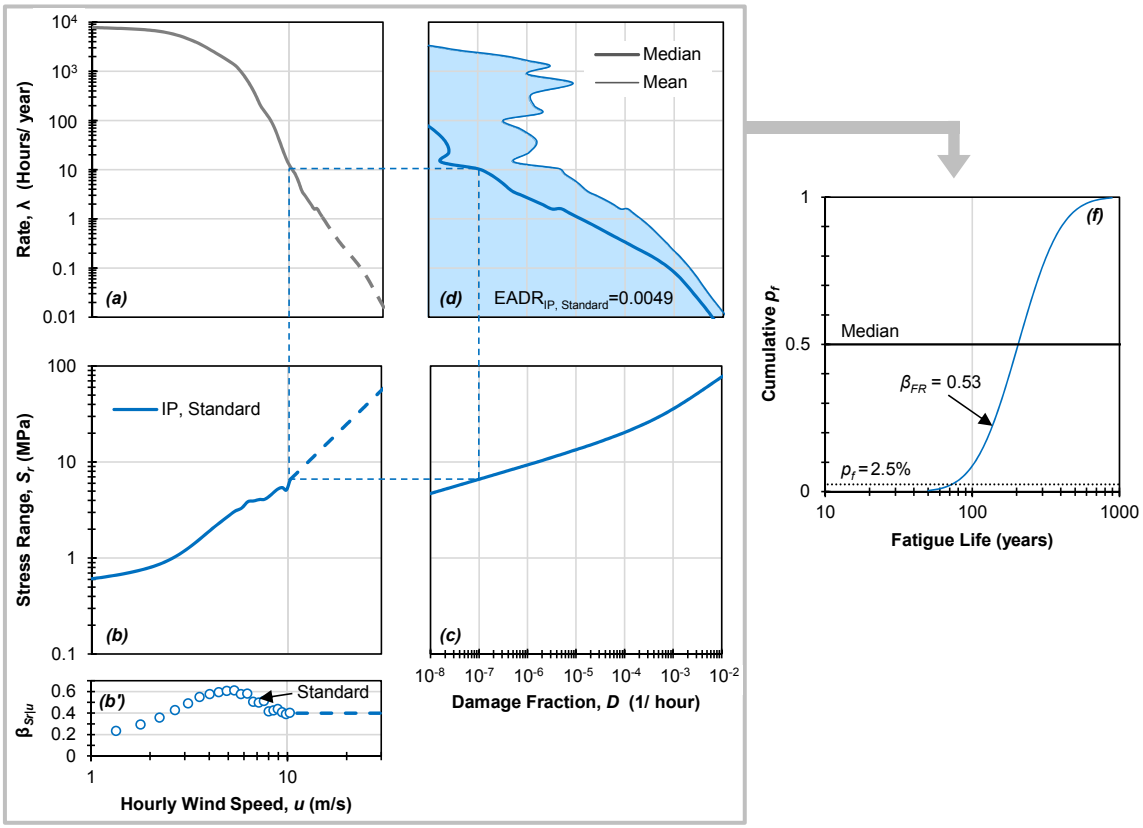

Figure 9-4. **Probabilistic fatigue damage analysis for the structure investigated within the (a) Bryan/College Station, TX, wind environment for the (b,b') standard structure in-plane response implementing the (c) total life-based damage model for (d) annual damage rate analysis and (f) estimation of dependable service life.**

Figure 9-5 depicts the results from repeated probabilistic fatigue assessments over the locations selected in this dissertation. As evaluated in Sections 6 and 8, the dependable life for a structure in Cheyenne, WY, remains under 10 years. When using a total life-based damage model, it can be seen that the dependable life for the other selected locations increases by an average of 75 percent. For each of these locations, the decreased median damage accumulated hourly was not completely offset by the increase in uncertainty, therefore the expected damage rated decreased.

9.5.2 Parameter Sensitivity Analysis

A swing analysis was conducted to investigate the sensitivity of various total life model parameters on the calculation of expected fatigue life (EFL). Each parameter was varied by ±10 percent and the corresponding change in EFL was calculated using the probabilistic framework then ranked. Figure 9-6(a) depicts the fair amount of scatter in the associated S-N curves resulting from individually varying 18 total life model parameters by ±10 percent. As can be seen, the modeled median capacity/resistance remains primarily within AASHTO Categories D and E'. In Figure 9-6(b), the envelope of the identified scatter is described by identifying the parameters whose variation most affected the S-N curve derived during swing analyses.

Figure 9-6(c,d) presents the results of swing analyses in the form of tornado diagrams from the College Station, TX, and Cheyenne, WY, wind environments, respectively. In each plot, the top 10 most sensitive parameters are depicted and seven of those affected the EAL by more than the 10 percent variation, highlighting the intrinsic

Location	Mean Annual Wind Speed (m/s)
College Station, TX	3.6
Miami, FL	3.9
Chicago, IL	4.6
Corpus Christi, TX	5.3
Cheyenne, WY	5.7

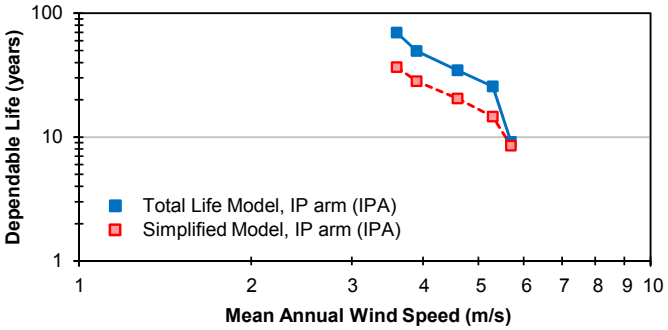

Figure 9-5. Comparing the effect of various damage models (simplified versus total life-based) on dependable service life estimates across several local wind environments.

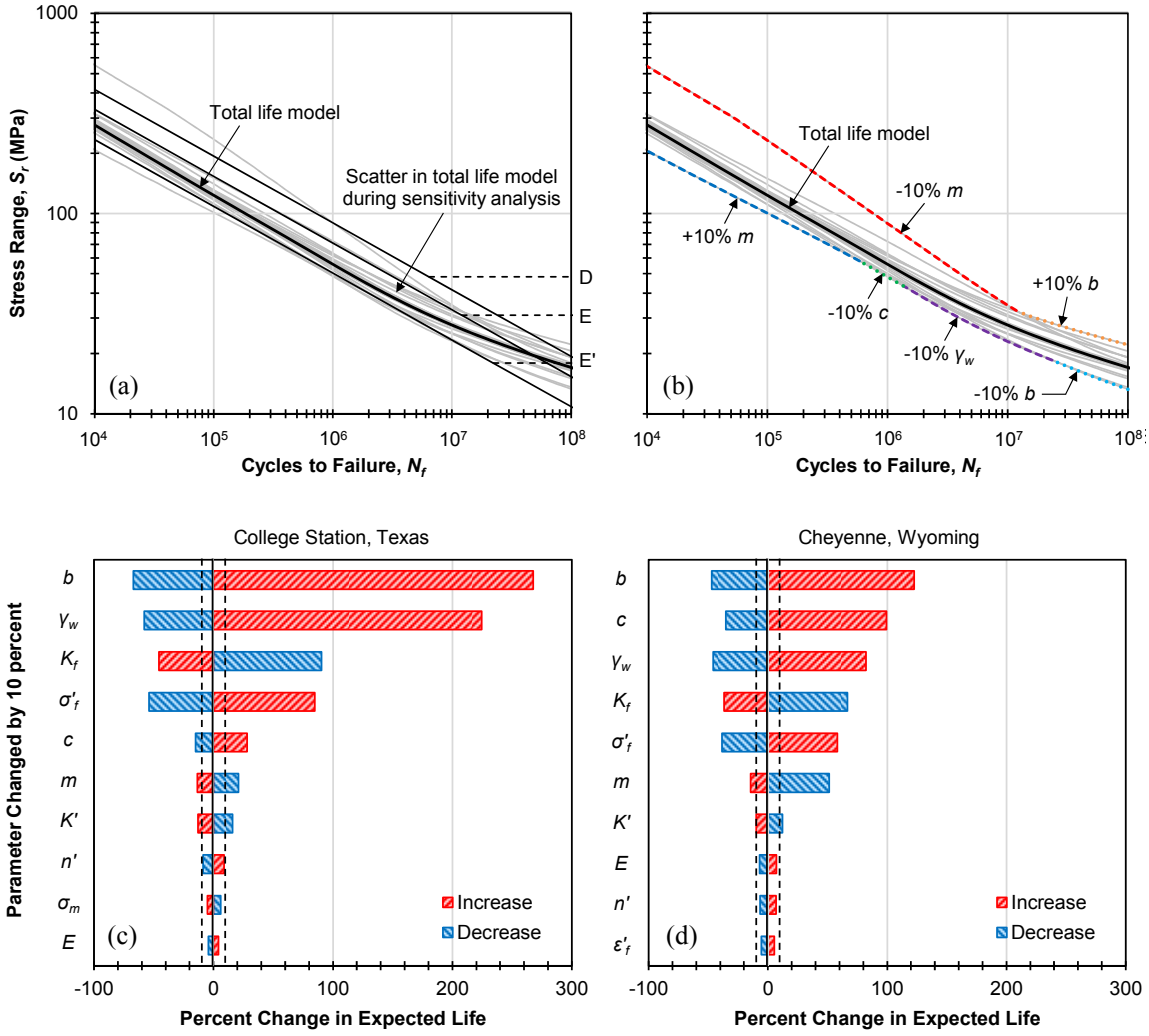

Figure 9-6. Model scatter and tornado diagrams resulting from swing analyses performed to determine the sensitivity of total life model parameters when calculating the expected fatigue life of a standard, fully equipped, traffic signal structure (150 MPa mean stress).

sensitivity of fatigue modeling (at long lives). Although ranked differently by location, the parameters b, γ_w, K_f, σ'_f, c, and m appear most influential. The parameters b, c, and m influence the slope of the stress life/damage models, while K_f is related to the notch tip stress intensity, resulting in model shift. The parameter γ_w shifts the model, however does so at varying levels with nominal stress range, thus also affecting model slope. Variation in the parameters b, K_f, and γ_w lead to changes in EFL greater than or equal to 100 percent. Each are material dependent and not expected to vary by this large of an amount. For example, a 10 percent change in ultimate strength σ_u (from 450 MPa) would lead to a maximum 1.1 percent change in γ_w (Dowling et al. 2009). Because K_f is related to notch tip stress intensity, which is dependent on connection detailing, it is expected that this parameter is of importance, however was selected to best fit the median fatigue capacity of the tube-to-transverse base plate connection family common to traffic signal structures. The influence of parameter b, however, necessitates that this parameter is appropriately selected.

For comparison, Figure 9-7 depicts the process of conducting a similar swing analysis for simplified stress-life/damage modeling. As shown in Figure 9-7(a,b), respectively, the slope (c, c_L) and shift $(S_{r,m})$ parameters each pointedly influence estimated fatigue life. Figure 9-7(c,d) present the results of swing analyses in the form of tornado diagrams from the College Station, TX, and Cheyenne, WY, wind environments, respectively. A 10 percent change in each studied parameter affects estimated life by more than that amount, highlighting their sensitivity. As reminder, $S_{r,m}$ specified in Sections 6

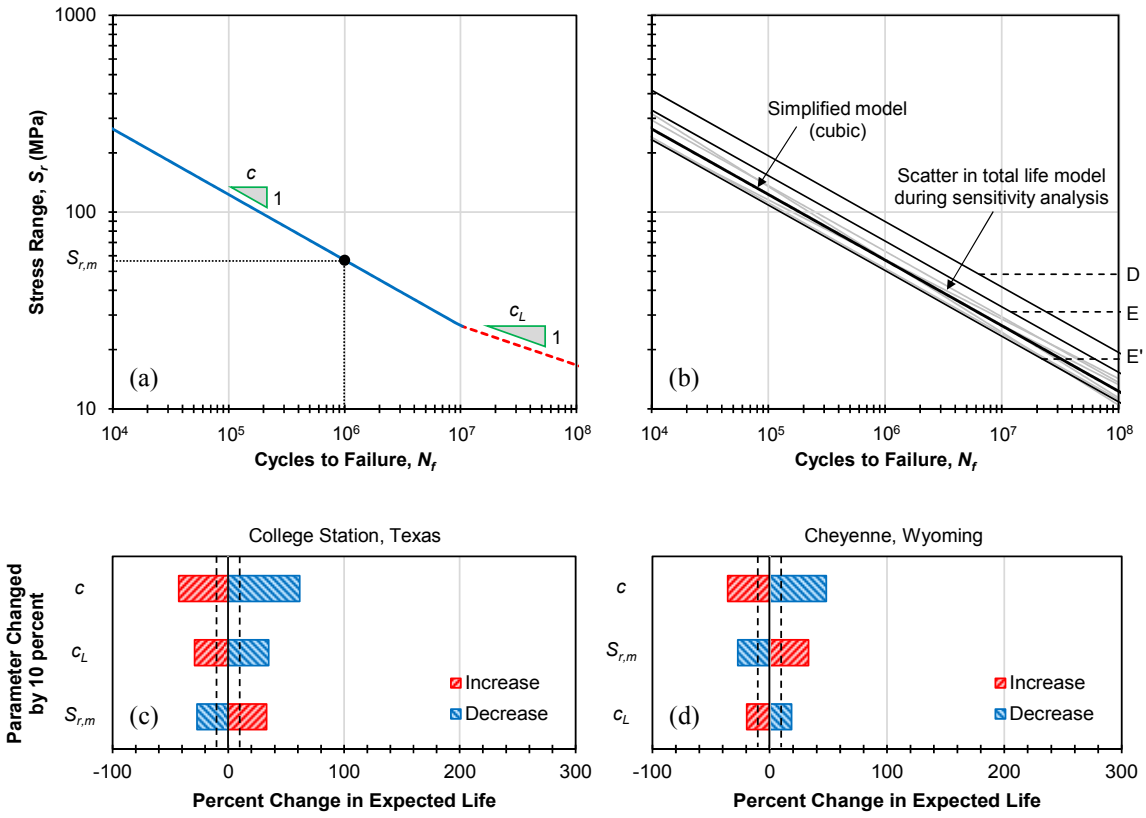

Figure 9-7. Description of and results stemming from swing analyses performed to determine the sensitivity of simplified model parameters when calculating the expected fatigue life of a standard, fully equipped, traffic signal structure (150 MPa mean stress).

and 8 are of parallel relation to K_f, where it was selected to best fit the median fatigue capacity of past connection tests. Thus, it can be inferred that parameter sensitivity is not necessarily model dependent as the fatigue/fracture phenomenon is innately quite sensitive to a multitude of factors.

9.5.3 Validity of Simplified versus Rigorous Connection Resistance Modeling

Finally, the validity of simplified connection resistance modeling was explored to investigate its impact on the implied efficacy of applying prestress to alleviate the adverse effect of mean tensile stress on the fatigue performance of cantilevered traffic signal structures. When simplified models were utilized, it was shown in Section 8 that full prestress could increase the dependable service (fatigue) life by nearly an order of magnitude, regardless of wind environment exposure.

Re-examining the Benefits of Applying Prestress to Connections

Figure 9-8 demonstrates the differences in each damage model (simplified versus total life-based) and their effect on calculated dependable service life for the structure subject to the local (College Station, TX) wind environment. For a fully loaded (equipped) structure with $\sigma_m = 150\,\text{MPa}$, the difference between the total life-based versus simplified models resulted in an increased EFL, thus a rightward shirt in the modeled distribution of fatigue life depicted in Figure 9-8(f). However, for the case in which tensile mean stress is fully relieved $(\sigma_m = 0)$, the difference between damage models shown in Figure 9-8(c) resulted in little to no change in EFL. Despite resulting in a

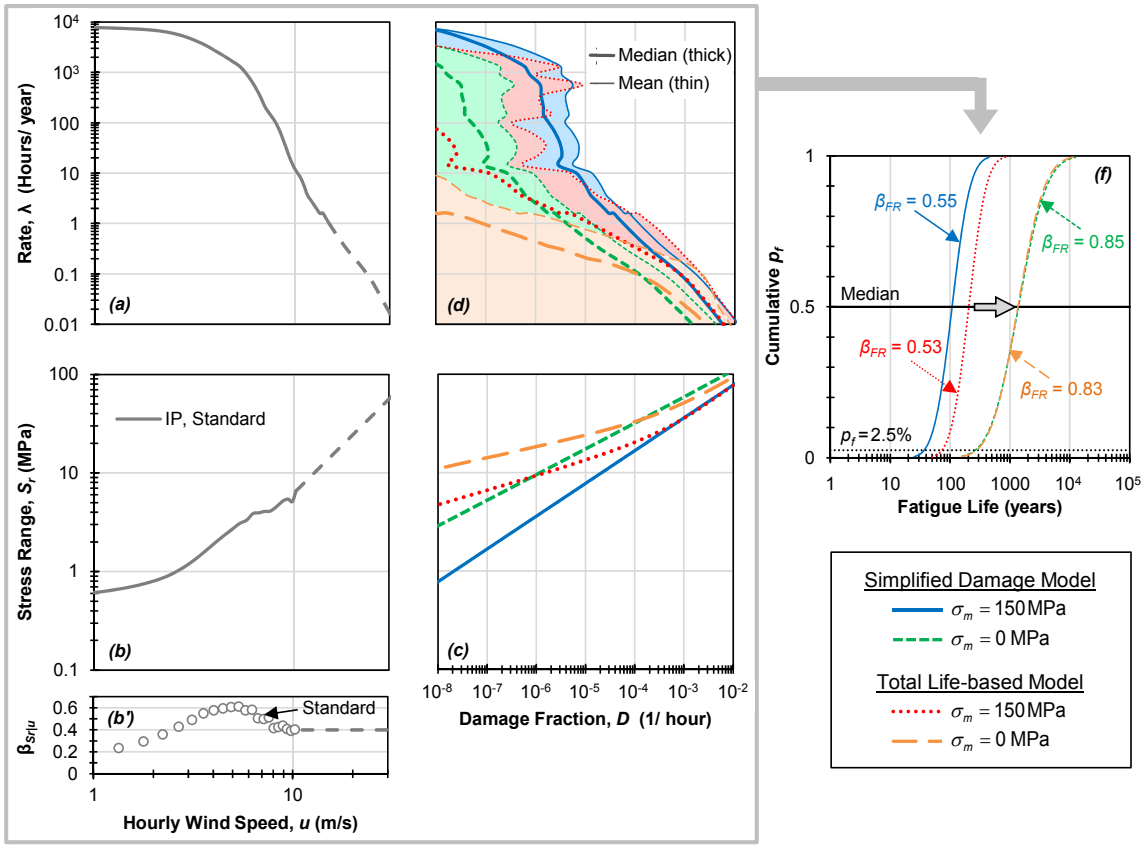

Figure 9-8. **Probabilistic fatigue damage analysis for the studied structure in the (a) Bryan/College Station, TX, wind environment for the (b,b') standard structure in-plane response implementing (c) standard and total life-based damage models for two levels of mean stress for (d) annual damage rate analysis and (f) estimation of dependable service life to re-evaluate the effectiveness of tensile mean stress relief via the application of prestress.**

modeled decrease in median accumulated damage fraction shown in Figure 9-8(c), the associated change in model slope c (see Section 6) increased the sensitivity of the measured uncertainty in structural stress response $\beta_{Sr|u}$ via Eq. (6-7). The only other difference of note is a slightly decreased value of β_{FR} related to the total life-based damage model derived in this section.

9.6 Discussion

Figure 9-9 depicts the results of the repeated probabilistic assessment, now implementing total life-based damage models for all five previously considered wind environments. As indicated, the standard structure dependable life estimate for Cheyenne, WY, remained similar to that obtained when using the simplified damage model, but differed for less harsh wind environments. Despite the merits of a robust initiation-propagation predictive analysis versus a more simplified fatigue analysis based on the customary nominal fatigue relationships, it should be noted that by either method the relative lowest-to-highest order of dependable service life is preserved. Location- or environment-based absolute life should be validated empirically from field evidence, where possible.

Upon review of dependable life estimates for the standard structure, it may be considered that conservative lower bound estimates result when implementing simplified stress-life-based damage models. On the other hand, estimates made using total life-based models tend toward an upper bound solution due to the manner in which crack initiation does not consider the influence of an initial flaw or discontinuity in material structure.

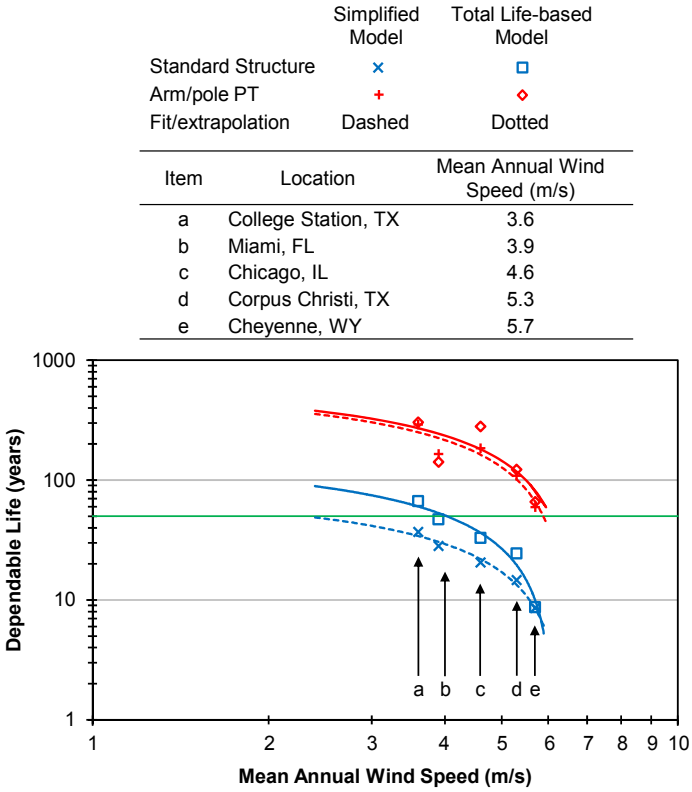

Figure 9-9. Effectiveness of the proposed applied prestress technique for traffic signal structure fatigue mitigation as determined using both simplified and total life-based damage models.

This is demonstrated by the large difference in S-N model slope beginning at $N_f \approx 10^7$ cycles for $\sigma_m = 150\,\text{MPa}$. Thus, it is not unreasonable for simplified stress-life based damage models to be used during probabilistic assessments as presented in this dissertation.

Figure 9-8(f) further demonstrates that the perceived benefit of tensile mean stress relief via the application of prestress is greater when simplified stress-life-based damage models are implemented. The effectiveness of full prestress application is best demonstrated at locations with the greatest mean annual wind speeds (harshest wind environments), where fatigue improvement is most necessary. Regardless, the benefit of applied prestress remains significant as Figure 9-9 depicts the increase in dependable service life well beyond the common 50 year threshold, and over 100 years for wind environments where the mean annual wind speed is below approximately 5.4 m/s. Only the probability of large windstorms (i.e. hurricanes) poses a threat to the 100 year threshold (see Corpus Christi, TX, and Miami, FL).

Although there are considerable differences between the simplified and total life-based stress-life/damage models at low levels of nominal structural stress response for the standard structure $(\sigma_m = 150\,\text{MPa})$, they are partially negated by their differences in slope. That is, increases in damage model slope parameter c (see Section 6) result in a greater influence of response uncertainty on expected damage rate. This finding is most clear for the case of full prestress $(\sigma_m = 0)$, where despite differences in resulting damage models the EFL remained practically unchanged for most wind environments considered.

Of ancillary importance to the development of the total life model in this section lies the distinction between traditional (mean stress-independent) fracture mechanics-based crack propagation analysis and a mean stress-dependent total life analysis. Figure 9-10 depicts the propagation component-based S-N curve for the fully reversed loading case along with the total life-based S-N relation for the dead loaded, $\sigma_m = 150\,\text{MPa}$ condition. Given the parameters as utilized in the total life model, except implementing the crack propagation parameters utilized by Fisher et al. (1983), the crack tip intensity factor K_f was set such that the zero mean propagation only-based stress-life model co-aligned with AASHTO Category E'. As shown, the models co-align over the range of nominal stress ranges investigated in previous works (Koenigs et al. 2003; Roy et al. 2011) and diverge at longer a live $N_f \approx 10^7$ (smaller S_r). This divergence is reminiscent of that suggested for analysis below the design CAFL for AASHTO Category E' (Crudele and Yen 2006; Sonsino 2007; Yen et al. 2013) and also provides insight into the behavior below the CAFL. Each reasonably models the stress-life behavior of the connection family.

Despite the available datasets, additional connection fatigue tests should, ideally, be conducted to investigate more thoroughly the fatigue resistance/life of common tube-to-transverse base plate connections below the AASHTO-specified CAFL. Unfortunately, this study will be time intensive as the corresponding N_f related to the onset of the CAFL for AASHTO Categories D, E, and E' are 6.4×10^6, 1.2×10^7, and 2.2×10^7, respectively. Nondestructive techniques should be used to determine the onset of crack propagation.

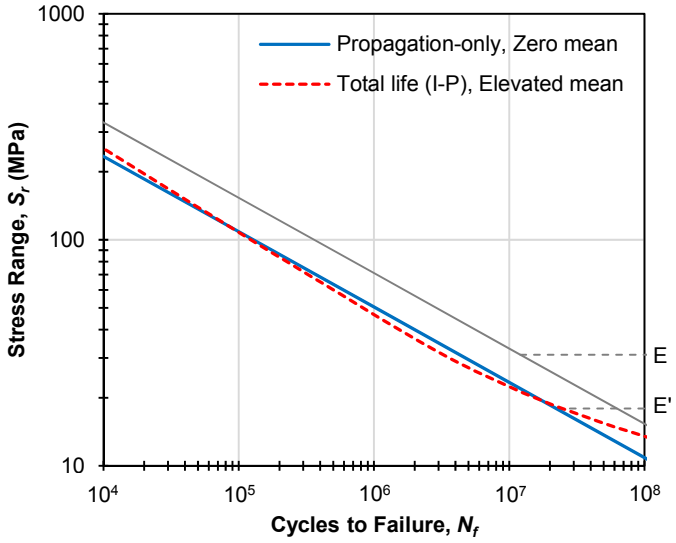

Figure 9-10. Similarities between stress-life relations based on fully reversed crack propagation and mean stress-dependent initiation-propagation analyses.

9.7 Closure and Key Findings

The following key findings are drawn based on the analysis described in this section:

i. A median S-N relationship for a family of tube-to-transverse base plate connections common to traffic signal structures was developed via a total life initiation-propagation model using parameters based on those reported in past studies. Accounting for notch tip stresses and nominal mean stress effects, the mean stress-dependent model reasonably modeled the benefit of tensile mean stress relief on connection fatigue resistance.

ii. The total life-based damage model was incorporated into the overall fatigue damage estimation framework. Despite the perceived differences from the previously-used simplified model, the total life-based framework provides a similar estimate of dependable life for Cheyenne, WY, but indicates greater dependable lives for locations with smaller mean annual wind speeds. It is reasoned that estimates derived using simplified damage models may be a conservative lower bound, while estimates made incorporating total life-based damage models approach an upper bound solution.

iii. A sensitivity study reveals that the expected fatigue life is most sensitive to total life model parameters affecting the long-life, right-sided tail of the stress-life model (that corresponds to the median damage incurred by the most common, small stress cycles that result from constant wind excitation).

iv. When exploring the repercussions of using simplified damage models, the efficacy of applied prestress was revisited. Despite leading to differences in dependable life estimates for a fully-equipped standard structure, estimates of dependable life for a full prestress structure led to similar relationships between dependable service life and mean annual wind speed for structures with relieved tensile mean stresses. When using total life-based damage models, applied prestress remains an effective technique to extend the dependable service life of traffic signal structures beyond today's common expectations, even in the severe wind environments studied herein.

v. Albeit potentially conservative for connections subject to dead load tensile mean stresses, simplified stress-life-based damage modeling is sufficient for use in probabilistic fatigue damage and life assessments. The clear benefit of the application of prestress to mitigate tensile mean stresses is to significantly extend the service life of common traffic signal structures.

10 SUMMARY, CONCLUSIONS, AND RECOMMENDED FUTURE WORK

10.1 Summary

This dissertation presents several studies that together aim to explore mitigating wind-induced fatigue in steel traffic signal structures, but more generally, all lightweight steel traffic support structures.

In Section 3, the natural wind response of a full-scale prototype structure was studied. The response was statistically characterized using the lognormal distribution where the median and lognormal standard deviation were used as a measure of central tendency and dispersion, respectively. The response of the prototype in its standard configuration was compared to its response with helical strakes installed in effort to determine excitation mechanisms. Helical arm strake installation resulted in a significant decrease in response as indicated by the elimination of large stress responses within the wind speed range associated with the vortex shedding mechanism.

In Section 4, a target-less computer vision technique to measure structure displacements was developed. Unlike similar non-contact approaches, the presented approach demonstrated high accuracy without dependence on a well-defined target geometry or background pattern. Using a low-cost, consumer-grade camcorder and the developed method, experimental modal analysis was conducted and stresses were successfully inferred when coupled with an analytical model of the structure.

Section 5 documents a study to assess the effectiveness of helical strake installation as a fatigue mitigation measure. Observed response was presented and a deterministic, code-based fatigue damage analysis framework was introduced. To quantify the benefit of arm strake installation, annual fatigue damage was studied as a function of wind speed for several differing wind environments. Although effective at reducing vortex-induced vibrations, the installation of helical strakes is of practical benefit to improve the in-plane dependable service life only in regions that do not typically experience wind speeds over 10 m/s.

Acknowledging the limitations of the code-based framework, Section 6 details the extension of a probabilistic framework to estimate expected annual wind-induced fatigue damage that was previously used to estimate the financial risk related to structural performance against seismic hazards. The formation of a fatigue damage-recurrence relationship results by inter-relating wind hazard, structural stress response, and fatigue damage submodels. Variability in wind-induced response and randomness in fatigue resistance are considered. The proposed framework was successfully demonstrated to determine the fatigue fragility of lightweight, wind excited traffic signal structures upon comparison against the results of an inspection program. The presented framework's submodels may be reformed or substituted to rapidly perform comparative studies.

In Section 7, the low-cost PT DAD system was proposed and evaluated using a code-based damage analysis framework. Supplemental load-balancing prestress transfers the dead load associated with the cantilevered arm to relieve the detrimental tensile mean stress from the fatigue-prone member connections. Prototype testing was conducted in

phases to quantify the effect that member PT has on wind-induced structural response. Dependable service life was estimated using the deterministic framework using the experimentally monitored response and mean stress-adjusted fatigue strength curves to assess the benefit of utilizing PT DAD concepts. Two dissimilar wind environments were considered, where results demonstrated that response reduction is not necessary to significantly improve the service life if dead load tensile stresses can be significantly relieved.

Later, in Section 8, an implementation-ready version of the proposed PT DAD system was presented. Previous field test observations were statistically characterized using the lognormal distribution, and results from past fatigue testing programs were used to statistically describe the mean stress-dependent fatigue resistance of tube-to-transverse base plate connections. Using the proposed probabilistic framework, expected annual fatigue damage, then later service life, was determined for several wind environments to demonstrate the efficacy of the proposed PT DAD system in improving the dependable service life of traffic signal structures. Fit relationships tie mean annual wind speed and dependable fatigue life without and with PT DAD. Mean stress reduction alone can increase dependable service life by an order of magnitude, regardless of wind environment.

Finally, work conducted in Section 9 studied the validity of using code-based connection fatigue models during probabilistic assessments performed throughout this dissertation. Total life (initiation-propagation) analysis was conducted to reason the detrimental effect that dead load tensile stresses have on traffic signal structure tube-to-

transverse base plate connections and the recommended change in slope below the design constant amplitude fatigue limit during finite life fatigue analyses. Probabilistic analyses are repeated for to allow a comparative study. It may be considered that implementation of simplified stress-life-based damage models produce lower bound dependable life estimates, while total life-based models tend toward an upper bound solution. The use of simplified models was deemed acceptable for use in the probabilistic framework proposed in this dissertation for mean stress-adjusted dependable life estimation

10.2 Conclusions

The following key conclusions can be drawn from the experimental testing and analytical modeling.

10.2.1 Traffic Signal Structure Excitation/Response

- Vibrations/stress reversals in the prototype traffic signal structure were caused by an interaction of two-dimensional buffeting and low-speed, across-wind vortex shedding. Although variable, the response may be characterized statically using the lognormal distribution. A lognormal standard deviation of 0.2 was observed for buffeting response, while response influenced by a prevalence of vortex shedding can be as high as 0.64.
- Vortex shedding was correlated with a specific wind condition and the characteristic dimension of the signal cluster attachments. Cantilevered traffic signal structure with slender mast arms and horizontal signal clusters are most

susceptible to signal cluster vortex shedding; as the diameter of the mast arm increases, mast arm vortex shedding shall begin to influence response.

- Optimally sized helical arm strakes reduced the effects of low-speed (signal cluster) vortex shedding. This demonstrates that the small-diameter mast arm section is critical to signal cluster vortex shedding.

10.2.2 Computer Vision for Traffic Signal Studies

- MQD-based computer vision is a fresh approach for non-contact methods to determine modal parameters and displacement time histories. When coupled with an analytical model, computer vision-measurements can be used to accurately infer stress histories.
- Computer vision is of greatest benefit in situations where the dynamic study of a structure is short term, the structure is access-limited, and/or the costs associated with traditional instrumentation would make a study infeasible.
- Although excellent results were obtained using a low-cost, consumer-grade camera, result accuracy may be increased using a higher resolution camcorder.

10.2.3 Helical Arm Strake Installation for Fatigue Mitigation

- The effectiveness of helical arm strakes to improve service life depends on the role that vortex shedding plays in fatigue damage accumulation. Thus, the efficacy of helical strakes as a fatigue mitigation measure depends on wind environment severity.

- The installation of helical mast arm strakes had a minimal effect on the buffeting-induced out-of-plane structural response and therefore strakes have little beneficial effect on extending out-of-plane service life.

10.2.4 Probabilistic Framework to Access Wind-Induced Fatigue (Fragility)

- A probabilistic methodology was successfully extended and demonstrated to predict the fatigue damage incurred in wind-excited traffic signal structures. Submodels related to wind environment, structural response, and/or fatigue resistance may be simply substituted, making the framework a choice option for comparative studies and for other hazard-response-damage problems.
- Common winds (return periods of less than one year) are responsible for the vast majority of fatigue damage accrued in traffic signal structure connections. This finding, however, does not indicate that severe damage does not occur during windstorm events, it only reflects the low occurrence rate of those events.
- When mean stress effects are not considered during fatigue damage accumulation, out-of-plane fatigue is of greater concern in locations with high annual wind speeds, whereas in-plane fatigue controls in most mild-to-moderate locations.
- In regions with mild-to-moderate wind conditions, the prevalence of low wind speeds and across-wind dominated response is primarily responsible for the premature fatigue failure of mast arm-to-pole tube-to-transverse base plate connections found in cantilevered traffic signal structures.

10.2.5 Damage Avoidance Solution to Mitigate Wind-Induced Fatigue

- Tensile mean stresses are detrimental to the fatigue performance of tube-to-transverse base plate connections. The proposed PT DAD concept is a low-cost solution to reduce the detrimental effects that tensile means stresses pose. PT systems could also be used in new designs to increase cantilever spans without increasing dead load stresses in fatigue-critical connections. Load-balancing redundancy is provided with potential for application in a variety of structural components/systems. Moreover, the alternative load path provides a fail-safe mechanism to prevent total arm collapse following extreme overloads or collisions, thus the frequency of inspection could be reduced.
- Prototype PT DAD was applied to the prototype traffic signal structure in phases. Field monitoring indicated an increase in mechanical damping when the eccentrically lace PT strand impacted the inner tube wall during large-amplitude vibrations. This significantly reduced the wind-induced structural response of the prototype structure. When not undergoing large-amplitude vibrations, a marginal increase in damping was observed. Installation of pole PT had little effect on structural response.
- When considering changes in both structural stress response and the fatigue resistance of PT tube-to-transverse base plate connections, fatigue damage accumulation reduces on the order of two orders of magnitude.

- Deterministic and probabilistic fatigue analyses each indicate that dead load, tensile mean stress relief can alone increase the dependable service life of traffic signal structures similar to that studied herein by an order of magnitude.

10.2.6 Rigorous versus Simplified Damage Modeling: Validity of Simplified Connection Models

- Dependable live estimates derived using simplified stress-life-based damage models may be seen as a conservative lower bound, while those made implementing total life-based models approach an upper bound solution.
- Probabilistic estimates of dependable life are susceptible to parameter sensitivity for both the simplified stress-life-based and total life-based damage models, highlighting the sensitive nature of the fatigue/fracture phenomenon.
- When using total life-based damage models, applied prestress remains an effective technique to extend the dependable service life of traffic signal structures beyond today's common expectations, even in the severe wind environments studied herein.
- Although yielding potentially conservative dependable life estimates, simplified stress-life-based damage models are sufficient for use in the probabilistic fatigue assessment framework proposed in this dissertation.

10.3 Recommended Future Work

Based on the studies conducted in this dissertation, the following areas have been identified as promising for future investigation to extend the state-of-the-art.

10.3.1 Devices for Wind-Induced Fatigue Mitigation

- The response of structures with most aerodynamic or mechanical response reduction techniques installed has not been quantified statistically. It would be beneficial for various vibration mitigation techniques to be installed, then for structural response to be described statistically for later probabilistic analysis. Fatigue service life estimates could be made for direct comparison to determine the best candidates for fatigue mitigation.

10.3.2 Damage Estimation Framework

- To refine the proposed fatigue damage estimation framework, wind direction dependence could be accounted for wind direction increments. Adding this third dimension would necessitate the use of surface plots to represent the wind hazard, structural response, and damage-recurrence submodels. Numerically integrating under the surface of plot (d) would yield the median annual damage rate.
- Regional assessments could be rapidly implemented upon gaining a better understanding of the effect of mean/median annual wind speed and its related dispersion. By using the lognormal distribution to model the recurrence of annual winds, a parameter sensitivity study could be conducted using the proposed framework. Regional estimates using approximate two-parameter lognormal parameters could be compared against those obtained using empirical wind hazard models, then validated using available inspection records.
- Scenario-based probabilistic fatigue damage accumulation assessments could be implemented to improve structure asset management practices. Given a

windstorm's time history (and spatial wind distribution), damage accumulated could be assessed as an equivalent amount of service life lost to update asset manage models. Likewise, the installation of applied prestress to existing structures could be reasoned by quantifying its benefit as a gain in structure service life following (or, ideally, prior to) an extreme wind event.

10.3.3 Computer Vision-Enabled Studies

- The use of computer vision could be used to conduct an expansive structural response study in effort to develop an acceptable code equation a static equivalent fatigue design load related to vortex shedding. Using computer vision and an anemometer, a vast inventory of wind speed-structural response relationships could be assembled for these access-limited structures. Using analytical models related to each monitored structures, stress response in the fatigue-critical tube-to-transverse base plate structures can be inferred.
- Computer vision could aid in performing more refined, regional service life analyses for traffic signal or other flexible, vibration-prone light pole structures. Not only location-specific, but also structure configuration-specific response curves could be used while assessing a large population of vibration prone structures.

10.3.4 Damage Avoidance Design

- Despite the availability of current datasets, the claims made herein concerning the mean stress-dependent nature of tube-to-transverse base plate fatigue resistance

should be experimentally substantiated by performing fatigue tests on similarly detailed specimens to allow for direct result comparison. Additional, computational analyses should be conducted to support the findings from the fatigue testing program. Once experimentally substantiated, future codes could, ideally, permit designers to incorporate fail-safe DAD concepts into designs to achieve improved service lives. These considerations could potentially dictate more cost efficient designs or allow longer distances to be spanned.

- The development of energy-dissipating connections could be used to further increase the benefit of PT DAD concepts applied herein. Because arm tip deflection is limited in the current specifications, relative rotation of the connections must kept to a minimum.

10.3.5 Total Life Analysis and the Detriment of Tensile Mean Stresses

- Ideally, additional fatigue tests should be conducted to investigate more thoroughly the fatigue resistance/life of common tube-to-transverse base plate connections with and without dead load tensile stresses below the specified CAFL. Testing would be time intensive due to large number of cycles necessary, yet beneficial to investigate the long-life onset of crack propagation under realistic, field-like conditions.

REFERENCES

AASHTO. (2001). "Standard specifications for structural supports for highway signs, luminaires, and traffic signals." 4th edition. American Association of State Highway and Transportation Officials, Washington, D.C., USA.

AASHTO. (2009). "Standard specifications for structural supports for highway signs, luminaires, and traffic signals." 5th edition. American Association of State Highway and Transportation Officials, Washington, D.C., USA.

AASHTO. (2013). "Standard specifications for structural supports for highway signs, luminaires, and traffic signals." 6th edition. American Association of State Highway and Transportation Officials, Washington, D.C., USA.

Ahearn, E. B., and Puckett, J. A. (2010). "Reduction of wind-induced vibrations in high-mast light poles." Report No. WY-10/02F. Wyoming Department of Transportation (WYDOT), Cheyenne, WY, USA.

Ajab J. J., Pekcan, G., and Mander, J. B., (2004). "Rocking wall-frame structures with supplemental tendon systems." Journal of Structural Engineering, 130(6), 895-903.

Albert, M. N, Manuel, L., Frank, K. H., and Wood, S. L. (2007). "Field testing of cantilevered traffic signal structures under truck-induced gust loads." Report No. 4586-2. Texas Department of Transportation (TxDOT), Austin, TX, USA.

Alderson, J. L. (1999). "Fatigue study of cantilevered traffic signal mast arms." M.S. thesis. University of Missouri, Columbia, MO, USA.

Allemang, R. J. (2003). "The modal assurance criterion-Twenty years of use and abuse." Sound and Vibration, 37, 14-23.

Azzam, D. (2006)."Fatigue Behavior of Highway Welded Aluminum Light Pole Support Structures." Ph.D. dissertation. The University of Akron, Akron, OH, USA.

Azzam, D., and Menzemer, C. C. (2006). "Fatigue behavior of welded aluminum light pole support details." Journal of Structural Engineering, 132(12), 1919-1927.

Bannantine, J. A., Comer, J. J., and Handrock, J. L. (1990). "Fundamentals of Metal Fatigue Analysis." Prentice Hall, Englewood Cliffs, NJ, USA.

Barsom, J. M., and Rolfe, S. T. (1999). "Fracture and Fatigue Control in Structure: Application of fracture Mechanics." 3rd edition. American Society for Testing and Materials (ASTM), Philadelphia, PA, USA.

Bartilson, D. T., Wieghaus, K. T., and Hurlebaus, S. (2015). “Target-less computer vision for traffic signal structure vibration studies.” Mechanical Systems and Signal Processing, 60-61, 571-582.

Beden, S. M., Abdullah, S., and Ariffin, A. K. (2009). "Modeling of fatigue crack growth under constant and variable amplitude loading." International Journal of Mechanical and Materials Engineering, 4(2), 131-135.

Blevins, R. D. (1977). “Flow-induced vibration.” Van Nostrand Reinhold, New York, NY, USA.

Busca, G., Cigada, A., Mazzoleni, P., Tarabini, M., and Zappa, E. (2013). "Static and dynamic monitoring of bridges by means of vision-based measuring system." Topics in Dynamics of Bridges, 3, 83-92.

Chang, C. C., and Ji, Y. (2007). "Flexible videogrammetric technique for three-dimensional structural vibration measurement." Journal of Engineering Mechanics, 133(6), 656-664.

Chen, G., Wu, J., Yu, J., Dharani, L. R., and Barker, M. (2001). “Fatigue assessment of traffic signal mast arms based on field test data under natural wind gusts.” Transportation Research Record, 1770, 188-194.

Chen, G., Barker, M., MacKenzie, D. S., Ramsay, C., Alderson, J., Dharani, L., and Yu, J. (2002). “Forensic investigation of failed mast arms of traffic signal supported structures.” Transportation Research Record, 1814, 9-16.

Chen, G., Barker, M., Dharani, L. R., and Ramsay, C. (2003). “Signal mast arm failure investigation.” Report No. RDT 03-010. Missouri Department of Transportation (MoDOT), Jefferson City, MO, USA.

Chopra, A. K. (2007). "Dynamics of structures: Theory and applications to earthquake engineering." 3rd edition. Prentice Hall, Upper Saddle River, NJ, USA.

Christenson, R. E., and Hoque, S. (2011). “Reducing fatigue in wind-excited support structures of traffic signals with innovative vibration absorber.” Transportation Research Record, 2251, 16-23.

Christenson, R. (2011). “Smart Vibration Absorber for Traffic Signal Supports.” WO Patent 2011085184.

Christopoulos, C., Filiatrault, A., Uang, C. M., and Folz, B. (2002). “Posttensioned energy dissipating connections for moment-resisting steel frames.” Journal of Structural Engineering, 128(9), 1111-1120.

Christopoulos, C., Tremblay, R., Kim, H. J., and Lacerte, M. (2008). “Self-centering energy dissipative bracing system for the seismic resistance of structures: Development and validation.” Journal of Structural Engineering, 134(1), 96-107.

Coffin, L. F. (1954). “A study of the effects of cyclic thermal stresses on a ductile metal.” Transactions of the American Society of Mechanical Engineers, 76, 931-950.

Connor, R. J., Collicott, S. H., DeSchepper, A. M., Sherman, R. J., and Ocampo, J. A. (2012). “Fatigue loading and design methodology for high-mast lighting towers.” National Cooperative Highway Research Program (NCHRP) Report 718. Transportation Research Board (TRB), Washington, D.C., USA.

Cook, R. A., Bloomquist, D., Richard, D. S., Kalajian, M. A., Cannon, V. A., and Arnold, D. P. (2000). "Design, testing, and specification of a mechanical damping device for mast arm traffic signal structures." Report No. BC-050. Florida Department of Transportation, Tallahassee, FL, USA.

Cook, R. A., Bloomquist, D., Richard, D. S., and Kalajian, M. A. (2001). “Damping of cantilevered traffic signal structures.” Journal of Structural Engineering, 127(12), 1476-1483.

Crudele, B. B., and Yen, B. T. (2006). “Analytical examination of S-N curves below constant amplitude fatigue limit.” Proceedings of the First International Conferences on Fatigue and Fracture in the Infrastructure: Bridges and Structures of the 21st Century, ATLSS Engineering Research Center, Lehigh University, Bethlehem, PA, USA.

Cruzado, H. J., Letchford, C., and Kopp, G. A. (2013). “Wind tunnel studies of cantilever traffic signal structures.” Wind and Structures, 16(3), 225-240.

Culp, J. (1990). “Action plan for cantilever sign problem, Report to management.” Michigan Department of Transportation, Lansing, MI, USA.

Cunha, A., and Caetano, E. (2006). "Experimental modal analysis of civil engineering structures." Sound and Vibration, 40(6), 12-20.

Deierlein, G. G., Krawinkler, H., and Cornell, C. A. (2003). “A framework for performance-based earthquake engineering.” Proceedings of the Pacific Conference on Earthquake Engineering, Christchurch, New Zealand.

Dexter, R. J., and Ricker, M. J. (2002). “Fatigue-resistant design of cantilevered signal, sign, and light supports.” National Cooperative Highway Research Program (NCHRP) Report 469. Transportation Research Board (TRB), Washington, D.C., USA.

Dhakal, R. P., and Mander, J. B. (2006). “Financial risk assessment methodology for natural hazards.” Bulletin of the New Zealand Society for Earthquake Engineering, 39(2), 91-105.

Dowling, N. E., Calhoun, C.A., and Arcari, A. (2009). “Mean stress effects in stress-life fatigue and the Walker equation.” Fatigue and Fracture of Engineering Materials and Structures, 32(3), 163-179.

Downing, S. D., and Socie, D. F. (1982). “Simple rainflow counting algorithms.” International Journal of Fatigue, 4(1), 31-40.

Duraisamy, R. (2005). “Finite element study of mast arm socket welded connections.” M.S. thesis. The University of Texas, Austin, TX, USA.

Elber, W. (1971). "The significance of fatigue crack closure." In STP 486. American Society for Testing and Materials (ASTM), Philadelphia, PA, USA, 230-243.

Fisher, J. W., Miki, C., Slutter, R. G., Mertz, D. R., and Frank, W. (1983). “Fatigue strength of steel pipe-base plate connections.” Engineering Structures, 5(2), 90-96.

Fisher, J. W., Nussbaumer, A., Keating, P. B., and Yen, B. T. (1993). “Resistance of welded details under variable amplitude long-life fatigue loading.” National Cooperative Highway Research Program (NCHRP) Report 354. Transportation Research Board (TRB), Washington, D.C., USA.

Florea, M. J., Manual, L., Frank, K. H., and Wood, S. L. (2007). “Field tests and analytical studies of the dynamic behavior and the onset of galloping in traffic signal structures.” Report No. 4586-1. Texas Department of Transportation (TxDOT), Austin, TX, USA.

Frank, K. (1980). “Fatigue strength of anchor bolts.” Journal of the Structural Division, 106(6), 1279-1293.

Gagvani, N. (2009). "Challenges in video analytics." In Advances in Pattern Recognition: Embedded Computer Vision, 237-256.

Garlock, M. M., Ricles, J. M., and Sause, S. (2005). “Experimental studies of full-scale posttensioned steel connections.” Journal of Structural Engineering, 131(3), 438-448.

Garlock, M. M., Sause, R., and Ricles, J. M. (2007). “Behavior and design of posttensioned steel frame systems.” Journal of Structural Engineering, 133(3), 389-399.

Gaul, L., Hurlebaus, S., Wirnitzer, J., and Albrecht, H. (2008). "Enhanced damping of lightweight structures by semi-active joints." Acta Mechanica, 195(1), 249-261.

Goode, J. S., and van de Lindt, J. W. (2007). “Development of a semiprescriptive selection procedure for reliability-based fatigue design of high mast lighting structural supports.” Journal of Performance of Constructed Facilities, 21(3), 193-206.

Goyal, R., Dhonde, H. B., and Dawood, M. (2012). “Fatigue failure and cracking in high mast poles.” Report No. 6650-1. Texas Department of Transportation (TxDOT), Austin, TX, USA.

Gray, B. (1999). ‘‘Fatigue effects on traffic signal structures.’’ M.S. thesis. University of Wyoming, Laramie, WY, USA.

Greenwood, M. (1926). “The natural duration of cancer.” Reports on public health and medical subjects. Her Majesty’s Stationery Office, London, England, 33, 1-26.

Gui, L., and Merzkirch, W. (2000). "A comparative study of the MQD method and several correlation-based PIV evaluation algorithms." Experiments in Fluids, 28, 36-44.

Hamid, N. H., and Mander, J. B. (2010). “Lateral seismic performance of multipanel precast hollowcore walls.” Journal of Structural Engineering, 136(7), 795-804.

Hamilton, H. R., Riggs, S. G., and Puckett, J. A. (2000). “Increased damping in cantilevered traffic signal structures.” Journal of Structural Engineering, 126(4), 530-537.

Hartnagel, B. A. and Barker, M. G. (1999). “Strain measurements on traffic signal mast arms.” Proceedings of the 1999 Structures Congress, New Orleans, LA, USA, 1111-1114.

Holmes, J. D. (2002). “Fatigue life under along-wind loading — closed-form solutions.” Engineering Structures, 24(1), 109-114.

Hurlebaus, S., and Gaul, L. (2006). "Smart structure dynamics." Mechanical Systems and Signal Processing, 20(2), 255-281.

Hurlebaus, S., and Mander, J. B. (2014). “Traffic signal supporting structures and methods.” US Patent 8756874.

Ince, A., and Glinka, G. (2011). "A modification of Morrow and Smith-Watson-Topper mean stress correction models." Fatigue and Fracture of Engineering Materials and Structures, 34(11), 854-867.

Kaczinski, M. R, Dexter, R. J, and Van Dien, J. P. (1998). “Fatigue-resistant design of cantilevered signal, sign, and light supports.” National Cooperative Highway Research Program (NCHRP) Report 412. Transportation Research Board (TRB), Washington, D.C., USA.

Kaplan, E. L., and Meier, P. (1958). “Nonparametric estimation from incomplete observations.” Journal of the American Statistical Association, 53(282), 457-481.

Kashar, L., Nester, M. R., Jones, J. W., Hariri, M., and Friezner, S. (1999). "Analysis of the catastrophic failure of the support structure of a changeable message sign." Proceedings of the 1999 Structures Congress, New Orleans, LA, USA, 1115-1118.

Keating, P. B., and Fisher, J. W. (1986). “Evaluation of Fatigue Tests and Design Criteria on Welded Details.” National Cooperative Highway Research Program (NCHRP) Report 286. Transportation Research Board (TRB), Washington, D.C., USA.

Kennedy, R. P., Cornell, C. A., Campbell, R. D., Kaplan, S., and Perla, H. F. (1980). “Probabilistic seismic safety study of an existing nuclear power plant.” Nuclear Engineering and Design, 59(2), 315-338.

Kerber, F., Hurlebaus, S., Beadle, B. M., and Stöbener, U. (2007). "Control concepts for an active vibration isolation system." Mechanical Systems and Signal Processing, 21(8), 3042-3059.

Kim, H. J., and Christopoulos, C. (2008). “Friction damped posttensioned self-centering steel moment-resisting frames.” Journal of Structural Engineering, 134(11), 1768-1779.

Kim, S. W., and Kim, N. S. (2013). "Dynamic characteristics of suspension bridge hanger cables using digital image processing." NDT&E International, 59, 25-33.

Koenigs, M. T., Botros, T.A., Freytag, D., and Frank, K.H. (2003). “Fatigue strength of signal mast arm connections.” Report No. 4178-2. Texas Department of Transportation (TxDOT), Austin, TX, USA.

Kumar, R. A, Sohn, C. H., and Gowda, B. H. L. (2008). “Passive control of vortex-induced vibrations: An overview.” Recent Patents on Mechanical Engineering, 1, 1-11.

Letchford, C., Cruzado, H., and Zuo, D. (2008). “Risk assessment model for wind-induced fatigue failure of cantilever traffic signal structures.” Report No. 4586-4. Texas Department of Transportation (TxDOT), Austin, TX, USA.

Li, L., Mander, J. B., and Dhakal, R. P, (2008). “Bidirectional cyclic loading experiment on a 3D beam-column joint designed for damage avoidance.” Journal of Structural Engineering, 134(11), 1733-1742.

Lin, Y. C., Sause, R., and Ricles, J. M. (2013). “Seismic performance of a large-scale steel self-centering moment resisting frame: MCE hybrid simulations and quasi-static pushover tests.” Journal of Structural Engineering, 139(7), 1227-1236.

Macchietto, C. (2002). Valmont Fatigue Testing Presentation, presentation given to the AASHTO T-12 committee, Las Vegas, NV, USA.

Magenes, L. (2011). "Fatigue assessment of high mast illumination poles using field measurements." M.S. thesis. The University of Texas, Austin, TX, USA.

Mander, J. B., Chen, S. S., Shah, K. M., and Madan, A. (1992). “Investigation of light pole base integrity.” Technical Report submitted to the Erie County Department of Public Works. Dept. of Civil Engineering, State University of New York (SUNY) at Buffalo, Buffalo, NY, USA.

Mander, J. B., and Cheng, C. T. (1997). “Seismic resistance of bridges based on damage avoidance design.” Technical Report NCEER-97-0014. National Center for Earthquake Engineering Research (NCEER), Buffalo, NY, USA.

Mander, J. B. (2003). “Beyond ductility: the quest goes on.” Bulletin of the New Zealand Society for Earthquake Engineering, 37(1), 35-44.

Mander, J. B., Dhakal, R. P., Mashiko, N., and Solberg, K. M. (2007). “Incremental dynamic analysis applied to seismic financial risk assessment of bridges.” Engineering Structures, 29(10), 2662-2672.

Mander, J.B. and Sircar, J. (2009). “Loss model for seismically damaged structures.” Proceedings of the 2009 Structures Congress, Austin, TX, USA, 1077-1086.

Mander, J. B., Sircar, J., and Damnjanovic, I. (2012). “Direct loss model for seismically damaged structures.” Earthquake Engineering and Structural Dynamics, 41(3), 571-586.

Manson, S. S. (1953). “Behavior of materials under conditions of thermal stress.” Heat Transfer Symposium, University of Michigan Engineering Research Institute, Ann Arbor, MI, USA, 9-75.

Manson, S. S., and Halford, G. R. (1981). "Practical implementation of the double linear damage rule and damage curve approach for treating cumulative fatigue damage." International Journal of Fracture, 17(2), 169-192.

Matsuishi, M., and Endo, T. (1968). “Fatigue of metals subjected to varying stress.” Proceedings of the Japan Society of Mechanical Engineers, Fukuoka, Japan.

McDonald, J. R., Mehta, K. C., Oler, W., and Pulipaka, N. (1995). “Wind load effects on signs, luminaires, and traffic signal structures.” Report No. 1303-F. Texas Department of Transportation (TxDOT), Austin, TX, USA.

McManus, P. S., Hamilton, H. R., and Puckett, J. A. (2003). “Damping in cantilevered traffic signal structures under forced vibration.” Journal of Structural Engineering, 129(3), 373-382.

Miki, C., Fisher, J. W., and Slutter, R. G. (1981). “Fatigue behavior of steel light-poles.” Report No. 200.81.714.1. Fritz Engineering Laboratory, Lehigh University, Bethlehem, PA, USA.

Miki, C., and Masakazu, S. (2001). “A Study on U-Shaped Rib Configuration with High Fatigue Resistance.” Document No. XIII-1885-01. International Institute of Welding (IIW), Paris, France.

Miner, M. A. (1945). “Cumulative damage in fatigue.” Journal of Applied Mechanics, 12(3), 159-164.

Mori, N., and Chang, K. A. "mpiv - MATLAB PIV toolbox: Introduction to mpiv." <http://www.oceanwave.jp/softwares/mpiv> (June 2013).

Morrow, J. (1968) “Fatigue Design Handbook.” Advances in Engineering. 4, 21-29. Society of Automotive Engineers (SAE), Warrendale, PA, USA.

Neuber, H. (1961). "Theory of stress concentration for shear-strained prismatical bodies with arbitrary nonlinear stress-strain law." Journal of Applied Mechanics, 28(4), 544-550.

Ocel, J. (2006). “The behavior of thin hollow structural section (HSS) to plate connections.” Ph.D. dissertation. University of Minnesota, Minneapolis, MN, USA.

Olaszek, P. (1999). "Investigation of the dynamic characteristic of bridge structures using a computer vision method." Measurement, 25, 227-236.

Paris, P., and Erdogan, F. (1963). "A critical analysis of crack propagation laws." Journal of Basic Engineering, 87, 528-534.

Pastor, M., Binda, M., and Harčarik, T. (2012). "Modal assurance criterion." Procedia Engineering, 48, 543-548.

Patel, K. and Freathy, P. (1984). “A simplified method for assessing wind-induced fatigue damage.” Engineering Structures, 6(4), 268-273.

Patsias, S., and Staszewski, W. (2002). "Damage detection using optical measurements and wavelets." Structural Health Monitoring, 1(1), 5-22.

Paulsen, U. S., Schmidt, T., and Erne, O. (2010). "Developments in large wind turbine modal analysis using point tracking videogrammetry." Structural Dynamics and Renewable Energy, 1, 187-198.

Peil, U., and Behrens, M. (2002). “Fatigue of tubular steel lighting columns under wind load.” Wind and Structures, 5(5), 463-478.

Pekcan, G., Mander, J. B., and Chen, S. S. (2000). “Balancing lateral loads using tendon-based supplemental damping system.” Journal of Structural Engineering, 126(8), 896-905.

Price, R. L., Puckett, J. A., and Barker, M. G. (2008). “Use of wind power maps to establish fatigue design criteria for traffic signal and high-mast structures.” Report No. 08-207. Mountain-Plains Consortium (MPC), Fargo, ND, USA.

Puckett, J. A., Garlich, M. G., Nowak, A., and Barker, M. (2014). “Development and Calibration of AASHTO LRFD Specifications for Structural Supports for Highway Signs, Luminaires, and Traffic Signals.” National Cooperative Highway Research Program (NCHRP) Report 796. Transportation Research Board (TRB), Washington, D.C., USA.

Pulipaka, N. (1995). “Wind-induced vibrations of cantilevered traffic signal structures.” Ph.D. dissertation. Texas Tech University, Lubbock, TX, USA.

Pulipaka, N., Sarkar, P. P., and McDonald, J. R. (1998). “On galloping vibration of traffic signal structures.” Journal of Wind Engineering and Industrial Aerodynamics, 77-78, 327-336.

Radaj, D., Sonsino, C. M., and Fricke, W. (2006). " Fatigue assessment of welded joints by local approaches." Woodhead Publishing, Cambridge, England.

Ramberg, W., and Osgood, W. R. (1943). “Description of stress-strain curves by three parameters.” Technical Note No. 902. National Advisory Committee for Aeronautics (NACA), Washington, D.C., USA.

Ren, W. X., Zhao, T., and Harik, I. E. (2004). "Experimental and analytical modal analysis of steel arch bridge." Journal of Structural Engineering, 130(7), 1022-1031.

Repetto, M. P. and Solari, G. (2001). “Dynamic alongwind fatigue of slender structures.” Engineering Structures, 23(12), 1622-1633.

Repetto, M. P. and Solari, G. (2002). “Dynamic crosswind fatigue of slender structures.” Wind and Structures, 5(6), 527-542.

Repetto, M. P. and Solari, G. (2004). “Directional wind-induced fatigue of slender vertical structures.” Journal of Structural Engineering, 130(7), 1032-1040.

Repetto, M. P. (2005). “Cycle counting methods for bi-modal stationary Gaussian processes.” Probabilistic Engineering Mechanics, 20(3), 229-238.

Repetto, M. P. and Solari, G. (2006). “Bimodal Alongwind Fatigue of Structures.” Journal of Structural Engineering, 132(6), 899-908.

Repetto, M. P. and Solari, G. (2007). “Wind-induced fatigue of structures under neutral and non-neutral atmospheric conditions.” Journal of Wind Engineering and Industrial Aerodynamics, 95(9-11), 1364-1383.

Repetto, M. P., and Solari, G. (2008). “Diagnosis of fatigue collapses of slender structures due to aerodynamic wind actions.” Proceedings of the BBAA VI International Colloquium on: Bluff Bodies Aerodynamics and Applications, Milan, Italy.

Repetto, M. P., and Solari, G. (2012). “Closed-form prediction of the alongwind-induced fatigue of structures.” Journal of Structural Engineering, 138(9), 1149-1160.

Reyer, M., Hurlebaus, S., Mander, J., and Ozbulut, O. E. (2011). "Design of a wireless sensor network for structural health monitoring of bridges." Proceedings of International Conference on Sensing Technology, Palmerston North, New Zealand, 515-520.

Rice, J. A., Foutch, D. A., LaFave, J. M., and Valdovinos, S. (2012). "Field testing and analysis of aluminum highway sign trusses." Engineering Structures, 34, 173-186.

Ricles, J. M., Sause, R., Garlock, M. M., and Zhao, C. (2001). “Posttensioned seismic-resistant connections for steel frames.” Journal of Structural Engineering, 127(2), 113-121.

Robertson, A. P., Hoxey, R. P., Short, J. L., Burgess, B. W., Holmes, J. D., and Ko, R. H. Y. (2001). “Wind-induced fatigue loading of tubular steel lighting columns.” Wind and Structures, 4(2), 163-176.

Robertson, A. P., Holmes, J. D., and Smith, B. W. (2004). "Verification of closed-form solutions of fatigue life under along-wind loading." Engineering Structures, 26(10), 1381-1387.

Rodgers, G. W., Chase, J. G., Mander, J. B., Leach, N. C., and Denmead, C. S. (2007). "Experimental development, tradeoff analysis and design implementation of high force-to-volume damping technology." Bulletin of the New Zealand Society for Earthquake Engineering, 40(2), 35-48.

Rodgers, G. W., Chase, J. G., and Mander, J. B. (2010). "Advanced model development and validation of damage-free precast structural connections with unbonded post-tensioned prestress." Proceedings of the New Zealand Society for Earthquake Engineering 2010 Conference, Wellington, New Zealand, 10p.

Rodgers, G. W., Solberg, K. M., Mander, J. B., Chase, J. G., Bradley, B. A., and Dhakal, R. P. (2012a). "High-force-to-volume seismic dissipators embedded in a jointed precast concrete frame." Journal of Structural Engineering, 138(3), 375-386.

Rodgers, G. W., Mander, J. B., and Chase, J. G. (2012b). "Modeling cyclic loading behavior of jointed precast concrete connections including effects of friction, tendon yielding and dampers." Earthquake Engineering and Structural Dynamics, 41(15), 2215-2233.

Rojas, P., Ricles, J. M., and Sause, R. (2005). "Seismic performance of post-tensioned steel moment resisting frames with friction devices." Journal of Structural Engineering, 131(4), 529-540.

Ronold, K. O., Wedel-Heinen, J., and Christensen, C. J. (1999). "Reliability-based fatigue design of wind-turbine rotor blades." Engineering Structures, 21(12), 1101-1114.

Roy, S., Park, Y. C., Sause, R., and Fisher, J. W. (2010). "Fatigue performance of groove-welded tube-to-end-plate connections in highway sign, luminaire, and traffic signal structures." Transportation Research Record, 2152, 63-70.

Roy, S., Park, Y. C., Sause, R., Fisher, J. W., and Kaufmann, E. J. (2011). "Cost-effective connection details for highway sign, luminaire, and traffic signal structures." National Cooperative Highway Research Program (NCHRP) Web-Only Document 176. Transportation Research Board (TRB), Washington, D.C., USA.

Roy, S., Park, Y. C., Sause, R., and Fisher, J. W. (2012). "Fatigue performance of stiffened pole-to-base plate socket connections in high-mast structures." Journal of Structural Engineering, 138(10), 1203-1213

Scruton, C., and Walshe, D. E. (1973). "Stabilisation of wind-excited structures." US Patent US3076533.

Shah, K. M. (1993). "Wind induced fatigue in steel pole bases." M.S. thesis. State University of New York (SUNY) at Buffalo, Buffalo, NY, USA.

Simiu, E., and Scanlan, R. H. (1996). "Wind Effects on Structures." 3rd edition. John Wiley and Sons, New York, NY, USA.

Smirnov, N. V. (1948). "Tables for estimating the goodness of fit of empirical distributions." Annals of Mathematical Statistics, 19(2), 279-281.

Smith, K. N., Watson, P., and Topper, T. H. (1970). "A stress-strain function for the fatigue of metals." Journal of Materials, 5(4), 767-778.

Solberg, K., Dhakal, R. P., Bradley, B., Mander, J. B., and Li, L. (2008a). “Seismic performance of damage-protected beam column joints.” ACI Structural Journal, 105(2), 205-214.

Solberg, K. M., Dhakal, R. P., Mander, J. B., and Bradley, B. A. (2008b). “Computational and rapid expected annual loss estimation methodologies for structures.” Earthquake Engineering and Structural Dynamics, 37(1), 81-101.

Solberg, K., Mashiko, N., Mander, J. B., and Dhakal, R. P. (2009). “Performance of a damage-protected highway bridge pier subjected to bidirectional earthquake attack.” Journal of Structural Engineering, 135(5), 469-478.

Sonsino, C. M. (2007). "Course of SN-curves especially in the high-cycle fatigue regime with regard to component design and safety." International Journal of Fatigue, 29(12), 2246-2258.

South, J. M. (1994). “Fatigue analysis of overhead sign and signal structures.” Physical Research Report No. 115. Illinois Department of Transportation (IDOT), Springfield, IL, USA.

Stephens, R. I., Fatemi, A., Stephens, R. R., and Fuchs, H. O. (2000). "Metal fatigue in engineering." 2nd edition. John Wiley and Sons, New York, NY, USA.

Teughels, A., and De Roeck, G. (2004). "Structural damage identification of the highway bridge Z24 by FE model updating." Journal of Sound and Vibration, 278(3), 589-610.

Topper, T. H., Wetzel, R. M., and Morrow, J. (1969). "Neuber's rule applied to fatigue of notched specimens." Journal of Materials, 4(1), 200-209.

Walker, K. (1970). “The effect of stress ratio during crack propagation and fatigue for 2024-T3 and 7075-T6 aluminum.” Effects of environment and complex load history for fatigue life, ASTM STP 462. American Society for Testing and Materials (ASTM), Philadelphia, PA, USA.

Walshe, D. E., and Wootton, L. R. (1970). “Preventing wind-induced oscillations of structures of circular section.” Proceedings of the Institution of Civil Engineers, 47, 1-24.

Warpinski, M. K. (2006). “The effect of base connection geometry on the fatigue performance of welded socket connections in multi-sided high-mast lighting towers.” M.S. thesis. Lehigh University, Bethlehem, PA, USA.

Whelan, M. J., Gangone, M. V., Janoyan, K. D., and Jha, R. (2009). "Real-time wireless vibration monitoring for operational modal analysis of an integral abutment highway bridge." Engineering Structures, 31(10), 2224-2235.

Wieghaus, K. T., Hurlebaus, S., Mander, J. B., and Fry, G. T. (2014a). “Wind-induced traffic signal structure response: Experiments and reduction via helical arm strakes.” Engineering Structures, 76, 245-254.

Wieghaus, K. T., Hurlebaus, S., Mander, J. B. (2014b). “Effectiveness of strake installation for traffic signal structure fatigue mitigation.” Structural Monitoring and Maintenance, an International Journal, 1(4), 393-409.

Wieghaus, K. T., Hurlebaus, S., and Mander, J. B. (2014c). “Natural wind response and fatigue assessment of a cantilevered traffic signal structure with helical arm strakes.” Proceedings of the Transportation Research Board 93rd Annual Meeting, Compendium of Papers, Washington, D.C., USA.

Wieghaus, K. T., Mander, J. B., and Hurlebaus, S. (2014d) “Fragility analysis of wind-excited traffic signal structures.” Submitted to Engineering Structures.

Wirsching, P. H. (1984). “Fatigue reliability for offshore structures.” Journal of Structural Engineering, 110(10), 2340-2356.

Wolski, M., Ricles, J. M., Sause, R. (2009). “Experimental study of a self-centering beam-column connection with bottom flange friction device.” Journal of Structural Engineering, 135(5), 479-488.

Yen, B. T., Hodgson, I. C., Zhou, Y. E., and Crudele, B. B. (2013). “Bilinear S-N curves and equivalent stress ranges for fatigue life estimation.” Journal of Bridge Engineering, 18(1), 26-30.

Yu, D., Butler, K., Kareen, A., Glimm, J., and Sun, J. (2013). “Simulation of the influence of aspect ratio on the aerodynamics of rectangular prisms.” Journal of Engineering Mechanics, 139(4), 429-438.

Zettlemoyer, N., and Fisher, J. W. (1977). "Stress gradient correction factor for stress intensity at welded stiffeners and cover plates." Welding Journal, 56(12), 393-398.

Zuo, D., and Letchford, C. (2008). "Investigation of wind-induced highway lighting pole vibration using full-scale measurement." Report No. 4586-5. Texas Department of Transportation (TxDOT), Austin, TX, USA.

Zuo, D., and Letchford, C. W. (2010). "Wind-induced vibration of a traffic-signal-support structure with cantilevered tapered circular mast arm." Engineering Structures, 32(10), 3171-3179.